ULTRASONIC ABSORPTION AND SPECTROSCOPIC STUDIES OF AQUEOUS SYSTEMS

A Thesis submitted by

DAVID WADDINGTON

for the Degree of

DOCTOR OF PHILOSOPHY

in the

FACULTY OF SCIENCE

of the

UNIVERSITY OF LEICESTER

Physical Chemistry Laboratory,
Department of Chemistry,
The University,
Leicester.

May, 1971.

ProQuest LLC
789 East Eisenhower Parkway
P.O. Box 1346
Ann Arbor, MI 48106-1346

S T A T E M E N T

This thesis is based upon work conducted by the author in the Department of Chemistry of the University of Leicester, mainly during the period between October 1968 and December 1970.

All the work recorded in this thesis is original unless otherwise acknowledged in the text or by references. This work is not being concurrently presented, in whole or in part, for any other degree.

May, 1971

David Waddington.

D. Waddington

ACKNOWLEDGEMENTS

I am pleased to acknowledge the advice and encouragement provided throughout the duration of this work by Professor M.C.R. Symons, whom I also thank for suggesting the field of study.

I am greatly indebted to Dr. M.J. Blandamer for his unfailing encouragement and interest, and his valued guidance as to the course of the study.

I also wish to express my gratitude to Dr. L.J. Bellamy, C.B.E., for many helpful discussions in the field of vibrational spectroscopy, and Dr. D.M. Adams for making available the laser-Raman equipment.

Sincere thanks are due to Dr. N.J. Hidden for many enlightening discussions and also, together with Mr. D.J. Burridge, for the construction and maintenance of the ultrasonic equipment.

I also thank Mr. T.R. Burdett, Mr. W.V. Nystrom and many other friends and colleagues in 'The Department' for stimulating discussions, criticisms and helpful suggestions.

I would like to thank Mrs. Sylvia Kent for patiently deciphering my handwriting and subsequently typing the manuscript, and Mrs. Ann Crane for drawing many of the diagrams.

I record here my gratitude to my Aunt and late Uncle, whose constant support and encouragement over many years has enabled me to pursue this study.

A Maintenance and Research Grant, provided by the Science Research Council, is gratefully acknowledged.

D. Waddington
Leicester, 1971.

CONTENTS

SUMMARY

This thesis is concerned with the theoretical and experimental aspects of ultrasonic absorption and vibrational spectroscopic studies of aqueous solutions. Emphasis is placed upon the role of water in these systems.

Measurements of ultrasonic absorption in the systems methyl cyanide + water and acetone + water are reported over the frequency range 200 kHz to 230 MHz. The construction of an apparatus for measurement of ultrasonic absorption over the frequency range 200 to 1500 kHz is described.

Ultrasonic velocity measurements are reported over a wide range of mixture compositions and temperatures for the system methyl cyanide + water.

Current theoretical models for ultrasonic absorption in binary liquid mixtures are reviewed and one model, that due to Romanov and Solovyev, is examined in detail. The model of Romanov and Solovyev is set down analytically in a convenient form for direct comparison with other models. The treatment of Romanov and Solovyev, together with the discrete relaxation model, is examined critically for the systems t butyl alcohol + water, acetone + water, methyl cyanide + water.

In addition, the Romanov-Solovyev theory, is extended to treat electrolyte solutions and, in its extended form,

is applied with some success to the systems tetra-alkylammonium bromide + water, and urea + water. The results of these applications reveal an important link between thermodynamic excess functions and ultrasonic absorption.

Infra-red and Raman spectroscopic studies of aqueous solutions of electrolytes and organic solutes are reported. Particular attention is given to the study of metal perchlorate solutions.

An attempt is made to distinguish between current models for the behaviour of salts when dissolved in HOD/H_2O solutions, with special reference to the influence of anions and cations on band parameters.

An ALGOL computer program for band deconvolution is described.

The design of a thermostatted Raman cell-holder for the CODERG Raman spectrometer is given.

"We live in the hope and in the faith that, by the advance of molecular physics, we shall by and by be able to see our way as clearly from the constituents of water to the properties of water, as we are now able to deduce the operations of a watch from the form of its parts and the manner in which they are put together."

T.H. Huxley

CHAPTER ONE

INTRODUCTION

The studies reported in this thesis are primarily concerned with ionic solvation and molecular interactions in aqueous solutions. Two techniques have been used; (i) ultrasonic relaxation and absorption, and (ii) vibrational spectroscopy (Raman and infra-red). The results of previous investigations of the ultrasonic absorption properties of binary aqueous mixtures are reviewed in Chapter 2, together with brief details of theoretical treatments of sound absorption.

In Chapter 3, details of the experimental methods of measuring ultrasonic absorption are discussed. In addition the construction of an apparatus for ultrasonic absorption measurements within the frequency range 200 to 1500 kHz, is described. The measurement of sound velocities, using an ultrasonic interferometer, is described.

Despite many investigations of the properties of binary aqueous mixtures,relatively little success has been achieved in linking such properties with molecular models. Only for those systems, in which the co-solvent is a monohydric alcohol, has any real success been achieved, and then only at low alcohol concentrations. In an attempt to extend these investigations, data are reported in Chapter 4 for two further liquid systems, acetone + water and methyl cyanide + water.

An analysis of the data has revealed several important features. One possible interpretation is that the ultrasonic absorption properties are controlled by water-

water, and water-solvent interactions.

Until very recently, the early theories of ultrasonic absorption have remained largely unchallenged, despite a growing bulk of experimental evidence against them.

In Chapter 5 the analytical details of two recent theoretical models of sound absorption are discussed and extended to enable application of these theories to experimental data. In particular, one of these models has been applied to aqueous electrolyte solutions and solutions of solids, such as urea, in water. One of these theories describes ultrasonic absorption in terms of composition fluctuations, whilst the second is a treatment of sound absorption in critical mixtures. The results of analyses of the systems, t butyl alcohol + water, acetone + water, methyl cyanide + water, tetraalkylammonium salts + water, and urea + water, in terms of the concentration fluctuation approach, are reported in Chapter 6. A clear link is established between ultrasonic absorption properties and thermodynamic properties of mixtures.

The role of water in solvating ionic species in solution has been the subject of many investigations, which are briefly reviewed in Chapter 7. The vibrational spectra (Raman and infra-red) of water are reviewed. Where appropriate, details of recent theoretical models for water are described. A detailed comparison of two major theories of solvation is given and an attempt to distinguish between these is reported. Briefly, one theory suggests

that the addition of sodium perchlorate to water increases the concentration of 'free' (non-hydrogen-bonded) OH groups. The second theory suggests that the perchlorate and sodium ions are solvated by the water.

The Raman and infra-red spectrometers used are described in Chapter 8, together with the design of a thermostated liquid cell for the Raman spectrometer, the formulation of a Gaussian (and Lorentzian) contour deconvolution program, and design of associated digital data output devices.

Experimental studies of the Raman and infra-red spectra of water and aqueous solutions of deuterium oxide containing salts such as sodium iodide are reported in Chapter 9. The uncoupled OD stretch of HOD, observed in dilute solutions of deuterium oxide in water, has been extensively investigated, and the effects of several inorganic salts upon the stretching band were studied.

In particular, interesting features were observed when sodium perchlorate and sodium fluoroborate were added to these HOD systems. The new features observed in the vibrational spectra have been assigned to solvent-anion interactions, and the effects of cations upon the spectra have also been studied. It has also been possible to obtain approximate solvation numbers for perchlorate and fluoroborate ions.

The effects of added alcohols, and other organic co-solvents, have been studied. This investigation has been,

perhaps, less fruitful owing to the considerable complexity of these systems, and the spectra obtained.

Finally, in Chapter 10, the results of these investigations outlined above, are briefly summarised.

CHAPTER TWO

ULTRASONIC ABSORPTION PROPERTIES OF BINARY AQUEOUS MIXTURES

2-1 INTRODUCTION

This chapter[1] reviews the application of ultrasonic absorption techniques to the study of aqueous binary mixtures. Several reviews[2-5] have touched upon the subject but little attention has usually been devoted to theoretical models for absorption in these systems. The importance of linking information gained from ultrasonic experiments with spectroscopic and thermodynamic observations is stressed. The importance of this approach has been indicated with reference to t butyl alcohol + water mixtures.[6,7] The design and operation of ultrasonic apparatus has been reviewed elsewhere.[8-10] Important features of ultrasonic theory and methods of analysing the experimental results are examined here.[4,5,11-17] The theories discussed treat the sound wave as a perturbation and no new chemical reactions take place when the sound wave passes (i.e. the power level is insufficiently high for cavitation). The technique may thus be regarded as involving a coupling between the sound wave and the dynamic changes taking place in solution.

2-2 ULTRASONIC ABSORPTION DATA

Three parameters are involved in measurements of ultrasonic absorption, α the absorption coefficient, (c) the sound velocity, and f the measurement frequency. Experimental data are conveniently summarised in four types of plot.

Plot A: The ratio α/f^2 is plotted against liquid composition at a fixed frequency and temperature, and at a pressure of 101325 Nm^{-2}. It is usual to express the composition in terms of mole fraction of component two x_2. An example is shown in Figure 2-1 for t butyl alcohol + water.[6,18,19]

Plot B: Here the quantity α/f^2 is plotted as a function of frequency (or log f) at fixed temperature and composition. A variant of this is to plot $\mu (= \alpha\lambda)$ the absorption per wavelength (λ) against composition. Many problems of interpretation are presented by this plot and these are considered below. An example is shown in Figure 2-2 for t butyl alcohol + water. It is desirable that a large frequency range be covered.

Plot C: The ratio α/f^2 is plotted as a function of temperature at a fixed frequency and composition. A typical example is given in Figure 2-3 for a ternary liquid mixture. This plot is of most use close to the critical temperature of liquids which show phase separation.[3,20,21]

Plot D: This plot shows the dependence of α/f^2 on pressure at fixed frequency, temperature and composition. This type of experiment has found little application to date because of a paucity of data.

2-3 WATER AND AQUEOUS SOLUTIONS

Water is not a typical liquid and thus it is not surprising that the ultrasonic absorption properties of

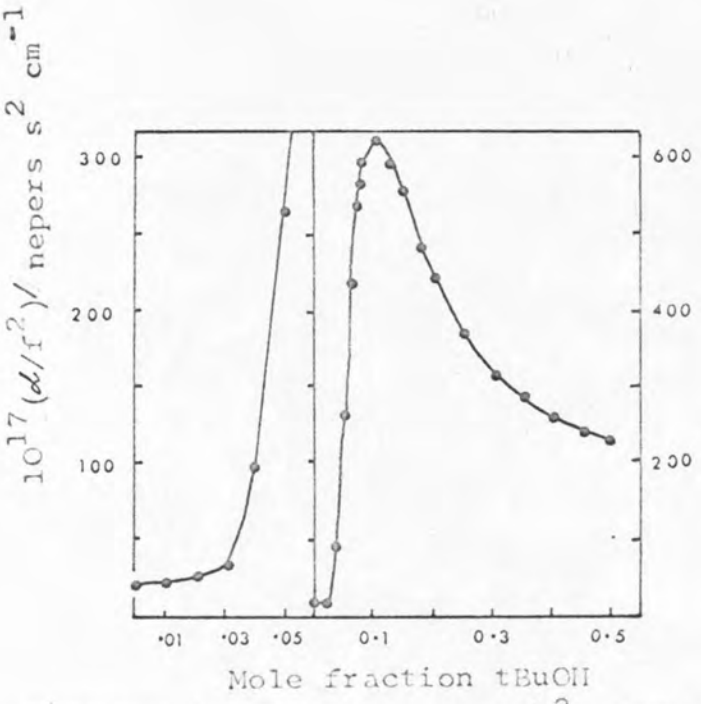

FIGURE 2-1 Variation of (α/f^2) with mixture composition for t butanol + water mixtures at 298 K and 70 MHz

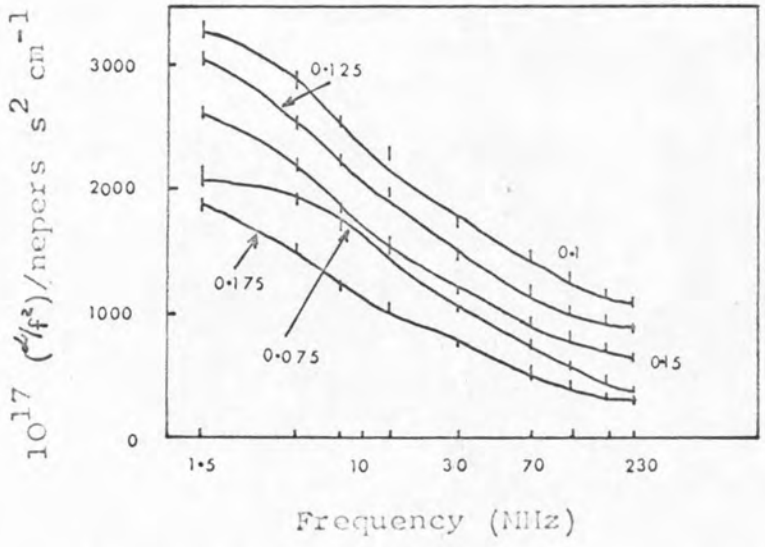

FIGURE 2-2 Typical Relaxation Curves for tBuOH + H_2O at 298 K. (For clarity each curve from 0.175 has been displaced 200 x 10^{-17} nepers s^2 cm^{-1})

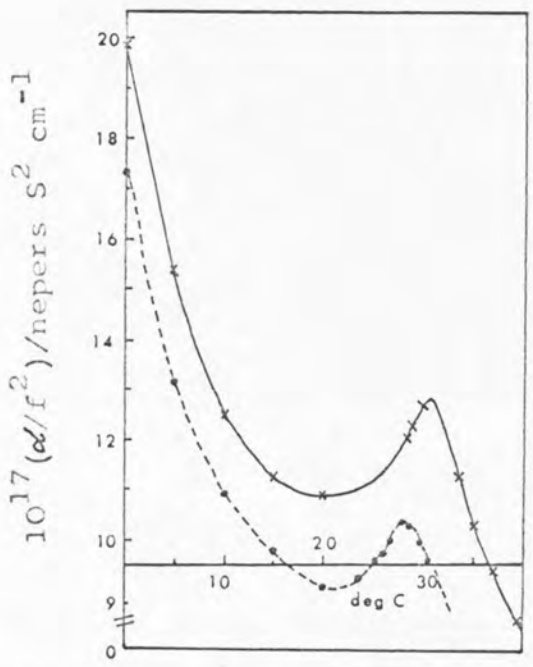

FIGURE 2-3 Sound Absorption at 1.5 MHz for 0.065(●) and 0.075(X) mole fraction (40:60 t AmOH-tBuOH) + water at different temperatures.

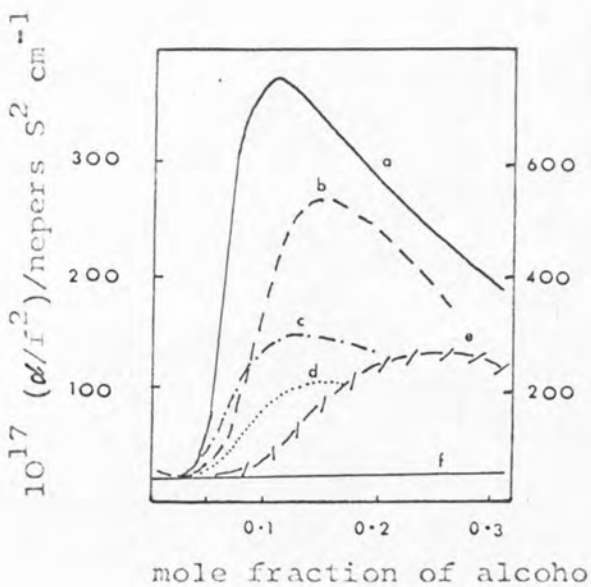

FIGURE 2-4 Ultrasonic absorption properties of water + alcohol mixtures at 70MHz and 298 K.

(a) n propyl alcohol
(b) allyl alcohol at 273 K (right hand scale)
(c) 2-bromoethanol
(d) 2-chloroethanol
(e) ethanol
(f) 2-cyanoethanol

aqueous mixtures are atypical of most other binary mixtures. The characteristic feature of PLOT A for aqueous systems is the intense maximum in α/f^2 observed in many binary aqueous mixtures. Maxima are detected for instance when the organic co-solvent is an alcohol,[2,18,22-25] substituted alcohol,[26,27] amine,[21,24,28,29] ketone,[22,24,30,31] cyclicether,[22,32,33] nitrile,[34,35] but not for t butyl alcohol + methanol mixtures.[22] A pattern is observed within each group of co-solvents. For instance, as the size of the alkyl group increases (the series Et, nPr, tBu, alcohols) $(\alpha/f^2)_{max.}$ increases and moves to lower co-solvent mole fraction. $(\alpha/f^2)_{max.}$ is relatively independent of temperature and the corresponding composition is termed the "peak sound absorption composition", PSAC. Andreae[24] has reported an extensive list of PSAC values for many systems. There is a considerable body of information regarding the properties of water.[36-39] A number of attempts at a theoretical treatment of sound absorption properties of water have been reported, that due to Hall[40] being of most significance historically. Hall used a mixture model[41] and not the uniformist model due to Bernal and Fowler.[42] The co-operative model of Frank and Wen[43] has also found application in ultrasonic absorption studies.

Often, much information can be gleaned from studies of crystalline clathrate hydrates in interpreting the behaviour of aqueous solutions.[44] There must, however, be certain reservations when solid hydrate information is

carried over to the liquid state because of the solid/liquid phase boundary separating these states. An interesting extension of this model is concerned with paraffins having one functional group. For instance, alcohols, ROH, may be treated as a solubilised paraffin with a hydrophilic hydroxyl group and hydrophobic R-group.[45,46] In dilute solutions the localised 'zones' of enhanced water structure interact to give a mutual enhancement of the water structure, accompanied by a further decrease in entropy. For some systems this mutual enhancement of water-water interactions is minimised by association of hydrophobic groups, the driving force being the resultant entropy increase.[47-50]

The thermodynamics of mixing is the key to the role of water in controlling processes in aqueous solutions.[51-53] Thus, the excess Gibbs function of mixing (G^E) is usually positive; the systems remain miscible where G^E is less than RT (2.5 kJ mol^{-1} at 298 K).[51] A link can be established between entropy changes in aqueous systems and tendencies toward phase separation at a lower critical solution temperature (LCST).[51,52] For example the critical solution behaviour of trimethylamine + water mixtures is well established.[54-56] There lies, in this property, another method of linking the hydrophobic character of the co-solvent with the properties of the mixture. Along the series Et_3N + water, Et_2NH + water, and $EtNH_2$ + water, the LCST increases,[54-56] and the intensity of $(\alpha/f^2)_{max.}$ (the PSAC)[21,24,28,57,58] at a fixed temperature decreases.

It thus seems, from this last comment, that ultrasonic absorption properties could be linked with liquid miscibility.[2,3,57,58] One suggestion is that the excess absorption in a binary liquid mixture (i.e. the PSAC) should correspond to the composition of the azeotrope.[59]

Not all non-polar solutes increase the ultrasonic absorption. Among the many examples, urea is the most frequently quoted,[60-62] the value of (α/f^2) decreasing as more urea is added. This has been interpreted as the structure breaking action of urea upon water.[63] It is likely that this approach is naive,[64,65] one puzzle being the near ideality of urea solutions.[66] In relation to the discussion in Section 2-4 it is of interest that Hammes et al.[60] found no evidence for self association in urea and water mixtures, despite the fact that such a model can fit the thermodynamic data.[67,68]

There is a striking contrast between the absorption properties (PLOT A) for aqueous mixtures where the co-solvent contains one hydrophilic group and the same properties when the co-solvent contains two hydrophilic groups. (Figure 2-4). It is of interest that despite a marked increase in the hydrophobic content of the molecule, polyhydric alcohols show little evidence for an excess absorption.[26,30] The effects of changes in the substituent X in $X \cdot CH_2 \cdot CH_2 \cdot OH$ was studied by Treloar[69] who noted a steady decrease in the excess absorption along the series CH_3, Br, Cl, H, OH, i.e. as X becomes more hydrophilic and less hydrophobic. The relatively small absorption of

sound by glycol + water mixtures has been used with advantage in studying the effects of solvents on the absorption properties of 2:2 electrolytes in water.[70,71] However, the replacement of a proton in ethyl alcohol to form chloroethanol or bromoethanol has little effect upon the absorption properties. The conclusion is that halogeno groups behave towards water in a fashion not unlike the methyl group.

2-4 ULTRASONIC THEORY

The theory of ultrasonic absorption can be thought of as an amalgam of two subjects, thermodynamics and kinetics. Similarities also exist between ultrasonics and spectrophotometry, both subjects being concerned with the absorption of energy at a chosen frequency. The vital difference is that a sound wave is not an electromagnetic wave but a pressure-temperature variation and requires a medium for propogation.

Conventional thermodynamics is only applicable when fluctuations in thermodynamic quantities are small, and this restricts its application to non-critical systems.[72-75] Initially therefore attention is confined to non-critical systems and those processes taking place when a plane progressive wave passes through it are reviewed briefly.[4,5,11,14,15]

The response of a system, measured in terms of extent, direction and rate, is a property of the system, as are

the parametersby which it is measured. The response is described by ξ indicating the change, and A indicating the affinity to undergo change. For stable equilibrium A = 0. Should the changes in the constraints (pressure, temperature) take place sufficiently fast for the system to be unable to respond, the system is described by a set of independent variables for which ξ is constant. An equilibrium isentropic compressibility can be defined, for example:

$$K_s(A=0) = - (1/V)(\partial V/\partial p)_{s,\ A\ =\ 0} \qquad \ldots\ldots (2\text{-}1)$$

and an instantaneous isentropic compressibility;

$$K_s(\xi) = - (1/V)(\partial V/\partial p)_{s,\xi} \qquad \ldots\ldots (2\text{-}2)$$

The difference between these two quantities is called the relaxational isentropic compressibility

$$\delta K_s = K_s\ (A=0) - K_s\ (\xi) \qquad \ldots\ldots (2\text{-}3)$$

Similarly, a relaxational heat capacity δC_p can be defined

$$\delta C_p = C_p\ (A=0) - C_p\ (\xi) \qquad \ldots\ldots (2\text{-}4)$$

It is possible to derive a series of important thermodynamic relations connecting equilibrium, frozen and relaxational properties.[5,53] At this stage the limit of thermodynamics is reached and it becomes necessary to appeal to kinetic information which characterises the rate of change in a system between the two situations of ξ fixed and equilibrium. Thus an expression for $\frac{d\xi}{dt}$ ($= \dot{\xi}$) is required in terms of the properties of the system. It is

at this point that the rigor of an approach to a theory of ultrasonic absorption is lost and simplifying assumptions are introduced. Thus the final expressions derived for the kinetics of changes in the system are very closely linked to the molecular interpretation of the phenomena. In one case, following the theory of dielectric relaxation, the relaxation processes occurring in solution are considered as stochastic or Markoffian processes and the analytical results are represented in terms of a number of Cole-Cole plots.[76,77] This diversion into a discussion of dielectric properties illustrates some of the problems encountered in studies of relaxational and decay processes.

The most straightforward approach to ultrasonic absorption is clearly to assume, following dielectric theory, that the system has an associated relaxation time $\tau_{s,p}$. This embodies two assumptions; (i) the rate of change, $\dot{\xi}$, is directly proportional to the affinity, and (ii) the displacement from equilibrium is small. For a perturbation due to a pressure wave of velocity, c and frequency f ($= \omega/2\pi$) an expression for the complex isentropic compressibility κ_s^* can be derived

$$\kappa_s^* = \kappa_s' - i\kappa_s'' = \kappa_s(\xi) + \left[\frac{\delta\kappa_s}{(1 + i\omega\tau_{s,p})}\right] \quad \ldots\ldots (2\text{-}5)$$

κ_s'' is the imaginary (out-of-phase) component and κ_s' the real (in-phase) component of the isentropic compressibility. If the velocity dispersion is small then

$$\kappa_s' = (1/c^2\rho) \text{ where} \quad \ldots\ldots (2\text{-}6)$$

ρ is the solution density and c the sound velocity.

By solving for the real and imaginary parts of κ_s^* a relation between (α/f^2) and frequency f is obtained.

$$(\alpha/f^2) = \left\{ A / [1 + (f/f_c)^2] \right\} + B \qquad \ldots\ldots (2\text{-}7)$$

where $A = (2\pi^2/c)\tau_{s,p} \left[\frac{\delta\kappa_s}{\kappa_{s(A=0)}} \right]$

and $fc = 2\pi\tau_{s,p}$ in the limit that

$$\left[\delta\kappa_s/\kappa_s(A=0)\right] \ll 1$$

B is the shear viscosity (η_s) contribution. The absorption per wavelength $\mu (= \alpha\lambda)$ has ideally the shape shown in Figure 2-5 which is similar to a plot of dielectric loss against frequency for a simple system. The data are more conveniently represented using equation (2-7) which has a sigmoid shape (Figure 2-5). This latter method permits easy identification of a B contribution. For a system with a spectrum of relaxation times, these expressions can be modified to give

$$\left[\frac{\alpha}{f^2}\right] = A \int_0^\infty \frac{F(\tau)\, d\tau}{1 + (\omega\tau)^2} \qquad \ldots\ldots (2\text{-}8)$$

with average relaxation time $\bar{\tau} = \int_0^\infty \tau F(\tau)\, d\tau$. This approach has been used in a study of polymer-water interactions.[78]

(i) WATER RICH MIXTURES

A remarkable feature of PLOT A for monohydric alcohols + water is the initial region of insensitivity of (α/f^2)

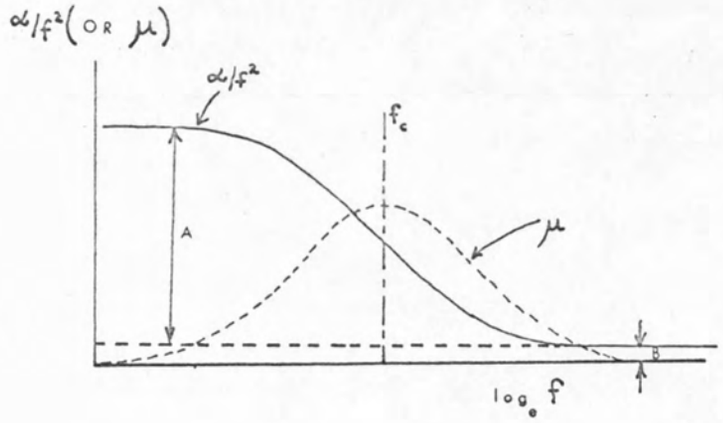

FIGURE 2-5 Idealised variation of (α/f^2) (_____) and (-----) with $\log_e f$ for a system with a single relaxation frequency f_c.

to added alcohol, prior to the rise to the PSAC. This transition is particularly marked for t butylalcohol + water mixtures[1,7] but less distinct for ethanol + water mixtures.[79] This region of insensitivity may be called a 'plateau', e.g. the region $0 \leqslant x_2 \leqslant 0.04$ for t butyl alcohol + water. There is a possibility that (α/f^2) does not remain completely independent of composition in the 'plateau' region, sometimes the points lie on a shallow curve and sometimes there is a small rise. For t butyl alcohol + water mixtures the plateau length increases as the temperature is lowered.

This initial insensitivity of (α/f^2) to added solute can be contrasted with other properties which show a change in this region. Examples are observed in the thermodynamic,[6,45,80-82] kinetic[81,83] and spectroscopic properties,[6,84] e.g. the rapid decrease in the relative partial molar volume $\overline{V}_2 - V_2^\circ$ of alcohol[45,85-88] and the shift to high energy of the charge-transfer-to-solvent (CTTS) spectra of iodide in the mixtures.[89,90]

Clearly those molecular processes which are responsible for the absorption at the PSAC play no part in these dilute solutions. Consequently one region can be identified and considered without regard to the region displaying a large excess absorption. At first sight it is difficult to reconcile the insensitivity of (α/f^2) with the marked sensitivity of spectroscopic techniques or volume parameters. These latter techniques lead to the conclusion that t butyl alcohol lowers the effective temperature of water.

Thus the alcohol could enhance water-water interactions such that the structure tends to resemble the alcohol clathrates. This is in opposition to the theory of Andreae,[24] who concluded that the alcohol destroyed the water structure. Andreae was, in fact, attempting to resolve the initial rise in both (α/f^2) and the sound velocity c. However, c increases whilst (α/f^2) remains constant, and there are grounds for examining not c but the deviation of c from ideality.

Although there is no direct evidence for a t butyl alcohol + water hydrate, ethanol + water is thought to form one.[91] Franks has shown,[46] by using molecular models, that t butyl alcohol could be accommodated in a hydrate lattice. This model accounts for the decrease in plateau length with increase in temperature since the latter effect will decrease the ability of the water to form cages.[18] Even if the liquid structure bears little relationship to the structure of the hydrate, the small change in (α/f^2) means that no new physical or chemical changes take place in the liquid which are sensitive to the sound wave. This can be contrasted with the amine + water mixtures where (α/f^2) increases when amine is added initially. This effect has been ascribed to an acid-base equilibrium of the form:

$$R_2NH + H_2O \rightleftharpoons R_2NH_2^+ + OH^-$$

The above conclusion was derived from a detailed analysis of the absorption properties of diethylamine + water[92] and can probably be extended to other amine + water systems.[15]

Addition of more amine causes a rapid increase in the absorption and a change is noticeable in the absorption behaviour (PLOT A) which is reminiscent of alcohol + water mixtures. Indeed there is good evidence that amine clathrate hydrates exist from freezing point data[93-95] and X-ray crystallography.[96-98] Also the thermodynamic properties are consistent, in many cases, with the idea that amines are structure makers.[99] It can thus be suggested that, in the absence of an acid-base equilibrium, each amine + water plot (PLOT A) would show a plateau region.

In the foregoing discussion attention has been concentrated on those mixtures where there is little excess absorption. This sets the stage for the discussion of those mixtures formed by adding more organic co-solvent. That is those mixtures where the absorption is large. By contrast to the dilute solutions, there is a real lack of understanding of these mixtures in terms of ultrasonic and spectroscopic data. In particular the kinetic contribution becomes difficult to assess. Thus there is no clear indication from other sources of how to set up theoretical treatments of these mixtures. Indeed, it is at this point that the development of ultrasonic theory becomes complex.

(ii) THE CHEMICAL APPROXIMATION

One way of explaining the sigmoid dependence of α/f^2 on f is to assume that the sound wave perturbs an equilibrium of the form:

$$A \underset{k_2}{\overset{k_1}{\rightleftharpoons}} B$$

Two simplifying assumptions are made (i) molecules A and B mix to form an ideal solution or are ideal solutes in a solvent, (ii) the thermodynamic equilibrium constant K is given by the ratio of the rate constants. A thermodynamic analysis of the system leads to an expression for $\mu_{max.}$ in terms of the standard volume $\Delta V^{\ominus}$ and enthalpy $\Delta H^{\ominus}$ differences.

$$\mu_{max} = \frac{\pi}{2} \frac{\rho c^2 \Gamma}{RT} \left[\Delta V^{\ominus} - \frac{\alpha_c \Delta H^{\ominus}}{\rho C_p} \right]^2 \frac{C_p}{C_{p_\infty}} \quad \ldots\ldots (2\text{-}9)$$

where Γ describes the sinusoidal variation of the equilibrium constant about its mean value caused by the sound wave. This equation cannot be solved for both $\Delta V^{\ominus}$ and $\Delta H^{\ominus}$ unless other assumptions are made. For example in dilute aqueous solutions $\Delta V^{\ominus}$ is thought to dominate. One feature of interest is that $|\Delta V^{\ominus}|$ and $|\Delta H^{\ominus}|$ could both be large but effectively cancel with respect to their effect on $\mu_{max.}$.

A kinetic analysis, based on an exponential decay of the calculated absorption, leads to a relaxation time for the equilibrium, $(k_1 + k_2)^{-1}$.

For a more complex equilibrium

$$A + mB \rightleftharpoons AB_m$$

additional factors come into the treatment. For instance, the chemical relaxation time is now a function of composition.

In some cases the dependence of (α/f^2) on frequency (PLOT B) cannot be fitted to a single relaxation but requires two or more frequencies:

$$\left[\frac{\alpha}{f^2}\right] = \sum_{i=1}^{n} \left[A_i \Big/ \left\{ 1 + \left(f / f_{c(i)} \right)^2 \right\} \right] + B \quad \ldots\ldots \quad (2\text{-}10)$$

Such an example is provided by 2:2 electrolytes in water.[15,100-103] The usual procedure is to fit the values of (α/f^2) over a range of frequencies to equation (2-10), using the smallest value of n consistent with the estimated experimental accuracy and the number of experimental points. The fit of the data to equation (2-10) is obviously improved the greater the value of n. The final, and most difficult, stage is to assign each derived relaxation time to a chemical reaction which involves setting up a series of chemical equilibria for the mixture. If the relaxation frequencies differ by a factor of ten or more then the two equilibria involved are considered to be effectively uncoupled.[104]

Often, in practice, an analysis of the absorption properties usually starts out with a consideration of PLOT A, followed by PLOT B. Storey[25] suggested that the absorption properties of ethanol + water mixtures can be considered in terms of an alcohol - water complex (1:4). He used as evidence of this the inflection in the freezing point curve at the same composition as the PSAC.

A more specific approach is to use an equilibrium of the form:

$$RX + mH_2O \rightleftharpoons RX \cdot MH_2O$$

where the absorption is attributed to intermolecular association. If m = 1 and RX, H_2O and $RX \cdot H_2O$ mix ideally then the theory predicts that $(\alpha/f^2)_{max.}$ for acetone + water occurs at $x_2 = 0.5$. Although for acetone + water the PSAC is 0.4 at 273 K.

In general x_2 (at $\alpha/f^2{}_{max.}$) = $1/(1+m)$ . . . . . (2-11)

and m can be obtained from PLOT A. Some values of m are shown in Table 2-1. This theory was extensively developed by Andreae and has been described uncritically in a number of reviews.[9,13] The essential features are examined below. Analysis of the dependence of (α/f^2) on frequency often shows that the assumption that ΔH° is zero is invalid.[29,105] It has been assumed that the association of RX with mH_2O is a single step process. Andreae and co-workers examined a stepwise model, a series of n-equilibria:

$$RX \cdot (m-1)\ H_2O + H_2O \rightleftharpoons RX \cdot mH_2O$$

where m = 1,2,3, ---n in which it is assumed that the forward rate constant, the association step, is independent of m. The calculations are formidable. A commendable treatment suggested by Andreae used a two state model having bound and 'free' water. Addition of an organic co-solvent brings about changes reflected by the two equilibria:

$$RX + H_2O \rightleftharpoons RX \cdot H_2O$$

$$H_2O \rightleftharpoons (H_2O)\ \text{bound}$$

TABLE 2-1 Approximate values of m derived from values of the peak sound absorption composition

System studied	Value of m
t butyl alcohol + water	10
acetone + water	1.5
diethylamine + water	9
methyl cyanide + water	1.5
ethyl alcohol + ethyl chloride	95

For acetone + water, assuming $\Delta H^{\circ} = 0$, a fair fit was achieved for the absorption and velocity results. The ultrasonic relaxation is associated with the former equilibrium, the latter being above 230 MHz. Thus generally when relaxations are observed within the range 1 to 230 MHz, these involve the added co-solvent. In many ways this model resembles more recent models which suggest that the added solute may dissolve in regions of bound or free water molecules.[64]

The above equilibria go some way towards describing the effects of urea as a structure breaker. In contrast, alcohols and acetone are more satisfactorily described as structure formers.Thus, addition of RX would involve[64] interaction with (H_2O) bound, thereby diluting the (H_2O) bound "phase" with the result that H_2O molecules associate to maintain the equilibrium:

$$H_2O \rightleftharpoons (H_2O) \text{ bound}$$

Hammes and Knoche[32] used a similar model to account for the absorption properties of dioxan. The excess absorption is small and the PSAC around 0.5 mole fraction dioxan. Their results were interpreted using two equilibria:

$$2H_2O + 2\ \text{DIOXAN} \rightleftharpoons \text{DIOXAN} + \text{DIOXAN}\cdot 2H_2O$$

$$\text{DIOXAN} + \text{DIOXAN}\cdot 2H_2O \rightleftharpoons 2\ \text{DIOXAN}\cdot 2H_2O$$

The formation of 1:1 and 2:1 complexes was indicated from previous dielectric relaxation data. Hammes et al discussed the results in terms of hydrophobic hydration of dioxan by the water.[52,85,106,107]

These treatments go some way towards an explanation of the important features of the absorption properties of aqueous mixtures, and have found wide acceptance. They have, however, several shortcomings which have become clearer as more data has become available.

A major criticism concerns the assumption of ideal mixing of all components involved in the equilibria. This requires that all non-ideal properties of these systems be explicable using the same equilibria. Other approaches find this analysis unsatisfactory, and the model does not satisfy the requirements of spectroscopic observations. The equilibrium constants and associated parameters (ΔH° and ΔV°) cannot be independently determined. It is certain that rates and equilibrium constants for chemical reactions are sensitive to the composition (x_2) of binary aqueous mixtures.[81,108]

Another major criticism is concerned with the shape of PLOT A. The theory predicts a large excess absorption at x_2 = 0.5 mole fraction of t butyl alcohol, whereas the observed absorption has almost fallen to zero at this stage.

None of the modifications often introduced to counter these criticisms can explain the shape of the curve at low mole fraction, namely the plateau and subsequent rise. Often the derived values of m are quite reasonable, but in the case of ethylene chloride + ethanol, it is quite unreasonable, i.e. 95.

Finally, the meaning of the equilibria invoked to

explain the absorption is often not clear. Consider the equilibrium,

$$R X + H_2O \rightleftharpoons RX \cdot H_2O.$$

If this equilibrium were present in a third, non-interacting, solvent, then RX, H_2O and $RX \cdot H_2O$ would be surrounded by solvent. In the present context RX is surrounded by water and RX molecules, the actual environment changing with x_2. Thermodynamic and spectroscopic evidence shows that at low x_2, RX molecules have an effect on neighbouring water molecules. Thus, the structural difference between RX in its environment in the solvent, and $RX \cdot H_2O$ in the solvent, is clearly not well defined by the above equilibrium.

In view of these difficulties, a new model has found application in these laboratories which overcomes qualitatively the major objections. This model directs attention towards the hydrophobic part of the RX molecule, previously shown to be the controlling factor in determining the magnitude of (α/f^2). The model followed the discovery that, in general, two relaxations were required to fit the data in PLOT B. For those mixtures where the thermodynamic properties indicated the organic co-solvent to be a structure former, a common pattern in the ultrasonic absorption parameters (derived using equation (2-10)) was found.[26,109] For alcohols, for example, fc_1, fc_2 and $(\mu_{max.})_1$ and $(\mu_{max.})_2$, have extrema at the PSAC. The temperature dependences of the relaxation frequencies are small and this suggests isothermal behaviour. Following the proposed clathrate hydrate model, it becomes clear that as more alcohol is added there will come a time when there is

insufficient water to satisfy the needs of all the alcohol molecules. Prior to this there were no major relaxation processes other than that of water.

The reduced availability of water leads to the rapid rise in (α/f^2) (PLOT A). In this region cavities are formed which can hold two or more co-solvent molecules possibly associated in a hydrophobic sense.

$$(ROH)_{H_2O} + (ROH)_{H_2O} \rightleftharpoons (HOR \cdot ROH)_{H_2O}$$

Such equilibria are thought responsible for the observed relaxations. A similar model may hold for methyl cyanide but a hydrate has not been characterised.[34,91,110]

A more quantitative link between thermodynamic and ultrasonic absorption data is clearly required. Such a link is briefly described in the next section and in subsequent chapters. This approach moves away from the chemical approximation and examines ultrasonic absorption phenomena from a different standpoint, which does not invoke the formation of well defined molecular associates.[111]

(iii) CONCENTRATION FLUCTUATIONS

Nomoto[112-114] made an interesting suggestion which does not require the chemical approximation approach. Instead he formulated a molecular mechanism for sound absorption[113] which he described as 'relaxation of molecular rearrangement' or 'diffusion relaxation mechanism'. As a basis it used the mixture model of Hall,[40] although there are similarities to the clathrate hydrate model. A link was woven between dynamic equilibria associated with 'bound' and 'free' water molecules and sound absorption. Added

alcohol causes partial collapse of the associated molecules. The sound wave (a pressure wave) passes through the liquid and groups of associated water molecules collapse. Solute molecules now diffuse into these zones because a solute molecule can only be accommodated in regions of single molecules. The transition to an equilibrium position is diffusion controlled. This mechanism avoids the problem that the equilibrium between associated and single water molecules is at higher frequencies than observed in aqueous solutions.

Many authors have noticed the resemblance between PLOT A and a similar plot of the intensity of scattered light.[115] It seems probable that a theory of concentration fluctuations, similar to that used to describe light scattering, may be able to offer a description of the ultrasonic absorption properties of binary aqueous mixtures. Subsequent chapters are given towards the development of one such theory proposed by V.P. Romanov and V.A. Solovyev.[116-118] A major advantage being the link provided by this theory between ultrasonic absorption and thermodynamic measurements.

(iv) CRITICAL PHENOMENA

Recently there has been a resurgence of interest in critical phenomena and a number of reviews are devoted to detailed analyses of critical properties.[119-126]

Many forms of critical phenomena occur in nature, for

example, in binary mixtures, liquid-gas transitions, and magnetic properties.

For ultrasonic absorption[3] it has been shown that for a single component system, the absorption increases rapidly as the critical temperature T_c is reached from above or below. A strong link has been established between ultrasonic absorption properties of critical phenomena and statistical treatments of the critical properties of magnetic materials.

It is of some importance when discussing the properties of mixtures to consider the effects of critical phenomena.

Several times during the previous discussion, reference has been made to upper or lower critical solution temperatures (UCST or LCST) which are close to the temperature at which the ultrasonic absorption properties were studied. Where measurements of the critical temperature are available a number of links can be drawn between critical behaviour and sound absorption. Thus Sette[2,3] first drew attention to the similarity in shape between the co-existence curve and PLOT A for n-hexane + nitrobenzene mixtures, which display a UCST at 298.17 K. The absorption properties of phenol + water have been measured close to the UCST.[3,127] The system water + (40:60 t amylalcohol + t butyl alcohol) has a lower critical solution temperature at 301 K at x_2 = 0.08 and $(\alpha/f^2)_{max.}$ occurs at x_2 = 0.08 at 298 K.[69]

The dependence of (α/f^2) upon temperature shows a

marked rise as the critical temperature is reached. An examination of the properties of alcohol + water mixtures reveals a number of puzzling features. For instance, as the critical temperature is approached, the heat capacity Cp of a binary liquid mixture increases with decrease in $|T-T_c|$.[128] The shape of these curves resembles PLOT A, especially the rise in (α/f^2) following the plateau. It is possible that the rise in (α/f^2) reflects a tendency towards phase separation. It was mentioned above that this rise in α/f^2 can be thought of as a consequence of the lack of sufficient water to accommodate all the alcohol molecules in a hydrate fashion. A further observation, which strengthens the link with incipient phase separation, is that the plots of C_v^E against x_2 for ethanol + water predict that C_v^E shows a large maximum before falling to zero at $x_2 = 0$. It may well be argued that those changes taking place in mixtures at mole fractions close to the end of the plateau region are in some way linked to incipient phase separation.

Changes also take place when salts are added to these mixtures. Some salts increase the absorption, whilst others decrease it. No clear evidence has been obtained for the effect on the absorption of ion size, but there is a general similarity with the effects of added salts on the solubility of partially miscible systems.[129,130]

If these properties do not reflect phase separation then they reflect the increasing intensity of composition fluctuations close to the position where (α/f^2) tends to

a maximum (PLOT A). This idea is borne out by X-ray scattering results,[131] despite an opposite temperature dependence of the scattering from that observed by ultrasonic absorption. However, the X-ray technique probably probes molecular interactions at a more microscopic level than ultrasonic absorption.

An early theoretical analysis of critical properties of ultrasonic absorption by Lucas[132] examined the effects of time dependent density fluctuations and linked these to sound absorption. Sette[3] reported that a test of this theory showed that the intensity of the absorption was not accountable for. A recent analysis by Fixman[133-139] has been much more successful in dealing with critical properties and is outlined in Chapter 5 for comparison with the Romanov-Solovyev approach.

Finally, it is noted that it is not yet possible to predict the magnitude of the excess absorption observed when two liquids are mixed. For binary aqueous mixtures the ability to make such predictions is closely linked with theoretical treatments of water structure.

CHAPTER THREE

ULTRASONIC ABSORPTION AND VELOCITY MEASUREMENTS

(EXPERIMENTAL)

3-1 INTRODUCTION

The construction and operation of the apparatus used for making ultrasonic absorption and velocity measurements is described in this chapter.

Two methods were used for absorption measurements, known as the pulse[7,8,140-143] and reverberation[144-147] techniques. The former technique covers the frequency range 1.0 to 230 MHz, using two instruments referred to as the Low Frequency Pulse Apparatus (LFPA) (1.0 to 30 MHz), and the High Frequency Pulse Apparatus (HFPA) (30 to 230 MHz). The pulse technique is unsuitable for accurate measurements below about 1.0 MHz because very large path lengths and, consequently, large volumes of liquid are required. An apparatus was built to cover the range 200 to 1500 kHz utilising the reverberation technique. The recorded applications of this technique are few and a brief comment upon some of these is included. The apparatus was constructed in these laboratories by Dr. N.J. Hidden. The high and low frequency pulse equipment has been described in detail elsewhere.[148,149]

In addition to the absorption measurements, a description of an apparatus for the measurement of ultrasonic velocities, at 2MHz, is also given.

3-2 REVERBERATION APPARATUS

(i) Low Frequency Ultrasonic Measurements

In principle a vessel containing the test liquid is ultrasonically excited so that standing waves are established in the fluid. The ultrasound source is then switched off and the decay of sound amplitude followed, using a detecting transducer connected to an amplifier and display oscilloscope.

Attempts to measure ultrasonic absorption in the frequency range 30 to 1000 kHz were reported in 1948 by C.E. Mulders.[150] Mulders, using aluminium cylinders to contain the fluid under examination, established some of the basic theory of this technique. If the only form of energy loss in the liquid is due to absorption by the liquid then the decay may be expressed as:

$$A_t = A_o \exp (-\alpha c t) \qquad \ldots\ldots (3\text{-}1)$$

where α is the amplitude absorption coefficient of the fluid, and c is the sound velocity in the fluid. However, Mulders suggested other sources of energy loss:

(a) added damping of the decay by the support of the vessel and transducer connections.

(b) radiation to the air from the outer surface of the container.

(c) absorption of sound in the walls of the container - 'wall loss'.

(d) losses due to viscous drag between the fluid and the walls of the container.

These additional losses are often represented by

$$k = k_a + k_b + k_c + k_d \qquad \ldots\ldots (3\text{-}2)$$

The total damping is given by

$$\delta = (\alpha c + k) \qquad \ldots\ldots (3\text{-}3)$$

A quantity τ, the decay time constant, is measured. $A_t = A_o \exp(-t/\tau)$ is the standard equation for any exponential.

Where $$A_t = A_o \exp(-t/\tau) = A_o \exp(-t(\alpha c + k)) \ldots (3\text{-}4)$$

Therefore $$\tau = \frac{1}{(\alpha c + k)}$$

The problem is thus resolved into one of determining the damping constant k by some independent method. Two methodsare available. Firstly, since k is dependent upon the surface area to volume ratio of the container, τ can be determined for several different sized vessels having similar geometry. Consequently k can be calculated. Secondly, a liquid of known absorption can be used as a standard for calibration. Low frequency measurement can be divided into two classes, those using a resonance[142,144,151-154] technique and those using a reverberation[146,147,150,155,156] technique. The former method involves the excitation of single radial modes in a spherical container. Low k-values are obtained since no fluid displacement takes place parallel to the liquid vessel boundary. It has been most successful in the range 30 to 300 kHz. Above 300 kHz the close spacing of radial modes makes them difficult to excite, without exciting the other modes as well.

Several workers[151-153] have shown that k varies with frequency according to

$$k = a + b f^2 \qquad \ldots\ldots (3\text{-}6)$$

The term $b f^2$, dominant at high frequency, is believed to represent residual viscous losses at the liquid-solid boundary, because 'b' depends upon the absorption of the liquid. It is likely that the term 'a' represents k_a and k_c loss. Stuehr[147] et al have used this technique, and an apparatus similar to that of Leonard and Wilson,[151] to make absorption measurements at 30 kHz on dilute potassium cyanide solutions. The estimated error is around $\pm$ 20%. Other noteworthy applications of this technique have been reported by Ohsawa and Wada[157] and Karpovitch.[144] The former workers studied toluene and aqueous solutions of magnesium sulphate at approximately 25 kHz. Karpovitch[144] studied rotational isomerism in cyclohexane derivatives. The reverberation technique has been employed more frequently than the resonance technique. No attempt is made to excite a particular resonance mode of the vessel and contents. Instead, all resonance frequencies within a small frequency range (usually about 8 kHz) are excited, and the average decay time recorded. If all the component modes have the same damping coefficient δ, then an exponential decay curve will be observed. Experiment shows that this holds for all non-radial modes. Occasionally, when a spherical container is used a long time constant 'trail off' is observed. In such cases the time constant of the initial decay is measured, since the 'trail off' is produced by radial modes.

Since excitation of radial modes is not necessary, containers of any shape may be used. Tamm[145] used cylinderical vessels. One disadvantage of this method is that uniform excitation of a number of modes often leads to a non-exponential decay curve. This effect can be partially eliminated by employing a noise generator and selecting an 8 kHz band of noise centred on the desired frequency.

The damping loss factor (k) is larger than in the resonance method and this tends to raise the low frequency limit of measurement. The method is simpler and more accurate than the resonance method and the dependence of k on frequency is said to obey the relation[146]

$$k = a + b f \qquad \ldots\ldots (3\text{-}7)$$

The limits of detectability are governed by the volume of sample and the sensitivity of the method used to measure the decay time constant. The frequency range of the method is limited to about 300-1500 kHz, for liquids of low absorption ($\alpha/f^2 \approx 200 \times 10^{-17}$ n.sec^2 cm^{-1}). This method has been applied, with moderate success.[150,155,156] The estimated error is about $\pm$ 20%.

Table 3-1 illustrates the systems studied, methods employed and frequency range covered up to date.

Recently another method for the measurement of ultrasonic absorption at low frequencies (200 to 1500 kHz) has been developed by Eggers.[158] This technique has not been widely used. An apparatus is at present

TABLE 3 - 1 Compilation of methods used by various experimentalists to study ultrasonic absorption in the frequency range 30 to 1000 kHz

Experimentalist and Date	Method	Frequency Range (kHz)	Modulation	Containers	Volume (dm^3)	Calibration Substance	Liquids Studied
Leonard and Wilson (1954)	Resonance	30 → 500 and 30 → 100	None	Pyrex Spheres	12	Water	Aqueous $MgSO_4$
Skudrzyk (1950)	Reverberation	20 → 600	F.M. 10 kHz	Aluminium Cylinders	500	Absolute	Pure water and sea water (?)
Mulders (1950)	Reverberation	730 → 1500	F.M. 15 kHz	Aluminium Cylinders	2-3	Absolute	Water and $MgSO_4$
Tamm (1950)	Reverberation	50 → 500	10 kHz noise	Aluminium Cylinders	100-900	Absolute	Water
	Resonance	5 → 50	None	Pyrex Spheres	20	Comparison solvent	$MgSO_4$
Moen (1951)	Resonance	140 → 1500	F.M.	Pyrex Spheres	0.2-12	Absolute	Water glycerol benzene toluene CS_2

TABLE 3 - 1 (Continued)

Experimentalist and Date	Method	Frequency Range (kHz)	Modulation	Containers	Volume (dm^3)	Calibration Substance	Liquids Studied
Bies (1953)	Resonance	20 ⟶ 500 and 20 ⟶ 200	None	Pyrex Spheres	12 and 50	Comparison solvent	$MgSO_4$ in water & water + dioxan
Karpovich (1954)	Resonance	20 ⟶ 1000 20 ⟶ 200	None	Pyrex Spheres	0.5	Comparison with standard liquids	Many organic liquids
Lawley and Reed (1955)	Reverberation	200 → 2000	Noise 15 kHz	Pyrex Spheres	0.5	Comparison with standard liquids	Several organic liquids
Muller (1960)	Reverberation	800	F.M.	Aluminium Cylinders	0.76 to 11.25	Absolute & Comparison with standard liquids	Water, MeOH, C_6H_5Cl, CCl_4, C_6H_6
Stuehr, Yeager, et al (1962)	Resonance Reverberation	30 ⟶ 300 300 → 1000	None 8 kHz noise	Pyrex Spheres	12 & 50 3	Comparison with solvent	Dilute Aqueous KCN Solutions

TABLE 3 - 1 (Continued)

Experimentalist and Date	Method	Frequency Range (kHz)	Modulation	Containers	Volume (dm^3)	Calibration Substance	Liquids Studied
Cerceo, Meister, Litovitz (1962)	Resonance	160 → 500	10 kHz Noise	Pyrex Spheres	12	Water as Calibration liquid	Toluene "
Eggers (1967)	Acoustic Resonator	200 → 15000		Specially designed resonator cell	0.040	Water as Calibration liquid	$MnSO_4$ + water, amino acids + water

under construction in these laboratories with a view to applying this method to aqueous and organic liquid mixtures.

In these laboratories low frequency measurements have been made using the reverberation technique. Preliminary experimental work has shown that the resonance technique is unsuited to routine ultrasonic absorption measurements. The operational difficulty and low accuracy and reproducibility also render this technique unsatisfactory.

(ii) Original Design of the Reverberation Apparatus

The apparatus shown diagrammatically in Figure 3-1, was designed to cover the frequency range 200 to 1500 kHz.[148] For liquids with high ultrasonic absorption this range was restricted. One and three dm^3 vessels of spherical geometry with very narrow necks were used. The vessels were suspended using three thin piano wires, thereby minimising sound losses in the suspension. Barium titanate transducers were coupled to the walls of the sphere, one for excitation and one for detection. An 8 kHz band of white noise centred about the desired frequency was selected by a tuneable amplifier and applied to one transducer. The receiving transducer followed the sound decay which was displayed on an oscilloscope. Two methods for measuring τ, the decay time constant, were used. In the first method an exponential decay of adjustable time constant and magnitude was

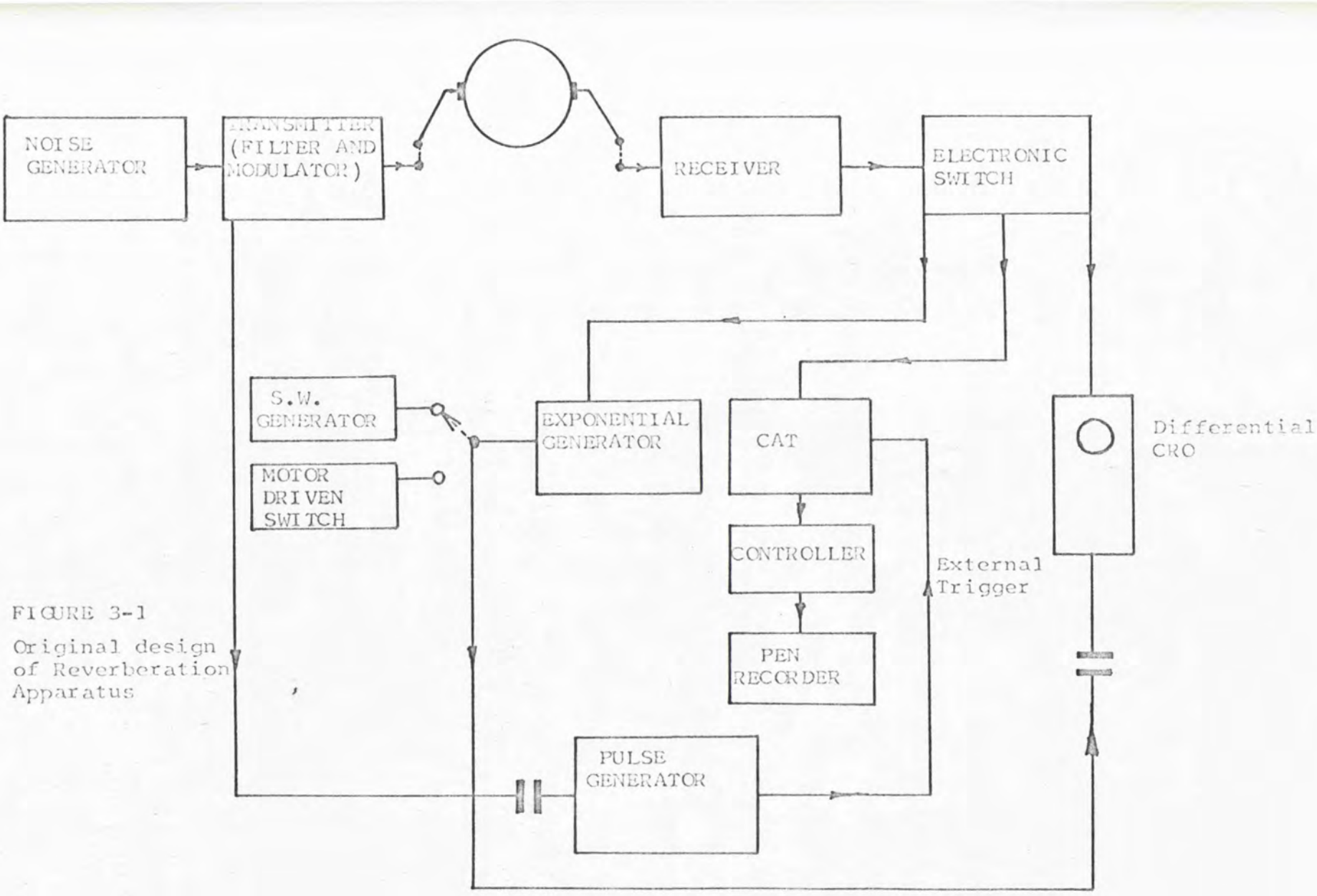

FIGURE 3-1

Original design of Reverberation Apparatus

generated and compared directly with that produced by the sphere. A differential oscilloscope was used and the generated exponential adjusted until the differences between the two signals was zero. In the second method a large number of decay curves were fed to a time averaging computer. The average decay curve was then recorded from the computer output.

Several problems were encountered with this apparatus. The results[148] showed a considerable scatter despite being in broad agreement with those obtained at 1.0 MHz. The measurements at certain compositions were repeated and considerable lack of reproducibility was evident. In consequence extensive modification of the apparatus was undertaken.

(iii) Reverberation Apparatus - Redesigned Version

(a) Construction

A block diagram of the apparatus is shown in Figure 3-2. Piezoelectric ceramic transducers (barium titanate, dimensions 12.5 mm dia.) were attached to thickness resonance 2 MHz. two metal mounting plates on diametrically opposite outside surfaces of a spherical vessel of capacity about one dm^3. Electrical contact was made to each of the transducers using small copper springs fitted with copper contacting plates. The vessel, filled with the fluid under examination, was suspended, using three piano wires in air in a sealed chamber. The chamber formed the

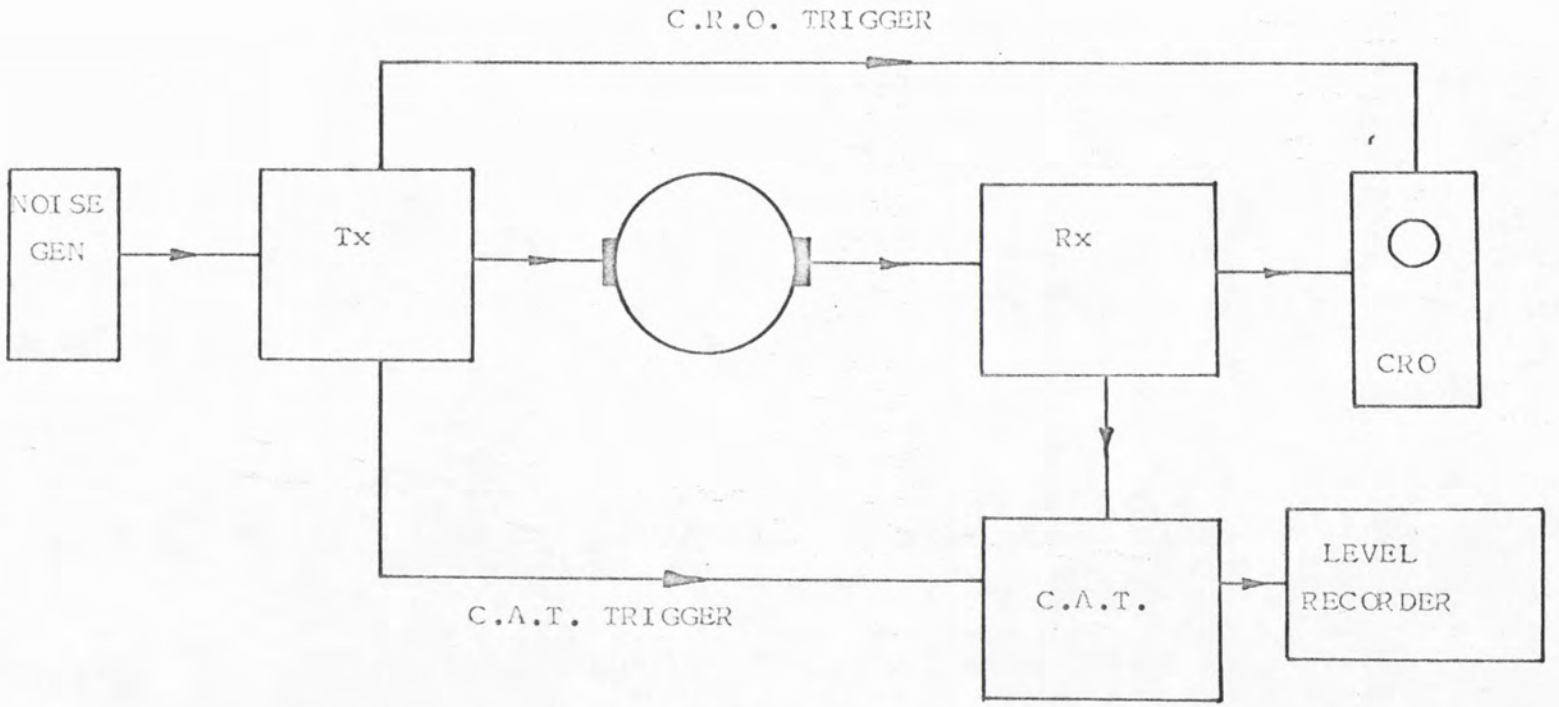

FIGURE 3-2 Redesigned Reverberation Apparatus

inside of a thermostatted tank. The thermostatting fluid, an ethylene glycol + water mixture, was circulated from a variable temperature thermostat bath. The temperature inside the air chamber was measured using a thermistor.

A white noise generator (Dawe Type 419 C) fed white noise to a tuneable transmitter and modulator unit. This produced an amplitude modulated square wave output of variable period (steps 1.6, 0.7, 0.42, 0.17 seconds) and having a band width of 8-10 kHz. Each pulse of sound at the transducer caused excitation of the sphere and a second transducer monitored the decay in energy of the sphere and contents between successive pulses. The signal from this transducer was amplified by a tuneable amplifier, a modified BC 433 receiver. A low pass filter removed the high frequency component of the noise. A signal from the transmitter triggered an oscilloscope which displayed the decay curve. An improvement in signal to noise ratio was achieved using a Varian Associates C-1024 Time Averaging Computer (C.A.T.). This stored and averaged 64 decay curves. The output level from the C.A.T. was recorded directly over a 25 db range, using a Bruel and Kjaer Type 2305 logarithmic pen recorder.

(b) Operation

The liquid under examination was thoroughly degassed in an ultrasonic degassing apparatus. This apparatus (shown in Figure 3-3) consisted of a high power generator Type L279 (Midland Equipment Ltd.),

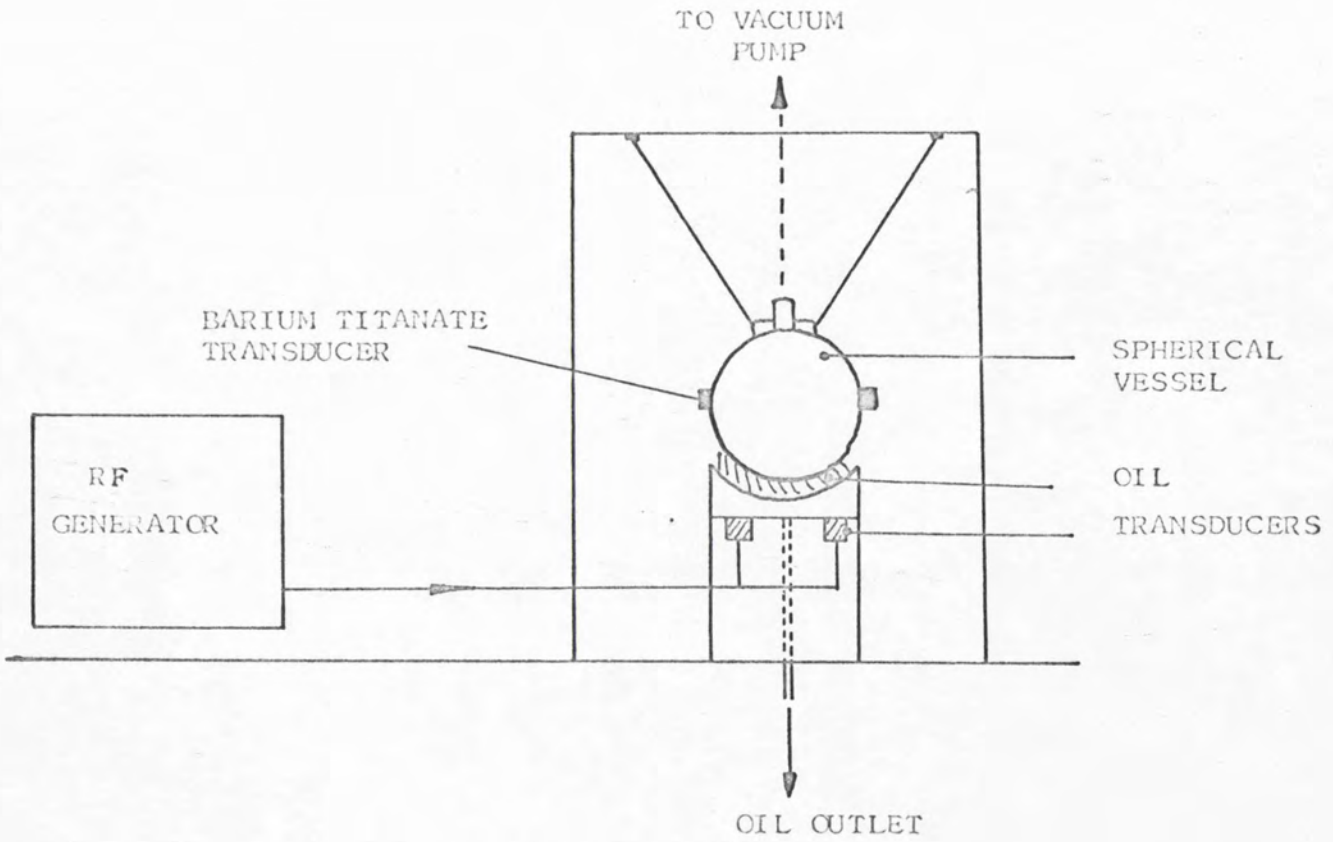

FIGURE 3-3 Ultrasonic Degassing Apparatus

connected to a series of barium titanate transducers attached to the mounting plate. The sound waves passed into the vessel via a layer of oil, which ensured acoustic contact with the transducer mounting.

Degassing produced by the ultrasonic treatment was assisted by reducing the pressure above the liquid to about 1 mm Hg. The sphere, after degassing, was completely filled with liquid, sealed and inserted into the air chamber and allowed to equilibrate for 24 hours. A frequency was selected and the apparatus tuned to maximise the signal amplitude at the receiver. A pulse repetition rate was selected such that the decay was essentially completed before transmission of the next pulse. The various waveforms involved are illustrated in Figure 3-4. The low pass filter was adjusted to minimise the high frequency component of the noise, care being taken not to alter the shape of the decay curve. The C.A.T. recorded and averaged 64 decay curves and the output was recorded using the logarithmic pen recorder. The C.A.T. readout time (p seconds), sweep time (s seconds) and the paper speed (q cm per second) were recorded. The best straight line was drawn through the recorder tracing and the time, measured by the distance on the chart paper (Δx cm) also recorded.

(c) Analysis of the Decay Curves

From equation (3-4)

$$\log_{10} \frac{A_o}{A_t} = \frac{t}{2.303\tau} \quad \ldots\ldots (3\text{-}8)$$

8 kHz band of noise

pulsed band of noise

exponential decay characteristic

FIGURE 3-4 Various waveforms observed during operation of Reverberation Apparatus

The first 25 db fall in level was recorded and thus, following the definition of the Bell,

$$\log_{10} \frac{A_o}{A_t} = \frac{25}{20} \qquad \ldots\ldots (3\text{-}9)$$

Now the time on the chart is $\frac{\Delta x}{q}$ seconds. The fraction of the total sweep time is thus

$$\frac{\Delta x}{q} \cdot \frac{1}{p}$$

This corresponds to a display time t of

$$t = \frac{\Delta x S}{pq} \qquad \ldots\ldots (3\text{-}10)$$

and so from equations (3-10), (3-9) and (3-8)

$$\tau = \frac{\Delta x S}{2.303 \cdot 1.25 \cdot pq} \qquad \ldots\ldots (3\text{-}11)$$

From equation (3-5)

$$\frac{\alpha}{f^2} = \frac{(1/\tau - k)}{c f^2} \qquad \ldots\ldots (3\text{-}12)$$

The apparatus required calibration with a fluid of known absorption ($\frac{\alpha}{f^2}$) in order to determine k. Water was used as a calibrating fluid.[154] It was assumed, therefore, that losses at the water/glass interface were unchanged when the binary liquid mixture under test was added.[156] Consequently measurements were made with a mixture having very different absorption properties from those of the calibration liquid. The system could have been calibrated with a liquid having absorption similar to that of the liquid under examination, if such a liquid were available. This,

however, required the more drastic assumption that losses at the interface remained constant.[152,154,156,159] A number of calibration methods were examined and that finally selected was as follows.

The value of 'k' was determined at each frequency by measuring the time constant of the decay when the sphere contained water. Figure 3-5 shows a typical plot of τ against frequency (kHz). The value of k was dependent upon the size of the transducers. The accuracy of (α/f^2) for a particular mixture was very sensitive to the value of the decay time constant. When τ was less than 1 millisecond the results were rejected, because this was very close to the time constant of the receiver circuit. The accuracy was also critically dependent upon the precision with which the distance on the recorder chart could be measured. If the displacement on the time axis of the recorder chart (Δx) was small, as was observed for highly absorbing liquids and at high frequencies (> 800 kHz), a large error in τ resulted. The estimated accuracy $\pm$ 20% is similar to that obtained by others[152-157] using this technique. In an attempt to solve some of these problems different sizes of transducers were used. Also various methods and periods of degassing were assessed. However, the main problem, calibration, remained. Unfortunately the sparsity and inaccuracy of low frequency acoustic measurements have imposed a serious limit on the testing of theoretical treatments of ultrasonic absorption.

FIGURE 3-5 Typical Calibration Curves for Reverberation Apparatus;
Plot of against frequency for water at 298 K

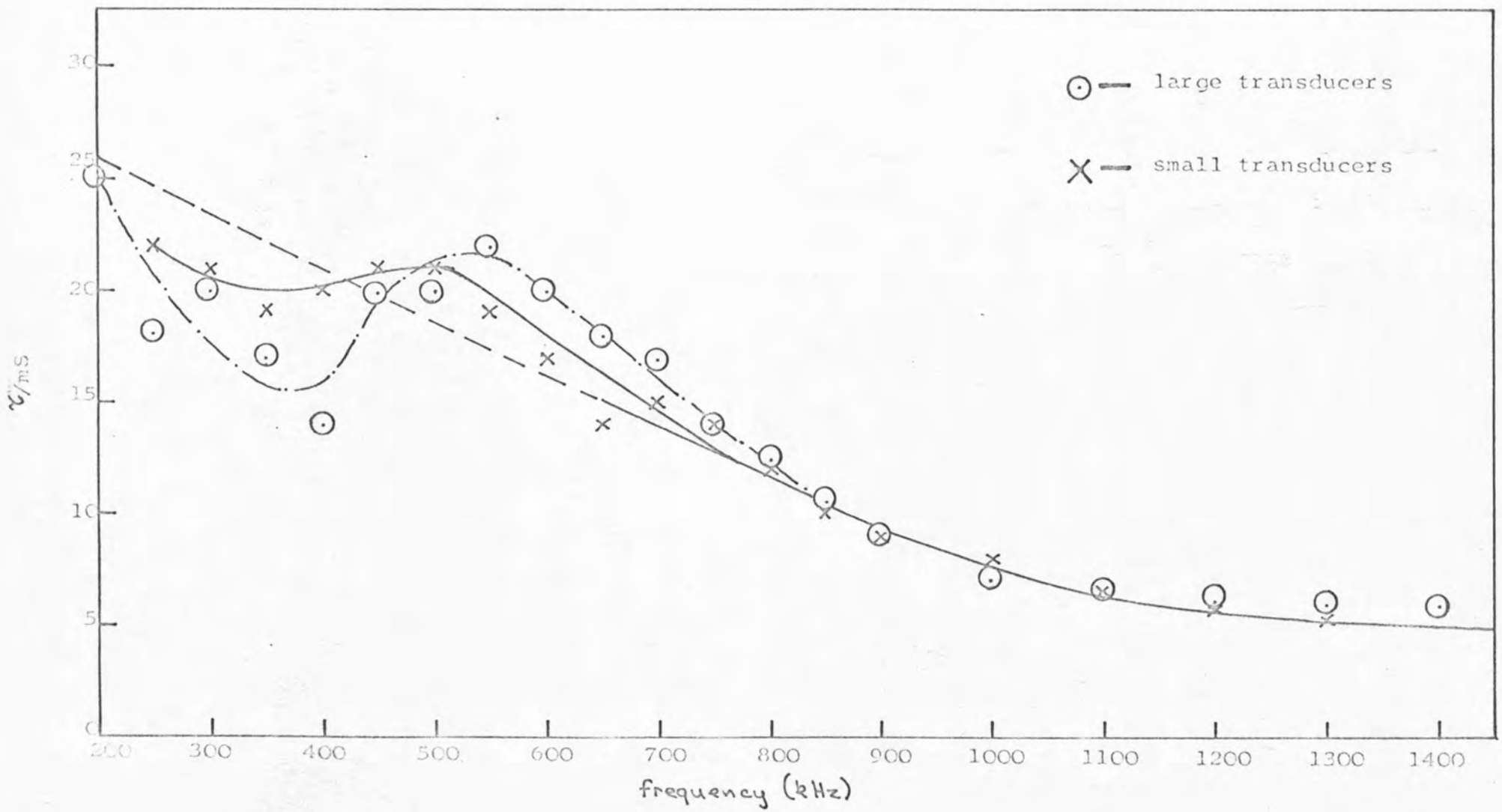

3-3 LOW FREQUENCY PULSE APPARATUS (LFPA)

(i) Description of Apparatus

A block diagram of the apparatus, Figure 3-6, shows the main features. The sample fluid (1000 cm^3), was contained in a vertical steel cylindrical vessel having double walls. Thermostatting fluid, from a variable temperature thermostat bath, was circulated between the outside walls of the cylinder. The cylinder was insulated by expanded polystyrene blocks. The upper end of the cylinder was fitted with a movable piston to which was attached the receiving piezoelectric transducer crystal. The lower end of the cylinder was sealed by the transmitting transducer. Delay rods of silica were attached to the two crystals and the ultrasonic waves entered the solution after passing along these. The delay rods served to increase the total path length traversed by the signal between the transmitting crystal and the receiving crystal. This ensured that the detector could distinguish the signal which passed through the liquid from that radiated directly from the transmitter. The receiving crystal was moved using a system of gears and magnetic clutches linked to a motor. The separation of the two crystals was measured using an electromechanical counter. A brass disc was rotated by the leadscrew which raised and lowered the receiving transducer. The disc was mounted between a light source and a phototransistor detector. Holes in the perimeter of the disc

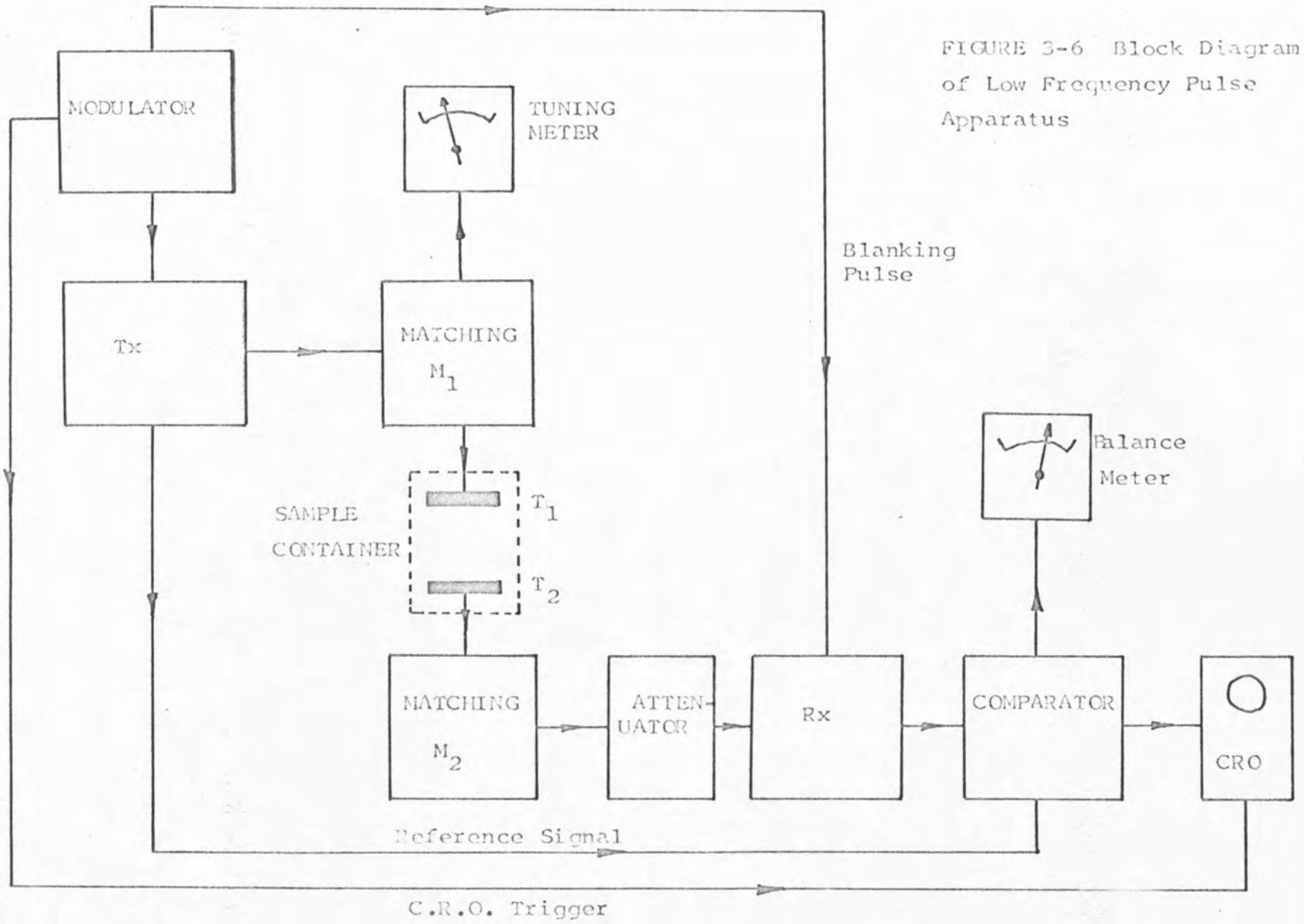

FIGURE 3-6 Block Diagram of Low Frequency Pulse Apparatus

permitted light to fall periodically on the photo-transistor, producing electrical pulses. These drove the counter which, after calibration, measured the displacement of the piston.

The transmitter output was modulated to produce r.f. pulses which were fed to the transmitting transducer T_1 via a matching network M_1. This network, consisting of a tuned circuit of which the transducer formed part, matched the transducer impedence with that of the transmitter. The potential across this tuned circuit was measured by a meter which was used for making tuning adjustments.

Measurements were made at all the odd harmonics of 1 MHz, the fundamental frequency and the crystal (1, 3, 5, 7, 9, ----29 MHz).

The receiving crystal T_2 converted the sound wave to an r.f. signal which passed through a second matching network M_2 (similar to the first). The signal then passed through an attenuator into the tuneable receiver Rx. A blanking pulse from the modulator reduced the level of any transmitter breakthrough. The received and amplified signal passed, together with a reference signal from the transmitter, into a comparator unit. A balance meter controlled by this unit indicated the difference (or error) between the reference signal and the received signal. In the balance position, the received signal level and the reference level were identical. The received

signal was also supplied to an oscilloscope, the time base of which was triggered by a signal from the modulator. This provided the tuning signal for the apparatus. The alignment of the two crystals such that they were both parallel was quite critical.

(ii) Operation

With the cell filled with liquid sample, a frequency was selected. The transmitter H.T. supply was switched on and set to about 500 v. The correct matching circuit was selected and tuned with fine tuning control. The H.T. voltage was adjusted for maximum reading on the tuning meter scale. The receiver tuning and receiving crystal matching were adjusted to maximise the signal intensity displayed on the oscilloscope. The tuning was then repeated to remaximise the signal displayed on the oscilloscope.

The crystals were driven together until a suitably large signal intensity was obtained using a fairly low attenuator setting. The attenuation was increased to zero the comparator 'balance' meter (a centre zero milliameter). Some attenuation (usually about 10 to 20 db) was removed and the transducers driven apart until a balance position was regained. The change in path length (p cm) registered on the electromechanical counter and the change in attenuation (Δa db) were recorded. The value of the absorption was obtained from equation (3-13).

$$\frac{\alpha}{f^2} = \frac{\Delta_a}{p} \cdot \frac{0.1115}{f^2} \quad \ldots\ldots (3\text{-}13)$$

The coefficient 0.1115 includes a factor for conversion of attenuation in db to nepers and a correction factor of 3% for the error in the pitch of the leadscrew thread.

It was possible to measure the change in path length to $\pm$ 0.1 mm and the change in attenuation to $\pm$ 0.1 db. At low frequencies (particularly 1 and 3 MHz) a diffraction correction had to be made.

3-4 HIGH FREQUENCY PULSE APPARATUS (HFPA)

(i) Description of Apparatus

A block diagram of the apparatus is shown in Figure 3-7. A X-cut quartz piezoelectric transducer was excited in the thickness expander mode by radio frequency pulses generated by an oscillator of known frequency. The ultrasonic pulses passed through the liquid contained in a thermostatted cell and were detected by a second quartz crystal. Discrimination could be made at the receiver between signals travelling through the liquid and signals radiated directly from the oscillator by virtue of the time delay of the ultrasonic waves in the silica delay rods. A variable attenuator was interposed between the transmitter and transducer. The total attenuation was held constant by servo-mechanical adjustment of the attenuation as the path length of solution was varied. A

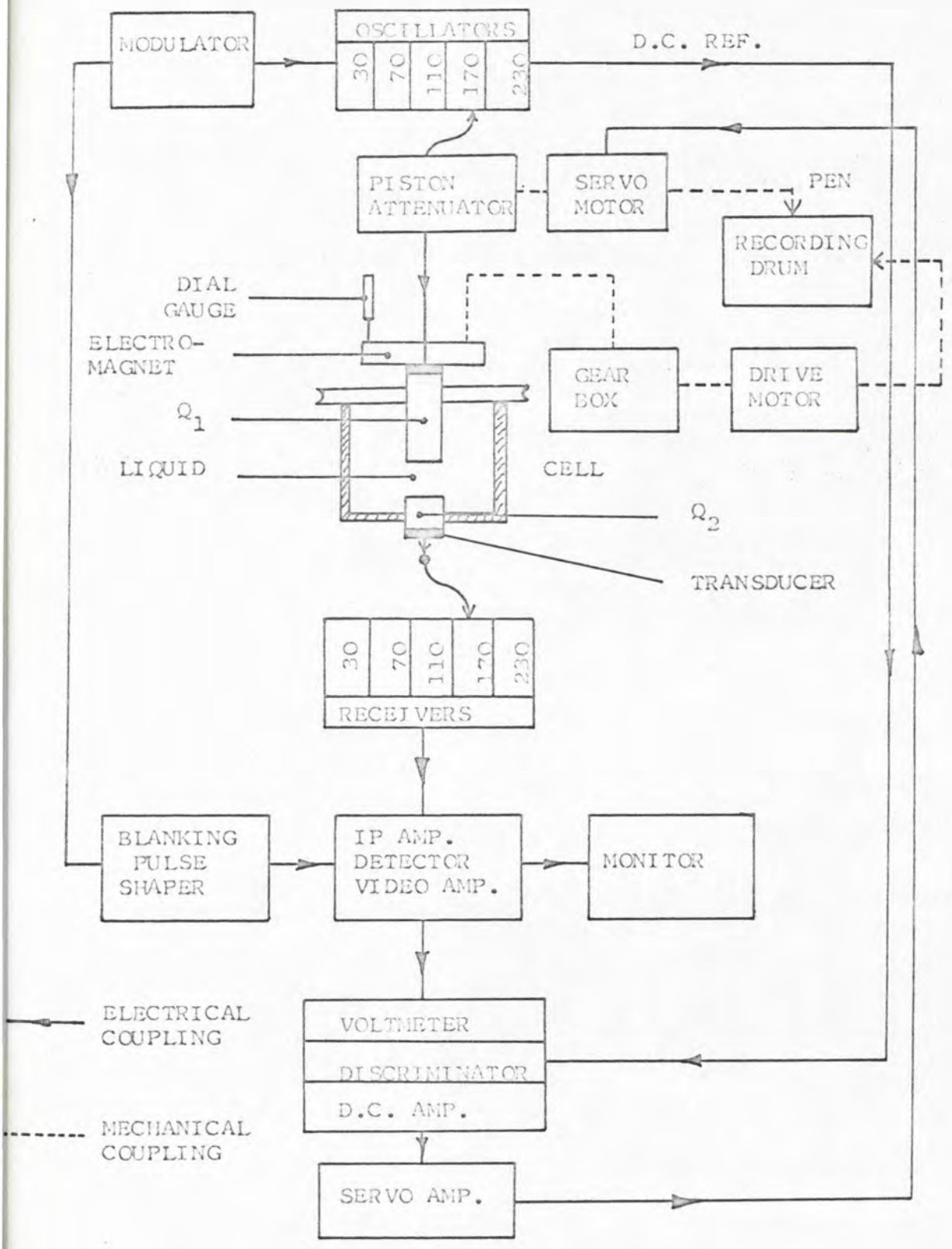

FIGURE 3-7 Block Diagram of High Frequency Pulse Apparatus

comparator compared a reference signal from the transmitter with the signal from the solution. Measurements were made at five frequencies 30, 70, 110, 170 and 230 MHz. The path lengths of liquid were in the range 0.1 to 4 cm; 10 cm^3 of sample was required.

(ii) Operation

The operation of the HFPA has been described in detail elsewhere.[7,148,149] The sample was contained in a cylindrical cell with hollow walls containing thermostatting liquid supplied from a thermostat tank. Delay rods, mounted vertically in the solution, were linked to a servo drive system. The upper rod, supported by an electromagnet, was movable and the lower rod fixed. A thermistor measured the liquid temperature and operated as a stirrer for the solution in the cell. The top of the cell was covered to prevent losses by evaporation. The maximum and minimum pathlengths were determined manually. The minimum position was located by lowering the upper rod until the peaks of the first pulse, and the first reflected pulse started beating. The maximum position was located by driving the upper rod out until either the maximum possible path length available was reached, or the signal level approximated to the noise level. Suitable gears were selected and a trace recorded on a rotating drum. The trace was linear. The absorption coefficient α was given by

$$\alpha = \Delta_{g.R} \qquad \ldots\ldots (3\text{-}14)$$

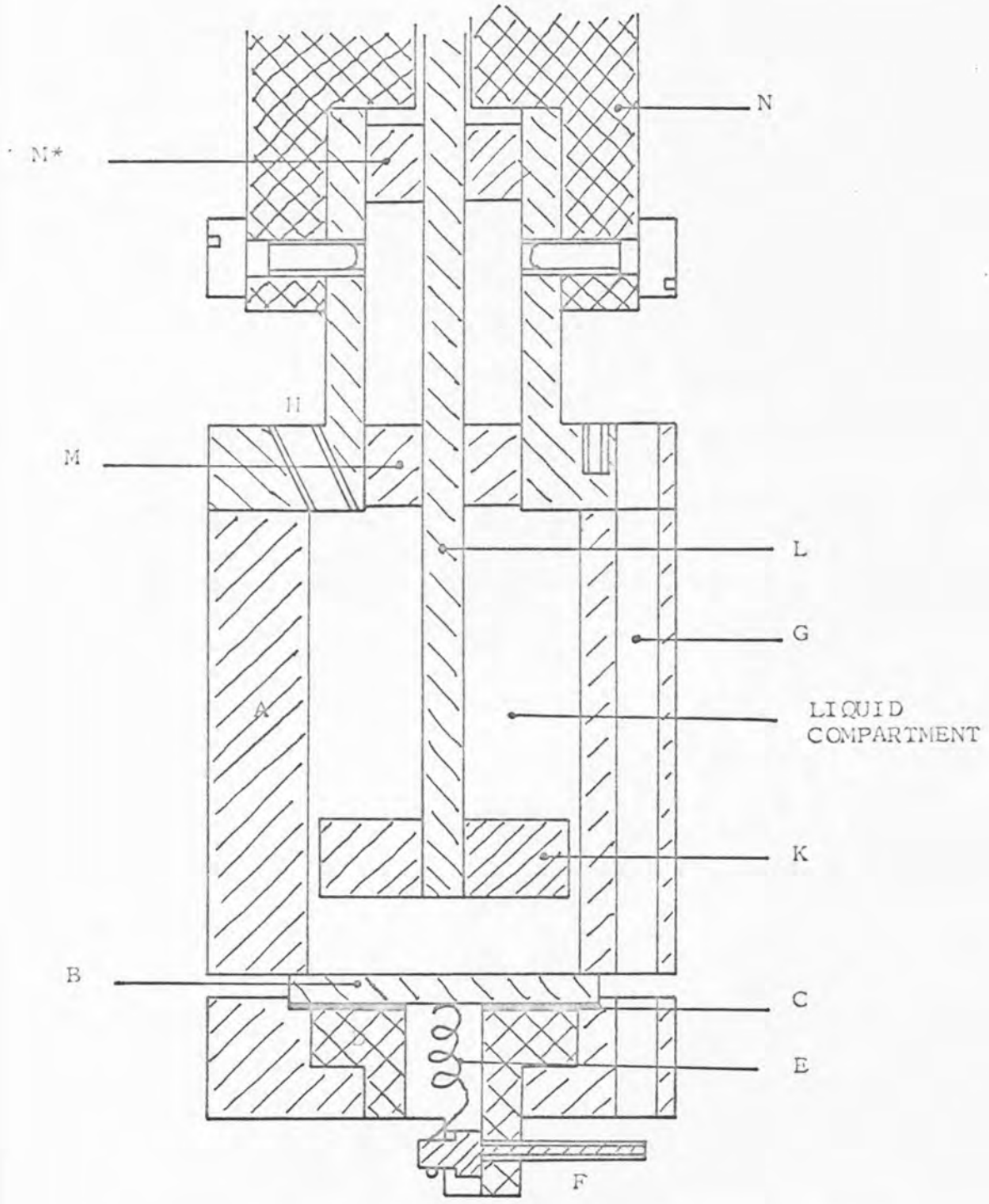

FIGURE 3-9 The Ultrasonic Interferometer Cell

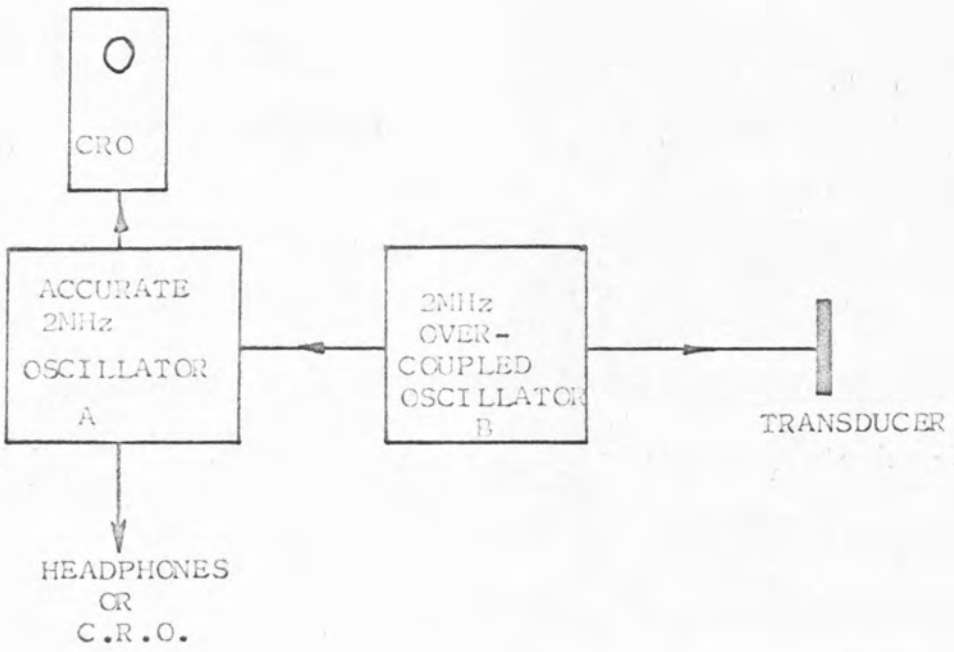

FIGURE 3-8 Block Diagram of Sound Velocity Apparatus

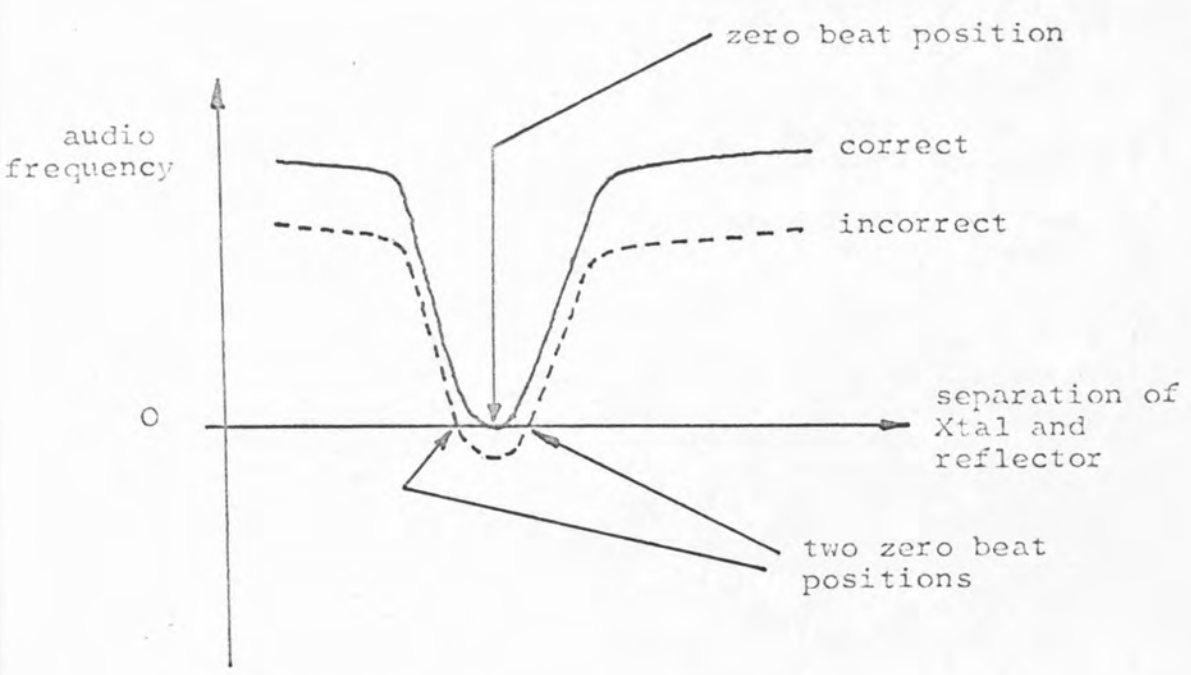

FIGURE 3-10 Illustration of Correct Zero Beat Position

where Δg and R are the slope of the trace and the gear ratio respectively.

The experimental accuracy was approximately 2%. Measurements were made at 263, 273, 283 and 298 K and temperature controlled to better than $\pm$ 0.25 K.

3-5 ULTRASONIC VELOCITY MEASUREMENTS

(i) Methods of Sound Velocity Measurement

Instruments for ultrasound velocity measurements[160,161] are usually termed 'interferometers'. The theory of the acoustic interferometer has been developed by Hubbard,[161-164] Mason[165] and Borgnis.[166] Fletcher and Parbrook[167] have shown how interferometric measurements can be used to measure absorption of sound also.

In general the technique consists of setting up 'standing' ultrasonic waves in the liquid sample and measuring the distance electronically, $\lambda/2$, where λ is the wavelength, between successive nodes or antinodes.

Then, $$c = f\lambda \qquad \ldots\ldots (3\text{-}15)$$

(ii) Description and Operation of Ultrasonic Interferometer

The instrument, Figure 3-8, was designed by J.H. Andreae[168] and P.D. Edmonds in 1961. A similar apparatus has been described by Bergman[160] (1938).

The cell, shown in Figure 3-9, comprised a stainless

steel tube A. The lower end of this tube was closed by a 2 MHz, 1 inch diameter X-cut quartz crystal, B. The flat edge of the tube made good electrical contact with the transducer. The clamping ring C was insulated from the lower surface of the crystal by a thin polythene disc, C. A Bakelite insulator D insulated spring E from C and supported the contact terminal F. A coaxial conductor passed down the hole G and the centre core was soldered to F. The outer sheath made contact with the stainless steel cell body A. The cell was filled through H and a thermocouple dipping into the liquid through this entrance recorded the temperature of the liquid. A non-rotatable stainless steel reflector K attached to a rod L was parallel to the transducer, closing the lower end of the tube. The rod L was guided by two bushes M, M*. The whole assembly was insulated from the measuring platform above by a Bakelite tube N. On the upper measuring platform a large nut geared to a fine screw moved the reflector K vertically but did not rotate it. A dial gauge measured the displacement of the reflector K. The cell was surrounded by a close fitting brass container suspended from a light Bakelite tube and immersed in a thermostat tank. Temperatures could be controlled to $\pm$ 0.1 K at all temperatures at which measurements were made.

The crystal was driven at 2 MHz by a conventional push-pull oscillator (see Figure 3-8) having an over-coupled output coupling coil. Over-coupling ensured that

small variations in crystal impedence altered the oscillator frequency. The change in frequency was followed by monitoring the audio beat frequency between this oscillator and a standard 2 MHz oscillator(BC221 frequency meter). The audio frequency was monitored using either headphones or an oscilloscope. The liquid was placed in the cell and allowed some thirty minutes to come to thermal equilibrium at the required temperature. The oscillator B (Figure 3-8) was adjusted to give zero beat frequency at some position of the reflector corresponding to a node in the standing wave form. This was achieved by adjusting alternately the position of the reflector, and the tuning of oscillator B to obtain a single beat position. If this was not carried out correctly a pair of close zero beat positions were observed (see Figure 3-10). The reflector was moved in close to the crystal and the positions of 20 successive zero beat positions were recorded on the dial gauge. This was repeated starting at some distance from the crystal and moving towards it. In all, three sets of measurements were recorded and the results averaged.

The mean distance between successive standing wave positions, $\lambda/2$, was calculated and the velocity of sound calculated using equation (3-15).

3-6 MATERIALS AND PREPARATION OF SOLUTIONS

(i) Materials

All materials used were purchased from British Drug

Houses or Koch-Light and were of 'AnalaR' or 'puriss' grades. These were used without further purification. Deionised water was used.

(ii) Preparation of Solutions

An appropriate volume of solution of the required mole fraction was prepared by mixing previously calculated volumes of the components. Solution densities were obtained from the literature.

CHAPTER FOUR

ULTRASONIC ABSORPTION MEASUREMENTS

(RESULTS)

4-1 INTRODUCTION

The ultrasonic absorption properties of mixtures of methyl cyanide and water at 273, 298 and 308 K and 70 MHz have been reported by Blandamer et. al.[35] Measurements have been made by Foster[148] over the frequency range 200 kHz to 230 MHz at several mixture compositions. In general an absorption in excess of that of the pure components was observed. The frequency range 200 to 1500 kHz was covered using the original reverberation apparatus described in section 3-2. These measurements were much less accurate than those made within the range 1.5 to 230 MHz for the reasons given previously.

The results, excluding those obtained over the range 200 to 1000 kHz, were analysed in terms of one, two and three relaxations (see Chapters 2 and 5). It was found that at low methyl cyanide concentrations and high temperatures a single relaxation fitted the data. At high concentrations of methyl cyanide and low temperatures two, and sometimes three, relaxations were required.

Ultrasonic velocity measurements for the system methyl cyanide + water have not been reported.[148] The system acetone + water has long been known to show a peak in the plot of sound velocity against mixture composition at about 0.08 mole fraction acetone (at 300 K).[22,30,169] Further, the composition at which (α/f^2) is a maximum is $x_2 = 0.4$ for both the methyl cyanide + water and acetone

+ water systems. Foster[148] suggested that, on the basis of the similarity between acetone + water and methyl cyanide + water, it might be expected that methyl cyanide + water mixtures should show a peak sound velocity at a similar composition. The suggested similarity between these two systems is substantiated by a comparison of the composition dependence of the excess functions of mixing G^E, H^E, and V^E.[170,171,172] The excess Gibbs function of mixing,[170] G^E, is positive and almost symmetrical for both systems. The excess volumes of mixing[35] V^E, are negative and show minima at about 0.4 mole fraction of solute for both systems. The excess enthalpies of mixing[172] are not identical. For acetone + water mixtures the excess enthalpy of mixing H^E crosses the axis at x_2 = 0.55 mole fraction of acetone, and in the region of the peak sound absorption is negative. Methyl cyanide + water mixtures,[110] conversely, show a similar sign inversion at x_2 = 0.1 mole fraction of methyl cyanide, and H^E is strongly positive at the peak sound absorption concentration (PSAC). The H^E behaviour of acetone + water mixtures is very similar to that for t butyl alcohol + water system.[7,148] The relative partial molar volume $\bar{V}_2-V_2^\circ$ for methyl cyanide does not, when plotted as a function of mole fraction of methyl cyanide, display a pronounced minimum, in contrast to similar plots for the alcohol + water mixtures.[148] This was also found to be the case for acetone + water mixtures. However the data available were less reliable than that used for the methyl cyanide

+ water system. Mixtures of methyl cyanide + water have an upper critical solution temperature at 272.1 ± 0.2 K at 0.38 ± 0.02 mole fraction of methyl cyanide.[35] Whereas methyl cyanide + water displays UCST behaviour, alcohol + water mixtures have a tendency toward LCST behaviour. A UCST is characteristic of a system where the mixing is thought to be enthalpy controlled, whereas with a LCST the mixing is entropy controlled.[51] Acetone + water mixtures do not have a UCST. However, Frank and Quist[173] have demonstrated the formation of a clathrate hydrate between acetone and water. No such hydrate has been reported for the system methyl cyanide + water.

In an attempt to investigate the similarity between the systems methyl cyanide + water and acetone + water, ultrasonic absorption measurements have been made which extend those reported previously.[22,30,148,169] The results have been analysed in terms of the simple models involving solute + water equilibria originally proposed by Andreae.[24] In a later chapter (Chapter 6) the data are analysed using two current theoretical treatments, detailed in Chapter 5.

4-2 METHYL CYANIDE + WATER

(i) Sound Velocity Measurements

Sound velocities were measured for the system methyl cyanide + water over a wide range of mixture compositions and at 273, 298 and 308 K. The apparatus and thermostating

system was described in Chapter 3-5. For each composition of methyl cyanide + water three measurements were made and averaged. The estimated accuracy was better than $^1/_2$ per cent. The results are tabulated in Appendix 4-1. The ultrasonic velocities for the methyl cyanide + water system are plotted as a function of mixture composition (x_2) in Figure 4-1. At each temperature a maximum was observed in the dependence of the sound velocity upon mole fraction of methyl cyanide in the highly aqueous region. The effect is most dramatic at low temperatures, but the position of the peak is, within experimental error, independent of temperature.

The maximum in the sound velocity occurs at a composition which corresponds closely with the end of the 'plateau region', i.e. at $x_2 = 0.08 \pm 0.02$ mole fraction of methyl cyanide.

(ii) Ultrasonic Absorption Measurements

The ultrasonic absorption of solutions of methyl cyanide in water were measured over the frequency range 200 to 1500 kHz at 298 $\pm$ 0.1 K at compositions corresponding to 0.1, 0.3, 0.4 and 0.5 mole fraction of methyl cyanide.[34] These measurements were made using the modified reverberation apparatus described in Chapter 3. The apparatus was calibrated using pure degassed water, assuming the ultrasonic absorption to be 21×10^{-17} nepers s^2 cm^{-1}. The measured values of the decay time constant defined in Chapter 3 are plotted against frequency in

FIGURE 4-1 Ultrasonic Velocities for Methyl Cyanide + water mixtures over the range 0.0 to 1.0 mole fraction.

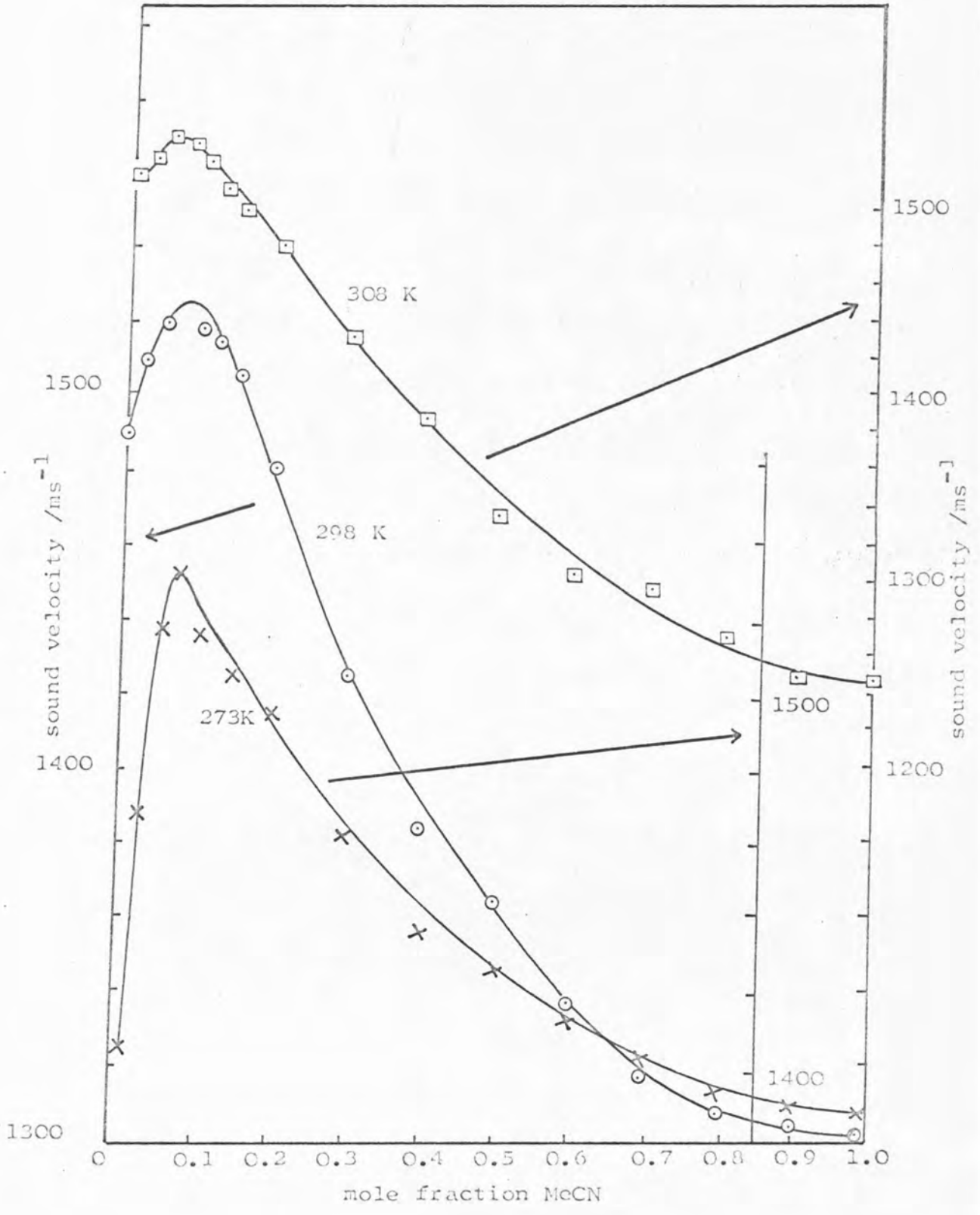

Figure 4-2 for three mixture compositions. With increase in the ultrasonic absorption the observed decay time constant decreased quite markedly and it became impossible, in many instances, to measure these accurately. Values of close to one millisecond were rejected since this value was too close to the time constant of the receiver circuit. A considerable scatter was noticed (Figure 4-2) but the trend was for the absorption to increase on going from 0.1 to 0.4 mole fraction of methyl cyanide. The probable error which could be assigned to the data was about $\pm$ 20 per cent. Despite the large error in the calculated values of the ultrasonic absorption, plotted as a function of frequency, as shown for 0.1 and 0.5 mole fraction methyl cyanide in Figure 4-3, the general trend was distinguishable. Thus the low frequency results show that the absorption continues to increase with decrease in frequency over the range 200-1500 kHz, for a mixture containing 0.5 mole fraction of methyl cyanide, but remains approximately constant for 0.1 mole fraction of methyl cyanide. These results would seem, in general, to be marginally better than those obtained by Foster.[148] The results are tabulated in Appendix 4-2.

4-3 ACETONE + WATER

(i) Composition Dependence of (α/f^2)

Ultrasonic absorption measurements were made on mixtures of acetone and water over a wide range of mixture

FIGURE 4-2 Expontential decay time constants for methyl cyanide + water mixtures at three compositions and 298 K and frequencies over the range 200 to 1500 kHz

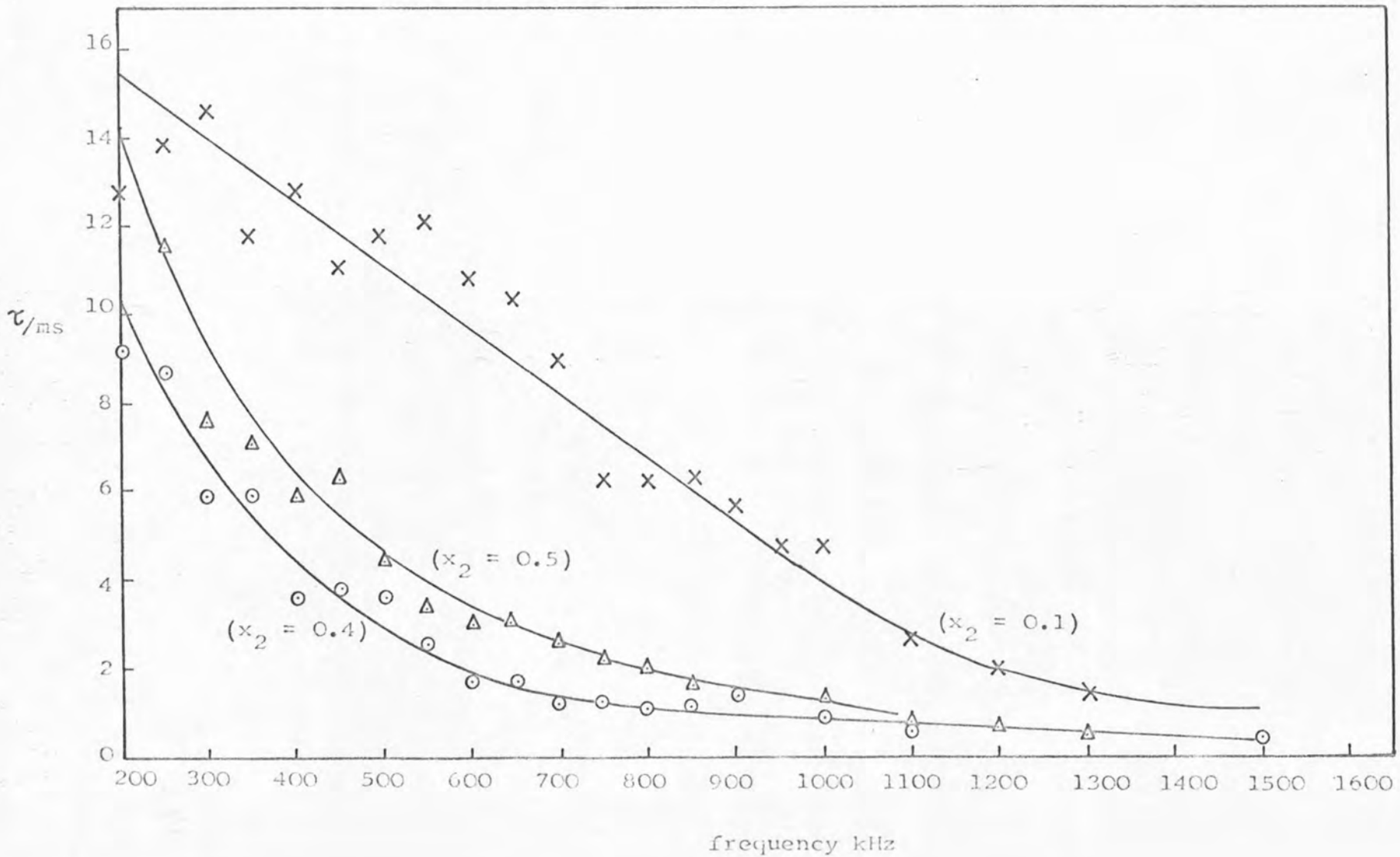

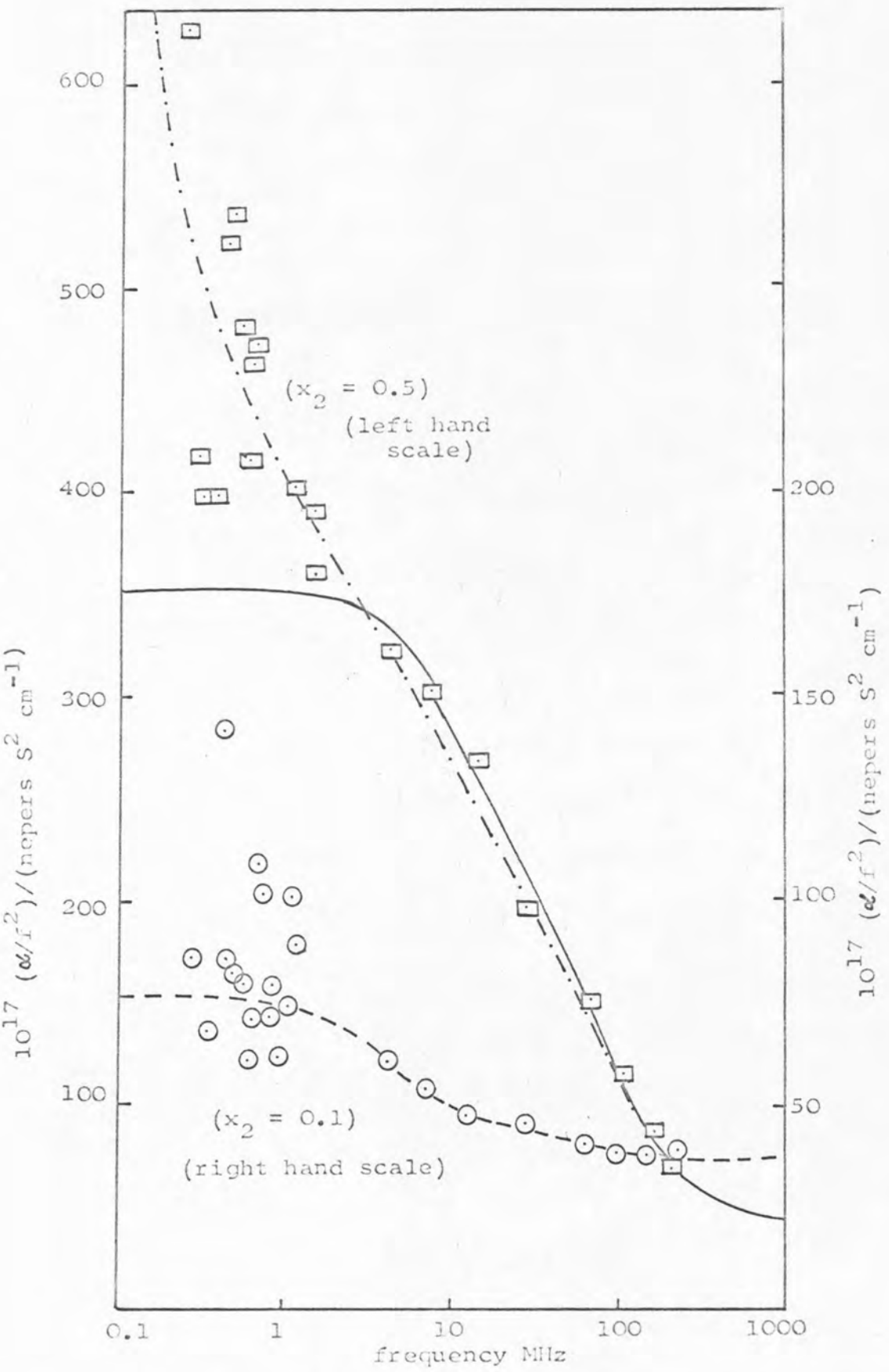

FIGURE 4-3 Ultrasonic absorption over range 200 kHz to 230 MHz for MeCN + H_2O at 298 K (——) and (-----) are two relaxation analysis curves.

composition and at 263, 273, 283 and 298 K and 70 MHz. The data are summarised in Figure 4-4 and are tabulated in Appendix 4-3. The data are in excellent agreement with the early measurements of Willard,[169] Willis[30] and Burton.[32] The peak sound absorption composition (PSAC) was located at 0.38 $\pm$ 0.02 mole fraction of acetone at 298 K. Measurements made at 263 K showed a PSAC at 0.3 $\pm$ 0.02 mole fraction of acetone. However between 273 and 298 K the PSAC is constant to $\pm$ 0.03 mole fraction of acetone.

The absorption in the low mole fraction of acetone region displays an initial insensitivity to added acetone up to about 0.07 $\pm$ 0.02 mole fraction of acetone. The absorption thereafter increases rapidly. This is clearly shown in Figure 4-5. At high mole fractions of acetone, $x_2 > 0.4$, the ultrasonic absorption steadily falls to the value for pure acetone.

(ii) Ultrasonic Absorption Measurements over the range 3 to 230 MHz.

Measurements of the ultrasonic absorption as a function of frequency were made at 273, 283 and 298 K at several compositions in the water and acetone rich mixtures. The results are tabulated in Appendix 4-3 and are summarised for 0.1 and 0.3 mole fractions of acetone in Figures 4-6, 4-7 and 4-8, at 273, 283 and 298 K respectively.

(iii) Ultrasonic Absorption Measurements over the range 200 to 1500 kHz.

FIGURE 4-4 Ultrasonic Absorption over the temperature range 263 to 298 K of mixtures of acetone and water.

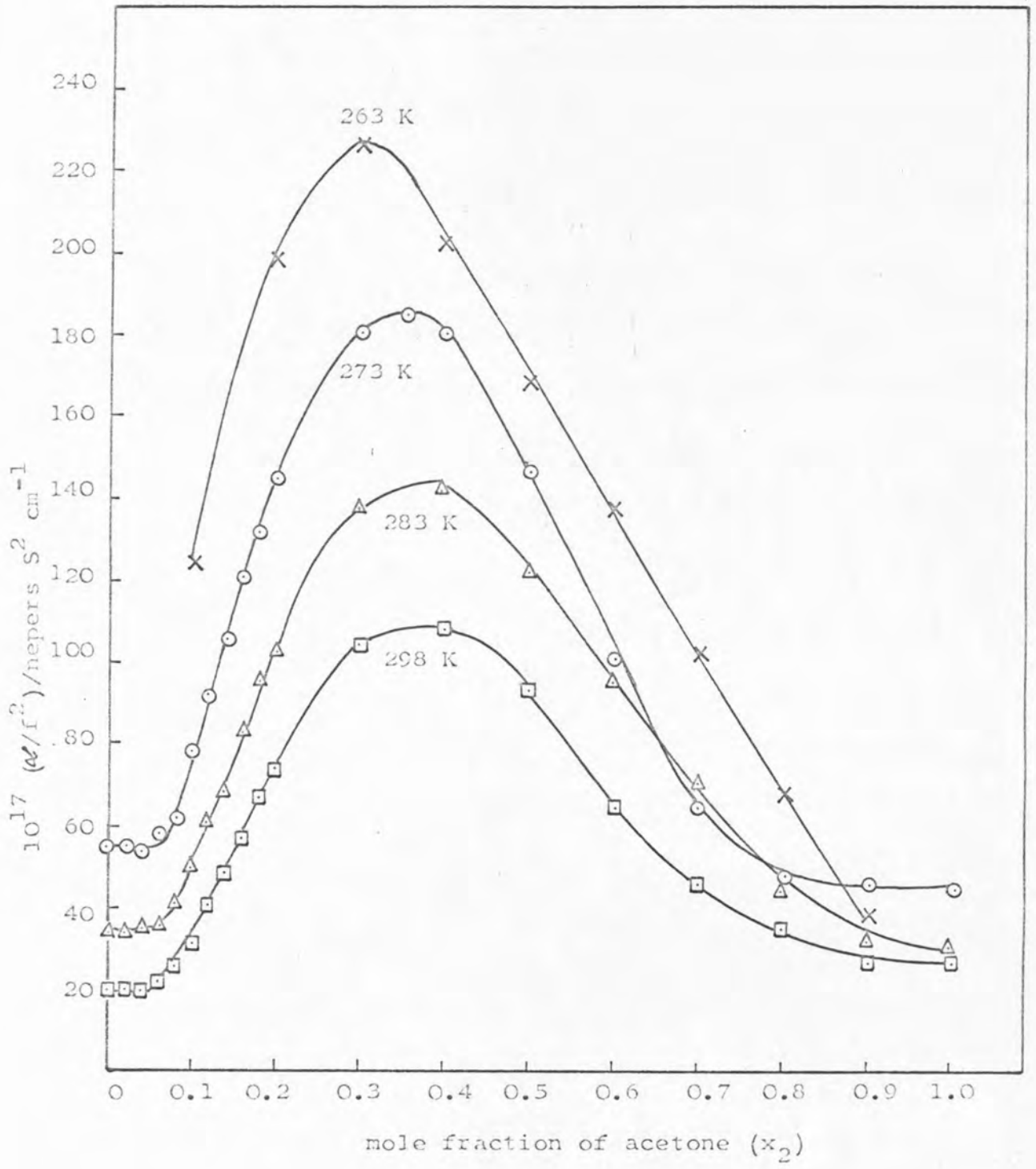

FIGURE 4-5 Ultrasonic Absorption at 273, 283 and 298 K for acetone + water mixtures over the composition range 0.00 to 0.18 mole fraction of acetone.

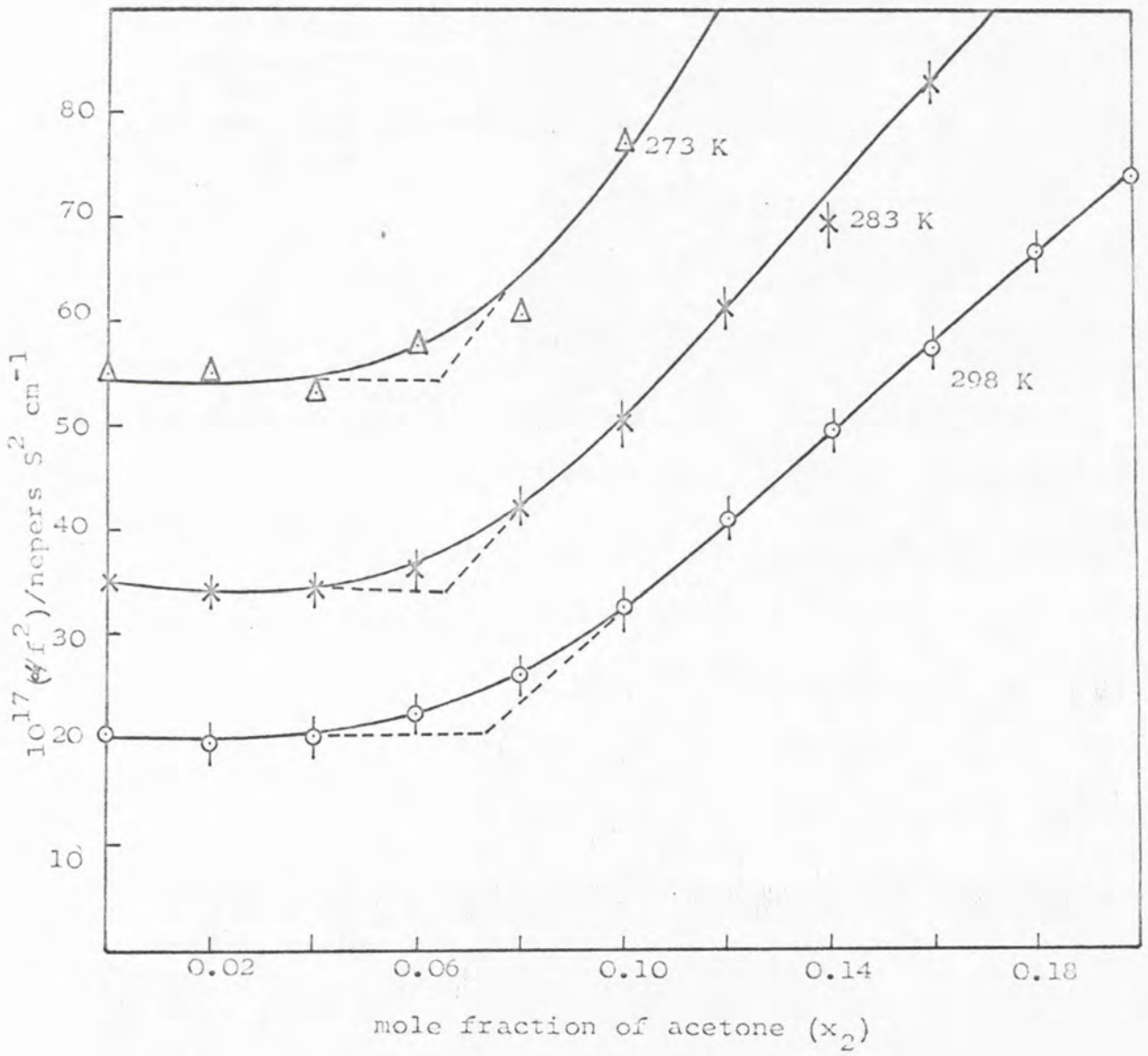

FIGURE 4-6 Ultrasonic Absorption over the frequency range 5 to 230 MHz for acetone + water mixtures at 273 K and 0.1 and 0.3 mole fraction of acetone.

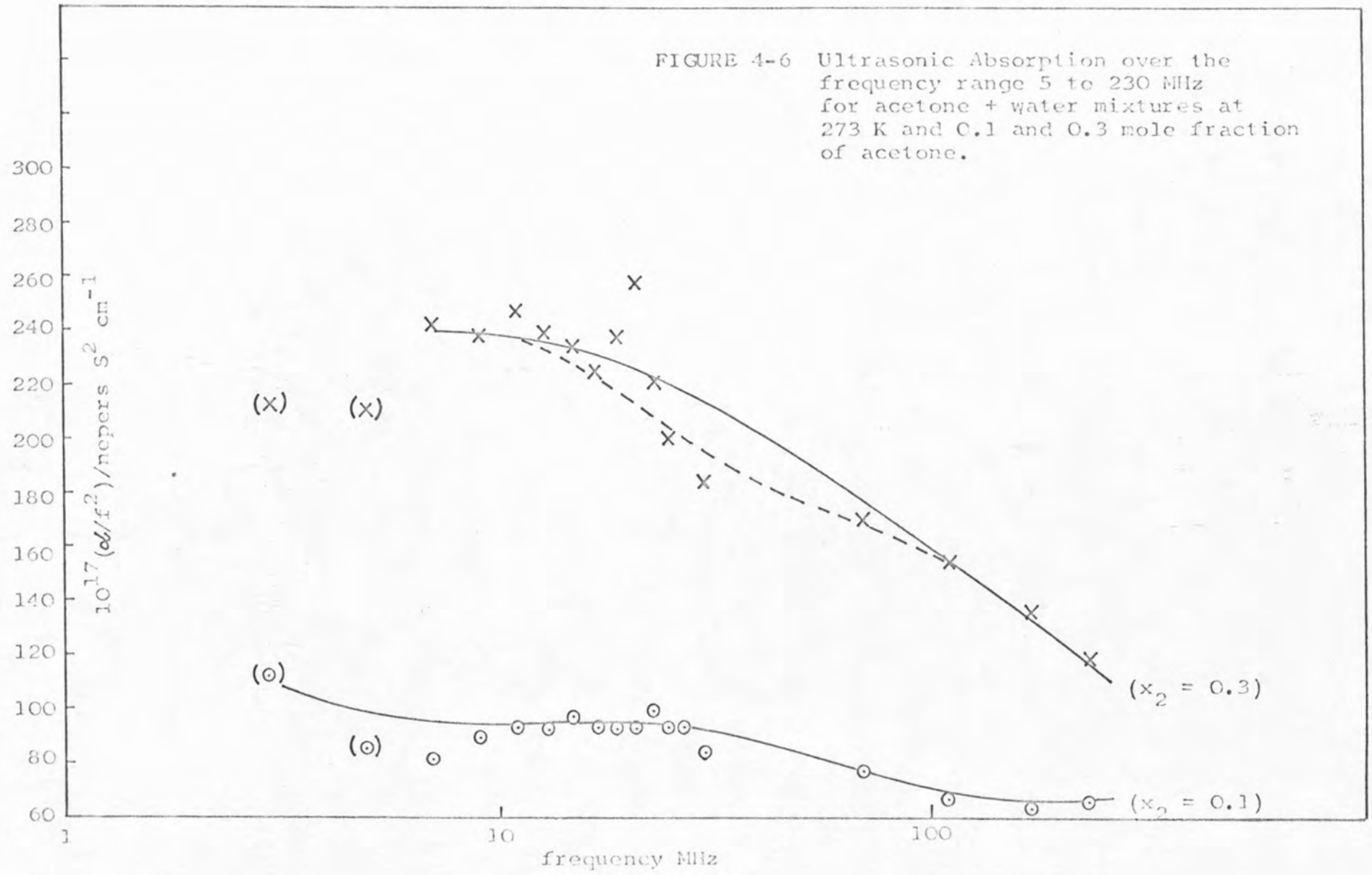

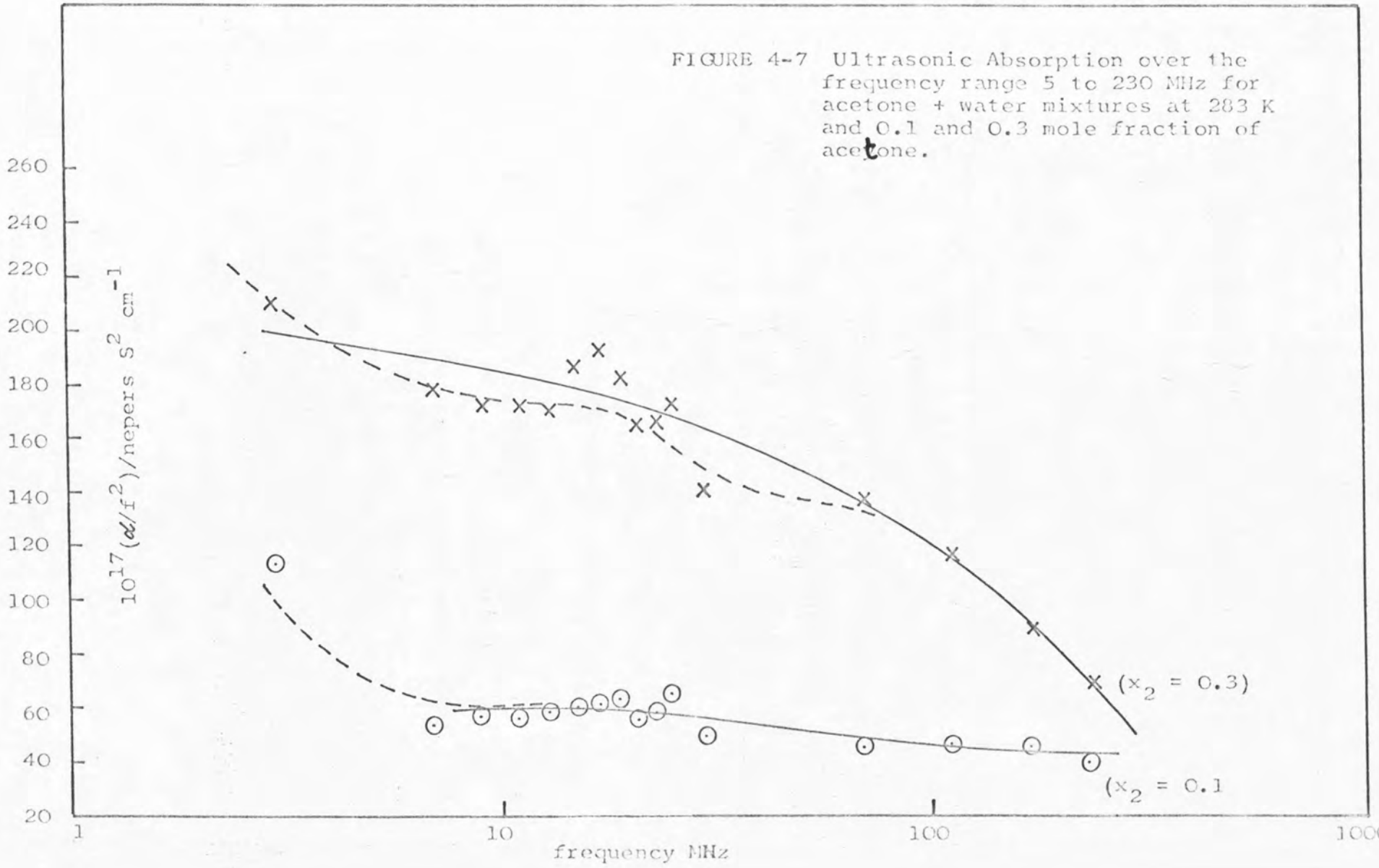

FIGURE 4-7 Ultrasonic Absorption over the frequency range 5 to 230 MHz for acetone + water mixtures at 283 K and 0.1 and 0.3 mole fraction of acetone.

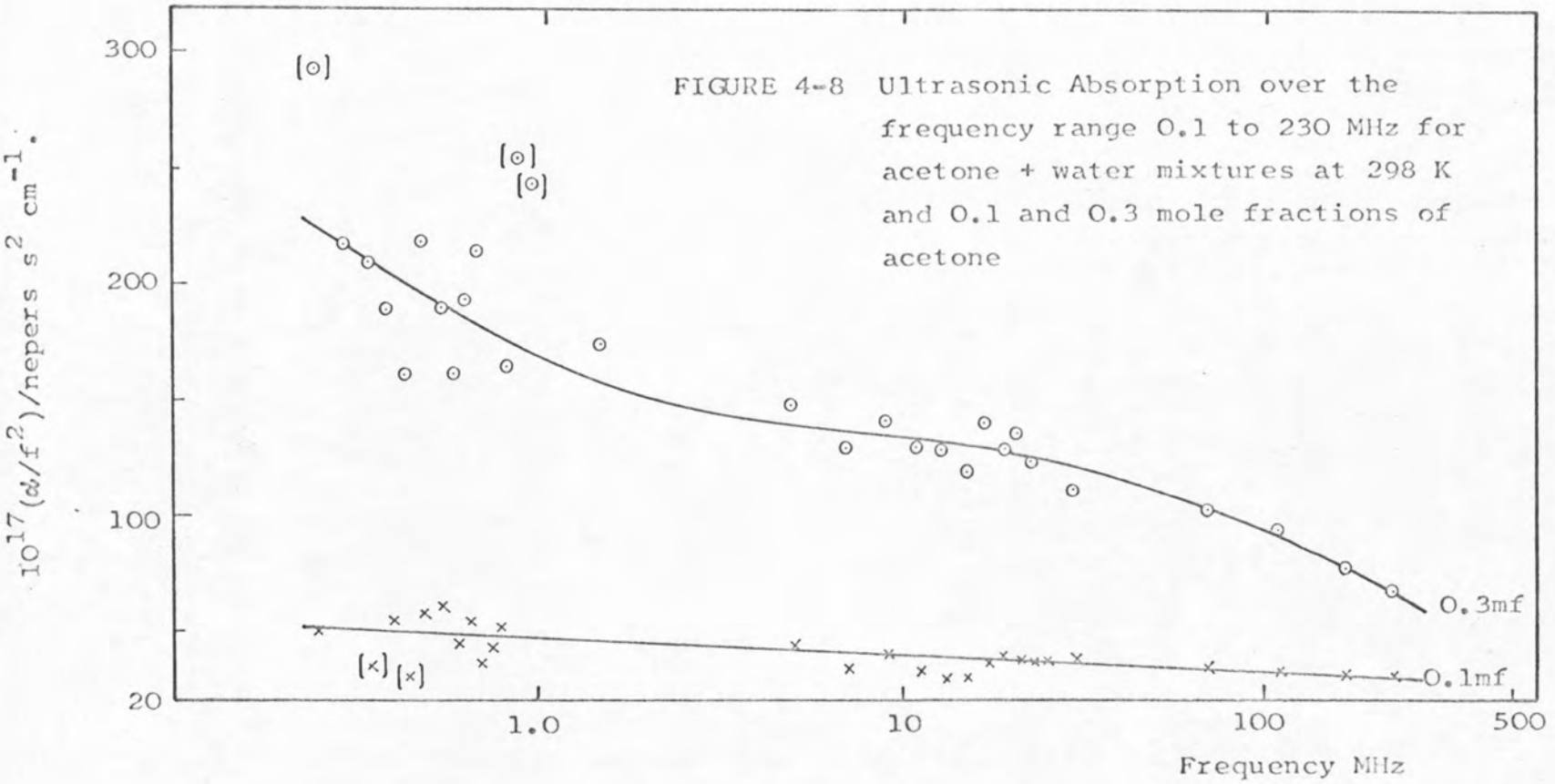

FIGURE 4-8 Ultrasonic Absorption over the frequency range 0.1 to 230 MHz for acetone + water mixtures at 298 K and 0.1 and 0.3 mole fractions of acetone

Figure 4-8 summarises the results obtained from ultrasonic absorption measurements in the frequency range 200 to 1500 kHz at 298 K, and compositions of 0.1 and 0.3 mole fraction of acetone. These data were obtained using a similar technique to that described in Chapter 3-2 and also in the previous section. The transducer size was, however, reduced on the assumption that the inflection in the plot of τ against frequency for calibration with degassed water at about 400-500 kHz (Chapter 3, Figure 3-5) was due to some form of transducer resonance. This seemed to reduce the scatter of the calibration points, but the inflection was not completely removed.

The observed inflection in τ is probably a function of the shape of the containing vessel. Possibly it is some form of sphere resonance. Certainly anomalous dependence of τ upon frequency contributes to the large experimental error in the measurements. The apparatus is still in its early stages of development, but these results show that spheres are not the ideal shape of containing vessel.

The data obtained does, however, show that the system acetone + water may be described in terms of two relaxation frequencies, one at about 200 kHz and one at about 100 MHz. The present data are not sufficiently accurate to render such an analysis possible. It would appear that an even greater range of frequencies is necessary to pinpoint the second relaxation at low frequencies. The analysis of the results in terms of one relaxation frequency,

excluding the data at frequencies below 3 MHz, is discussed in Chapter 6. The results are tabulated in Appendix 4-4.

(iv) Composition dependence of (α/f^2) for Acetonyl Acetone + Water Mixtures

Prompted by the early investigations of Andreae et. al.[24] and the need for a comparison between a simple ketone and a diketone the ultrasonic absorption of a wide range of compositions of acetonyl acetone + water were measured at 273, 283 and 298 K. The resulting data is summarised in Figure 4-9 and is tabulated in Appendix 4-5.

The general outline of the plot resembles that for acetone + water. The absorption at the PSAC is remarkably similar to that for acetone + water at each temperature. The striking feature, however, is that the PSAC occurs at $x_2 = 0.25 \pm 0.02$ at 298 K and is slightly temperature dependent. This is in accord with the preliminary results reported by Andreae et. al.[13] Further, there seems to be no indication of a 'plateau' region.

Andreae identified a single relaxation frequency of 84 MHz.

4-4 DISCUSSION

The ultrasonic absorption properties of the systems acetone + water and methyl cyanide + water may be considered

FIGURE 4-9 Dependence of Ultrasonic Absorption upon composition for mixtures of acetonylacetone + water

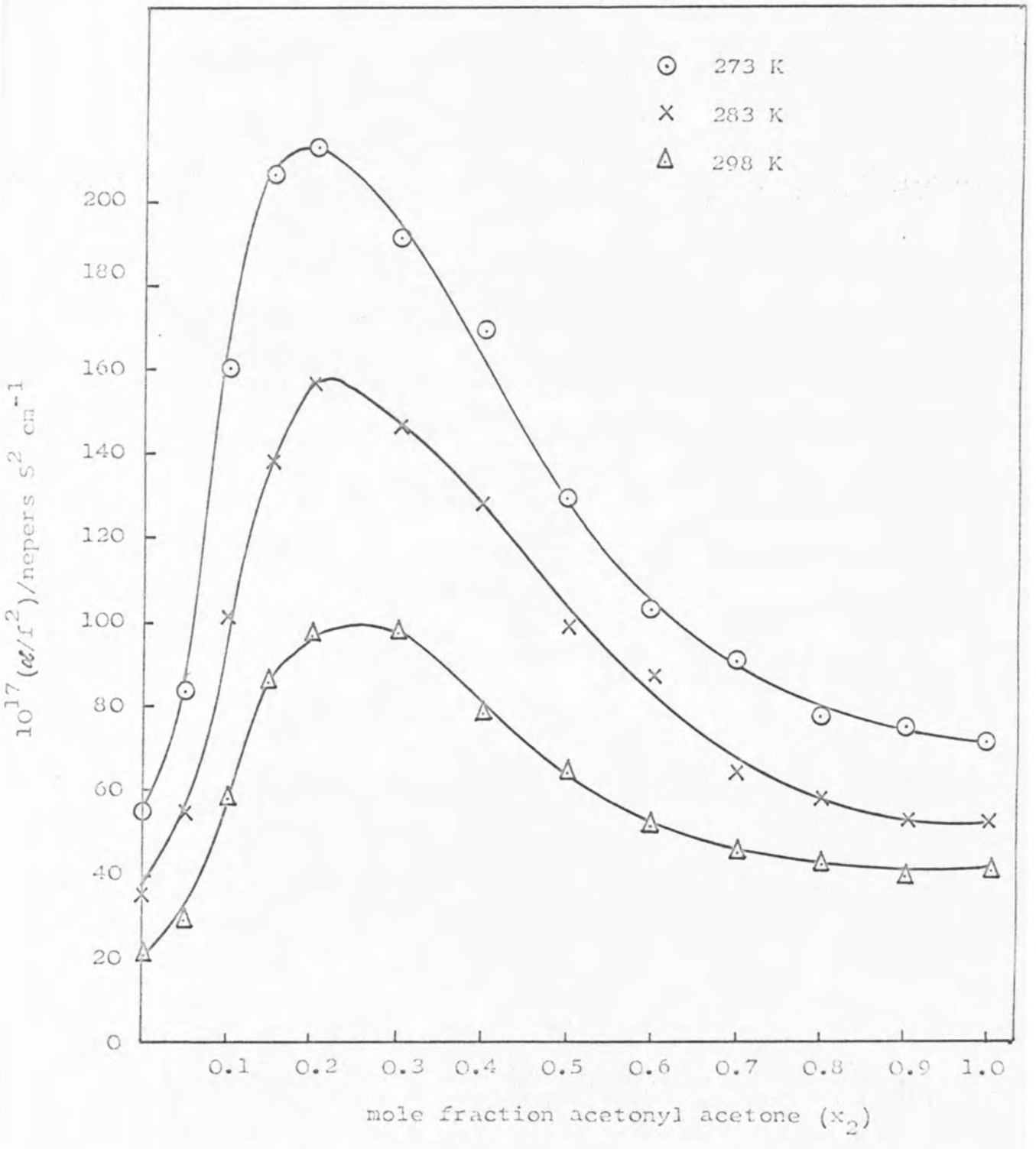

as arising from the relaxation of a series of chemical equilibria. The relaxation data is summarised in Appendix 6-3. In accounting for the type of behaviour, many workers[24,148] have proposed an equilibrium of the type:

$$A + B_m \rightleftharpoons AB_m$$

where m molecules of type B (say water) are associated with one molecule of type A. If the PSAC is due to the perturbation of an equilibrium of this nature, then the position of the PSAC can be explained by simple adjustment of m. Thus $x_2 = \frac{1}{1+m}$; where x_2 is the mole fraction of molecules of type A at the PSAC. In the cases of methyl cyanide + water and acetone + water x_2 = 0.38 $\pm$ 0.02 and so m = 1.63 or 5/3. Thus, a probable equilibrium would be

$$(MeCN)_3 + (H_2O)_5 \rightleftharpoons 3MeCN \cdot 5H_2O$$

or $$((CH_3)_2C{=}O)_3 + (H_2O)_5 \rightleftharpoons 3\ Acetone \cdot 5H_2O$$

If x_2 is taken as 0.4, then m = 1.5 and the equilibria become

$$2(Acetone) + 3H_2O \rightleftharpoons 2(Acetone) \cdot 3H_2O$$

and

$$2(MeCN) + 3H_2O \rightleftharpoons 2(MeCN) \cdot 3H_2O$$

This shows that a change in the PSAC (say $\pm$ 0.02) results in different equilibria.

Further, whilst such a simple model accounts approximately for the PSAC at 0.38, it cannot account in an obvious way for the temperature dependence or intensity

of the absorption. Further, the model cannot account for the observed shapes of the plots of (α/f^2) against composition and frequency. Attempts have been made to clarify this situation, notably by Andreae et. al.[24] with reference to the acetone + water system.

(i) The water-rich region

The 'plateau' region for methyl cyanide + water extends to higher concentrations of methyl cyanide as the temperature is raised. This trend is also observed for mixtures of acetone + water and over the temperature range 273 to 298 K the 'plateau' lengths x_2^* in these two liquid systems are roughly equal.

For aqueous solutions of alcohols in the water rich region, Clarke[7] has noted the similarity between the compositions of the 'plateau' and the sound velocity maximum. This observation has been discussed in terms of an enhancement of water structure by the alcohol.[7] An increase in sound velocity requires a decrease in the isentropic compressibility which implies a structuring of the solution. The acetone + water and methyl cyanide + water systems also show an increase in the ultrasonic velocity in the region close to the end of the plateau. This strongly suggests that it is in this region that some form of water structure enhancement takes place. The increase in the 'plateau' length with increase in temperature, however, suggests that methyl cyanide in these regions does not enhance the water structure (i.e. an

enhancement of water-water interactions). Rather some short lived methyl cyanide water complex is formed. Previous studies[7,35,148] have explained the presence of a plateau region by introducing a second equilibrium

$$AB_m \rightleftharpoons AB_m^*$$

The two complexes differ in structure only and this equilibrium is of most significance at low solute concentrations, where water structure is still taking a dominant role in the liquid mixture. Such a model does not seem unreasonable and its plausibility is further established by a consideration of some other properties of these systems.

Thus, the enthalpies of mixing for the two systems are exothermic in the low solute mole fraction region (considerably so in the case of acetone) and only become endothermic beyond this region. The infra-red absorption results have also shown (see Chapters 8 and 9) that enhancement of water-water interactions does not dominate but rather it is the water-solute hydrogen bonded interaction which is significant. Acetone in particular forms quite strong hydrogen bonds with water.

These observations are completely in accordance with the situation portrayed in the second model and with the temperature dependence of the 'plateau' lengths and sound velocity peaks. (see Tables 4-1 and 4-2). Thus, it seems that the 'plateau' regions in acetone + water and methyl cyanide + water, which are much less sharply defined

TABLE 4 - 1

Plateau lengths (x_2^*) and sound velocity peak locations - methyl cyanide + water

Temp/K	Plateau Length (x_2^*)	Location of Sound Velocity Peak
273	0.07 ± 0.02	0.08 ± 0.02
283	-	-
298	0.08 ± 0.02	0.08 ± 0.02
308	-	0.08 ± 0.02
323	0.12 ± 0.02	-

TABLE 4 - 2

Plateau lengths (x_2^*) and sound velocity peak locations - acetone + water

Temp/K	Plateau Length (x_2^*)	Location of Sound Velocity Peak
273	0.06 ± 0.01	-
283	0.06 ± 0.01	-
298	0.07 ± 0.01	0.09 ± 0.02
300	-	0.08 ± 0.02

than those of the alcohol + water mixtures, correspond to the formation of a solute + water hydrogen bonded complex. Further support for this explanation, at least in the case of acetone + water, is found in the isolation of an acetone hydrate by Frank and Quist.[3] These workers showed that the composition of the hydrate was about 9 to 14 weight per cent acetone. Allowing for the evaporation of acetone during the determination of the composition, it seems that a composition of 14 weight per cent acetone is most probable. This corresponds to about 0.06 mole fraction of acetone and is very similar to the composition at the end of the 'plateau'. No such hydrate has yet been reported for methyl cyanide + water. It is possible that the entropy term dominates in this region.

(ii) The methyl cyanide or acetone rich region

This region, beyond x_2 = 0.7 mole fraction of solute, is of little interest in an investigation of the properties of water. Methyl cyanide and acetone cannot be regarded as possessing a rigid structure akin to that postulated in water. Any equilibria of the type proposed earlier would be strongly displaced towards the complex. There are little data available to demonstrate the presence of such equilibria in this region.

(iii) The PSAC region

The region lying between the water-rich and acetone-rich regions previously described contains the maximum

ultrasonic absorption. The location of the absorption maximum, the peak sound absorption concentration, occurs at $x_2 = 0.38 \pm 0.02$ mole fraction over the temperature range 273 to 298 K for both systems. The presence of this PSAC has been previously described in terms of simple equilibria. To glean information which will help in the construction of a model for this region, other data are required. Examination of G^E, H^E and V^E shows no direct indication of which parameter could be responsible for the appearance of a PSAC and this is also found to be the case for the alcohol + water mixtures. Usually water attempts to retain its own structure and the formation of complexes takes place in opposition to this. This situation can, in some cases, be resolved by phase separation, the mixture exhibiting critical behaviour. For methyl cyanide + water mixtures this is the case and the upper critical solution temperature composition corresponds well with the location of the PSAC.[35] However, for the system acetone + water critical solution behaviour has not been reported. The only thermodynamic difference between these two systems is apparent in the dependence of H^E upon mixture composition. For acetone + water mixtures, which display hydrate formation, H^E is strongly negative, whereas for methyl cyanide + water mixtures H^E is only weakly negative in the water rich region (0.0 to 0.1 mole fraction of methyl cyanide) but becomes strongly positive beyond. A condition for phase separation and an upper critical solution temperature is that $\frac{\partial^2 H}{\partial x_2^2}$ should be less

than zero. As will be illustrated in a later analysis (Chapter 5 and 6) this is the case for methyl cyanide + water mixtures, whereas in the case of acetone + water mixtures $\frac{\delta^2 H}{\delta x_2^2}$ is greater than zero over most of the range up to x_2 = 0.7 mole fraction of acetone.

Comparison of the H^E dependence upon concentration for acetone + water with that for t butyl alcohol + water shows a marked similarity. This suggests that the ultrasonic behaviour of acetone in water lies between that of t butyl alcohol + water and methyl cyanide + water, but is more closely comparable with the methyl cyanide + water system. The importance of the double differentials of thermodynamic functions of mixing will be shown in Chapter 6 to be paramount in describing the dependence of ultrasonic absorption on mixture composition.

If the peak in the sound absorption of methyl cyanide + water mixtures reflects the critical behaviour and the tendency of the mixture to phase separation, then it is difficult to see how a simple equilibrium model can describe the situation. It would be incorrect to suggest that complex formation does not take place at low mole fractions of methyl cyanide, but it seems likely that the controlling feature in the PSAC region is the tendency toward phase separation.

Summary

Whilst there are striking similarities between the

systems water + methyl cyanide, and water + acetone as originally suggested by Foster,[148] there are important differences. The general ultrasonic absorption properties of acetone + water and methyl cyanide + water mixtures cannot be accounted for completely by the use of simple models such as proposed by Andreae et. al. In particular the differences between the systems manifest in the behaviour of the enthalpy of mixing cannot be accounted for. A later analysis (Chapter 6) in terms of a spectrum of relaxation times pinpoints the similarities and differences between these systems.

The simple equilibrium approach can, however, go some way towards describing the ultrasonic absorption behaviour in the water-rich region close to the 'plateau'.

CHAPTER FIVE

THEORETICAL INTERPRETATION OF ULTRASONIC ABSORPTION DATA

5-1 INTRODUCTION

The theoretical interpretation of the absorption of sound by liquids and liquid mixtures is complex. Many theoretical treatments are difficult to apply experimentally and require knowledge of parameters which are at present inaccessible. Current theories may be divided into two groups. Those of the first group assume that a chemical equilibrium is perturbed by the sound wave. The second group is based on an analysis of localised composition or density fluctuations. One example of the latter group is provided by the theory of Romanov and Solovyev.[1]

These two approaches, the chemical equilibrium and the composition fluctuation theories, have been applied to the data reported in Chapter 4, along with other data taken from the literature.

There is an important difference between these two models. The former considers that the response of the system to a perturbation can be characterised by a small number of discrete relaxation times. The latter model considers a 'spectrum' of relaxation times.

A further theory, due to Fixman[133,135-139] has been examined in less detail. This theory describes the absorption of sound by binary mixtures close to their critical point.

5-2 THE RELAXATION APPROACH

(i) Origin of the Relaxation Equations

The passage of a sound wave through a fluid is accompanied by local changes in volume and temperature (i.e. adiabatic compression). Experimental observations have shown that the attenuation of a sound wave travelling through a liquid cannot be wholly ascribed to sheer viscosity effects.[5] (For liquid systems the absorption arising from heat loss is negligibly small). The additional attenuation can be described in terms of a volume viscosity (η_v). Thus, Litovitz and Davis[12] write,

$$\left(\alpha/f^2\right)_{obs} = \frac{2\pi^2}{\rho c^3}\left\{\frac{4}{3}\eta_s + \eta_v\right\} \qquad \ldots\ldots (5\text{-}1)$$

where η_s is the 'classical', or shear, viscosity. However, in real liquids η_v is frequency dependent. Thus, the response of the system to a change in pressure is controlled by the system. Therefore, the compressibility κ_s (isentropic) is frequency dependent. Equation 5-1 is correct at low frequencies where the rate of change of pressure (or temperature) is much lower than the longest response time of the liquid system. With increase in f , $(\alpha/f^2)_{obs}$ decreases. In order to describe the rate control by the system, the mode of response of the system and its kinetic parameters must be understood.

Any theoretical description of ultrasonic absorption must, therefore, be linked with an analysis of the volume

viscosity contribution.

Many different molecular mechanisms for the change in the system following adibatic compression have been proposed. For example, in unassociated liquids isomeric and vibrational relaxation are said to be the causes of frequency dependent volume viscosity. In associated liquids η_v is ascribed to some form of structural relaxation. Two methods of derivation of the structural volume viscosity η_v have been examined. That described in section (5-3) relates the volume viscosity to composition fluctuations in the liquid. The interpretation discussed in this section is due to Andreae and Lamb.[175] They suggest that this viscosity, and hence the excess ultrasonic absorption, arises from the perturbation of a molecular equilibrium due to the temperature alternations in a compressional wave. Lamb,[5] in an analytical treatment of this relaxation process, has derived the equations below.

$$\frac{\alpha}{f^2} = \sum_{i=1}^{n} \frac{A_i}{1 + \{f/f_c(i)\}^2} + B \quad \ldots\ldots (5\text{-}2)$$

where;

$\tau_i = \left(1/2\pi f_c(i) \right)$ is the ith relaxation time,

B is a constant representing the high frequency absorption (e.g. includes shear viscosity).

The maximum value of the absorption per wavelength for the ith relaxation process, $\mu_{max.}$, is given by:

$$\mu_{max}(i) = \tfrac{1}{2} A_i \, c \, f_c(i) \qquad \ldots\ldots (5\text{-}3)$$

μ, the absorption per wavelength, is given by

$$\mu = \alpha \lambda \qquad \ldots\ldots (5\text{-}4)$$

$\mu_{max.}$ can also be derived thermodynamically from the expression below:

$$\mu_{max} = \frac{\pi}{2} \frac{\rho c^2 \Gamma}{RT} \left[\Delta V^{\ominus} - \frac{\alpha_e \Delta H^{\ominus}}{\rho C_p} \right]^2 \frac{C_p}{C_{p_\infty}} \qquad \ldots\ldots (5\text{-}5)$$

where;

$\Delta V^{\ominus}$ and $\Delta H^{\ominus}$ represent the standard volume and enthalpy changes associated with the reaction equilibrium.

α_e is the thermal expansion coefficient of the liquid and ρ its density. C_p and C_{p_∞} are the equilibrium and limiting high frequency values of the heat capacity. The function Γ represents the sinusoidal variation of the equilibrium constant about its mean position brought about by passage of the sound wave.

Equation (5-5) cannot be solved for both $\Delta V^{\ominus}$ and $\Delta H^{\ominus}$ and so, in the absence of additional evidence, one or other is assumed to be dominant. For reactions in dilute aqueous solution at around 277 K, $\Delta V^{\ominus}$ is thought to be much larger than the enthalpy term. Several applications of this equation have been reported,[5,12,175] but none of these provides a clear link between the ultrasonic data and the values of $\mu_{max.}$ calculated from thermodynamic data. Further, $\Delta V^{\ominus}$ and $\Delta H^{\ominus}$ are difficult parameters to determine experimentally.

Whenever ultrasonic absorption measurements are reported equation (5-2) has generally been used to deduce the relaxation times. These times are then assigned to postulated equilibria in solution but the interpretation is far from straight forward. The derived A and f_c values for many aqueous systems have shown similar trends which may be considered as highlighting the important role of water in these systems.

(ii) Computer Analysis

Ultrasonic absorption data was fitted to equation (5-2) using a least squares program originally written by Dr. A. Weinmann.[176] This program, written in ALGOL, modified to provide further controlled output is listed in Appendix 5-1. The observed values of $\left(\frac{\alpha}{f^2}\right)_{obs}$ are required by the program at various frequencies f, making N observations in total. If F is defined as

$$F = \sum \left[\left(\frac{\alpha}{f^2}\right)_{obs} - \left(\frac{\alpha}{f^2}\right)_{cal}\right]^2 \qquad \ldots\ldots (5\text{-}6)$$

then $\frac{\partial F}{\partial A_i} = \frac{\partial F}{\partial f_c(i)} = \frac{\partial F}{\partial B} = 0$ at the minimum.

The program estimated values of the parameters, together with upper and lower limits and 'variation lengths' and repeatedly computed F whilst varying one or more parameters until F was a minimum. The values of $\left(\frac{\alpha}{f^2}\right)$ calc, f, fc(i) and A(i) were output. This program was, however, found to

be unsatisfactory because the squares of the differences in the two quantities $\left[\left(\frac{\alpha}{f^2}\right)_{obs} - \left(\frac{\alpha}{f^2}\right)_{calc}\right]$ were not normalised. Thus, large values of $\left(\frac{\alpha}{f^2}\right)_{obs}$ or $\left(\frac{\alpha}{f^2}\right)_{calc}$ were given greater 'weight' by the program than other values. This was effectively overcome by normalising the squares; redefining F as;

$$F = \sum \left\{ \frac{\left(\frac{\alpha}{f^2}\right)_{obs} - \left(\frac{\alpha}{f^2}\right)_{calc}}{\left(\frac{\alpha}{f^2}\right)_{obs}} \right\}^2 \qquad \ldots\ldots (5\text{-}7)$$

The program listed in the Appendix 5-1 uses this 'weighted' form of the sum of the squares of the deviations.

Another method of fitting equation (5-2) to the observed experimental quantities follows that discussed in Chapter 8 for the analysis of spectral band contours.[177] This method used the approximation that for any generalised parameter p_{o^i} a refined or 'better' value can be obtained from the equation

$$p_i = p_{oi} - \tau \frac{\partial F/\partial p_{oi}}{\partial^2 F/\partial p_{oi}^2} \qquad \ldots\ldots (5\text{-}8)$$

where τ is an adjustable minimising parameter having a value between 1.0 and 0. The relevant equations are summarised below.

Let $\frac{\alpha}{f^2} = \Phi$ and $\Phi = \Phi\ (A_i, f_c(i)f, B)$

then $$F = \sum_{j=1}^{N} \left\{ \Phi_{obs}^{(j)} - \Phi_{calc}^{(j)} \right\}^2 \quad \ldots\ldots (5\text{-}9)$$

Thus, $$\frac{\partial F}{\partial p_i^o} = -2 \sum_{j=1}^{N} \left\{ \Phi_{obs}^{(j)} - \Phi_{calc}^{(j)} \right\} \frac{\partial \Phi_{calc}^{(j)}}{\partial p_i^o} \quad \ldots\ldots (5\text{-}10)$$

and $$\frac{\partial^2 F}{\partial p_i^{o\,2}} = 2 \sum_{j=1}^{N} \left(\frac{\partial \Phi_{cal}}{\partial p_i^o} \right)^2 - 2 \sum_{j=1}^{N} \left(\Phi_{obs} - \Phi_{cal} \right) \frac{\partial^2 \Phi_{calc}}{\partial p_i^{o\,2}} \quad \ldots\ldots (5\text{-}11)$$

This method reduces the computing time required for data analysis. In addition the minimisation is improved and 'false minima' are eliminated.

One criticism of the use of equation (5-2) in analysing ultrasonic absorption data is that this theory describes a closely defined situation which is difficult to understand in dynamic terms. Further, the values of A(i) and $f_c(i)$ for the 'ith relaxation' cannot be endowed with a simple meaning.

5-3 THE THEORY OF ROMANOV AND SOLOVYEV

(i) Fluctuation Model

The theory of Romanov and Solovyev attempts to explain the presence of a maximum in the plot of (α/f^2) against the concentration. The usual explanation is founded upon the formation and decomposition of polymeric molecular associates,[175] all having rigorously defined stoichiometry.

Vuks and Lisnyanskii[178,179] drew attention to the similarities between the concentration dependence of sound

absorption and light scattering. They accounted for the excess sound absorption in liquid mixtures in terms of concentration fluctuations. The analysis which follows assigns the absorption to fluctuations which are treated as regions of variable concentration in a continuous medium. This approach is only rigorous for large scale fluctuations but it may be considered as offering an approximate description of small scale inhomogeneities also. Some sound absorption can be attributed to heat exchange, the Zener-Isakovitch[180] effect, but a simple estimate[116] shows that this effect is small. A more likely mechanism considers the relaxation of the fluctuations.

(ii) Derivation of the Romanov-Solovyev Equation

The volume occupied by one mole of solution V is divided into elements dV, sufficiently small that the concentration may be considered constant throughout the elemental volume. The thermodynamic potential of the element is

$$G(x)\frac{dV}{V} = \left[G_0(x_2) + \frac{\partial G_0}{\partial x_2}(x-x_2) + \frac{1}{2}\frac{\partial^2 G_0}{\partial x_2^2}(x-x_2)^2 + \cdots\right]\frac{dV}{V} \quad \ldots\ldots (5\text{-}12)$$

where x is the concentration in the volume element dV, and x_2 is the concentration of the bulk solution in mole fraction units. $G_0(x_2)$ is the thermodynamic potential per mole in the absence of fluctuations. Further terms are omitted in the absence of experimental data for the determination of the correction coefficients.

Integrating over the volume V gives the molar thermodynamic potential in the presence of fluctuations.

$$G(x_2) \approx G_0(x_2) + \frac{1}{2V} g'' \int_V (x - x_2)^2 dV \qquad \ldots\ldots (5\text{-}13)$$

that is

$$G(x_2) \approx G_0(x_2) + \tfrac{1}{2} g'' \langle (x - x_2)^2 \rangle \qquad \ldots\ldots (5\text{-}14)$$

The molar enthalpy H and molar volume V are similarly derived as

$$H(x_2) \approx H_0(x_2) + \tfrac{1}{2} h'' \langle (x - x_2)^2 \rangle \qquad \ldots\ldots (5\text{-}15)$$

$$V(x_2) \approx V_0(x_2) + \tfrac{1}{2} v'' \langle (x - x_2)^2 \rangle \qquad \ldots\ldots (5\text{-}16)$$

where $g'' = \frac{\partial^2 G}{\partial x_2^2}$ and $h'' = \frac{\partial^2 H}{\partial x_2^2}$ and $v'' = \frac{\partial^2 V}{\partial x_2^2}$

These quantities g'', h'', v'' are derivable from experimental data. Thus V, H and G are dependent upon the mean square fluctuation.

The passage of a sound wave is accompanied by variations in pressure (p) and temperature (T). These p and T variations alter the distribution and magnitude of the fluctuations.

(note that; $v'' = \frac{\partial G}{\partial p}$ and $h'' = -T^2 \frac{\partial}{\partial T}\left(\frac{G}{T}\right)$)

The rate at which the new distribution is established is controlled by diffusive processes. It is assumed that

the restoration of the distribution of fluctuations proceeds according to the equation

$$\frac{\partial x}{\partial t} = D \nabla^2 x \qquad \ldots\ldots (5\text{-}17)$$

where D is the diffusion coefficient.
Further, it is assumed that the rate of formation of a new distribution takes place independently of the distribution of fluctuations already established.

The instantaneous concentration distribution may be represented as a Fourier spectrum

$$x - x_2 = \sum_f B_f(t) \exp(i(f, r)) \qquad \ldots\ldots (5\text{-}18)$$

The amplitudes (B_f) may be shown to vary as

$$\frac{\partial B_f}{\partial t} = -\frac{1}{\tau_f}(B_f - \bar{B}_f) \qquad \ldots\ldots (5\text{-}19)$$

$\bar{B}_f$ is the average value of B_f at a given pressure and temperature, and B_f is the amplitude of the harmonic wave vector f. The relaxation time $\tau_f = \frac{1}{Df^2}$. In any sound wave $p = p_o + \delta p$, $T = T_o + \delta T$, and $\delta p \approx \delta T \approx \exp(i\omega t)$, thus

$$\delta B_f = \frac{\delta \bar{B}_f}{1 + i\omega\tau_f} \qquad \ldots\ldots (5\text{-}20)$$

For a small volume increment δV

$$\delta V = \left(\frac{\partial V}{\partial p}\right)_{T,x} \delta p + \left(\frac{\partial V}{\partial T}\right)_{p,x} \delta T + \frac{1}{2} \sigma'' \langle (x - x_2)^2 \rangle$$

$$= -V\beta_\infty \delta p + V\alpha_\infty \delta T + \frac{1}{2}\upsilon'' \langle (x-x_2)^2 \rangle \quad \ldots\ldots (5\text{-}21)$$

where α_∞ and β_∞ are the instantaneous coefficients of expansion and compressibility.

Now $$\langle (x-x_2)^2 \rangle = \sum_f B_f^2 \quad \ldots\ldots (5\text{-}22)$$

so $$\delta \langle (x-x_2)^2 \rangle = \delta \sum_f B_f^2$$

$$= 2\sum_f B_f \cdot \delta B_f = 2\sum_f B_f \frac{\delta B_f}{1+i\omega\tau} \quad \ldots\ldots (5\text{-}23)$$

but $\overline{B}_f \approx \sqrt{\frac{kT}{g''}}$ and hence

$$\delta \overline{B}_f = \left(\frac{\partial \overline{B}_f}{\partial p}\right)_T \delta p + \left(\frac{\partial \overline{B}_f}{\partial T}\right)_p \delta T = \frac{\overline{B}_f}{2g''}\left(\upsilon'' \delta p - \frac{h''\delta T}{T}\right) \quad \ldots\ldots (5\text{-}24)$$

From equation (5-21)

$$\frac{\delta V}{V} = -\tilde{\beta}\delta p + \tilde{\alpha}\,\delta T \qquad \text{where}$$

$$\tilde{\beta} = \beta_\infty + \frac{kT(\upsilon'')^2}{2V(g'')^2}\sum_f \frac{1}{1+i\omega\tau_f} \quad \ldots\ldots (5\text{-}25)$$

$$\tilde{\alpha} = \alpha_\infty + \frac{k(\upsilon'' h'')}{2V(g'')^2}\sum_f \frac{1}{1+i\omega\tau_f} \quad \ldots\ldots (5\text{-}26)$$

By analogy $$\delta H = \tilde{C}_p \delta T - TV\tilde{\alpha}\delta p \quad \ldots\ldots (5\text{-}27)$$

and $$\tilde{C}_p = C_{p_\infty} + \frac{k(h'')^2}{2(g'')^2}\sum_f \frac{1}{1+i\omega\tau_f} \quad \ldots\ldots (5\text{-}28)$$

The complex adiabatic modulus $\tilde{K}$ may be expressed as

$$\tilde{K} = K + i\omega\eta_v = \left[\tilde{\beta} + (TV\tilde{\alpha}_e^2/\tilde{C}_p)\right]^{-1} \quad \ldots\ldots (5\text{-}29)$$

By substituting for $\tilde{\beta}$, $\tilde{\alpha}_e$ and $\tilde{C}_p$ from equations (5-25), (5-26), (5-27), and extracting the real and imaginary parts of the complex adiabatic modulus Romanov and Solovyev showed that

$$K = K_\infty - K_\infty^2 \frac{VkT}{2(g'')^2}\left(\frac{v''}{V} - \frac{\alpha_{e\infty} h''}{C_{p\infty}}\right)^2 \sum_f \frac{1}{1+\omega^2\tau_f^2} \quad \ldots\ldots (5\text{-}30)$$

and from the imaginary part;

$$\eta_v = K_\infty^2 \frac{VkT}{2(g'')^2}\left(\frac{v''}{V} - \frac{\alpha_{e\infty} h''}{C_{p\infty}}\right)^2 \sum_f \frac{\tau_f}{1+\omega^2\tau_f^2} \quad \ldots\ldots (5\text{-}31)$$

where η_v is the volume viscosity coefficient. The instantaneous quantities $\alpha_{e\infty}$, K_∞, $C_{p\infty}$ may be replaced, to a good approximation, by their equilibrium values α_e, Cp, K. Romanov and Solovyev made use of the Debye wavenumber distribution function

$$n(f)\,df = \frac{Vf^2}{2\pi^2}\,df \quad \ldots\ldots (5\text{-}32)$$

in order to convert the summation in equation (5-33) to an integral; they obtained

$$\eta_v = \frac{K^2 V^2 kT}{4\pi^2 (g'')^2}\left(\frac{v''}{V} - \frac{\alpha_e h''}{C_p}\right)^2 \frac{f}{D}\, L\left(\frac{\omega}{Df_m^2}\right) \quad \ldots\ldots (5\text{-}34)$$

where $$L\left(\frac{\omega}{Df_m^2}\right) = \frac{1}{f_m\sqrt{D/\omega}} \int_0^x \frac{x^4\,dx}{1+x^4} \quad \ldots\ldots (5\text{-}35)$$

and $x = f_m\sqrt{D/\omega}$.

f_m is the maximum wavenumber of the Fourier expansion and defines the limit of the model. The model is only strictly applicable for $f \ll 1/\ell$ where ℓ is the mean distance between the molecules with the lower concentration. Taking into consideration the approximate nature of the model we have set $fm = 1/\ell_m$.

The link between the volume viscosity η_v and the quantity $\alpha' = \alpha - \alpha$ classical is[5,12]

$$\alpha' = \frac{\omega^2}{2c^3\rho}\eta_v \qquad \ldots\ldots (5\text{-}36)$$

from which it is easily shown that

$$\frac{\alpha' V}{\omega} = \frac{\omega V}{2c^3\rho}\eta_v$$

Following Litovitz[59] and writing $f = 1/\ell$ and redefining $\tau_\ell = \ell^2/2D \; (\equiv \tau_f)$;

$$\frac{\alpha' V}{\omega} = \left\{\frac{2\pi^3 V^2 kT}{\beta_o (g'')^2}\right\}\left[\frac{v''}{V} - \frac{\alpha_e h''}{c_p}\right]^2 \int_{\ell_m}^{\infty} \frac{2}{\ell^4}\frac{\omega(\ell^2/2D)\,d\ell}{1+\omega^2(\ell^2/2D)^2} + B \qquad \ldots\ldots (5\text{-}37)$$

$$\text{thus} \quad \frac{\alpha'}{f^2} = \left\{\frac{8\pi^3 V^2 kT}{\omega c \beta_o (g'')^2}\right\}\left[\frac{v''}{V} - \frac{\alpha_e h''}{c_p}\right]^2 \cdot \int_{\ell_m}^{\infty} \frac{2}{\ell^4}\frac{\omega(\ell^2/2D)\,d\ell}{1+\omega^2(\ell^2/2D)^2} + B \qquad \ldots\ldots (5\text{-}38)$$

writing

$$I(\ell) = \int_{\ell_m}^{\infty} \frac{2}{\ell^4}\frac{\omega(\ell^2/2D)\,d\ell}{1+\omega^2(\ell^2/2D)^2} \qquad \ldots\ldots (5\text{-}39)$$

The integral $I(\ell)$ has been evaluated as below; putting

$a = \omega/2D$

$$I(\ell) = \int_{\ell_M}^{\infty} \frac{2}{\ell_1^4} \frac{a\ell^2}{(1+a^2\ell^4)} d\ell \qquad \ldots\ldots (5\text{-}40)$$

$$= 2\int_{\ell_M}^{\infty} \frac{a\, d\ell}{\ell^2(1+a^2\ell^4)} \qquad \ldots\ldots (5\text{-}41)$$

by partial fractions

$$\frac{1}{\ell^2(1+a^2\ell^4)} = \frac{1}{\ell^2} - \frac{a^2\ell^2}{[1+a^2\ell^4]} \qquad \ldots\ldots (5\text{-}42)$$

thus;

$$I(\ell) = 2a\int_{\ell_M}^{\infty} \frac{d\ell}{\ell^2} - 2a^3\int_{\ell_M}^{\infty} \frac{\ell^2 d\ell}{1+a^2\ell^4}$$

$$= \frac{2a}{\ell_M} - 2a^3\int_{\ell_M}^{\infty} \frac{\ell^2 d\ell}{1+a^2\ell^4} \qquad \ldots\ldots (5\text{-}43)$$

let the integral $\int_{\ell_M}^{\infty} \frac{\ell^2 d\ell}{1+a^2\ell^4} = J$

using partial fractions J becomes

$$J = \frac{1}{2\sqrt{2a}}\left[\int_{\ell_M}^{\infty} \frac{\ell\, d\ell}{(a\ell^2-\sqrt{2a}\,\ell+1)} - \int_{\ell_M}^{\infty} \frac{\ell\, d\ell}{(a\ell^2+\sqrt{2a}\,\ell+1)}\right] \qquad \ldots\ldots (5\text{-}44)$$

which may be rewritten as

$$J = \left(\frac{1}{2\sqrt{2a}}\right)\left(\frac{1}{2a}\right)\left[\int_{\ell_M}^{\infty} \frac{(2a\ell-\sqrt{2a})\,d\ell}{(a\ell^2-\sqrt{2a}\,\ell+1)} + \int_{\ell_M}^{\infty} \frac{\sqrt{2a}\,d\ell}{(a\ell^2-\sqrt{2a}\,\ell+1)}\right.$$

$$\left. - \int_{\ell_M}^{\infty} \frac{(2a\ell+\sqrt{2a})\,d\ell}{(a\ell^2+\sqrt{2a}\,\ell+1)} + \int_{\ell_M}^{\infty} \frac{\sqrt{2a}\,d\ell}{(a\ell^2+\sqrt{2a}\,\ell+1)}\right] \qquad \ldots\ldots (5\text{-}45)$$

writing $x^2 = a\ell^2$ and integrating gives;

$$J = \left(1/4a\sqrt{2a}\right)\left[\left\{\ln\left(\frac{x^2-\sqrt{2}x+1}{x^2+\sqrt{2}x+1}\right)\right\}_{\sqrt{a}\,\ell_m}^{\infty} + \int_{\ell_m}^{\infty}\frac{\sqrt{2}\,dx}{(x^2-\sqrt{2}x+1)} + \int_{\ell_m}^{\infty}\frac{\sqrt{2}\,dx}{(x^2+\sqrt{2}x+1)}\right] \quad \ldots\ldots (5\text{-}46)$$

But $(x^2 + \sqrt{2}x + 1)$ may be written as $(x + \frac{\sqrt{2}}{2})^2 + (\frac{\sqrt{2}}{2})^2$

and $(x^2 - \sqrt{2}x + 1)$ may be written as $(x - \frac{\sqrt{2}}{2})^2 + (\frac{\sqrt{2}}{2})^2$

Thus the two integrals in equation (5-46) become similar to the standard integral

$$\int\frac{dx}{A^2+x^2} = \frac{1}{A}\tan^{-1}\left(\frac{x}{A}\right) + \text{const.}$$

Thus, after integration, the expression for J is

$$J = \left(1/4a\sqrt{2a}\right)\left[2\pi - \ln\left(\frac{a\ell_m^2-\sqrt{2a}\,\ell_m+1}{a\ell_m^2+\sqrt{2a}\,\ell_m+1}\right) - 2\tan^{-1}\left(\sqrt{2a}\,\ell_m+1\right) - 2\tan^{-1}\left(\sqrt{2a}\,\ell_m-1\right)\right] \quad \ldots\ldots (5\text{-}47)$$

The resulting expression for $\frac{\alpha}{f^2}$ may be summarised as follows;

$$\frac{\alpha}{f^2} = \frac{Q}{\omega}\,I(\ell) + B \qquad \ldots\ldots (5\text{-}48)$$

where

$$Q = \frac{8\pi^5 V^2 k T}{c\,\beta_o (g'')^2}\left[\frac{\sigma''}{V} - \frac{\alpha_a h''}{C_p}\right]^2$$

and

$$I(\ell) = \omega\left[\frac{1}{D\ell_m} - \frac{\omega^{1/2}\,p}{8D^{3/2}}\right]$$

(note $\kappa_s = \beta_o$ = isentropic compressibility)

where P =

$$2\pi - \ln\left\{\frac{a l_m^2 - \sqrt{2a}\, l_m + 1}{a l_m^2 + \sqrt{2a}\, l_m + 1}\right\} - 2\left(\tan^{-1}\left(\sqrt{2a}\, l_m + 1\right) + \tan^{-1}\left(\sqrt{2a}\, l_m - 1\right)\right)$$

and $a = \omega/2D$.

(iii) The Quantity Q

A quantity, Q, defined in equation (5-49)

$$Q = \frac{8\pi^5 k T V^2}{c \kappa_s (g'')^2}\left[\frac{v''}{V} - \frac{\alpha_e h''}{C_p}\right]^2 \qquad \ldots\ldots (5\text{-}49)$$

has been identified since it contains, in principle, all those quantities which are independently determinable. To a close approximation at a fixed frequency the quantity P is independent of composition. Thus the dependence of α/f^2 upon composition should be reflected in the behaviour of the quantity Q as a function of mixture composition. In an attempt to test this hypothesis the variables contained within Q were determined from experimental data.

The composition dependence of the quantities g", h", v", α_e, Cp, κ_s, V, c and ρ were required. The quantities α_e, Cp, c and ρ were directly obtained from the literature.

The isentropic compressibility κ_s was obtained using the equation of Newton and Laplace.

$$\kappa_s = \left(\partial \ln V/\partial P\right)_s = (1/\rho c^2) \qquad \ldots\ldots (5\text{-}50)$$

Further details of these parameters are given in Chapter 6.

The quantities g", h", v" and V were obtained, using the analysis below, from reported excess volume, enthalpy and Gibbs function measurements.

Consider a binary mixture comprising mole fractions x_1 and x_2 with molar free energy G.

$$G = x_1 \overline{G}_1 + x_2 \overline{G}_2 \qquad \ldots\ldots (5\text{-}51)$$

where $\overline{G}_1$ and $\overline{G}_2$ are the partial molar free energies of the two components.

For a real system;

$$G = x_1 \overline{G}_1^{\circ} + x_2 \overline{G}_2^{\circ} + x_1 RT \ln x_1 f_1 + x_2 RT \ln x_2 f_2$$

For an ideal system;

$$G = x_1 \overline{G}_1^{\circ} + x_2 \overline{G}_2^{\circ} + x_1 RT \ln x_1 + x_2 RT \ln x_2$$

so that the excess molar free energy of mixing G^E is;

$$G^E = G_{real} - G_{ideal} = x_1 RT \ln f_1 + x_2 RT \ln f_2$$

For a real system

$$G = x_1 \overline{G}_1^{\circ} + x_2 \overline{G}_2^{\circ} + x_1 RT \ln x_1 + x_2 RT \ln x_2 + G^E$$

Thus, after differentiation with respect to x_2,

$$\frac{\partial^2 G}{\partial x_2^2} = \frac{\partial^2 G^E}{\partial x_2^2} + \frac{RT}{x_2(1-x_2)} \qquad \ldots\ldots (5\text{-}52)$$

Similarly, it can be shown for the heats of mixing and volumes of mixing that;

$$\frac{\partial^2 H}{\partial x_2^2} = \frac{\partial^2 H^E}{\partial x_2^2} \quad ; \quad \frac{\partial^2 V}{\partial x_2^2} = \frac{\partial^2 V^E}{\partial x_2^2}$$

For any general excess function X^E the derivation of

$\frac{\partial^2 X^E}{\partial x_2^2}$ (= X") places rigorous demands on the thermodynamic data for a binary mixture. The following technique of analysis of the data has been applied.

The general excess function may be represented as a power series,[51]

$$X^E = x_2(1-x_2)\sum_{i=0}^{n} A_i(1-2x_2)^i \qquad \ldots\ldots (5\text{-}53)$$

By differentiation with respect to x_2 we derive,

$$\frac{\partial^2 X^E}{\partial x_2^2} = 4(1-x_2)x_2\sum_{i=0}^{n} i A_i(1-2x_2)^{i-2}(i-1) -$$

$$2\left\{\sum_{i=0}^{n} i A_i(1-2x_2)^i + \sum_{i=0}^{n}(i-1)A_i(1-2x_2)^i\right\} \qquad \ldots\ldots (5\text{-}54)$$

Where data was not reported in the literature liquid-vapour equilibrium measurements were used to obtain G^E as a function of composition using the method of Barker.[181] The molar volumes were obtained from excess volume measurements using the equation

$$V = \frac{x_1 M_1}{\rho_o(1)} + \frac{x_2 M_2}{\rho_o(2)} + V^E \qquad \ldots\ldots (5\text{-}55)$$

where $\rho_o(1)$ and $\rho_o(2)$ are the densities and M_1 and M_2 the molecular weights of the pure components.

(iv) Computer Analysis

(a) The Computation of Ω

An ALGOL computer program was written to evaluate the quantity Q as a function of liquid mixture composition. The program, together with a summary of the input data, is given in Appendix 5-2. For calculation of the parameters v", h" and g" as a function of mixture composition the constants A_i (i = 0,1,2,---n) had to be evaluated in equation (5-53). This was accomplished by a least squares procedure as follows;

If $$F = \sum_{\text{data points}} \left(X^E_{\text{input}} - X^E_{\text{calc}} \right)^2 \qquad \ldots\ldots (5\text{-}56)$$

$$\frac{\partial F}{\partial A_i} = 0 \text{ for all i at a minimum.}$$

Now

$$\frac{\partial F}{\partial A_i} = -2 \sum_{\text{data points}} \left(X^E_{\text{input}} - X^E_{\text{calc}} \right) \frac{\partial X^E_{\text{calc}}}{\partial A_i} \qquad \ldots\ldots (5\text{-}57)$$

Thus the set of n equations in the n parameters A_i may be represented by

$$2 \sum_{\text{data points}} \left(X^E_{\text{calc}} - X^E_{\text{input}} \right) \frac{\partial X^E_{\text{calc}}}{\partial A_i} = 0 \qquad \ldots\ldots (5\text{-}58)$$

for i = 0,1,2,---n.

The set of equations so generated were solved on an Elliott 4130 computer using an ALGOL program[182] which incorporated an Elliott Library program for the solution of a series of linear equations (cf e.g. (5-58)). Successive

series of equations were solved for values of n increasing from zero to 10. The set of parameters A_i which gave the 'best fit' were then used in the program to evaluate Q.

(b) The Romanov-Solovyev Equation

A computer program was written in ALGOL which derived the values of Q, l_m, D and B in the 'full' Romanov-Solovyev equation. (See equation (5-48)).

The frequency dependence of $(\frac{\alpha}{f^2})$ was fitted to equation (5-48) using a modified form of the program described in section 5-2 (ii). Initial approximate values of Q, l_m, D, and B (defined previously) were input to the program which refined these values in order to minimise the sum of the squares of the deviations. The output consisted of the values of the constants above, together with a table of f, $(\alpha/f^2)_{obs}$ and $(\alpha/f^2)_{calcd.}$. A description of the program is included in Appendix 5-3.

5-4 ULTRASONIC ABSORPTION IN CRITICAL MIXTURES

The thermodynamic condition for critical mixing is that $g'' = 0$.[51] The Romanov-Solovyev treatment requires that α/f^2 is infinite at the critical point. This is in agreement with experimental observation.

However, critical phenomena cannot be treated using conventional fluctuation theory, since the fluctuations become large close to the critical point.

According to equation (5-13) a fluctuation in composi-

tion or density is reflected in a change in G. However at a critical point there is little change in G and the fluctuations become very large. Another approach to this problem has been proposed by Fixman[111,133,135-139,174]

(i) Outline of the theory of Fixman

The treatment proposed by Fixman discusses ultrasonic absorption in terms of a coupling between the fluctuating anomalousheat capacity of a system close to a critical point, and the oscillating temperature changes induced by the sound wave. The limit of applicability of the theory requires that $|T - T_c| < 1$ K.[51] The theory has connections with the Ornstein-Zernike[183] theory of correlation and the Debye[184] theory of light scattering.

If two points A and B are separated by distance r such that Δ_A and Δ_B represent local fluctuations in some property of the system, then $\langle \Delta_A \Delta_B \rangle$ is the average product of the fluctuations at a fixed distance apart.[1] As $r \longrightarrow 0$; $\langle \Delta_A \Delta_B \rangle \longrightarrow \langle \Delta^2 \rangle$ and as $r \longrightarrow \infty$ $\langle \Delta_A \Delta_B \rangle$ decreases. The extent of this dependence is measured by a correlation function c(r). c(r) = 1.0 when $r = \infty$ and c(r) = 0 when r = 0. The value of r corresponding to c(r) = 0.5 is called the correlation or persistence length L. Debye[184] showed that for a fluid at critical density and critical temperature T_c;

$$L^2 = \ell^2 / \left[(T/T_c) - 1 \right] \qquad \ldots\ldots (5\text{-}59)$$

The length l is characteristic of intermolecular interactions. The classical equation of Ornstein and Zernike[183] provides a means of dealing with these correlation functions.

If g is the Gibbs function per unit volume and n_i the number of molecules of species i, then the change in g, following a composition fluctuation, is

$$dg = -(2n_2V_1^\circ)^{-1}(\partial\mu_1/\partial n_2)(\delta n_2)^2 \qquad \ldots\ldots (5\text{-}60)$$

Assuming no volume change on mixing

$$\delta S = -\{(\partial(\delta g)/\partial T)\} \qquad \ldots\ldots (5\text{-}61)$$

Using these two equations, an expression for the average entropy change associated with a critical fluctuation may be derived;

$$\langle \delta S \rangle = \Phi\,(2V_1^\circ)^{-1}(\partial^2\mu_1/\partial\Phi_2\partial T)\int_0^{k_{max}} G_k(r)\,dk \qquad \ldots\ldots (5\text{-}62)$$

where Φ_2 is the volume fraction of species 2 and G_k is the Fourier component of the pair distribution function g(r) with wave vector k.

The form of g(r) is taken as;

$$h(r) = g(r) - 1 = a\exp(-\kappa r)/r \qquad \ldots\ldots (5\text{-}63)$$

where $h(r) = c(r) + n\int c(r)\,h(r)\,dr$, and h(r) is the total (or long range) correlation function. n is the number

of molecules in the system.

Absorption arises from an out-of-phase component of the fluctuating heat capacity. The frequency dependence of the heat capacity arises out of the properties of the Fourier transform of g(r). The response of the system is governed by diffusion processes and if the excess heat capacity per unit volume Δ is

$$\Delta = T_c \langle \delta S \rangle / \delta T \qquad \ldots\ldots (5\text{-}64)$$

then, Fixman writes;

$$\Delta = k \left[T_c \frac{\partial \kappa^2}{\partial T} \right]^2 \left(\frac{1}{4\pi^2} \right) \left(\frac{h}{\omega} \right)^{\frac{1}{2}} f(d) \qquad \ldots\ldots (5\text{-}65)$$

where h is a diffusion coefficient, and

$$f(d) = \frac{\pi}{2} i d^{3/2} \left\{ 1 - i(1 + 4 i d^{-2})^{-\frac{1}{2}} (\chi_1^{5/2} + \chi_2^{\frac{5}{2}}) \right\} \qquad \ldots\ldots (5\text{-}66)$$

The imaginary root Im(f) is required[133,135-139] in an analysis of the sound absorption,

$$\alpha / f^2 = \frac{\pi H I_m(f)}{c f} \qquad \ldots\ldots (5\text{-}67)$$

where

$$H = (\gamma_0 - 1) \frac{R}{C_{p_0}} \left[T_c \frac{d \kappa^2}{d T} \right]^2 \left(\frac{(n_1 + n_2)^{-1}}{4\pi^2} \right) \left(\frac{h}{2\pi f} \right)^{\frac{1}{2}} \qquad \ldots\ldots (5\text{-}68)$$

putting $H = f^{\frac{1}{2}} H'$ equation (5-67) becomes

$$\frac{\alpha}{f^2} = \left\{ H' c^{-1} I_m(f) \right\} f^{-\frac{5}{4}} + B' \qquad \ldots\ldots (5\text{-}69)$$

where c is the sound velocity. This equation is simplifiable to;

$$\frac{\alpha}{f} = \Psi f^{-5/4} + B' \quad \ldots\ldots (5\text{-}70)$$

where Ψ and B' are constants.

(ii) Application of the Fixman Theory

Many attempts have been made to explain the shape of the plot of α/f^2 against f for a critical mixture.

Attempts to apply the "full" Fixman equation have proved difficult since the theoretical treatment incorporates several parameters which cannot be satisfactorily estimated. These parameters include one term used to define h and the quantity $\frac{\partial \kappa^2}{\partial T}$. κ may be re-expressed as a function of $\mathbb{D}$, and κ is used to determine the quantity d, which in turn lead to a deduction of Im(f).

Several authors,[1] including Fixman,[133,135-139] have attempted to calculate these parameters and have thus attempted to predict the dependence of (α/f^2) upon f. These tests show the theory to be satisfactory in a description of the absorption properties of critical mixtures. Unfortunately, the theory fails to predict[133,135-139] the observed dependence of the sound velocity on frequency.

The theory does predict that (α/f^2) should show a maximum at some intermediate composition, but the agreement between the observed and predicted curve is unsatisfactory.

A program was written in ALGOL to 'fit' equation (5-70), using a least squares procedure, to the experimental values of $(\alpha/f^2)_{obs}$ at various values of f for an aqueous solution, showing critical behaviour.

The analysis showed broad agreement between the experimental results and the theoretical treatment.[1,69]

CHAPTER SIX

APPLICATIONS OF THE THEORY OF ROMANOV AND SOLOVYEV AND DISCUSSION OF RESULTS

6-1 t BUTYL ALCOHOL + WATER MIXTURES

Recently much attention has been devoted to studies of the properties of t butyl alcohol and water mixtures. This is, in part, because t butyl alcohol is the last of the lower alcohols which is completely miscible with water.

Clarke[7,19] measured the ultrasonic absorption properties of mixtures of t butyl alcohol and water over a wide range of compositions, and at several temperatures. Burton[22] reported sound velocity measurements at various compositions and 298 K.

The thermodynamic properties of t butyl alcohol and water mixtures have been extensively examined by Kentamaa et al.[185]

(i) Calculation of Q

The calculation of the values of the quantity Q, defined by equation (5-49), were undertaken as described in Chapter 5. Sound velocity data, taken from reference 22 and values of V^E, H^E and G^E obtained from reference 185 were used. The values of Q calculated at several mole fractions (x_2) are plotted in Figure 6-1, together with the ultrasonic absorption measurements of Clark.[7,19] Figure 6-2 displays the dependence upon the mole fraction of t butyl alcohol (x_2) of the computed parameters g", v"/V and $\alpha_e h''$/Cp which have been previously defined.

Figure 6-3 shows the composition dependence of the

FIGURE 6-1 Dependence of (α/f^2) and Ω(thermo) upon mixture composition for tBuOH + water at 298 K.

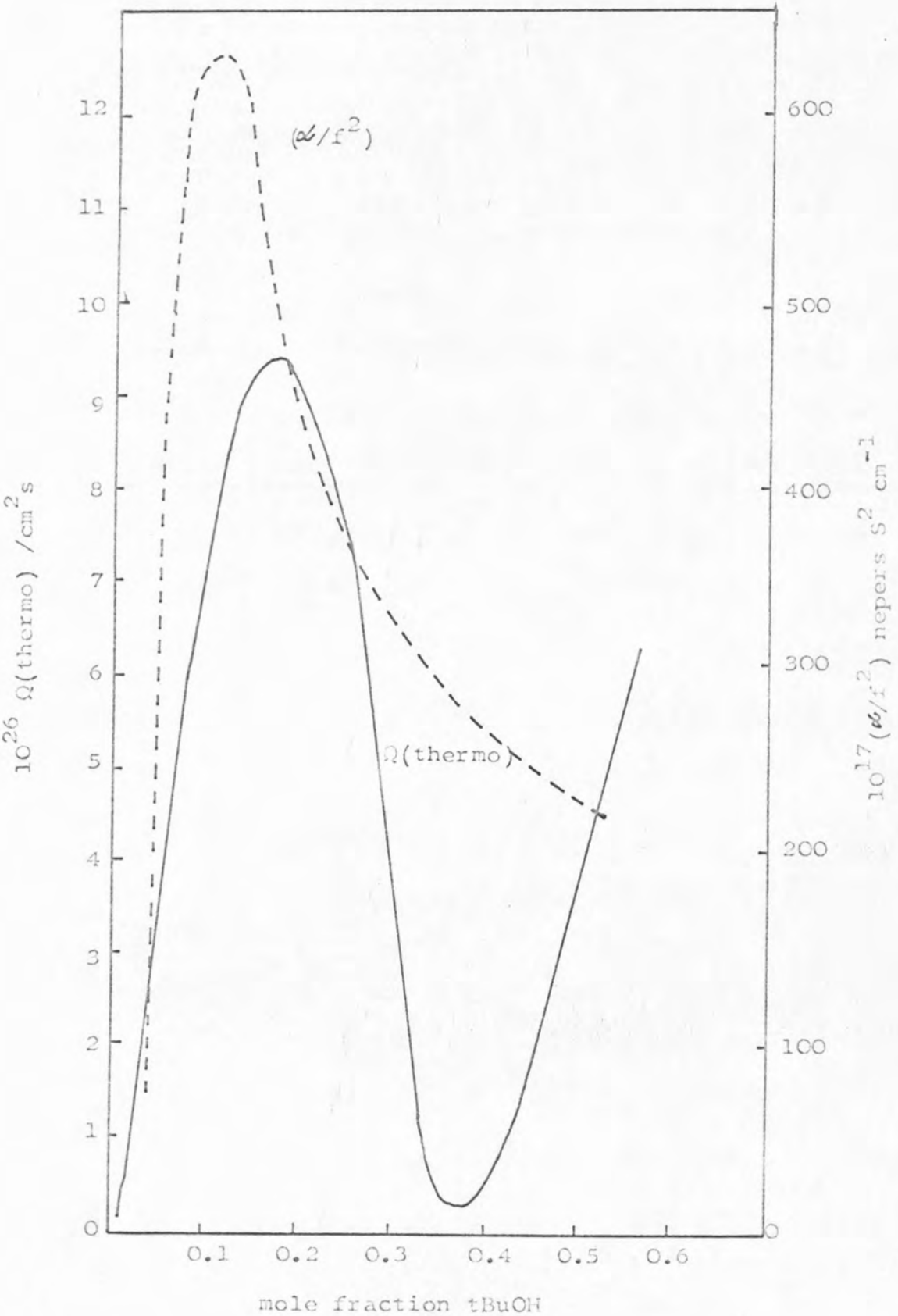

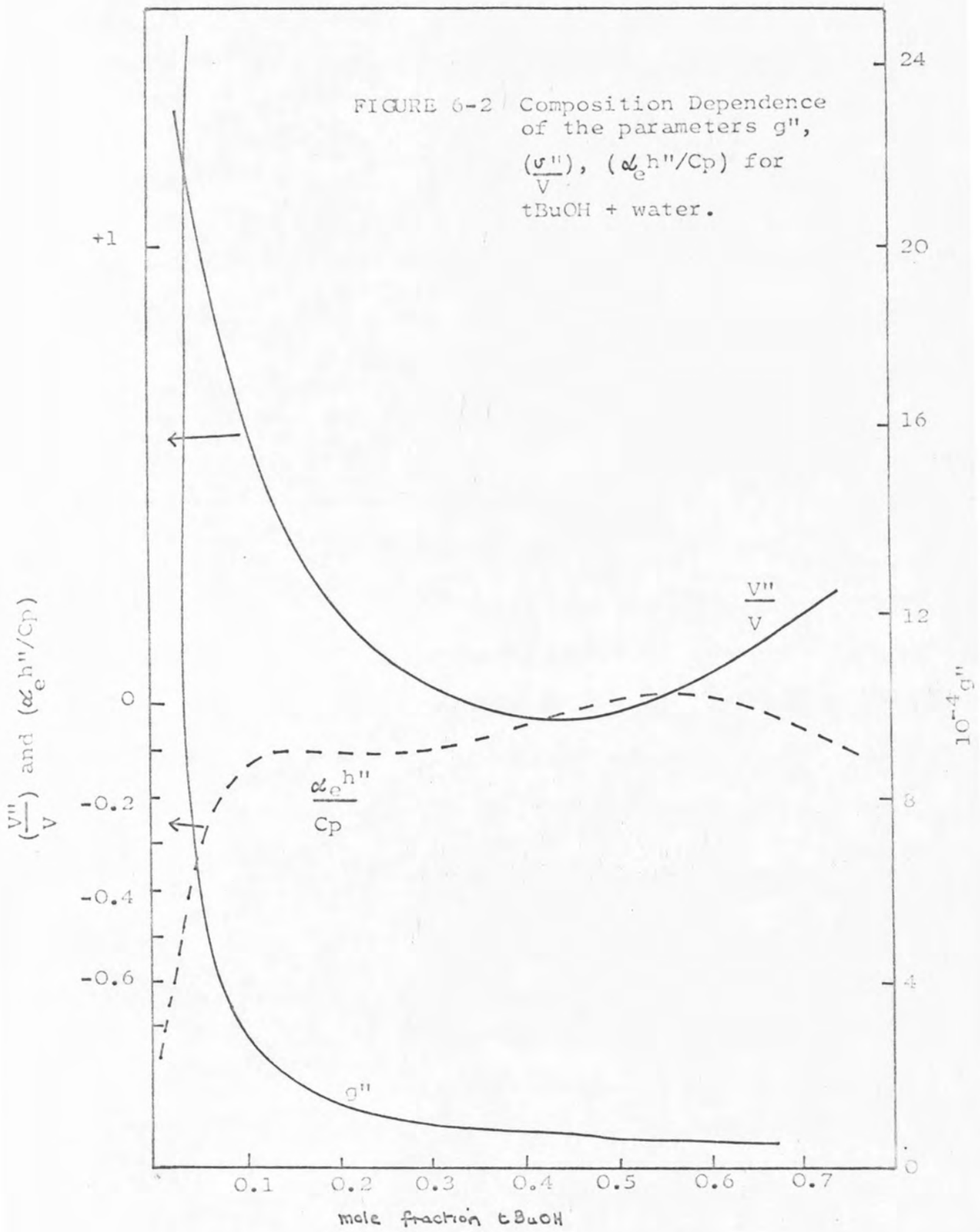
FIGURE 6-2 Composition Dependence of the parameters g", $(\frac{v''}{V})$, $(\alpha_e h''/Cp)$ for tBuOH + water.
+1
0
-0.2
-0.4
-0.6
24
20
16
12
8
4
0
$(\frac{V''}{V})$ and $(\alpha_e h''/Cp)$
$10^{-4} g''$
$\frac{V''}{V}$
$\frac{\alpha_e h''}{Cp}$
g"
0.1
0.2
0.3
0.4
0.5
0.6
0.7
mole fraction tBuOH

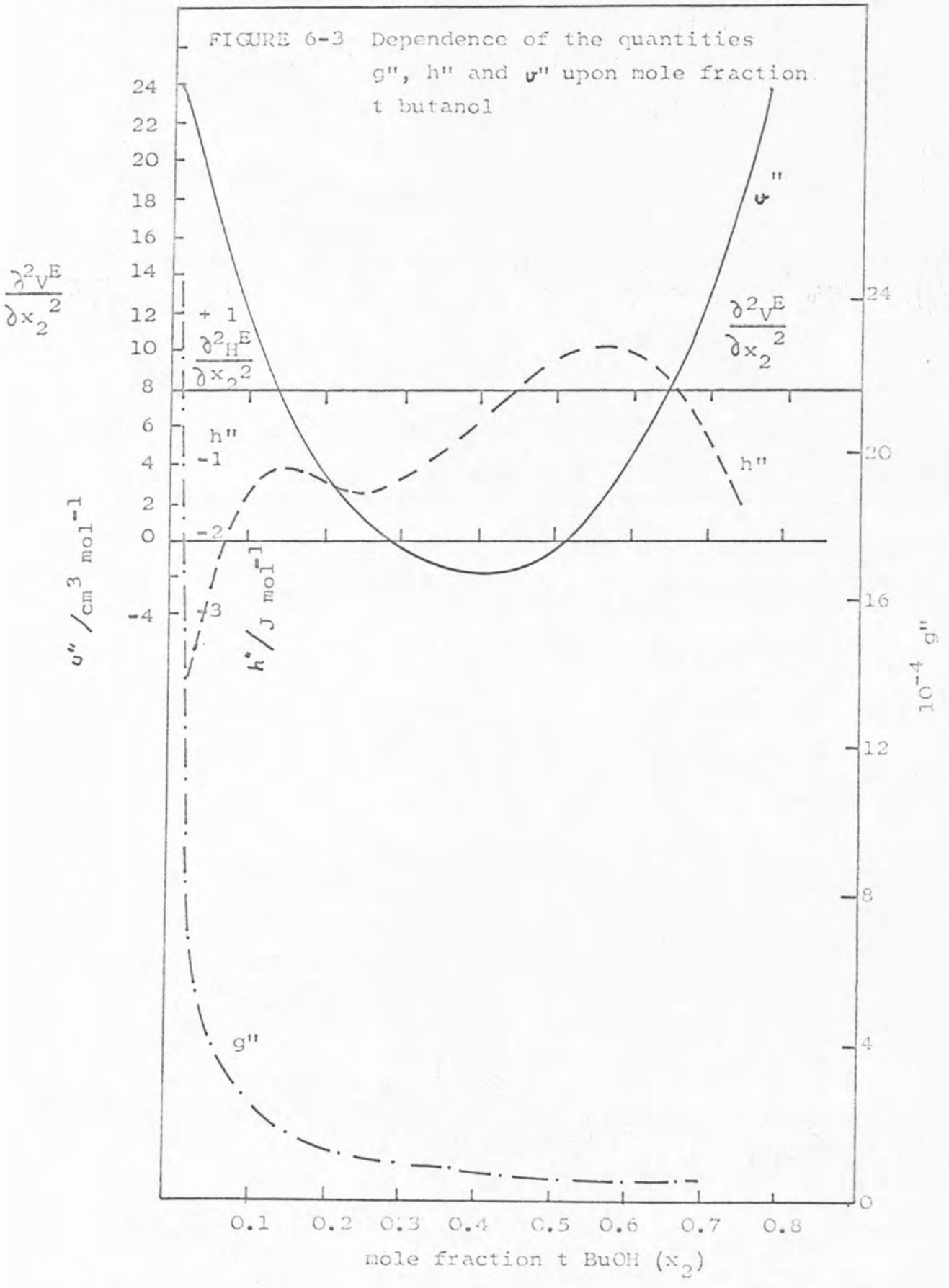
FIGURE 6-3 Dependence of the quantities g", h" and υ" upon mole fraction t butanol
$\frac{\partial^2 V^E}{\partial x_2^2}$
+ 1 $\frac{\partial^2 H^E}{\partial x_2^2}$
h" -1
-2
-3
υ" /cm³ mol⁻¹
h* /J mol⁻¹
g"
υ"
h"
$\frac{\partial^2 V^E}{\partial x_2^2}$
10⁻⁴ g"
24
22
20
18
16
14
12
10
8
6
4
2
0
-4
0.1 0.2 0.3 0.4 0.5 0.6 0.7 0.8
mole fraction t BuOH (x_2)

quantities g", h", v" which were evaluated from the excess function measurements in reference 185 using the technique discussed in Chapter 5.

Some difficulty was experienced in obtaining values of α_e, the coefficient of expansion and C_p, the heat capacity as a function of composition. Thus values for these two quantities had to be estimated. It was found that the analysis was not significantly affected by small variations in these two quantities. One final point regarding the accuracy of the analysis is relevant. The magnitude of Q (therm) evaluated is critically dependent upon the second derivatives of the excess thermodynamic functions of mixing. Thus these derivatives cannot be obtained by taking tangents to a plot of X^E versus x_2 but must be derived using an analytical method similar to that described in Chapter 5.

Tables of the input data to the program (entitled QCALC) and the values of Q, g", h", v", $\alpha_e h''/Cp$ and v''/V output by the program are given in Appendix 6-1.

(ii) The Significance of Q (therm.)

In the last chapter it was noted that the Q factor calculated from thermodynamic measurements should behave in a manner similar to α/f^2. At least the form of a plot of Q (therm.) versus x_2 should have a shape similar to a plot of α/f^2 versus x_2. Figure 6-1 confirms this prediction.

The quantity Q (therm.) is relatively small over the range $0 \leq x_2 \leq 0.03$, where α/f^2 is only slightly different from that of water and then rises sharply to a maximum close to the composition at which (α/f^2) is a maximum (at $x_2 = 0.17$). Unfortunately the high melting point of t butyl alcohol precludes extension of the comparison between Q and (α/f^2) to higher mole fractions. At low alcohol mole fractions σ''/V and $\alpha_e h''/Cp$ would combine to yield a large value of Q (Figure 6-2) but this is prevented by large values of g". As more alcohol is added g" decreases and up to $x_2 = 0.1$ the volume parameter (σ''/V) becomes increasingly more important. However, it should be noted that the enthalpy term $(\alpha_e h''/Cp)$ is not negligible. The decrease in Q (therm.) following the maximum at about $x_2 = 0.17$ arises initially from the decrease in (σ''/V) while $(\alpha_e h''/Cp)$ remains relatively constant.

At $x_2 = 0.365$, Q (therm.) is almost zero since (σ''/V) and $(\alpha_e h''/Cp)$ are small and g" is small and changing very slowly.

Previously the mole fraction for which (α/f^2) changes rapidly ($x_2 = 0.04$), was linked with the minimum in the partial molar volume.[6,35] It is now clear that the trends in the volume dependent parameters would require rapid variations in the absorption which g" essentially offsets, at least initially. The intense maximum in Q (thermo) at $x_2 = 0.17$ bears out the previous conclusion[7,185] that water is an important feature in systems with intense ultrasonic

absorptions. This clearly demonstrates that the link between ultrasonic absorption and the excess thermodynamic functions of mixing is a key one.[1]

6-2 ACETONE + WATER

The ultrasonic absorption properties of mixtures of acetone and water were presented in Chapter 4. The velocity of sound in these mixtures has been reported by Burton.[22,171] Heats of mixing,[172,186-188] liquid-vapour equilibrium[189-192] and density measurements[193-197] have been reported by many groups of workers.

Frank and Quist[173,198] have characterised a solid hydrate of acetone and water, the composition of which, as noted in Chapter 4, corresponds to the end of the plateau region.

(i) Calculation of Q (thermo)

The calculation of values of Q (thermo) at 293 K was carried out as described in Chapter 5 (see Appendix 6-2). The excess volumes of mixing were calculated from the density measurements of Young[197] and used to evaluate v". Heats of mixing were obtained from a compilation by Mobius,[172] and used to calculate h". Excess free energies of mixing were calculated from the liquid-vapour equilibrium data of Taylor[189] using the method of Barker.[181,199] These values were used in the evaluation of g" as a function of mixture composition.

Sound velocity measurements reported by Jacobson[171] were used together with estimated values for the expansion coefficient α_e and the molar specific heat C_p. The values of Ω (thermo) at 293 K were then computed at various mole fractions of acetone (x_2) and are shown in Figure 6-4 together with (α/f^2) at 298 K for comparison.

The parameters g", (υ''/V) and ($\alpha_e h''/Cp$) are shown as a function of composition in Figure 6-5.

(ii) The Significance of Ω (thermo)

The striking feature of Figure 6-4 is the close correspondence of the predicted and observed plateau lengths (x_2 = 0.06).

From Figure 6-5 it is clear that in the region where the concentration of acetone is low, the value of g" is large, υ''/V and $\alpha_e h''/Cp$ are quite often small, and thus the plateau region is again dominated by the magnitude of g". As the concentration of acetone is increased beyond 0.06 mole fraction, the term υ''/V shows a dramatic increase and the value of g" becomes very small.

Further examination of Figure 6-5 reveals that the term $\alpha_e h''/Cp$, although initially large, is offset by the terms υ''/V and g".

Thus the 'plateau region' would seem to be dominated by g", whilst the region of peak sound absorption, and the initial rise to this peak, are dominated by the volume parameters (υ''/V). The correspondence between the predicted

FIGURE 6-4 Comparison of (α/f^2) and Ω(thermo) for acetone+ water mixtures at 293 K

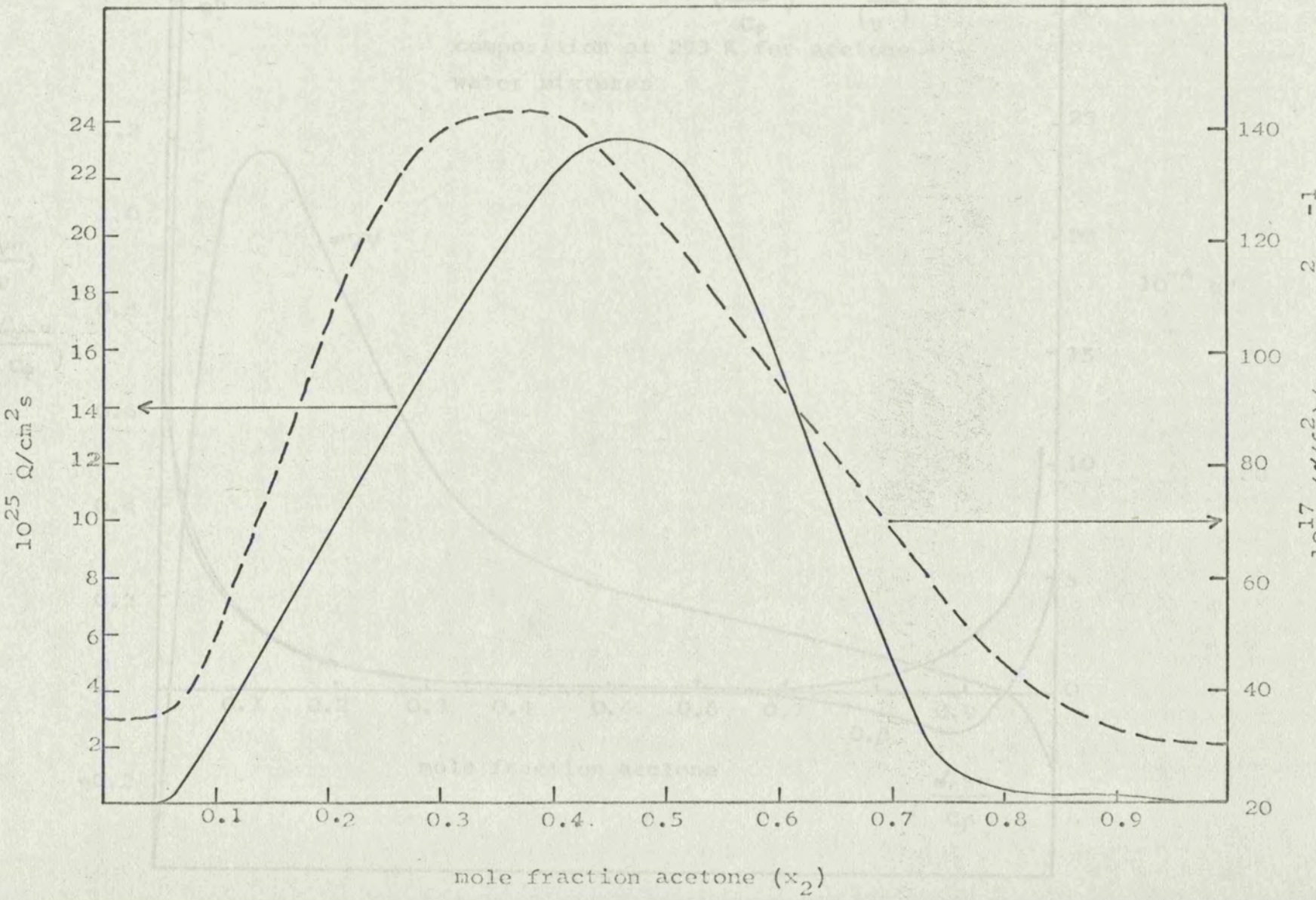

FIGURE 6-5 Dependence of g", $(\frac{\alpha_{eh}''}{C_p})$ and $\frac{v''}{(V)}$ upon composition at 293 K for acetone + water mixtures

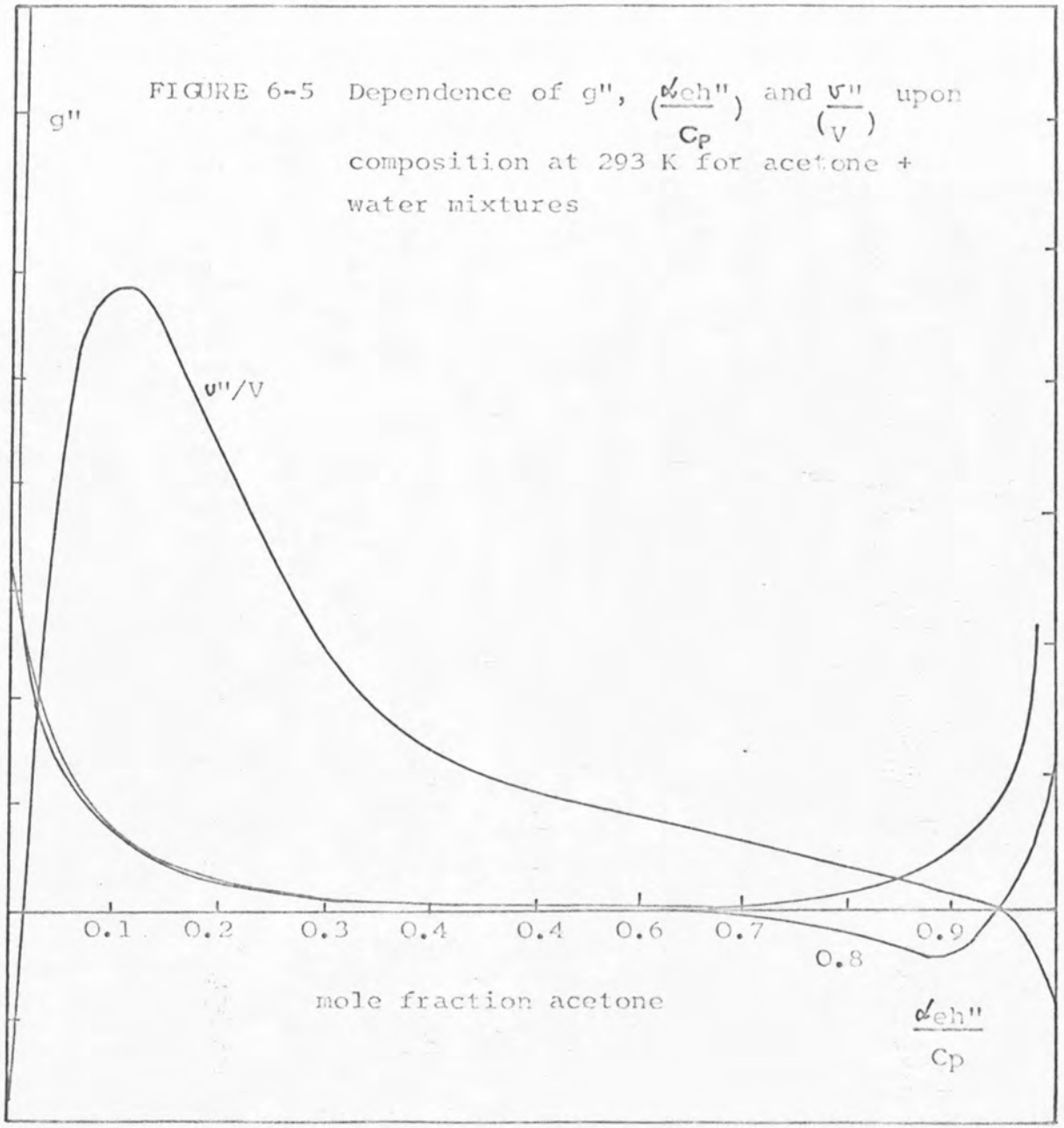

or $(\frac{V''}{V})$ $\frac{\alpha_{eh}''}{(C_p)}$

(x_2 = 0.46) and observed (x_2 = 0.38) peak sound absorption compositions is not so close as in the 'plateau region'. This may, however, be due in part to the approximations used for α_e and Cp in the calculation.

This would again seem to support the close link provided by the Romanov-Solovyev theory between thermodynamic observables and ultrasonic parameters.

(iii) Analysis in terms of the Discrete Relaxation Approach

The ultrasonic absorption data presented in Chapter 4-3 has been analysed using equation (5-2), for a single relaxation process. The results of this analysis are given in Table 6-1. Certain general trends in the relaxational behaviour are clear. Firstly, the relaxation frequency increases with concentration up to x_2 = 0.3 mole fraction, except at 273 K. Secondly, the relaxation frequency increases with decrease in temperature. The relaxation frequency in general is around a value of 50 to 70 MHz. This means that the relaxation process giving rise to the absorption has an associated relaxation time lying in the range 2×10^{-8} to 1×10^{-8} seconds.

The results were examined in terms of two relaxations. A better fit of the experimental data to the computed curve was observed, but this is only to be expected in view of the larger number of variables (5) involved in the minimisation. Until better experimental accuracy can be obtained with the present apparatus, the analysis of data in terms

TABLE 6 - 1 Relaxation Parameters.

298 K	$10^{17}A$	10^{6} fc	$10^{17}B$	RMS
x_2	nepers s^2 cm^{-1}	Hz	nepers s^2 cm^{-1}	
0.1	15	5	33	-
0.3	69	60	69	0.06
0.4	67	34	79	0.05

283 K	$10^{17}A$	10^{6} fc	$10^{17}B$	RMS
x_2	nepers s^2 cm^{-1}	Hz	nepers s^2 cm^{-1}	
0.1	18	59	41	0.07
0.3	115	70	66	0.08
0.4	103	70	83	0.08

273 K	$10^{17}A$	10^{6} fc	$10^{17}B$	RMS
x_2	nepers s^2 cm^{-1}	Hz	nepers s^2 cm^{-1}	
0.1	33	78	59	0.05
0.3	116	67	115	0.07
0.4	134	67	105	0.08

of two relaxation processes is probably invalid. However, if a cage-like interstitial model is to be accepted, then two relaxations would be predicted associated with the equilibria between cavities containing zero, one and two molecules of acetone. This assumes, however, that these two equilibria are not concerted or very fast (> about 10^{-12}s).

6-3 METHYL CYANIDE + WATER MIXTURES

Ultrasonic absorption properties for mixtures of water and methyl cyanide have been reported at 273, 298 and 308 K over the frequency range 1.5 to 230 MHz by Foster.[34,35,148] Sound velocities have been measured[34] at 273, 298 and 308 K and are presented in Chapter 4-2. Methyl cyanide + water mixtures show an upper critical solution temperature at 272.10 $\pm$ 0.2 K at a composition corresponding to 0.38 $\pm$ 0.02 mole fraction of methyl cyanide.[35] For this system a plot of (α/f^2) against x_2 at 4.5 MHz has a peak sound absorption composition (PSAC) at x_2 = 0.4 mole fraction. The intensity of the absorption at the PSAC increases with decrease in temperature to a greater extent than the intensity at the PSAC in t butyl alcohol + water mixtures,[7] a system showing a tendency to phase separation but with a LCST.[45,51] The increased sensitivity to temperature of $(\alpha/f^2)_{max.}$ for methyl cyanide + water mixtures may well be due to the combined effects of those processes which bring about absorption in the alcohol and those which bring about absorption in mixtures close to

their critical point. Based on the assumption that this is correct, there are grounds[21,138,200,201] for suggesting that α/f^2 should continually rise with decrease in frequency and not level off.

(i) Calculation of Ω (thermo)

Values of Ω (thermo) were calculated as described (equation 5-49) using the enthalpies of mixing reported by Morcom and Smith,[110] the excess volume measurements of Armitage et al,[35] and the liquid-vapour equilibrium data of Vierk.[170] The liquid-vapour equilibrium data was used to compute values of G^E, the excess Gibbs function of mixing as a function of mixture composition using the method of Barker.[181,199] Values of the molar heat capacity Cp and coefficient of expansion α_c were estimated from literature data.[202,203]

The computed Ω (thermo) factors are displayed, together with (α/f^2) at 4.5 and 70 MHz and 273 and 298 K in Figure 6-6 as a function of mixture composition. The dependence of the quantities v^u/V, $\alpha_c h^n/Cp$ and g'' upon mixture composition is shown in Figure 6-7. The data is also presented in detail in Appendix 6-3.

(ii) Analysis in terms of the Concentration Fluctuation Model

A method of deriving the parameters Ω, l_m, D and B from the Romanov-Solovyev equation (equation (5-48)) was described in Chapter 5-3. This method has been employed

FIGURE 6-6 Comparison of (a) Q(thermo); (b) α/f^2 at 273 K and 4.5 MHz; (c) α/f^2 at 273 K and 70 MHz; (d) α/f^2 at 298 K and 70 MHz; (e) α/f^2 at 298 K and 4.5 MHz

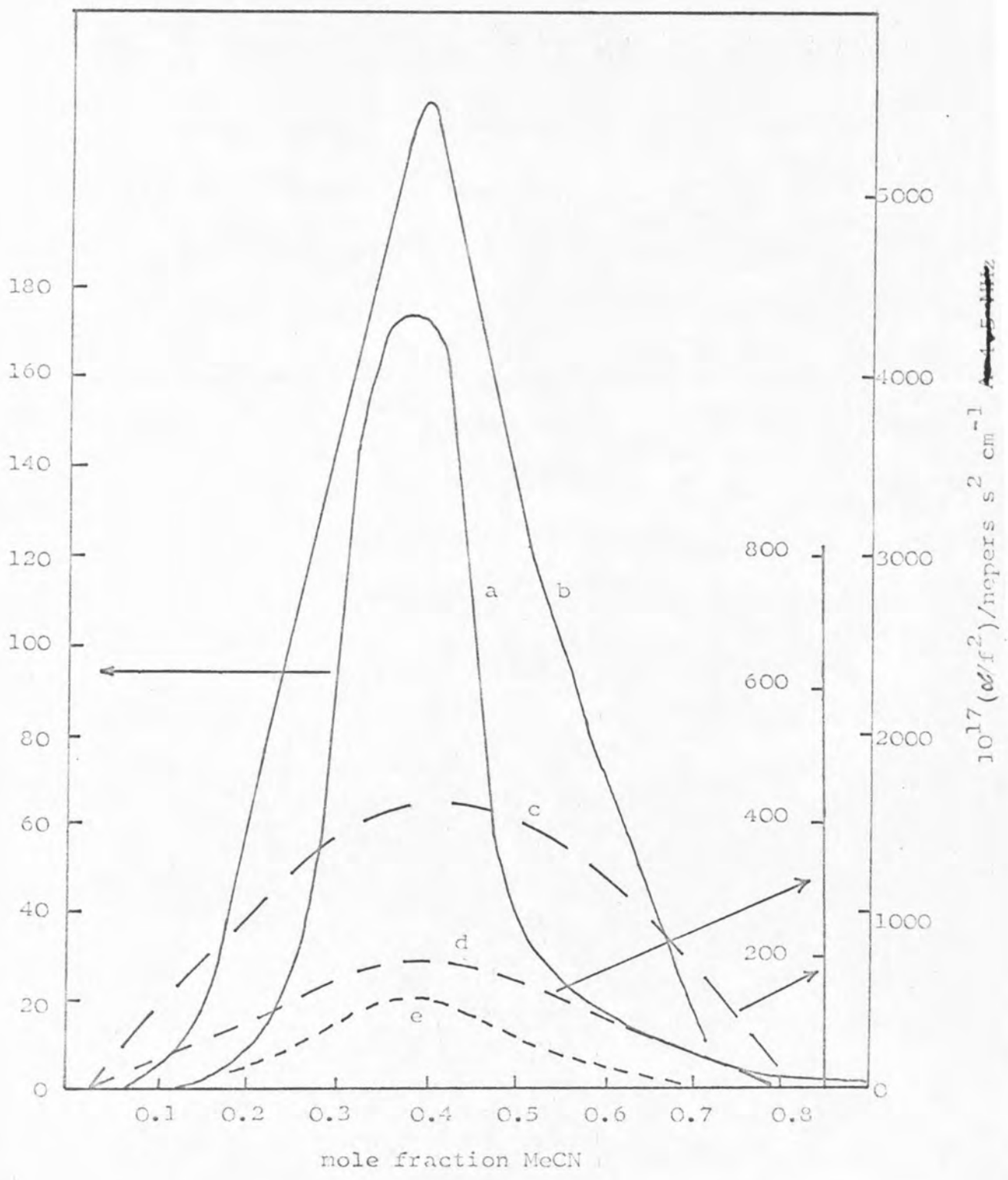

FIGURE 6-7 Variation of g", $(\frac{\alpha_{eh}''}{C_p})$, and (υ''/V) with mixture composition for methyl cyanide + water mixtures

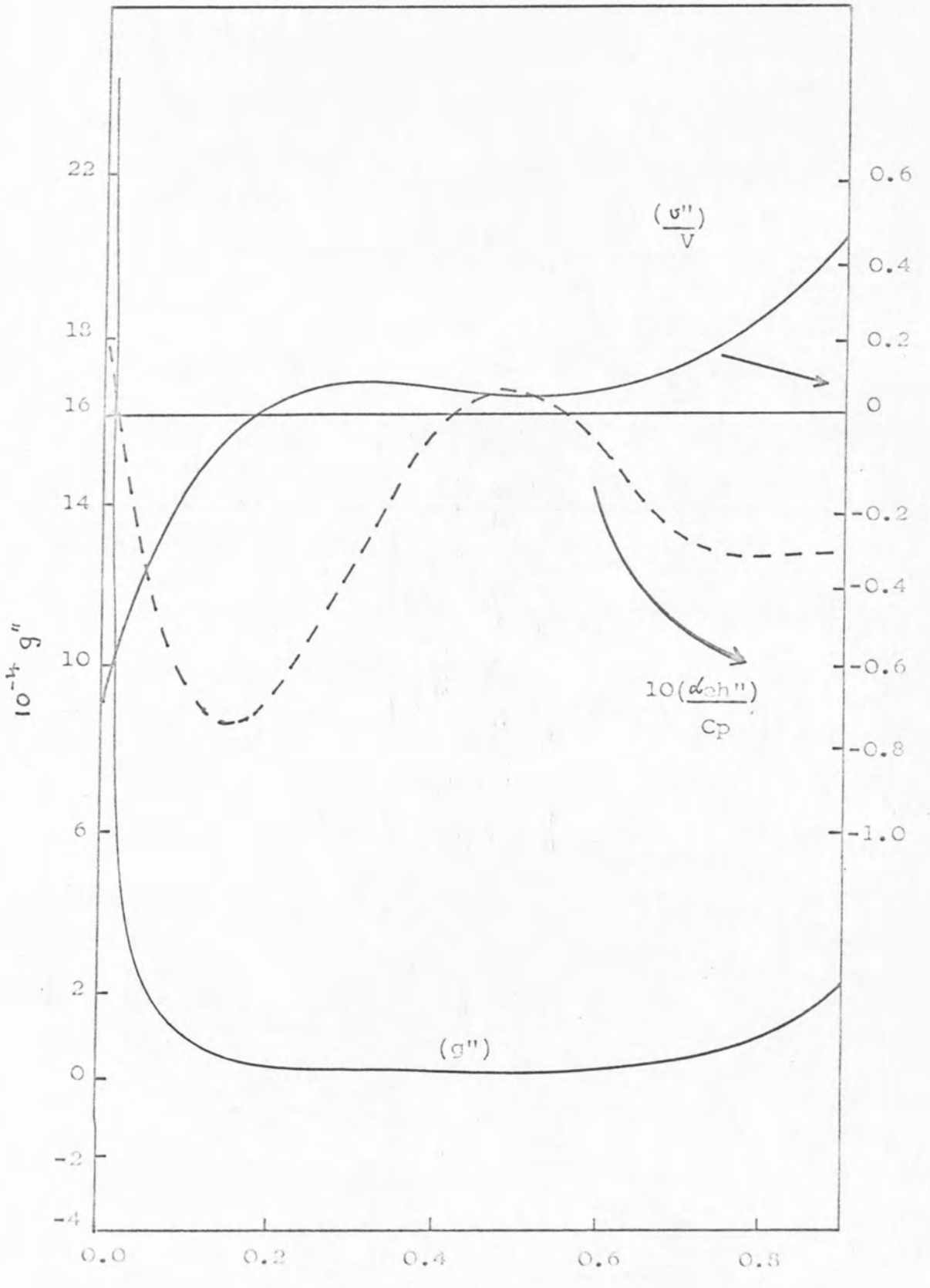

to derive the parameters from the dependence of (α/f^2) on frequency at 273 K using an ALGOL program (RSCF - see Appendix 5-3). The program required a provisional estimate of the four parameters which it then refined to minimise the sum of the squares of the deviations.

In some cases difficulty was experienced in obtaining a satisfactory fit (tested by the variation in the root-mean-square deviation) of the experimental points to the equation. One reason for this difficulty was the occurence of the product and ratio ($D\,l_m$ and $l_m^2/2D$) in equation (5-48). This also would account for the lack of success in deriving the parameters at 298 K, where the difference between the low and high frequency values of (α/f^2) is less than 1000×10^{-17} nepers.s^2.cm^{-1}. The analysis was successful, however, at 273 K and the derived parameters Q, l_m, D are presented in Figure 6-8.

The dotted curves shown in Figure 6-9 represent the computed 'best fit' curve resulting from the application of the Romanov Solovyev equation (equation (5-48)) to the data at 4.5 MHz and 273 K. (x_2 = 0.1; 0.3; 0.5 mole fraction MeCN). A table of the data obtained at each composition is presented in Appendix 6-4.

(iii) Analysis using the Discrete Relaxation Equation

The ultrasonic absorption data measured over the range 1.5 to 230 MHz were fitted to equation (5-2) using the new weighted version of the regression program described

FIGURE 6-8 Parameter obtained by curve fitting ultrasonic absorption data at 273K for methyl cyanide+water(____) diffusion coefficient,(----)Ω,(_ _ _) interaction length..

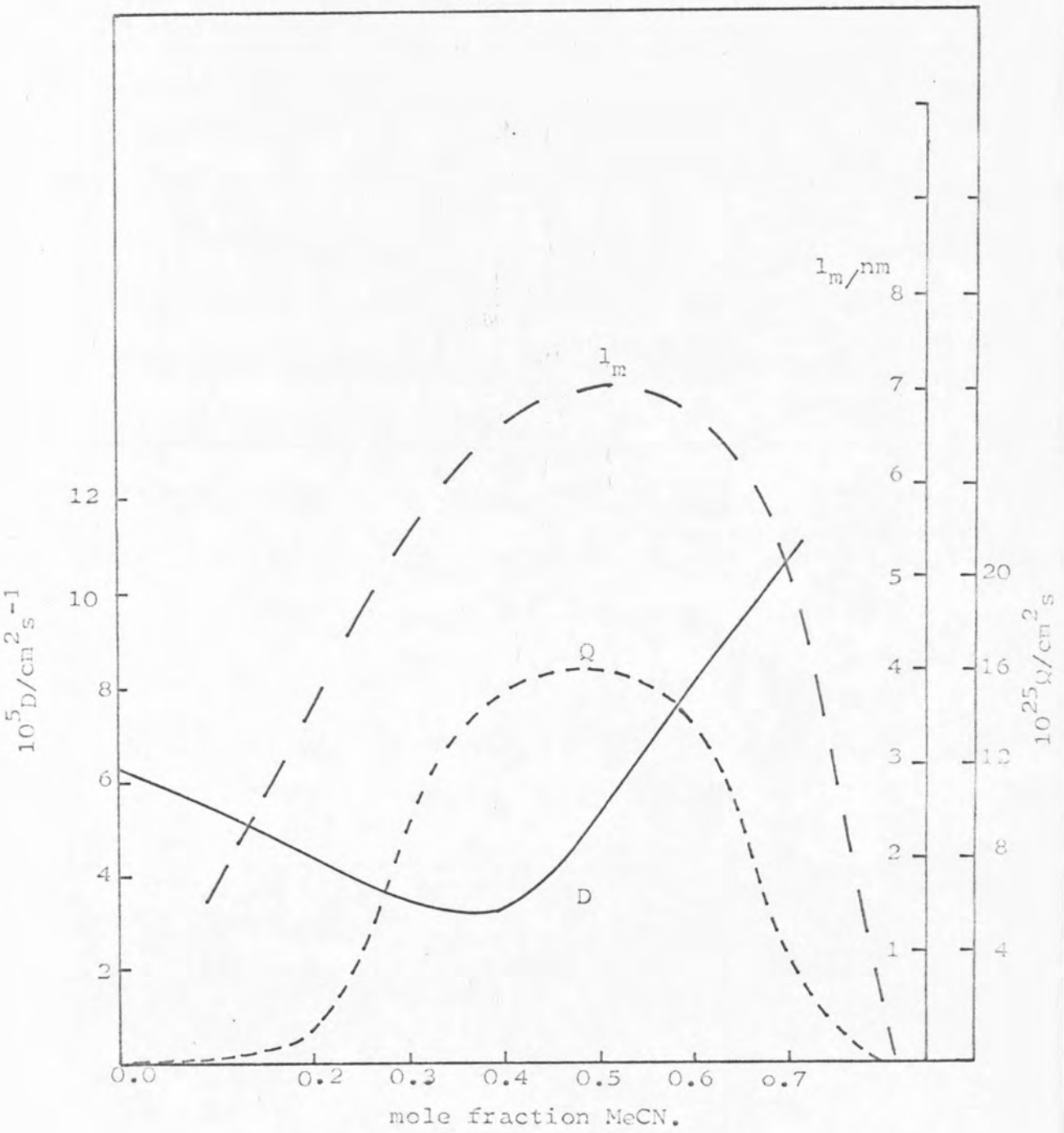

FIGURE6-9 Variation of ultrasonic absorption over the range 1.5-230MHz at 273K showing Romanov-Solovyev (----) and two relaxation curves (___) for three typical compositions.

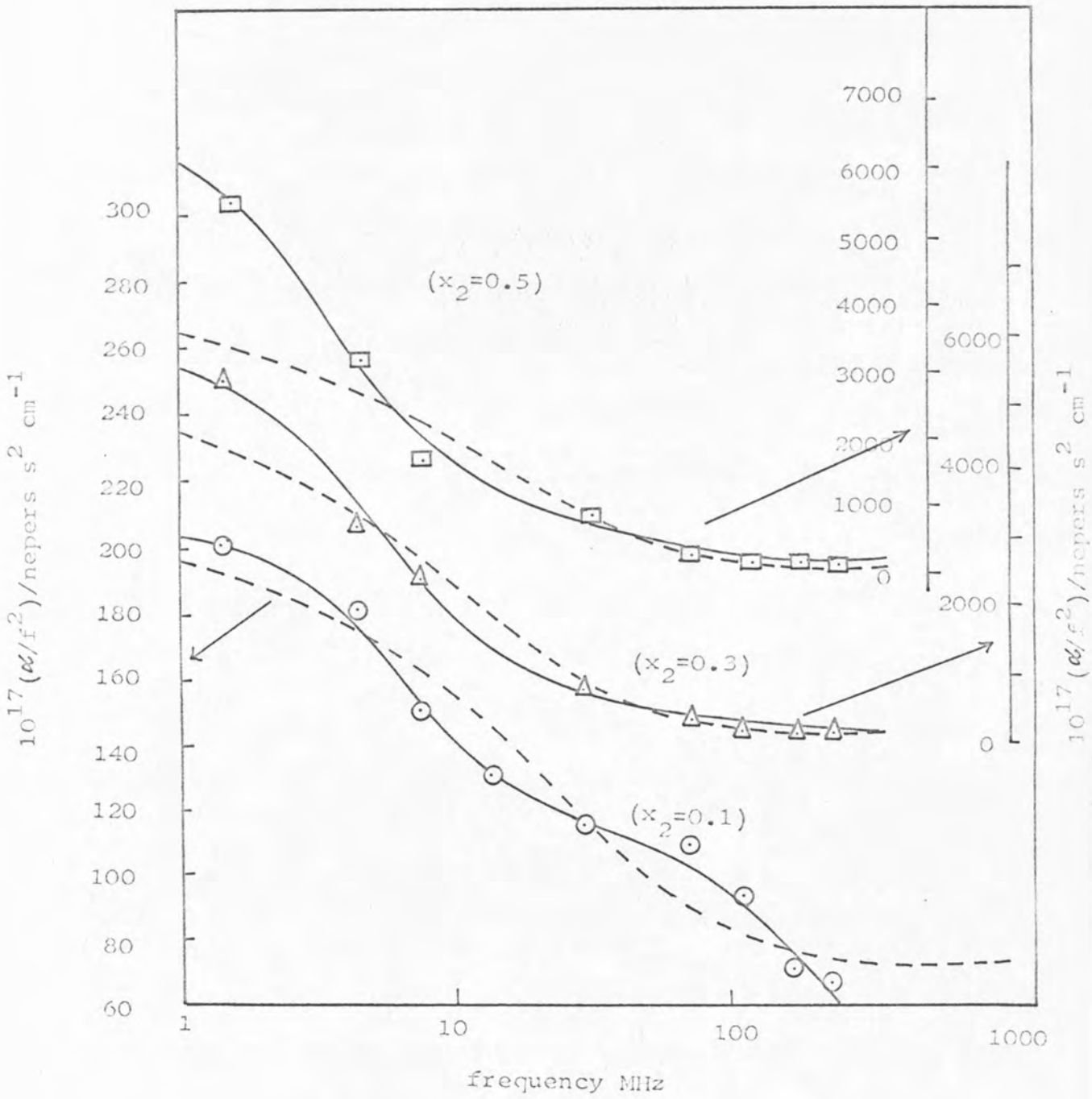

in Chapter 5-2. An original estimate of the values of the parameters was required and this was obtained from a graphical representation of the data. These values were then refined to constant minimum root-mean-square deviation. Each point was given an equal weighting such that the final sum of the squares of the deviations (F) was equally sensitive to each data point. Thus a point corresponding to a large ($> 1000 \times 10^{-17}$ nepers s^2 cm^{-1}) absorption could not dominate the magnitude of F. This had been the case in a previous analysis.[148]

The fit obtained for a single relaxation (n = 1 in equation (5-2)) was unsatisfactory. Since there were only nine experimental points, any analysis for more than two relaxations (n = 2 in equation (5-2)) is invalid. Thus an analysis for two relaxations was carried out for five variable parameters (average root-mean-square deviations ~ 0.03 - normalised). The results are presented in Appendix 6-5 and the values of $\mu_{max}(1)$ and $\mu_{max}(2)$ (cf equation (5-3)) are represented in Figure 6-10. Both $\mu_{max}(1)$ and $\mu_{max}(2)$ show a peak at $x_2 = 0.4$ mole fraction, whereas using the unweighted program no correlation was obtained.[148]

The relaxation frequency $f_c(1)$ was relatively insensitive to composition (1.5 to 6 MHz over the range $0.1 \leq x_2 \leq 0.7$ mole fraction), whereas the relaxation frequency $f_c(2)$ initially changed rapidly from 145 MHz at $x_2 = 0.1$ to 60 MHz at $x_2 = 0.2$ and thereafter varied over the range 34 to 50 MHz. The computed 'relaxation' curves are compared in Figure 6-9 with the observed

FIGURE 6-10 Dependance of the maximum relaxation strength upon composition (⊙) $\mu_{max}(1)$; (X) $\mu_{max}(2)$.

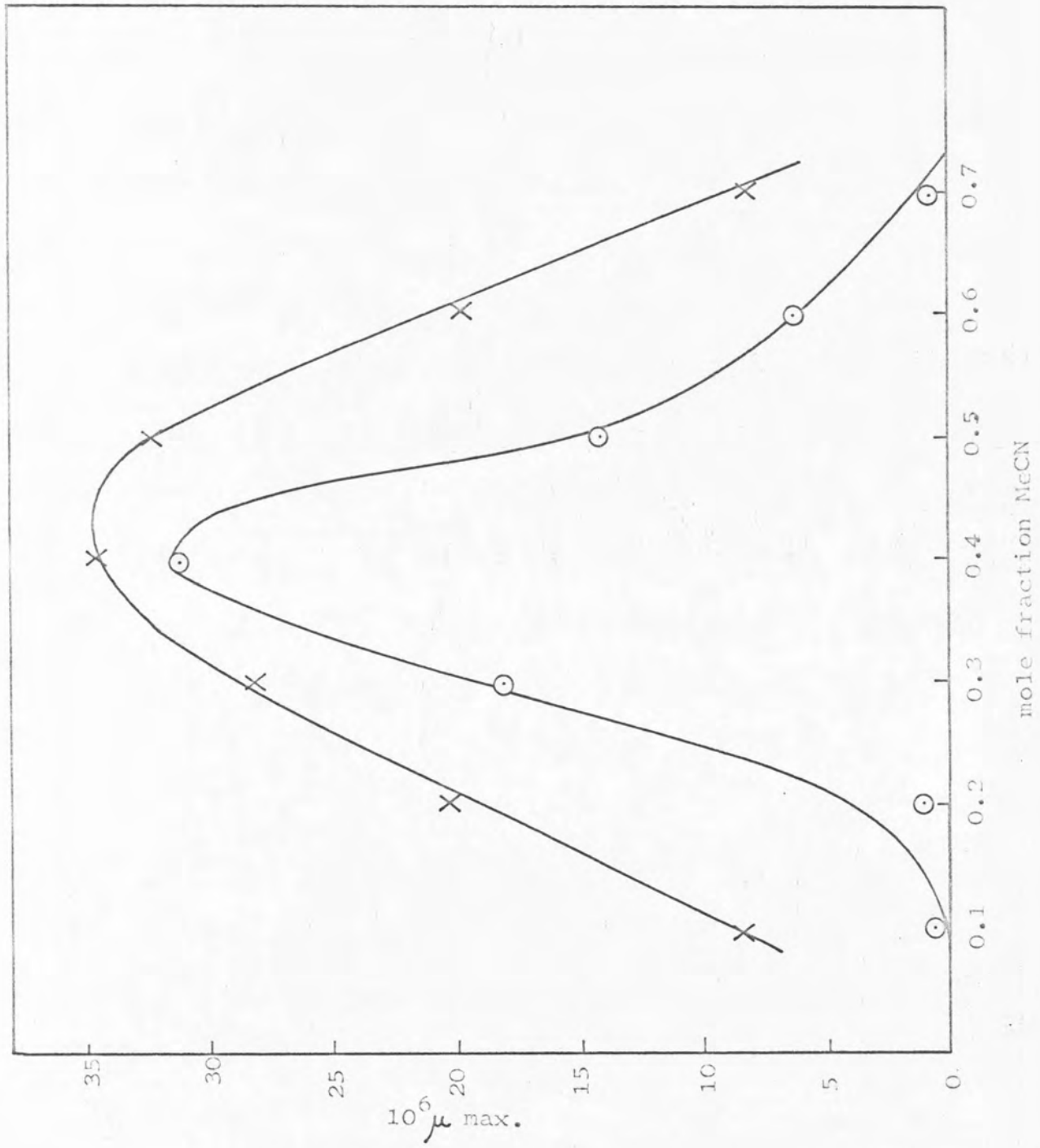

frequency dependence of α/f^2. The total absorption at 298 K was insufficiently large to place any great confidence on the parameters but the shape of the curve produced was consistent with equation (5-2). Figure 6-9 compares these curves at 298 K with the observed frequency dependence of α/f^2.

(iv) Discussion of Results for the System Methyl Cyanide + Water and Comparison with t Butyl Alcohol + Water

For the methyl cyanide + water system the maxima in Q (thermo) and α/f^2 correspond to 0.4 molefraction of methyl cyanide. In t butyl alcohol + water mixtures Q (thermo) shows little variation over the range $0 \leqslant x_2 \leqslant 0.04$, the range for which α/f^2 is insensitive to added alcohol. That such a region also exists in methyl cyanide + water mixtures is not clear from the experimental data, but the calculated values of Q (thermo) suggest strongly that such a region does exist (Figure 6-6). Evidence in support of the suggestion that the thermodynamic excess functions of mixing and the excess ultrasonic absorption are strongly linked[59] is provided by the close agreement between the values of Q calculated from thermodynamic data (Q (thermo)) and the values of Q derived from fitting equation (5-48) to the experimental data. Thus the importance of enthalpy or volume parameters in determining the absorption can be assessed. The major problem in applying equation (5-5) has been in separating the terms $\Delta V^{\ominus}$ and $\Delta H^{\ominus}$. Usually one of these terms is

assumed to be zero , i.e. '$\Delta V^{\ominus} = 0$' for conformational isomerisms and '$\Delta H^{\ominus} = 0$' for equilibria in water. For MeCN + water the quantities (v''/V) and g'' remain fairly constant over the region $0.2 \leqslant x_2 \leqslant 0.7$. Thus the marked changes in Q (thermo), and consequently in (α/f^2), arise from the concentration dependence of ($\alpha_e L''/Cp$). For t butyl alcohol + water mixtures it is (v''/V) which seems to be the controlling parameter.[1] The fact that the enthalpy dependent term dominates the absorption in methyl cyanide + water mixtures can be linked with the presence of an upper critical solution temperature which is usually the case for mixtures where enthalpy of mixing, ΔH^m, controls the sign and magnitude of G^E.[51]

The analysis using equation (5-48) reveals, however, that α/f^2 is not totally controlled by Q, but that the frequency dependent term leads to a mutual diffusion coefficient D and an interaction length l_m (see Figure 6-8).

The minimum in the diffusion coefficient close to $x_2 = 0.4$ mole fraction is consistent with the model which requires that the lower the diffusion coefficient, the less rapid the re-establishment of equilibrium, and thus the greater the contribution to the out of phase component of the isentropic modulus, i.e. the absorption. No independent measurements of the diffusion coefficients for methyl cyanide + water mixtures have been reported, but (α/f^2) often shows a maximum at the composition for which the diffusion coefficient shows a minimum for other systems.[204-206] l_m describes the distance over which the

composition fluctuations can correlate and shows a maximum close to x_2 = 0.4 mole fraction.

The treatment of Romanov and Solovyev predicts that α/f^2 should vary smoothly with frequency. This is a consequence of the assumption of a distribution of relaxation times. Unlike the thermal relaxation equation, the equation of Romanov and Solovyev is unable to account directly for more than one 'relaxation' in the plot of α/f^2 against frequency. In order to use the treatment given by Romanov and Solovyev to account for two relaxations, the equation (5-48) would have to be rewritten as

$$\frac{\alpha}{f^2} = \sum_{\text{relaxations}} (Q/\omega) I(\Omega) + B' \qquad \ldots\ldots (6\text{-}1)$$

However, such an extension of the theory is probably unrealistic.

One method of interpretation of the results envisages that the water-water interactions encourage the methyl cyanide molecules to cluster and this process may clearly be approximated as a series of equilibria. At low temperatures the water-water interactions become so strong as to eject nearly all the methyl cyanide in the interstices, and this may be considered as phase separation. In contrast, the alcohols, which tend towards the formation of hydrates, are more easily accommodated at lower temperatures by water.

When x_2 = 0.5, (α/f^2) for MeCN + water apparently shows a continual rise with decrease in frequency. This

rise resembles that required by the theory of Fixman.[30] Possibly the experimental data at $x_2 = 0.5$ indicates a transition from systems where the composition fluctuations are small, to those where the fluctuations are large. However, it seems unlikely that this can be the complete explanation since the temperature is around 25 K from its critical temperature.

6-4 TETRA-ALKYLAMMONIUM SALTS + WATER

When tetra-n-butylammonium bromide is added to water, the ultrasonic absorption at 298 K and 70 MHz changes only slowly at first, but then shows a sharp increase at concentrations greater than 0.8 mol dm^{-3}.[148,207] In marked contrast, when tetraethylammonium bromide is added to water, the change in (α/f^2) is much more gradual, and the absorption much smaller. Aqueous solutions of alkylammonium salts have generated considerable interest[208,209] and Franks[52] has indicated the wide variety of experimental information available. The ultrasonic absorption properties remain puzzling, however. Atkinson[210] has considered a number of models based upon the concept of ionic association/dissociation equilibria. A further complication has been added by the discovery that the excess absorption may be a product of alkyl chain reorganisation.[211] A possible rationalisation of some of the ultrasonic absorption results with the observed thermodynamic behaviour has been obtained as a direct result of applying the Romanov

Solovyev treatment to these systems.[212]

(i) Application of the theory of Romanov and Solovyev to Aqueous Electrolyte Solutions

The analysis of the Romanov and Solovyev equation described in Chapter (5-3) is only directly applicable to binary liquid mixtures. The application of the analysis to aqueous electrolyte solutions is not so straightforward. The mole fraction (x_2) of alkylammonium salt in a solution containing m_2 moles of salt in 1 kg of solvent, relative molecular mass M_1, is defined as follows[213]

$$x_2 = m_2 \nu (\nu m_2 + 10^3/M_1)^{-1} \quad \ldots\ldots (6\text{-}2)$$

ν = 2 for tetra-alkylammonium salts.

The analysis is simplified by defining, for any given thermodynamic function X, the following quantities:

X(total) for a solution of molality m_2,
X(salt) which equals X(total)/m_2 and
X(solution) which equals X(total) $(2m_2 + 10^3/M_1)^{-1}$.

These properties are required in the analysis. A related set of excess functions X^E were also used. The standard state chemical potential for the salt is $\mu_2^\ominus$, where the standard state is the hypothetical 1 mol dm^{-3} solution with the mean activity coefficient $\gamma_\pm$ equal to one. The standard state for the solvent is the pure liquid when the osmotic coefficient ϕ is one, at constant pressure and temperature, and the chemical potential is μ_1°. The

problem is conveniently divided into two parts; (a) relating the required parameters g", h", v" to the excess functions, (b) curve fitting the excess functions to a suitable equation.

Gibbs Functions:

$$G(\text{total}) = n_1\mu_1 + n_2\mu_2 \quad \ldots\ldots (6\text{-}3)$$

The chemical potential of the solvent μ_1 may be written in two ways defined below. This leads to dual definition for G(total). A choice of the appropriate definition is controlled by the function used to evaluate G^E (total). Both of these definitions are derived below. Taking the solute as component (2) and the solvent as component (1);

For the solute: $\mu_2 = \mu_2^{\ominus} + 2RT \ln m_2\gamma_{\pm}$ . . . . . (6-4)

For the solvent: $\mu_1 = \mu_1^{\ominus} + RT \ln x_1 f_1$ . . . . . (6-5)

From the definition of the osmotic coefficient,[213] ϕ;

$$\ln x_1 f_1 = -2\phi m_2 (M_1/10^3) \quad \ldots\ldots (6\text{-}6)$$

thus; $$\mu_1 = \mu_1^{\ominus} - 2\phi m_2 RT (M_1/10^3) \quad \ldots\ldots (6\text{-}7)$$

Thus two definitions for G(total) may be derived;

$$G(\text{total}) = \frac{10^3}{M_1}\left[\mu_1^{\ominus} + RT \ln x_1 f_1\right] + m_2\left[\mu_2^{\ominus} + 2RT \ln m_2\gamma_{\pm}\right] \quad \ldots\ldots (6\text{-}8)$$

or

$$G(\text{total}) = \frac{10^3}{M_1}\left[\mu_1^{\ominus} - 2\phi RT m_2 M_1 10^{-3}\right] + m_2\left[\mu_2^{\ominus} + 2RT \ln m_2\gamma_{\pm}\right] \quad \ldots\ldots (6\text{-}9)$$

For an ideal mixture (or solution) $f_1 = 1$, $\phi = 1$ and $\gamma_{\pm} = 1$.

Thus two ideal Gibbs functions can be derived.

$$G(\text{ideal,total}) = \frac{10^3}{M_1}\left[\mu_1^{\ominus} + RT\ln x_1\right] + m_2\left[\mu_2^{\ominus} + 2RT\ln m_2\right] \quad \ldots (6\text{-}10)$$

or

$$G(\text{ideal,total}) = \frac{10^3}{M_1}\left[\mu_1^{\ominus} - \frac{2RT m_2 M_1}{10^3}\right] + m_2\left[\mu_2^{\ominus} + 2RT\ln m_2\right] \quad \ldots (6\text{-}11)$$

Using the relationship that

$$G^E(\text{total}) = G(\text{total}) - G(\text{ideal,total}) \quad \ldots (6\text{-}12)$$

two excess functions are derivable.

$$G^E(\text{total}) = (10^3/M_1)RT\ln f_1 + 2m_2RT\ln\gamma_{\pm} \quad \ldots (6\text{-}13)$$
$$= G^E(f_1, \gamma_{\pm}, \text{total})$$

or

$$G^E(\text{total}) = (10^3/M_1)2RT(1-\phi)\frac{m_2 M_1}{10^3} + m_2 2RT\ln\gamma_{\pm} \quad \ldots (6\text{-}14)$$
$$= G^E(\phi, \gamma_{\pm}, \text{total})$$

Rearranging equation (6-14) yields

$$G^E(\phi, \gamma_{\pm}, \text{total}) = 2m_2RT(1-\phi+\ln\gamma_{\pm}) \quad \ldots (6\text{-}15)$$

In general G^E per mol of salt is given by

$$G^E(\phi, \gamma_{\pm}, \text{total}) = 2RT(1-\phi+\ln\gamma_{\pm}) \quad \ldots (6\text{-}16)$$

Two definitions of G(total) are thus arrived at.

$$G(\text{total}) = \frac{10^3}{M_1}\left[\mu_1^{\ominus} + RT\ln x_1\right] + m_2\left[\mu_2^{\ominus} + 2RT\ln m_2\right] + G^E(f_1, \gamma_{\pm}, \text{total}) \quad \ldots (6\text{-}17)$$

or

$$G(\text{total}) = \frac{10^3}{M_1}\left[\mu_1^{\ominus} - \frac{2RT\, m_2 M_1}{10^3}\right] + m_2\left[\mu_2^{\ominus} + 2RT \ln m_2\right] + G^E(\phi, \gamma_{\pm}, \text{total}) \quad \ldots (6\text{-}18)$$

For a 1:1 electrolyte the total number of moles in solution will be $(2m_2 + 10^3/M_1)$.

Thus G = Gibbs function per mol total solution =

$$\frac{G(\text{total})}{(2m_2 + 10^3/M_1)} \quad \ldots (6\text{-}19)$$

so, using equation (6-2) with $\nu = 2$;

$$G = x_1\left\{\mu_1^{\ominus} + RT \ln x_1\right\} + \frac{x_2}{2}\left\{\mu_2^{\ominus} + 2RT \ln m_2\right\} + G^E(f_1, \gamma_{\pm}) \quad \ldots (6\text{-}20)$$

or

$$G = x_1\left\{\mu_1^{\ominus} - \frac{2RT\, m_2 M_1}{10^3}\right\} + \frac{x_2}{2}\left\{\mu_2^{\ominus} + 2RT \ln m_2\right\} + G^E(\phi, \gamma_{\pm}) \quad \ldots (6\text{-}21)$$

Note that $G^E(f_1, \gamma_{\pm})$ and $G^E(\phi, \gamma_{\pm})$ are both per mole of solution now.

If m_2 is substituted for in terms of x_2 and both equations (6-20) and (6-21) differentiated twice with respect to x_2 then

$$g'' = \frac{\partial^2 G}{\partial x_2^2} = \frac{RT}{x_2} + \frac{3RT}{(1-x_2)} + \frac{x_2 RT}{(1-x_2)^2} + \frac{\partial^2 G^E}{\partial x_2^2}(f_1, \gamma_{\pm}) \quad \ldots (6\text{-}22)$$

or

$$g'' = \frac{\partial^2 G}{\partial x_2^2} = \frac{RT}{x_2(1-x_2)^2} + \frac{\partial^2 G^E}{\partial x_2^2}(\phi, \gamma_{\pm}) \quad \ldots (6\text{-}23)$$

The relationship between the two derived excess functions is given by

$$\frac{\partial^2 G^E(\phi,\gamma_\pm)}{\partial x_2^2} = \frac{RT}{(1-x_2)} + \frac{\partial^2 G^E(f_1,\gamma_\pm)}{\partial x_2^2} \quad \ldots (6\text{-}24)$$

Now G^E(solution) = $\frac{x_2}{2}$ G^E(salt) and if G^E(salt) = y then;

$$\frac{\partial G^E(\phi,\gamma_\pm,\text{soln.})}{\partial x_2} = \frac{y}{2} + \frac{x_2}{2}\frac{\partial y}{\partial x_2}$$

and

$$\frac{\partial^2 G^E(\phi,\gamma_\pm,\text{soln.})}{\partial x_2^2} = \frac{\partial y}{\partial x_2} + \frac{x_2}{2}\frac{\partial^2 y}{\partial x_2^2} \quad \ldots (6\text{-}25)$$

$$\text{but } \frac{\partial y}{\partial x_2} = \frac{\partial y}{\partial m_2}\cdot\frac{\partial m_2}{\partial x_2} = \frac{\partial y}{\partial m_2}\cdot\frac{a}{(1-x_2)^2} \quad \ldots (6\text{-}26)$$

where $a = 10^3/M_1$ and so;

$$\frac{\partial^2 y}{\partial x_2^2} = \frac{2a}{(1-x_2)^3}\frac{\partial y}{\partial m_2} + \left[\frac{a}{(1-x_2)^2}\right]^2\frac{\partial^2 y}{\partial m_2^2} \quad \ldots (6\text{-}27)$$

This combination of equations (6-26), (6-25), (6-27) leads to the result

$$g'' = \frac{\partial^2 G}{\partial x_2^2} = \frac{RT}{x_2(1-x_2)^2} + \frac{a}{(1-x_2)^3}\frac{\partial y}{\partial m_2} + \frac{a^2 x_2}{2(1-x_2)^4}\frac{\partial^2 y}{\partial m_2^2} \quad \ldots (6\text{-}28)$$

A similar expression could have been derived using G^E (f_1, $\gamma_\pm$, solution). However, the available data in the literature provides values of ϕ and $\gamma_\pm$ as functions of m_2 mol dm^{-3}. Thus, for our purposes this definition in terms of ϕ and $\gamma_\pm$ is most useful.

Wu and Friedman,[214] have shown that for a general electrolyte the excess function X^E(salt,per mol) may be

expressed as

$$X^E(\text{salt}) = A_o m_2^{1/2} + E m_2 \ln m_2 + A_1 m_2 + \cdots \quad \ldots\ldots (6\text{-}29)$$

For a 1:1 electrolyte the coefficient E=0 and it was found convenient to extend the equation to the form

$$X^E(\text{salt}) = A_o m_2^{1/2} + \sum_{i=1}^{n} A_i m_2^i \quad \ldots\ldots (6\text{-}30)$$

If $y = X^E(\text{salt})$ then

$$\frac{\partial y}{\partial m_2} = \left(A_o / 2 m_2^{1/2}\right) + \sum_{i=1}^{n} i A_i m_2^{(i-1)} \quad \ldots\ldots (6\text{-}31)$$

and

$$\frac{\partial^2 y}{\partial m_2^2} = -\frac{A_o}{4 m_2^{3/2}} + \sum_{i=1}^{n} i(i-1) A_i m_2^{(i-2)} \quad \ldots\ldots (6\text{-}32)$$

Thus values of g'' as a function of composition can be calculated using equation (6-25) after deriving the quantities $\frac{\partial y}{\partial m_2}$ and $\frac{\partial^2 y}{\partial m_2^2}$ from equations (6-31) and (6-32) where $X^E(\text{salt}) = G^E(\phi, \gamma_{\pm}, \text{salt})$. This latter quantity can be calculated from equation (6-16).

Enthalpies

The derivation of expressions for the enthalpy parameter h'' follows from a similar analysis to that above. Consider a solution containing m_2 mol of solute (component 2) and $10^3/M_1$ mol of solvent (component 1).

The real total enthalpy H =

$$(10^3/M_1)\,\bar{H}_1 + m_2\,\bar{H}_2 \quad \ldots\ldots (6\text{-}33)$$

The ideal total enthalpy H_{id} =

$$(10^3/M_1)\,\overline{H_1^\circ} + m_2\,\overline{H_2^\circ} \qquad \ldots\ldots (6\text{-}34)$$

Now the relative molal heat content ϕ_H is defined such that the real total enthalpy is given by

$$H = (10^3/M_1)\,H_1^\circ + m_2\,\phi_H^\circ \qquad \ldots\ldots (6\text{-}35)$$

thus ϕ_H° is identified with H_2° .

But H^E(total) = H(real) - H(ideal)

$$= (10^3/M_1)(\overline{H}_1 - H_1^\circ) + m_2(\overline{H}_2 - \overline{H_2^\circ})$$

$$= m_2\,[\,\phi_H - \phi_H^\circ\,] \qquad \ldots\ldots (6\text{-}36)$$

Let L = H(real) - H(ideal) then

$$\overline{L}_1 = \overline{H}_1 - H_1^\circ \;;\; \overline{L}_2 = \overline{H}_2 - H_2^\circ \;;\; \phi_L = \phi_H - \phi_H^\circ$$

thus $\phi_L = H^E$ (per mol of salt) $\qquad \ldots\ldots (6\text{-}37)$

Hence,

$$H(\text{real, per mol solution}) = (1 - x_2)H_1^\circ + \frac{x_2}{2}\,H_2^\circ + \frac{x_2}{2}\,\phi_L$$

and so, differentiating twice with respect to x_2

$$h'' = \frac{\partial^2 H}{\partial x_2^2} = \frac{\partial \phi_L}{\partial x_2} + \frac{x_2}{2}\,\frac{\partial^2 \phi_L}{\partial x_2^2} \qquad \ldots\ldots (6\text{-}38)$$

This is the required form because ϕ_L is known as a function of m_2. This dependence is fitted to equation (6-30) and since,

$$\frac{\partial \phi_L}{\partial x_2} = \frac{\partial \phi_L}{\partial m_2} \cdot \frac{\partial m_2}{\partial x_2}$$

then,

$$h'' = \frac{\partial^2 H}{\partial x_2^2} = \left\{\frac{a}{(1-x_2)^3}\right\}\frac{\partial \phi_L}{\partial m_2} + \left\{\frac{a^2 x_2}{2(1-x_2)^4}\right\}\frac{\partial^2 \phi_L}{\partial m_2^2} \qquad \ldots\ldots (6\text{-}39)$$

Volumes

An analysis for V(total) and v'' similar to that described under Enthalpies follows.

$$\text{Real Volume} = V(\text{total}) = (10^3/M_1)\overline{V}_1 + m_2\overline{V}_2 \quad \ldots\ldots (6\text{-}40)$$

$$\text{Ideal Volume} = V_{id}(\text{total}) = (10^3/M_1)V_1^\circ + \overline{V}_2^\circ m_2 \quad \ldots\ldots (6\text{-}41)$$

The excess volume is given by;

$$V^E(\text{total}) = (10^3/M_1)(\overline{V}_1 - V_1^\circ) + m_2(\overline{V}_2 - V_2^\circ) \quad \ldots\ldots (6\text{-}42)$$

Thus the total volume may be expressed as;

$$V(\text{total}) = (10^3/M_1)\, V_1^\circ + m_2 V_2^\circ + V^E(\text{total}) \quad \ldots\ldots (6\text{-}43)$$

$$V(\text{per mol solution}) = x_1 V_1^\circ + \frac{x_2}{2}\, V_2^\circ + V^E(\text{per mol solution})$$

and differentiating this latter equation twice with respect to x_2 gives

$$v'' = \frac{\partial^2 V}{\partial x_2^2} = \frac{\partial^2 V^E}{\partial x_2^2} \quad \ldots\ldots (6\text{-}44)$$

but $\frac{\partial V^E}{\partial m_2} = \frac{\partial V^E}{\partial x_2} \cdot \frac{\partial x_2}{\partial m_2}$ and using this expression equation (6-44) becomes;

$$v'' = \frac{\partial^2 V}{\partial x_2^2} = \frac{2a}{(1-x_2)^3}\frac{\partial V^E}{\partial m_2} + \frac{a^2}{(1-x_2)^4}\frac{\partial^2 V^E}{\partial m_2^2} \quad \ldots\ldots (6\text{-}45)$$

Thus if V^E is fitted as a function of m_2 to equation (6-30), then values of v'' at various compositions can be derived. The usual experimental volume parameter is ϕ_v, the apparent molal volume.

$$\phi_v = \frac{V - x_1 V_1^\circ}{x_2} \quad \text{by definition} \qquad \ldots\ldots (6\text{-}46)$$

$V(\text{total}) = (10^3/M_1)\, V_1^\circ + m_2\, \phi_v$ and

$V_{id}(\text{total}) = (10^3/M_1)\, V_1^\circ + m_2\, \phi_v^\circ$ where ϕ_v° is the apparent molal volume at infinite dilution.

Hence V^E (per mol of solution) $= \frac{x_2}{2}\,(\phi_v - \phi_v^\circ)$ . . . (6-47)

Thus values of the excess volume of mixing per mol of solution can be calculated from equation (6-47). $\phi_v^\circ \equiv V_2^\circ$, the standard partial molar volume of the salt in solution.

Densities

Densities were calculated from the apparent molal volume using the equation

$$\rho\,(\text{solution}) = \frac{(1000 + m_2 M_2)}{(10^3/\rho_\circ + m_2 \phi_v)} \qquad \ldots\ldots (6\text{-}48)$$

where $\rho_\circ$ is the density of the solvent and M_2 the molecular weight of the solute.

(ii) Calculation of Q(thermo) for aqueous solutions of tetra-n-butylammonium bromide and tetraethylammonium bromide at 298 K.

Osmotic and activity coefficients reported by Lindenbaum and Boyd[215] were used in the analysis for g". Enthalpy data reported by Lindenbaum[216] were used to derive h". The volume data of Wen and Saito[217] were used together

with V_2° values reported by Franks and Smith[86] in order to derive v".

An ALGOL program for an Elliott 803 computer employed a multiple regression method similar to that described in Chapter 5-3 (cf excess functions of binary liquid mixtures) to fit the excess functions for the salt to equation (6-30) as a function of salt molality. The program is similar to that previously described (Appendix 6-6).

Figure 6-11 shows the fitted curve (solid line) obtained using this method for the G^E(salt) data of tetraethylammonium bromide. The derived parameters are presented in Appendix 6-6.

The values of Q(thermo) as a function of composition were calculated using equation (5-49) for each salt and are shown, together with (α/f^2) in Figure 6-12. The thermal expansivities[55] and heat capacities[219] of these mixtures were taken as estimated values in the absence of sufficient data over the entire range. Nevertheless, it was found that the effects of salts upon these parameters are very small. The isentropic compressibilities were calculated using the equation of Newton and Laplace, using the density data of Wen and Saito.[217]

The dependence upon salt molarity of the parameters g", $\alpha_e h''/Cp$ and v''/V is shown for tetraethylammonium bromide in Figure 6-13 and for tetra-n-butylammonium bromide in Figure 6-14.

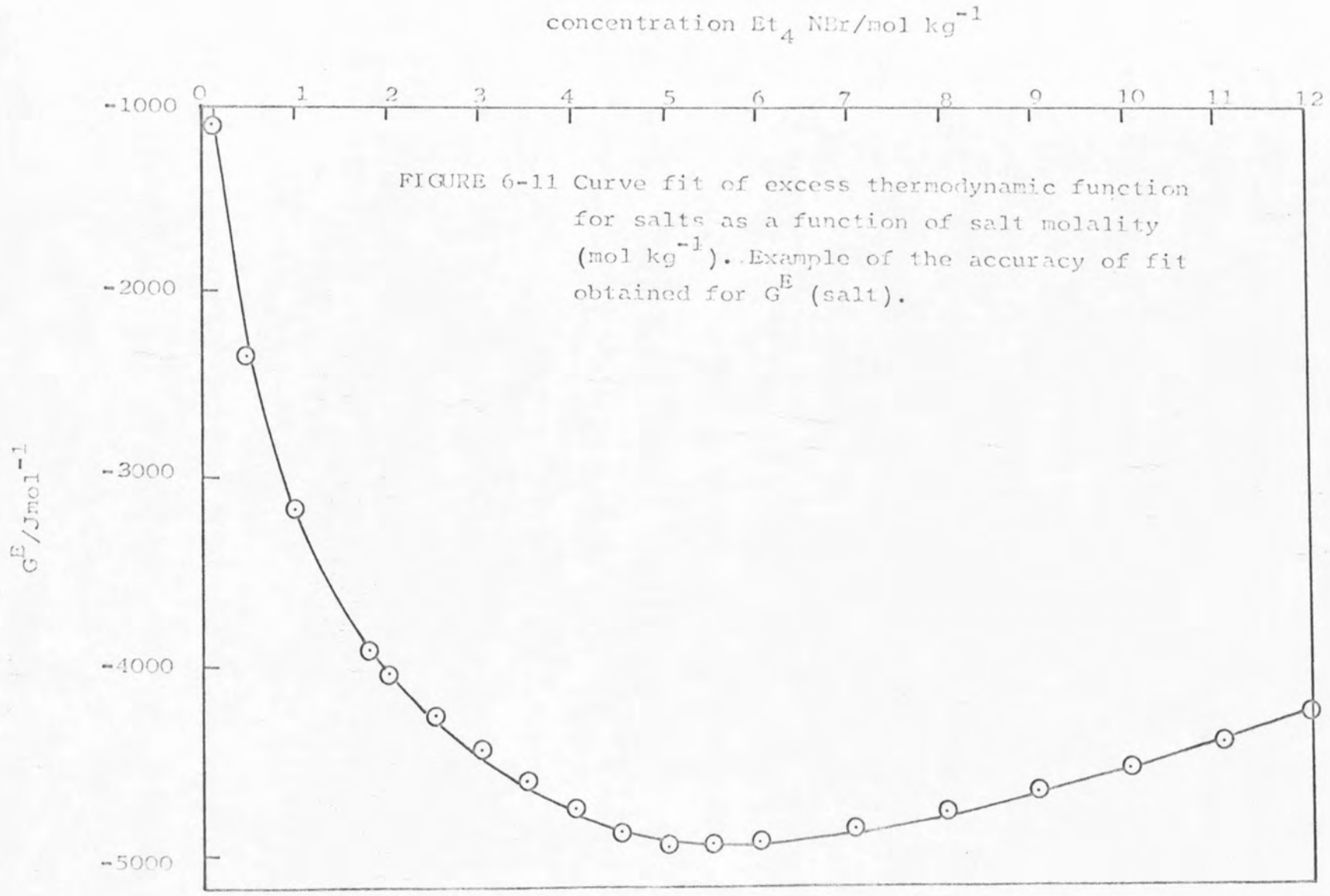

FIGURE 6-11 Curve fit of excess thermodynamic function for salts as a function of salt molality (mol kg^{-1}). Example of the accuracy of fit obtained for G^E (salt).

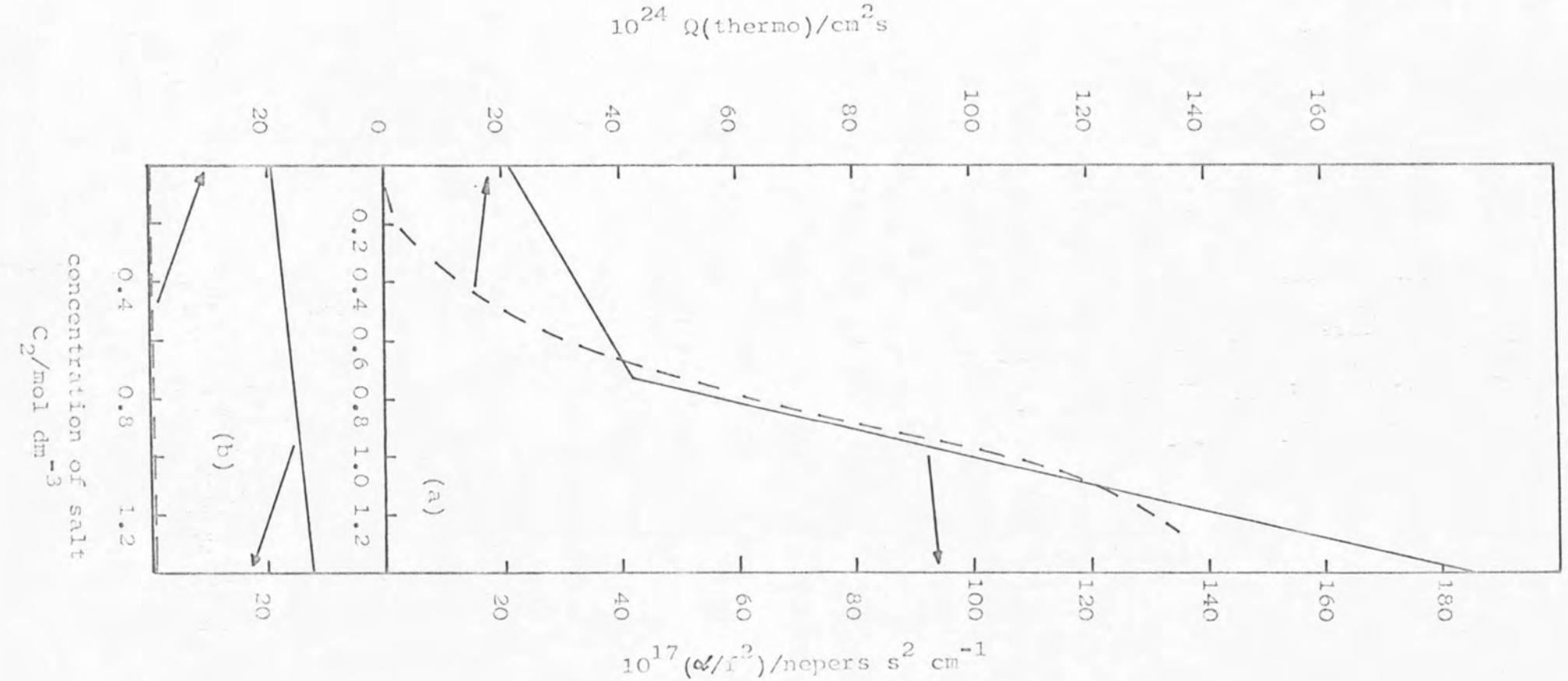

FIGURE 6-12. Composition dependence of Ω(----) and α/f^2 (____) for (a) tetra-n-butyl ammonium bromide and (b) tetraethyl ammonium bromide + water mixtures at 298K..

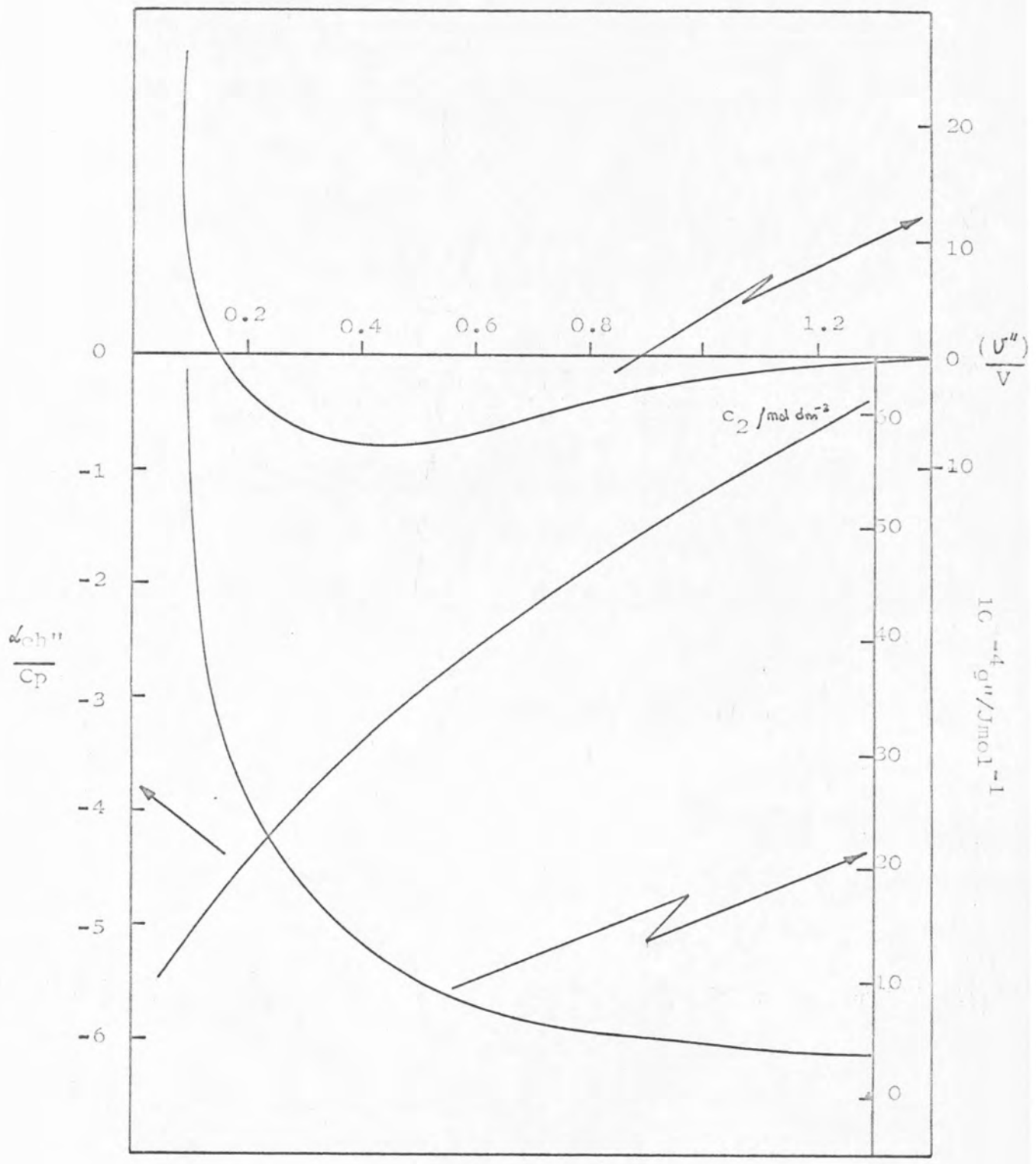

FIGURE 6-13 Dependence of g", $\frac{\upsilon''}{V}$ and $\frac{\alpha eh''}{Cp}$ upon concentration of Et_4NBr.

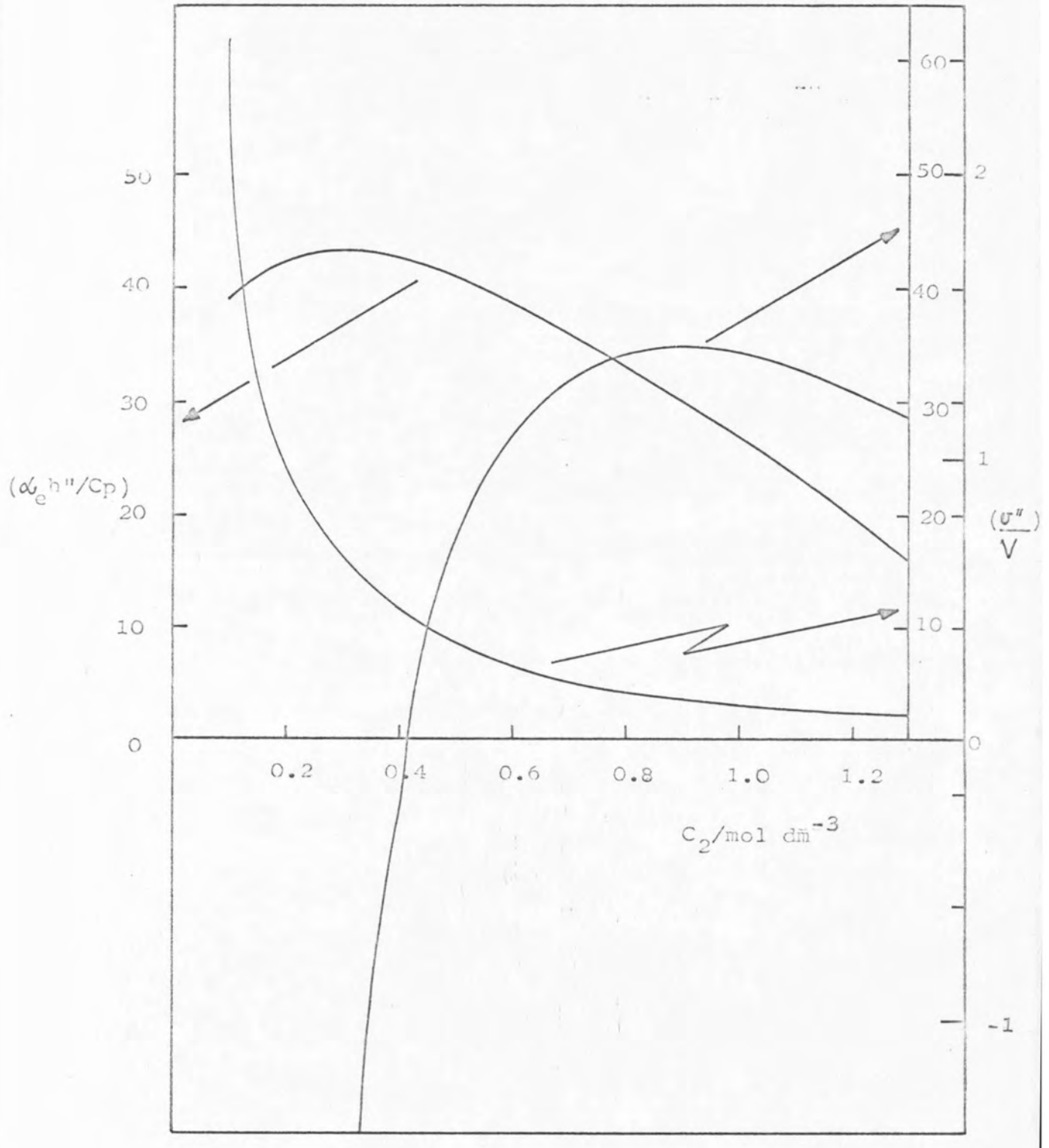

FIGURE 6-14. Dependence of g", $\frac{\upsilon''}{V}$ and (α_{eh}''/Cp) upon concentration of Bu_4NBr.

(iii) Discussion

The key feature of Figure 6-12 is the dramatic increase in Q(thermo) for tetra-n-butylammonium bromide in water at 298 K, where $c_2 > 0.8$ mol dm^{-3}, a trend also observed in (α/f^2). In sharp contrast, Q(thermo) for tetraethylammonium bromide in water remains quite small, as also does (α/f^2), when the salt concentration is increased.

Comparison of the parameter (α_h''/Cp) and $(^{v''}/V)$ shows that the enthalpy controlled term dominates the large absorption in aqueous solutions of tetra-n-butylammonium bromide. It will be recalled that H^E(salt) $(\equiv \phi_L)$ for the butylammonium salt in water is large and positive, whereas H^E(salt) for the ethylammonium salt in water is small and negative. For the tetraethylammonium salt in water the perameters (α_h''/Cp) and $(^{v''}/V)$ are of the same order of magnitude. The low values of Q(thermo) at low concentrations of the butylammonium salt can be related to the large positive value of g''. The parameter g'' falls with increase in salt concentration c_2, the fall being less marked for the ethylammonium salt.

6-5 UREA + WATER MIXTURES

Urea has played a prominent role in many studies of water structure and is frequently cited as a water structure breaking solute.[220] Not the least among such studies

are ultrasonic absorption measurements. Addition of urea to water at 273 K brings about a decrease in (α/f^2) over the range $0 \leqslant c_2 \leqslant 8$ mol dm^{-3}.[221]

No evidence has been found for a relaxation over the frequency range $5 \leqslant f \leqslant 230$ MHz.[221] Further, the ultrasonic velocity (measured at 5 MHz) increases with increase in pressure, concentration and temperature.[62]

Subtraction of the viscosity contribution[62,221] results in the structural contribution showing a sharp decrease with increase in urea concentration, before eventually levelling out.

These trends are consistent with the theory that urea acts as a structure breaker, although the mechanism for this structure breaking action is not fully understood.[220]

(i) Calculation of Q(thermo) for Urea + Water

The Q(thermo) values for urea + water mixtures were derived following an analysis similar to that used for the tetra-alkylammonium salts (see section 6-4).

Stokes[67] has presented an extensive compilation of thermodynamic data for the system urea + water, and his data were used in this analysis.

Free Energies

Following the treatment for tetra-alkylammonium salts and defining the mole fraction of urea (x_2) as;

$$x_2 = \frac{m_2}{m_2 + 10^3/M_1} \qquad \ldots\ldots (6\text{-}49)$$

then G/mol = G = $x_1\{\mu_1^{\circ} + RT \ln x_1 f_1\}$

$+ x_2\{\mu_2^{\circ} + RT \ln \left(\frac{x_2 10^3}{(1-x_2)M_1} \cdot \gamma_2\right)\}$ . . . . . (6-50)

and differentiating this equation twice with respect to x_2, and employing the Gibbs-Duhem[213] relationship, gives

$$\frac{\partial^2 G}{\partial x_2^2} = RT\left\{ \frac{\left(1 + \phi + x_2\left[\frac{\partial \phi}{\partial x_2}\right]\right)}{(1-x_2)} - \left(\frac{1+\phi x_2}{(1-x_2)^2}\right) + \frac{1}{x_2} + \frac{\partial \ln \gamma_2}{\partial x_2} \right\} \quad \ldots (6\text{-}51)$$

where Ø is the osmotic coefficient and γ_2 the activity coefficient of the urea.

Now Stokes[67] gives the relationship between the osmotic coefficients and the salt molality (m_2) as

$$\phi = 1 - \frac{a m_2}{1+bm_2} - \frac{c m_2^2}{(1+bm_2)^2} \quad \ldots (6\text{-}52)$$

where a = 0.042783, b + 0.15 and c = 0.0004198.
After a little algebra and a further application of the Gibbs-Duhem relationship

$$g'' = RT\left[\frac{(1-2x_2^2)}{x_2(1-x_2)^2} - \frac{2a10^3}{A(1-x_2)^2} + \frac{(ab-3c)x_2 10^6}{A^2(1-x_2)^2} + \frac{2bcx_2^2 10^9}{A^3(1-x_2)^2}\right] \quad (6\text{-}53)$$

where $A = \{M_1(1 - x_2) + bx_2 10^3\}$.

Enthalpies

The parameter h'' was derived following section 6-4 as

$$h'' = \frac{\partial^2 H}{\partial x_2^2} = 2\frac{\partial \phi_L}{\partial x_2} + x_2 \frac{\partial^2 \phi_L}{\partial x_2^2} \quad \ldots (6\text{-}54)$$

Stokes[67] has shown that the dependence of ϕ_L upon m_2 may be expressed by

$$\phi_L = - am_2 + bm_2^2 - cm_2^3 + dm_2^4 \qquad \ldots\ldots (6\text{-}55)$$

where a = 85.87, b = 6.815, c = 0.4569 and d = 0.01470.

Thus, differentiating equation (6-55) and substituting the results into equation (6-54) gives

$$h'' = \frac{\partial^2 H}{\partial x_2^2} = \frac{2(bx_2 - a)10^3}{M_1(1-x_2)^2} - \frac{2ax_2 10^3}{M_1(1-x_2)^3} + \frac{2(2b - 3cx_2)x_2 10^6}{M_1^2(1-x_2)^3}$$

$$+ \frac{4bx_2^2 10^6}{M_1^2(1-x_2)^4} + \frac{6(2dx_2 - c)x_2^2 10^9}{M_1^3(1-x_2)^4} - \frac{6cx_2^3 10^9}{M_1^3(1-x_2)^5}$$

$$+ \frac{8dx_2^3 10^{12}}{M_1^4(1-x_2)^5} + \frac{8dx_2^4 10^{12}}{M_1^4(1-x_2)^6} \qquad \ldots\ldots (6\text{-}56)$$

Thus h'' as a function of m_2 can be calculated.

Volumes

An equation relating v'' to the apparent molar volume ϕ_v was derived.

$$v'' = \frac{\partial^2 V}{\partial x_2^2} = 2\frac{\partial \phi_v}{\partial x_2} + x_2 \frac{\partial^2 \phi_v}{\partial x_2^2} \qquad \ldots\ldots (6\text{-}57)$$

A relationship has been derived by Stokes[67] connecting the apparent molal volume ϕ_v with the molar volume at infinite dilution ϕ_v°.

$$\phi_v = \phi_v^\circ + \frac{am_2}{1 + bm_2} \qquad \ldots\ldots (6\text{-}58)$$

where ϕ_v° = 44.17, a = 0.212 and b = 0.15, at 298 K. Using equations (6-57) and (6-58) a relation for v'' was derived.

$$v'' = \frac{\partial^2 V}{\partial x_2^2} = \frac{2a10^3}{A(1-x_2)} - \frac{2ab\,x_2 10^6}{A^2(1-x_2)} + \frac{2a x_2 10^3}{A(1-x_2)} - \frac{2ab x_2 10^6}{A^2(1-x_2)^2} - \frac{2ab\,x_2^2 10^6}{A^2(1-x_2)^2} - \frac{2ab^2 x_2^2 10^9}{A^3(1-x_2)^2} \quad \ldots\ldots (6\text{-}59)$$

where $A = \{ M_1(1 - x_2) + bx_2 10^3 \}$.

Thus the dependence of v'' upon m_2 could be calculated. Heat capacity data and thermal expansion coefficients reported by Stokes,[67] together with the sound velocity data of Beauregard and Barrett[62] were used to evaluate Q(thermo) at 298 K as a function of composition. An ALGOL program for an Elliott 803B computer was used and all relevant data is given in Appendix 6-7.

Figure 6-15 shows the dependence of Q(thermo) and (α/f^2) upon molality of urea. Figure 6-16 displays the dependence of the parameters g'', $(\alpha_e h''/Cp)$ and (v''/V) upon mixture composition, at 298 K.

(iii) Discussion of Q(thermo) for Urea + Water

Consideration of Figure 6-15 shows that over the range $0 \leq m_2 \leq 5$ mol dm^{-3} the calculated value of Q(thermo) is very small, (α/f^2) also shows no increase, but rather

FIGURE 6-15 Comparison of the composition dependence of (α/f^2) and Ω(thermo) for Urea + water

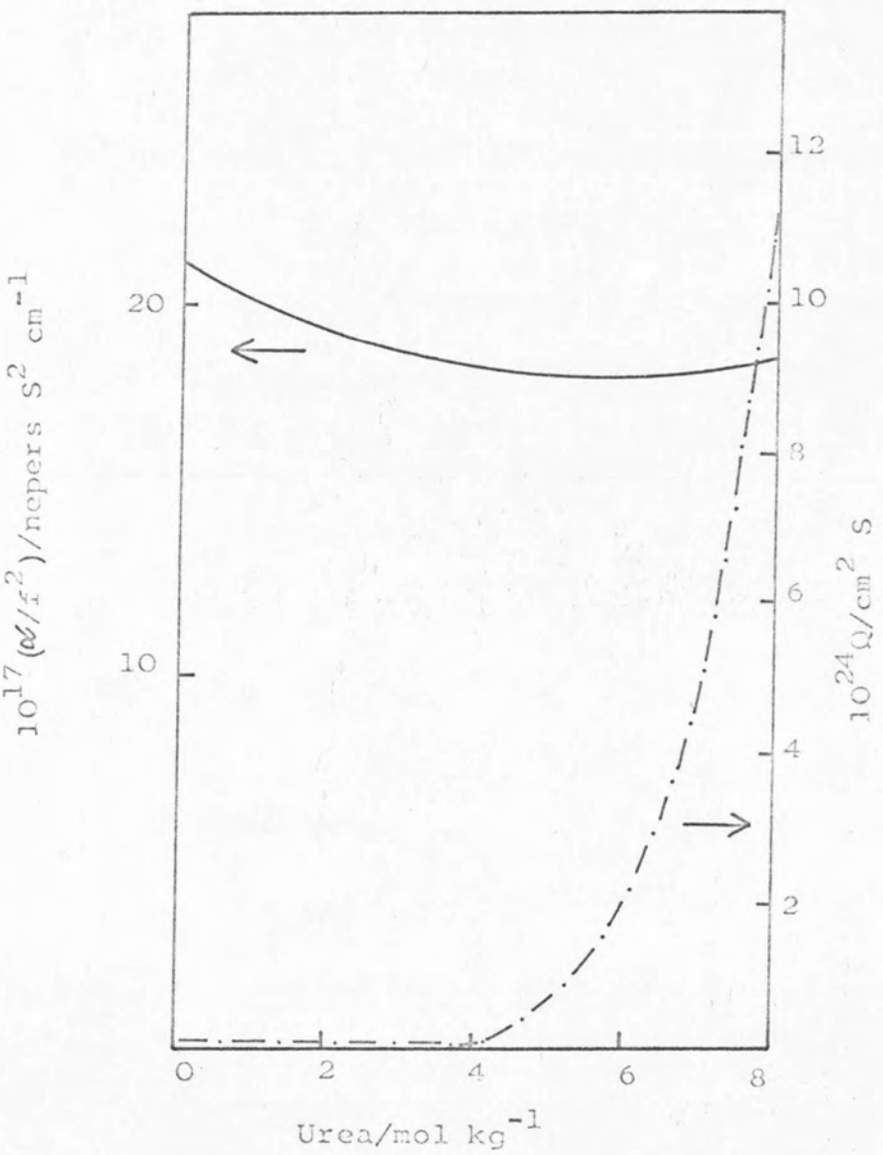

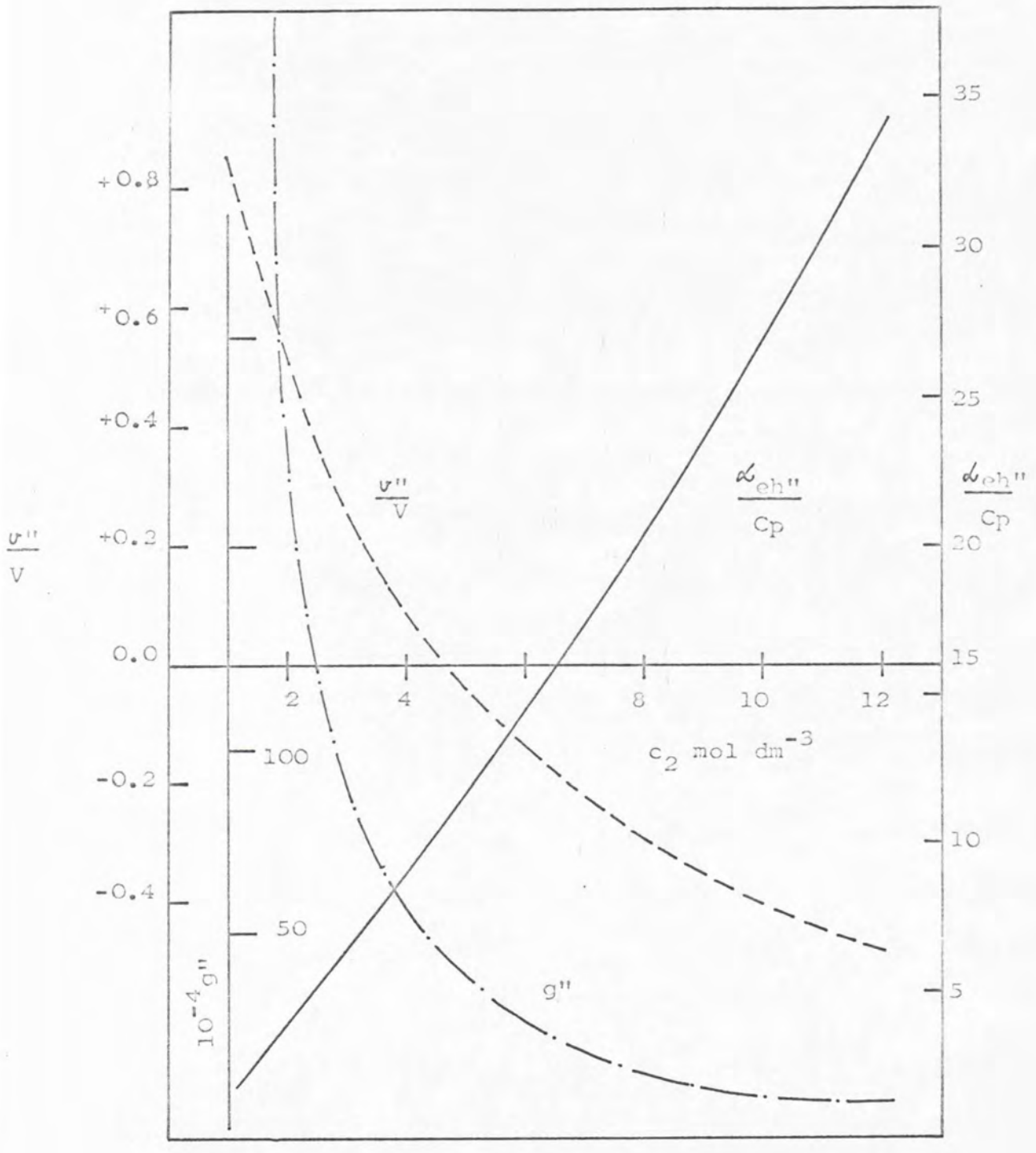

FIGURE 6-16 Composition dependence of the quantities g", (υ"/V) and (α_eh"/Cp) for urea + water mixtures

a gradual decrease, over this region. At around m_2 = 8 mol dm^{-3} urea the value of (α/f^2) is tending to increase and this is qualitatively reflected in Q(thermo). The relatively large value of g" seems to dominate the Q factor (Figure 6-16) and appears to be responsible for the lack of absorption in the low molarity of urea region.

This analysis again confirms the usefulness of the link developed between thermodynamic measurements and ultrasonic absorption.

6-6 GENERAL DISCUSSION

The results of the applications of the Romanov - Solovyev analysis lend support to the contention that the parameter Q(thermo) provides a useful link between thermodynamic and ultrasonic measurements. In itself, it should be stressed that the absolute magnitude of Q(thermo) indicates little. It does however provide an excellent qualitative indication of the presence or absence of an excess ultrasonic absorption in binary liquid and electrolyte mixtures. In particular it is helpful in pinpointing 'plateau regions' and PSAC regions.

The trends in the evaluated parameters g", $(\alpha_s h''/Cp)$ and $(^{V''}/V)$ are also helpful in deciding which thermodynamic parameters exert a controlling influence over the ultrasonic absorption. In general it would appear that g" controls the 'plateau region', suggesting that in this

region energy considerations are paramount. The PSAC region may be enthalpy ($\alpha_e h''/Cp$) or volume (v''/V) controlled and the analysis allows separation of these effects.

The analysis, applied in particular to methyl cyanide, of the ultrasonic absorption data at 273 K as a function of frequency is less satisfactory. The Romanov-Solovyev equation (5-48) produces a sigmoid shaped curve and, unlike the discrete relaxation equation, it cannot account for the subtleties in the shape of the experimental plots - some of which lie outside experimental error.

It may therefore be concluded that the Romanov - Solovyev approach is more useful than the thermal relaxation approach for prediction of the qualitative features of the plot of (α/f^2) against x_2. It does not, however, lend itself towards quantitative application in an attempt to analyse the subtle features of the frequency dependence of (α/f^2). This is, in part, due to the difficulty in defining values of l_m, the interaction length.

The major difficulty encountered in attempts to apply the original Romanov-Solovyev theory, or the extensions developed therein, to mixturesis the sparsity of thermodynamic measurements (particularly G^E data) available.

CHAPTER SEVEN

VIBRATIONAL SPECTRA OF WATER AND AQUEOUS ELECTROLYTE SOLUTIONS

7-1 INTRODUCTION

There have been several recent reviews of the properties of aqueous electrolyte solutions,[37,203,222-224] but no comprehensive account is available of progress in the application of Raman and infra-red spectroscopic techniques to the study of these systems. The aim of this chapter is, therefore, to review the Raman and infra-red spectra of water and aqueous solutions of electrolytes. Where relevant, details of recent models for the structure of liquid water are included. No attempt has been made to review in detail theoretical models of water structure since these are dealt with in many excellent reviews and papers.[2,5,6-12,36,37,45,224-229] The theory and techniques of Raman and infra-red spectroscopy have been the subject of an excellent book by Herzberg[230] and are not reviewed here.

At the outset it must be made clear that the so called 'structure' of water depends upon the way in which it is observed. A photograph of a moving object, taken at a rate which is fast compared with the rate of motion of the object, will reveal nothing of that motion. However, if the same photograph is taken at a much slower rate the motion of the subject is revealed in the blurred image obtained. A similar situation exists in the observation of molecular motion in a liquid. If an observation of the molecules were made with a 'camera', three types of structure would be broadly observed. An 'instantaneous'

photograph would reveal molecules in clearly defined positions. Such a structure is described as the I (instantaneous) - structure. If the photograph were taken in a time corresponding to the time taken for a molecular vibration to occur, (10^{-14} to 10^{-10} S) then a different structure, the V (vibrationally controlled) - structure would be observed. Finally, if the liquid is examined over a time of the order of that taken for molecular diffusion processes, the D (diffusion controlled) - structure would be observed. These three basic structural types are illustrated[36] in Figure 7-1. In contrast to the nuclear magnetic resonance[222] experiment, the Raman and infra-red spectroscopic techniques probe direct molecular environments (I-structure) whilst the n.m.r. observes the average environment of the magnetic nucleus studied (D-structure). Thus the vibrational time scale is of the order of 10^{-12}S, whereas the n.m.r. time scale is 10^{-2} S. In principle vibrational spectroscopy is the most suitable technique for a study of liquid structure and solvent-solute interactions. However, in practice, thermal disorder in the liquid and the non-rigorous periodicity of the vibrational motions leads to broad spectral bands having ill defined maxima.

Indeed, a major difficulty in formulating a statistical mechanical model for water is the imprecise assignment of the vibrational spectrum of water over the region 4000 to 0 cm^{-1}; the frequencies are required in a calculation of the vibrational partition function.[226]

FIGURE 7-1 (from reference 36)

D-structure V-structure I-structure

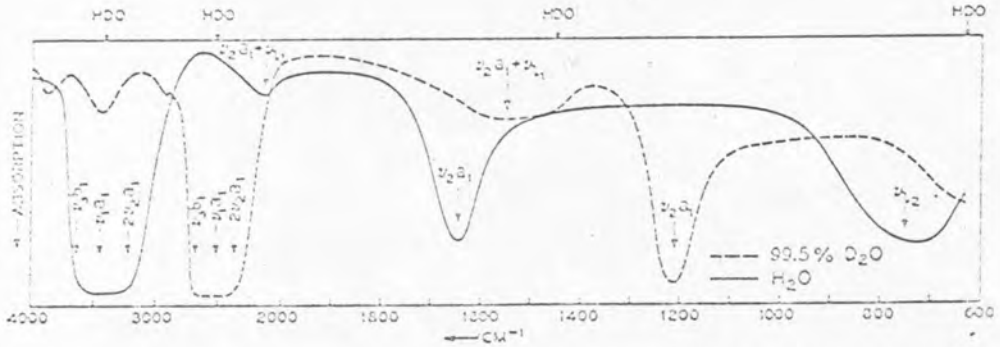

Infrared spectra of water and heavy water. (Weak bands in the spectrum of 99.5% D_2O, which coincide with characteristic HDO frequencies shown by arrows, are indicative of the sensitivity of the infrared spectrum to impurities.)

FIGURE 7-2 (from reference 259)

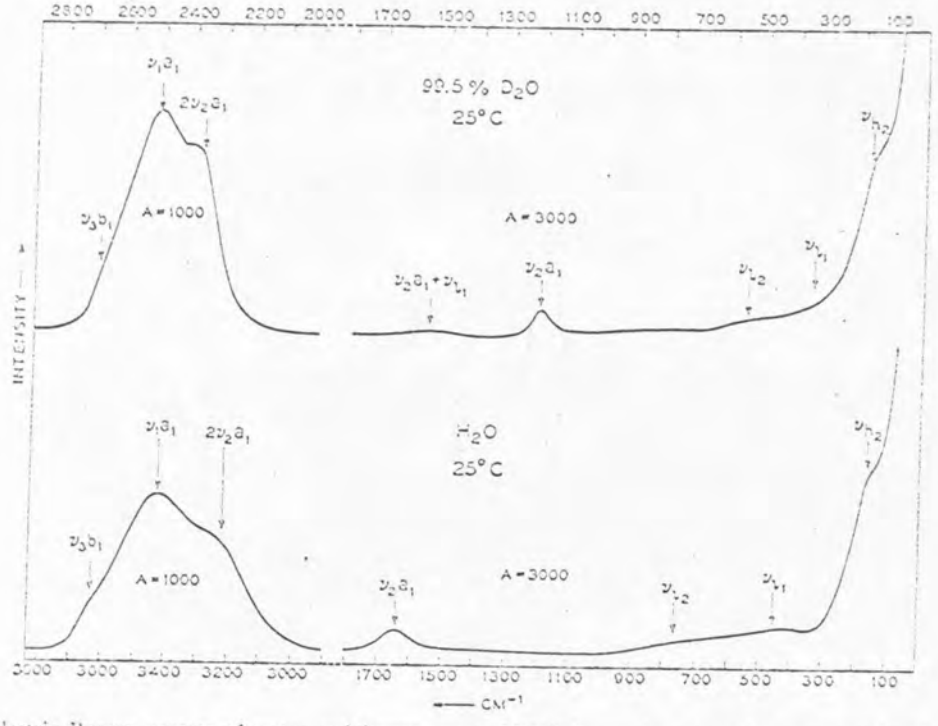

Photoelectric Raman spectra of water and heavy water. Identical sample geometries were employed in both cases. = amplification.

FIGURE 7-3 (from reference 259)

TABLE 7 - 1

Spectroscopic stretching and bending frequencies for H_2O molecule

	ν_1	ν_2	ν_3
Water (vapour)	3650	1595	3755
Liquid 276 K	3448	1642	3397
Liquid 343 K	3448	1642	3434
Ice	3360	1585	3210

Notwithstanding these difficulties, useful information can be retrieved from detailed Raman and infra-red spectroscopic studies of water.

7-2 VIBRATIONAL SPECTRA OF WATER AND DEUTERIUM OXIDE

The infra-red and Raman spectra of water and deuterium oxide are shown in Figures 7-2 (a and b) and 7-3 (a and b) respectively. The major region of interest is the OH stretching region and some typical values of the stretching frequencies[231,232] and their assignments are given[37] in Table 7-1. Whilstthe assignment of the bands for water vapour is not in doubt, there is some uncertainty with regard to the liquid state. Hornig et al[232] accepted that ν_1 (the symmetric water stretching mode) and ν_3 (the assymetric stretching mode - see Table 7-1) become transposed on going from the vapour to liquid states. Other workers do not accept that this is so. The question has not been satisfactorily resolved. Many authors ignore the intensity evidence used in support of the assignments made in Table 7-1 by Hornig and have assumed that the frequencies in ice remain in the order $\nu_3 > \nu_1$. The bending frequency ν_2 is little affected by phase change.

The study of the stretching region (4000 to 3000 cm^{-1}) of liquid water is facilitated by isotopic substitution. Figure 7-4 shows the infra-red and Raman spectra of dilute solutions of D_2O in H_2O and H_2O in D_2O. (Taken from reference 36). The stretching vibrations of water are

(a)

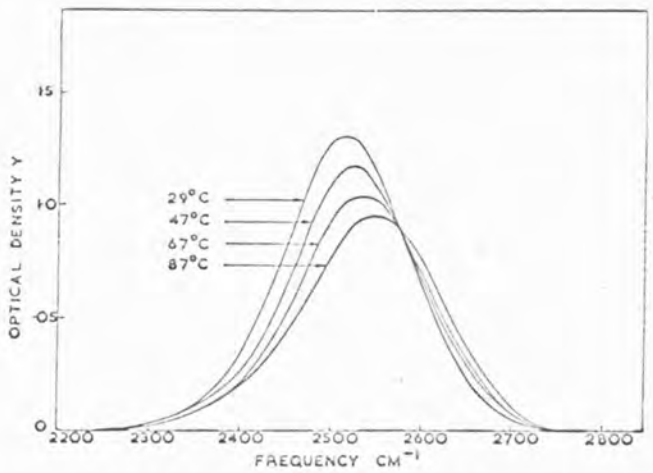

Plot of optical density *vs.* frequency for the ir absorption of HOD at ~2500 cm^{-1} for various temperatures. The presence of an isosbestic point at ~2575 cm^{-1} is clearly shown.

(b)

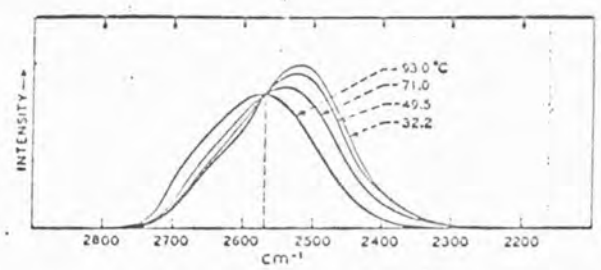

Quantitative Raman intensities as functions of frequency transferred to horizontal baselines from mercury-excited spectra corresponding to a 6.2*M* solution of D_2O in H_2O at temperatures from 32.2° to 93.0°C. The 4358-Å line of mercury and a slitwidth of 15 cm^{-1} were employed. The 4916-Å line of mercury was removed from the original photoelectric tracings. The dashed vertical line near 2570 cm^{-1} refers to the isosbestic frequency (see text for definition). The intensity scale is arbitrary.

FIGURE 7-4 Infra-red and Raman Spectra of dilute HOD in H_2O. The spectra of HOD in D_2O are similar (taken from reference 36)

decoupled[36] and it is possible to study the OH and OD stretches of the HOD formed in solution. On average, the five nearest neighbours of each OH oscillator in D_2O (say) are deuterated. Some of the early Raman studies of water were made by Magat[233] who laid the foundations of the investigations reviewed here.

Wall and Hornig[234] made photoelectric Raman studies of HOD in D_2O and H_2O. They observed narrower bands than in water and suggested that the band-width could be related to the distribution of O----O distances in liquid water. Further, it was shown that the nearest neighbour distribution function obtained from the spectra was in good agreement with previous X-ray data. Also the band contours were smooth and this, together with the relatively small temperature dependence led Wall and Hornig to conclude that a continuous distribution of O----O distances is present with one 'preferred' value at the band maximum.

Falk and Ford[235] confirmed the results obtained by Wall and Hornig after an exhaustive infra-red investigation of HOD in D_2O and H_2O. Thus the conclusion was drawn that a continuous distribution of hydrogen bond strengths exists in water, any discrete species of specific hydrogen bond strength must be ruled out.

Walrafen[236,237] studied the intermolecular vibrations of water and obtained evidence which prompted an alternative interpretation.

A band at 170 cm^{-1} was assigned to hydrogen bond

stretching by Walrafen, and a band at 60 cm^{-1} to hydrogen bond bending. Following a study of the temperature dependence of the intensities of these bands, Walrafen suggested that hydrogen bond breaking occurs. In a Raman study of a broad band in the region 300 to 1000 cm^{-1}, associated with molecular libration in water, Walrafen found strong evidence for the single step breakage of hydrogen bonds. This was taken to imply that different energy levels can be assumed for water molecules forming one to four bonds. The infra-red spectra in the low frequency region (1000 to 100 cm^{-1}) are less informative.[238] Walrafen has also examined, by an analogue computer technique, the water OH stretching region (3000 to 4000 cm^{-1}). He found an isosbestic point[237,240] (a point at which the intensity is not temperature dependent) at 3460 cm^{-1} and judged this behaviour, together with the results of the computer analysis, irrefutable evidence for an equilibrium between hydrogen bonded and non-hydrogen bonded water. Recently Walrafen[241-243] has shown that laser-Raman spectroscopic studies of dilute solutions of D_2O in H_2O and H_2O in D_2O show slight but definite asymmetries on the high frequency side of the bands (see Figure 7-4 a and b). Further, he has observed an isosbestic point in a study of 6.0 mol dm^{-3} D_2O in H_2O (i.e. the OD stretching band). Franck and Roth[244] have studied the infra-red absorption spectra of D_2O in H_2O at constant density up to 673 K and observed that at high temperature the band becomes asymmetric and shifts to high frequencies.

This adds further support to the model which requires that a simple equilibirum is present in solution between hydrogen bonded water and non-hydrogen bonded water. (It is assumed that non-hydrogen bonded water refers here to non-bonded OH groups). In support of this Senior and Verrall[245] studying the infra-red spectra of D_2O in water, observed that numerical differentiation of digitally recorded spectra from these solutions reveals an extra component in the infra-red band. They were able to derive a value for the heat of dissociation of the hydrogen bond of 9.5 ± 1.5 kJ mol^{-1} in good agreement with the value derived from the Raman spectra reported by Walrafen.

Schiffer[246] criticised the model proposed by Walrafen and, in conjunction with Hornig,[247] demonstrated theoretically that a continuum model could account for the observed asymmetry in the Raman spectra of Walrafen. Schiffer and Hornig[247] proposed that collisional distortion occurs in liquid water which perturbs the two bonds in H_2O differently. They concluded that even if Walrafen's approach was taken at face value, it requires a two state continuum model rather than a simple two state model.

Wall[248] using a treatment by Gordon[249] analysed the vibrational bandwidths in liquid water, and drew attention to the important part played by hindered rotatory and translatory motions in contributing to bandwidths. It was also concluded that long time diffusions are not evident in water. This would tend to support the analysis of Schiffer and Hornig.[247] It is evident that there is

considerable disagreement between the interpretations of spectroscopic results in the fundamental inter- and intramolecular regions. In addition there is a lack of a universally acceptable interpretation of the spectra obtained in the stretching region. This may be resolved by the earlier suggestion that different methods of investigation 'see' different effects. Alternatively a radically new approach is required.

One criticism[234] which has been used by adherents to the 'continuum' model is that the concentration of D_2O in the solutions examined by Walrafen is too high. It is suggested that the observed shoulder could be due to coupled OD oscillators. A recent investigation[250] of the infra-red spectrum of a very dilute solution of D_2O in H_2O showed that 96% of the D_2O added was present as HOD and 4% as D_2O. Although not conclusive, this would suggest that such coupling is unlikely.

Another region of considerable spectroscopic interest extends over the range 5000 to 11000 cm^{-1}, the near infra-red. In this region there are a number of overtone and combination bands whose assignments are the subject of current debate. A number of detailed investigations of this region (5000 to 11000 cm^{-1}) have been undertaken - notably by Buijs and Choppin,[251,252] Luck[253] and Worley and Klotz.[254]

Buijs and Choppin[251,252] assigned bands at 8620 cm^{-1}, 8330 cm^{-1} and 8000 cm^{-1} to water molecules forming zero, one and two hydrogen bonds respectively. They were able

to calculate the mole fractions of these species present in water and a significant proportion of broken hydrogen bonds was inferred to be present in water.

Luck[253] challenged the analysis of Buijs and Choppin on the basis of their supposition that non-hydrogen bonded water molecules could be detected easily by infra-red spectroscopy. For hydrogen bonded OH groups, Luck assigned an absorption at 8000 cm^{-1} to those involved in linear bonds and an absorption at 8700 cm^{-1} to those involved in bent bonds. Following an analysis similar to that of Buijs and Choppin, Luck was also able to calculate the percentage of broken hydrogen bonds. The wide range of estimated values for the percentage "broken hydrogen bonds" in water[235] (Table 7-2) clearly indicates the confused state of the subject. Recent analyses[255] are moving towards the idea that the concentration of 'monomeric water' in water is very small.

Glew[256] suggested that for dilute solutions of water in organic solvents monomer bands are only found for 'non-interacting' solvents, and thus it is unlikely that in water there can be a high monomer concentration.

Worley and Klotz[254] studied the near infra-red (Fig. 7-5) spectrum of OH in the overtone region (1.3$\mu$to 1.8μ) using 6.0 mol dm^{-3} HOD in D_2O against D_2O as reference. From a study of the temperature dependence of the spectra they were able to identify two features, one at 1.416μ (7062 cm^{-1}) assigned to non-hydrogen bonded OH and one at 1.556μ (6427 cm^{-1}) assigned to hydrogen bonded OH groups. In addition they reported an isosbestic point

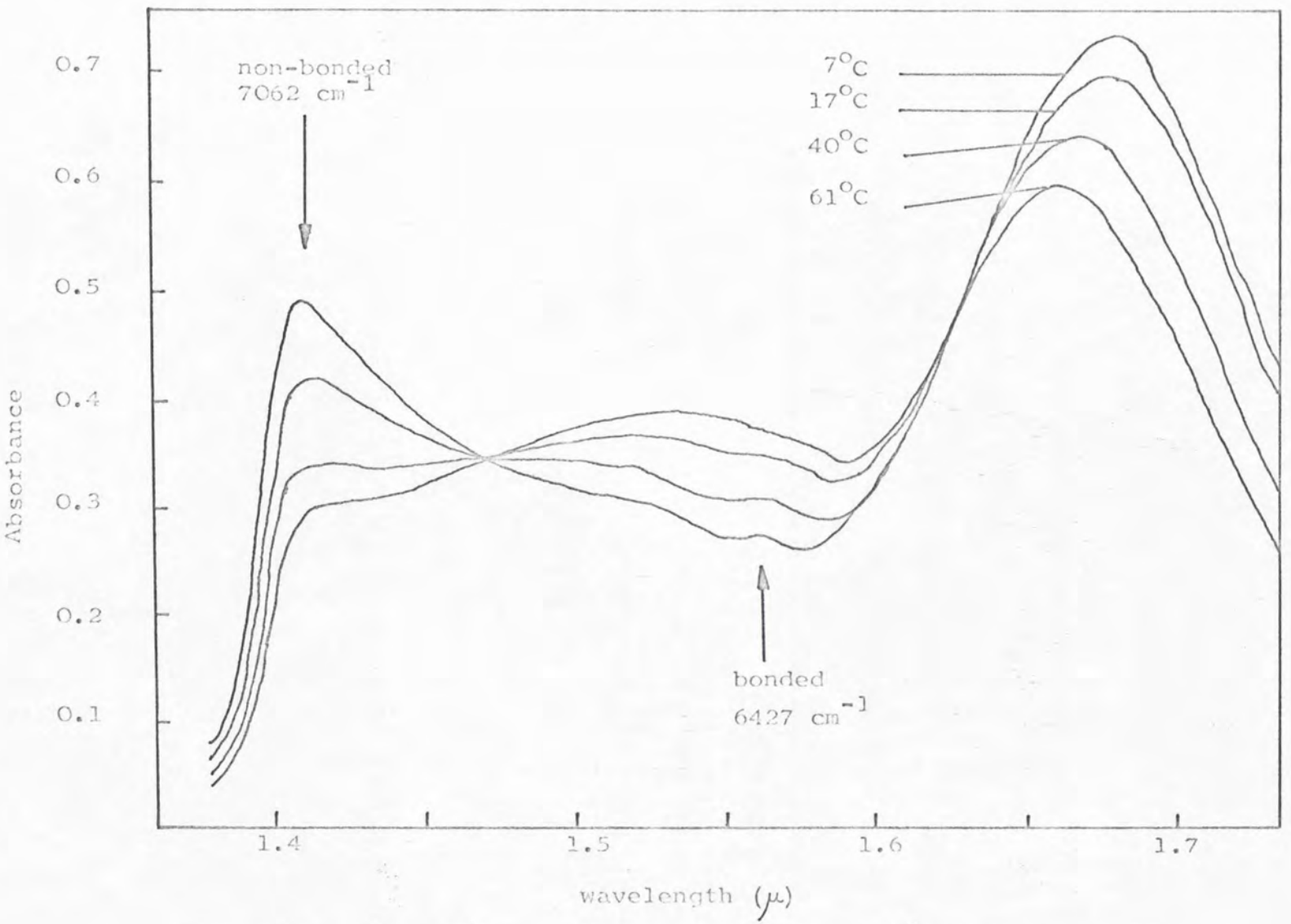

FIGURE 7-5 Near infra-red spectra of 6 mol dm^{-3} HOD/D_2O solution at four temperatures (from reference 254)

TABLE 7 - 2

(Taken from paper by Falk and Ford[235])

Author	T/K	% broken H-bonds
Litovitz, Carnevale	273	71.5
Eucken	273	66
Fox, Martin	273	60
Wada	273	57.5
Gojotheim and Krogh Moe	273	56
Cross et al	299	50
Némethy and Scheraga	273	47
Ewell and Eyring	273	46
Buijs and Choppin	273	46
Thomas et al	273	38
Goldstein and Penner	273	32
Hall	273	30
Pauling	273	28.5
Danford and Levy	298	20
Frank and Quist	273	18
Davis and Litovitz	273	18
Nomoto	293	17.5
Pauling	273	15
Luck	273	9-16
Walrafen	273	10.5
Haggis et al	273	9
Marchi and Eyring	273	2.5
Stevenson	298	0.1

at 1.468μ (7062 cm^{-1}) which they consider strong evidence for a simple equilibrium between hydrogen bonded and non-hydrogen bonded OH groups in water. They defined a parameter R (= $\frac{A\ 6427\ cm^{-1}}{A\ 7062\ cm^{-1}}$) which was observed to decrease with increase in temperature. When salts were added to the solution at a fixed temperature, the ratio R decreased and this was taken to indicate that these salts operated a water structure breaking effect. A decrease in R from the water value being taken as a structure breaking effect. Wootten[257] has used this technique to examine the effects of t butyl alcohol and methyl cyanide on water structure. He found that the ratio R increased when t butyl alcohol was added and decreased when methyl cyanide was added. This has been interpreted as a structure forming effect by t butyl alcohol and a structure breaking effect by methyl cyanide.

Luck and Ditter[258] confirmed the findings of Worley and Klotz[254] and studied the HOD near infra-red spectrum over a temperature range from 273 to 673 K (Figure 7-6). They assigned the band at 1.4μ (7062 cm^{-1}) to the second overtone of the stretching band, and the band at 1.6μ (6427 cm^{-1}) to a combination of the bending and stretching vibrations.[235,258]

In the foregoing outline of developments in the vibrational spectroscopy of water, the ways in which infra-red and Raman spectra can reveal structural information have been indicated. This approach can be extended by an examination of the effects of solutes upon the types of

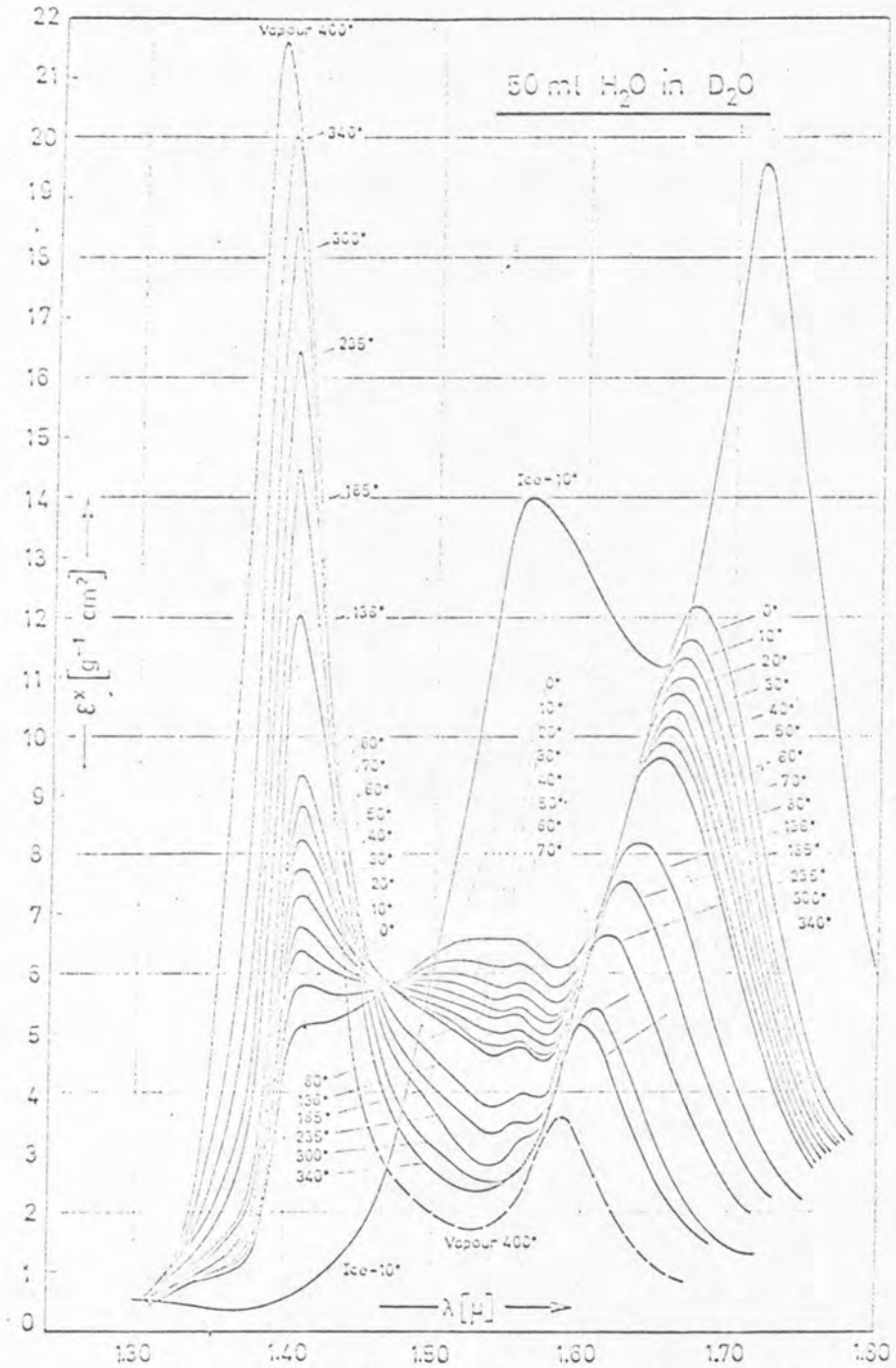

Temperature-dependence of the HOD spectrum. 50 ml H_2O/l D_2O liquid phase under saturation conditions.

FIGURE 7-6 (from reference 258)

spectra described.

7-3 VIBRATIONAL SPECTRA OF AQUEOUS ELECTROLYTE SOLUTIONS

The Raman and infra-red spectra of water may be regarded as having three major regions of interest;
(i) the low frequency region (1000 - 10 cm^{-1}),
(ii) the high frequency region (4000 - 2000 cm^{-1}) and
(iii)the overtone region (5000 to 12000 cm^{-1}). The effects of added electrolytes on the Raman and infra-red spectra in each of these regions have been examined in some detail. The results of such examinations have revealed much useful information concerning the spectra and structure of water and the solvation of ions in solution.

Walrafen[259] studied the effects of added electrolytes on the 175 cm^{-1} band in the Raman spectrum of water. He concluded that;
(i) all the electrolytes studied brought about an intensity decrease in the 175 cm^{-1} band,
(ii) no marked cationic effects were produced,
(iii) the largest effects were produced by bromides.
Walrafen concluded that a fall in the intensity of the 175 cm^{-1} band can be directly attributed to a breaking of O-H----O bonds by the added electrolytes. It was also concluded that the large decrease in intensity produced by bromides indicated that certain ions are very effective at breaking O-H---O units when forming strongly hydrated anionic units.

Further, the fact that NH_4Br and NH_4Cl produce a similar effect to the other halides is significant when it is recalled that NH_4^+ is known to produce little distortion of the water structure.[260]

In another study, Walrafen[261] examines the Raman spectra of water in the region 200 to 1000 cm^{-1}, i.e. the region where the librational modes of water are observed. In addition he also assigns the spectrum of water and this is given in Table 7-3. The suggestion was made by Magat[262] that the bands at 450 and 780 cm^{-1} in water are due to librations of water molecules hydrogen bonded to four nearest neighbour water molecules. The intensities of the various librational bands studied were observed to increase linearly with electrolyte concentration. Also marked intensity increases with increasing anionic size were noted. The effects of cations were relatively small. Walrafen explains the intensity increases in terms of the concentration of electrostricted water in hydration shells. Walrafen,[263] in a later publication, confirmed these large anionic effects by librational intensity studies. Further, he suggested that primary hydration may account for the linear dependence of intensity on salt concentration and the insensitivity of the spectra to temperature changes. He concludes that Raman spectroscopy can reveal information about cation effects and confirms his previous conclusion that such effects are smaller than those of anions.

The far infra-red spectra of a number of electrolytes

TABLE 7 - 3

Frequency/cm^{-1}	Assignment	
175	ν_o	hydrogen bond stretching
450	ν_{L1}	hydrogen bonded libration
780	ν_{L2}	hydrogen bonded libration
1645	$\nu_2\ a_1$	bending
2115	$\nu_{L1} + \nu_2\ a_1$	combination
3225	$\sim 2\ \nu_2\ a_1$	Fermi resonance
3450	$\nu_1\ a_1$	symmetric stretching
3630	$\nu_3\ b_1$	asymmetric stretching
3990	$\sim 2\ \nu_2\ a_1 + \nu_{L2}$	combination

have been reported by Draegert and Williams[264] in the range 75 to 650 cm^{-1}. These authors studied the spectra of solutions (4 mol dm^{-3}) of electrolytes in D_2O (see Figure 7-7). They note that the spectra of even the most concentrated solutions bear a strong resemblance to the solvent spectrum. Two bands were observed in the spectrum;

(i) a broad intense feature attributable to hindered rotation of water molecules, and

(ii) a weak band due to hindered translatory modes of water.

The frequencies, intensities and shapes of these bands were compared. The anions were thought to have the greater effect, and their structure breaking effect was assessed as:

$$NO_3^- < ClO_3^- < ClO_4^- < Cl^- < Br^- < I^-$$

The most interesting changes in spectra occurred for solutions of sodium perchlorate and sodium chlorate where a new feature was observed at about 650 cm^{-1}. This was interpreted as indicative of further, unresolved, components within the hindered rotational band in solution.

In summary, the low frequency studies described go some way towards obtaining an indication of the effects of electrolytes in solution. However, detailed interpretation is hindered by the large widths and low intensities of the bands.

At this stage it is appropriate to examine the information available from studies made at higher frequencies (4000 to 2000 cm^{-1}) of the stretching modes (coupled

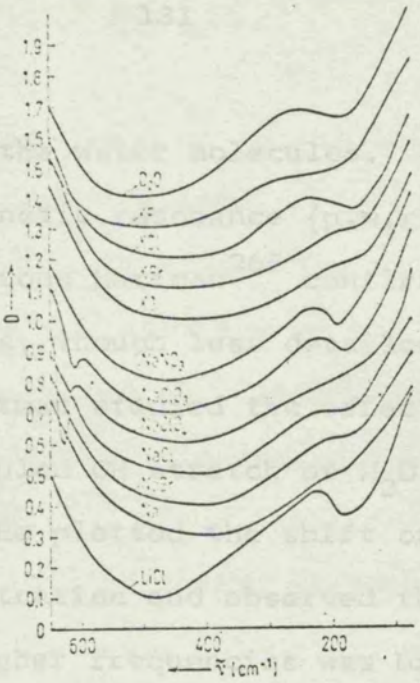

Normalized IR transmittance D of D_2O solutions of some electrolytes in the low wave number range. The concentration is 4 mole/l in every case. For clarity, the curves are displaced vertically in relation to one another. The interval between lines on the ordinate is always 0.1; after *D. A. Draegert* and *D. Williams*

FIGURE 7-7 (from reference 222)

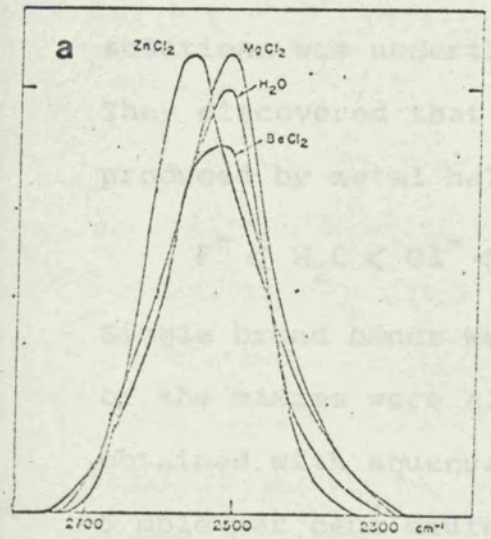

The OD stretching band of HDO in solutions of some divalent metal chlorides in 5 mole % deuterated water at 27°C and 30-cm^{-1} resolution.

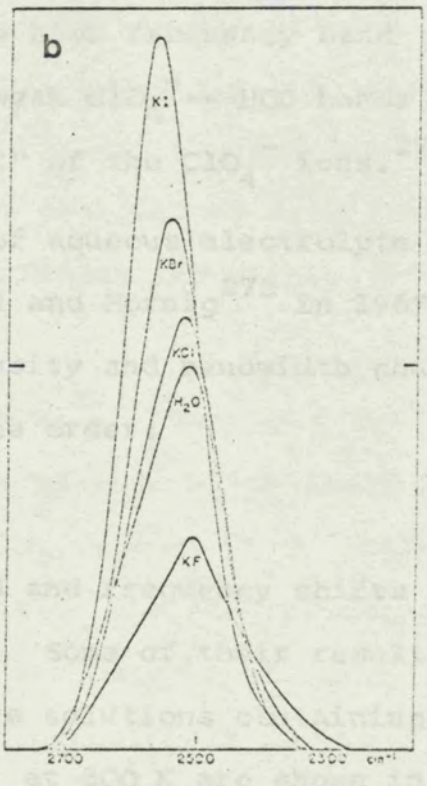

The OD stretching band of HDO in solutions of the potassium halides in 5 mole % deuterated water at 27°C and 30-cm^{-1} resolution.

FIGURE 7-8 (from reference 272)

and uncoupled) of the water molecules. In an infrared and proton magnetic resonance (p.m.r.) study of aqueous salt solutions Hartman[265] confirmed the results of several previous, though less detailed, investigations.[266-270] Hartman studied the effect of added electrolytes on the uncoupled OH stretch of H_2O in dilute solution in D_2O. He plotted the shift of the band maximum against concentration and observed that, in general, a shift towards higher frequencies was brought about by alkali halides, whereas salts such as sodium acetate produced a low frequency shift. In particular, he noticed that addition of sodium perchlorate produced a high frequency feature in these spectra. Further the greatest shift was produced by sodium chlorate. In the spectrum of sodium perchlorate in D_2O the high frequency band was assigned by Hartman to the weak ClO_4^----HOD bands in the "negative hydration layer" of the ClO_4^- ions.[271]

An exhaustive Raman study of aqueous electrolyte solutions was undertaken by Wall and Hornig[272] in 1967. They discovered that large intensity and bandwidth changes produced by metal halides had the order:

$$F^- < H_2O < Cl^- < Br^- < I^-$$

Single broad bands were observed and frequency shifts of the maxima were always small. Some of their results obtained with aqueous electrolyte solutions containing 5 mole per cent deuterated water at 300 K are shown in Figure 7-8 a and b. On the basis of these observations Wall and Hornig concluded that there is no indication of

ion-water association leading to the changes in intensity and bandwidth, as would be implied by a rigid hydration model. For a solution of KI containing 160D oscillators per iodide ion, six are affected by the ion and ten are remote. The six affected oscillators and six of the remote ones have scattering cross sections twice that of a bulk OD oscillator.[273] Thus the intensity ratio of bulk to hydration band is 16/12, it being important only that they are of comparable intensity, so that one is not lost under its neighbour. However, if it is assumed that only four instead of six oscillators are affected by iodide and twelve remain remote then the Wall and Hornig calculation above predicts an intensity ratio of 18/8; thus the 'hydrate' band could be lost under the bulk band. Indeed, the fact that hydrates of tetraalkyl halides excluding iodide all have four water oscillators associated with each halide ion, leads one towards the conclusion that iodide also has four and not six oscillators associated with it.[274] This clearly demonstrates the dangers of such calculations.

Kecki, Dryjanski and Kozlowska[275] have recently undertaken a study of the infra-red absorption spectra of ternary solutions of HOD, $NaClO_4$, D_2O and H_2O. They interpreted the splittings of the OH and OD stretching contours observed in terms of the breakdown of water structure and the failure of the perchlorate ion to hydrate.

Walrafen[276] obtained photoelectric laser Raman spectra

of a series of ternary solutions of HDO, D_2O, H_2O and perchlorates (Li^+, Na^+, K^+). Addition of perchlorates to aqueous solutions of D_2O produced a splitting of the OD contour (Figure 7-9). Similar effects were observed when the coupled stretching region of water was studied. The Raman intensities of the high frequency components increased as more perchlorate was added in all the cases studied.

The following conclusions were drawn by Walrafen from these studies;

(i) perchlorate ion produces extensive destruction of the hydrogen bonded water structure equivalent to the structural changes produced by a large increase in temperature,

(ii) perchlorate does not form hydrogen bonds with water whereas Cl^- and Br^- are able to form nearly linear hydrogen bonds,

(iii) hydration of the cations (Li^+, Na^+ or K^+) does not have a marked effect upon the OH and OD stretching vibrations.

The first conclusion followed from earlier work reported by Walrafen[241] in which he interpreted the temperature dependence of the OD stretching contour in terms of a two state model for water structure. It is concluded that the effect of the addition of one mole of sodium perchlorate is equivalent to a temperature rise of 34 K. The Raman spectral evidence for the failure of perchlorate to hydrate required the comparison of perchlorate spectra

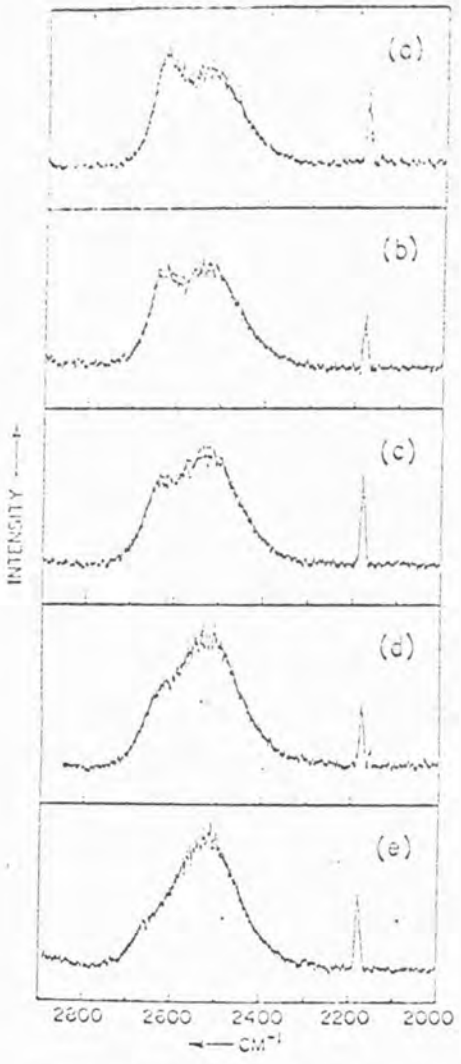

Photoelectric Raman recordings of argon-ion-laser-excited spectra (4880 Å) in the OD stretching region of HDO *from binary solutions*, 5.51*M* D_2O in H_2O, (e), and ternary solutions, 1-4*M* $NaClO_4$, 5.51*M* D_2O, in H_2O, (d)–(a). The amplification was constant for all spectra, but only neighboring spectra are approximately comparable with respect to intensities. The electric vector was oriented perpendicular to the slit of the spectrometer. The slitwidth was 10 cm^{-1}, and the time constant 1 sec. The spectral lines at 2180 cm^{-1} are produced by A^+—they are not Raman lines

FIGURE 7-9 (from reference 276)

with the spectra from ternary solutions containing K Br or K Cl. Previous Raman studies suggest that Br^- and Cl^- are strong structure breakers and the large intensity enhancements produced by salts of these ions is taken as evidence of anionic hydration.[261] There is clearly a conflict of opinion here between the conclusions of Wall and Hornig and Walrafen.

Recently Walrafen et al[277] have studied the stimulated Raman spectra from H_2O, D_2O, HDO, and perchlorate solutions. Exclusive stimulation of either hydrogen bonded or non-hydrogen bonded components was observed for the OH stretching vibrations. Interpretation of these spectra is complex but certain broad conclusions are reached. Firstly, the broad contours observed suggest a wide range of molecular environments encountered by a water molecule and are discussed in terms of refractive index modulation. Secondly, the results are interpreted as suggesting that two species at least, hydrogen bonded and non-hydrogen bonded water, are present. These can only be preliminary conclusions, and further developments in this field should prove of considerable importance. The conclusion that a wide distribution of ion-water environments is encountered in aqueous solutions of salts was also reached by Wyss and Falk[278] in an infra-red study of sodium chloride - HOD solutions.

Brink and Falk[279] have made a systematic study of the infra-red spectra of water in the crystalline hydrates $NaClO_4 \cdot H_2O$, $LiClO_4 \cdot 3H_2O$ and $Ba(ClO_4)_2 \cdot 3H_2O$. The infra-red

spectra of the deuterated and undeuterated hydrates were examined. Early crystallographic data by West[280,281] for $LiClO_4 \cdot 3H_2O$ points to a weak hydrogen bond between water molecules and the perchlorate ion. This was confirmed by the high HOD stretching frequencies for this compound. Brink and Falk also conclude that the near identical HDO stretching frequencies in the hydrates studied and in aqueous solutions of these salts points to a weak hydrogen bond between solvent and perchlorate in all the hydrates and their solutions. They estimated a bond energy for the water-perchlorate interaction of about 8 kJ mol^{-1}.

A very recent study by Brink and Falk[282] of the infra-red spectra of ternary solutions of perchlorate and fluoroborate goes some way towards demonstrating the existence of weak solvent-anion interactions in these solutions. In particular they observed in the infra-red OH and OD contours a difference in the locations of the high frequency components of about 14 cm^{-1}. They concluded that these features were due to oscillators solvating the perchlorate and fluoroborate anions. These conclusions are discussed in greater detail in the following chapters.

Few attempts have been made to study the effects of organic co-solvents of the OH and OD contours. Walrafen,[276,283] has briefly examined the effects of dimethyl sulphoxide, urea and sucrose.

7-4 CONCLUSION

The considerable theoretical advantages apparently

provided by the study of water and aqueous electrolyte solutions by infra-red and Raman spectroscopy are not fully realised in practice. The evidence seems to point towards a choice between continuum and two state models, though the problem of water structure will probably be finally resolved by a fusion of ideas drawn from both of these interpretations. At present the superiority of neither model is indicated although the two state model of Walrafen seems to account for the temperature dependence of the uncoupled OD stretching contours.

In regard to the study of electrolyte solutions certain conclusions can be drawn. Anions, for instance, would seem to exert most influence on the spectral bands observed in water. The effects of cations is apparently second order. A degree of confusion exists as to whether addition of an electrolyte to water causes an increase in the concentration of non-hydrogen bonded water (O-H) oscillators, or whether ionic hydration takes place. This now seems to have been fairly well resolved and the evidence points towards solvation of anions, especially in the case of perchlorates, in aqueous solutions.

Many problems still remain unresolved and there is a need for further study, especially in the region of the water librational modes. It seems that the packing of water molecules in solution differs from their arrangement in water. Hertz[222] concluded that the changes brought about by electrolytes in aqueous solution must be very different from the changes which take place on heating or

cooling water. Whilst this has an element of truth in it, the recent evidence of Walrafen, and Brink and Falk, suggests that such differences are perhaps less marked.

A final question which remains, as yet, unanswered concerns the directional arrangement of the molecules solvating an anion in solutions of electrolytes.[284,285]

CHAPTER EIGHT

INSTRUMENTATION AND EXPERIMENTAL DETAILS

8-1 INTRODUCTION

Vibrational spectra of aqueous solutions were recorded using several instruments. In the infra-red region (600-4000 cm^{-1}) the UNICAM SP100, followed more recently by a UNICAM SP200G, was used. The near infra-red region (5000-10000 cm^{-1}) was adequately covered using a BECKMANN DK-2A recording spectrophotometer. Raman spectra were obtained using two instruments, the CODERG PH_o and PH_1. In both cases 488.0 nm argon-ion laser excitation was used.

8-2 INFRA-RED INSTRUMENTATION

(i) UNICAM SP100

At the outset of this investigation the only available infra-red spectrophotometer having a low temperature Nernst source was a UNICAM SP100. The instrument required considerable rennovation after more than two years inactivity. Owing to the lack of satisfactory technical assistance from UNICAM, extensive repairs had to be undertaken before the machine could be used. One particular problem, which eventually prompted the acquisition of an SP200G, was the slowness and operational complexity of the SP100.

A diagram of the essential features of the optical system of the SP100 is presented in Figure 8-1. The instrument monochromator and photometer sections were

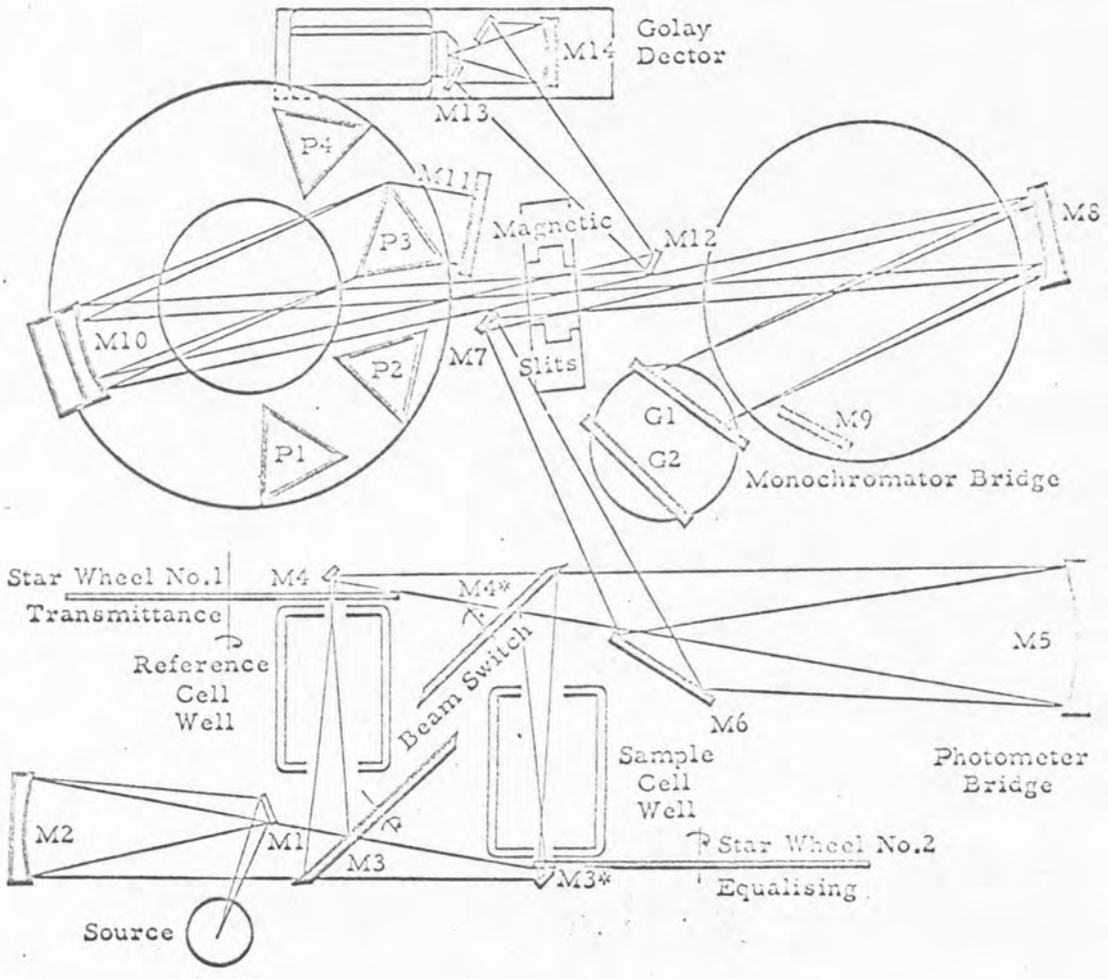

FIGURE 8-1 SP100 OPTICS

mounted on two separate girders. The monochromator consisted of a prism-grating system. Light from the photometer unit was reflected by mirror M7 through a magnetically operated slit mechanism onto M8, a parabolic mirror which reflected a parallel beam of light onto the selected grating (or, when the gratings were not in use, onto plane mirror M9). The light was dispersed by the grating and travelled back along a similar path to strike mirror M10, mounted on the rotatable prism table (similar to the grating table). M10 reflected the light through the selected prism onto a Littrow mirror M11, which was rotated by the scanning motor. Light from M11 returned along a similar path and was passed via the slits to M2, whence it entered the Pfund condensing system and Golay detector. The photometer unit, mounted in front of the monochromator bridge, operated on a null system as follows.

Light from the Nernst source was reflected by M1 to M2, and thence onto M3,a rotating beam switch which allowed the light to pass through the reference cell well or the sample cell well. From the reference cell well the light passed through a starwheel (number 1) (a rotating sectored wheel) which was moved by the balancing servo system and connected to the pen carriage. An equalising starwheel (number 2) was placed close to the sample cell and connected to the 100% transmission adjustment control. The light from these two cell wells was recombined by a M4 rotating sectored mirror and focused into the monochromator via mirrors M5 and M6. The signal from the Golay detector

passed through a discriminator and servo system to provide drive for the balancing transmission starwheel (No. 1). Two gratings and two prisms were available to give coverage of 200 to 5000 cm^{-1} in four ranges.

The wavenumber calibration was initially found to be some 300 cm^{-1} in error. This was only corrected after re-allignment of the gratings had been undertaken. Another problem, and one which could not be entirely eliminated, concerned the automatic prism, grating, cam and filter change assembly. The selection of the appropriate cam, prism, filter and grating was semi-automatic and required that some 20 relays and microswitches operated perfectly. This could not be expected of an instrument which was about 12 years old. Lack of replacement parts made this fault impossible to remedy and range interchange was a truly hazardous affair.

A final criticism of the SP100 concerns the very limited space available in the cell wells. Nevertheless this instrument has the attractive feature of being able to be operated under vacuum or dry nitrogen and also optimum resolution can be achieved with the prism-grating monochromator. However, it will have become clear from previous comments in Chapter 7 that resolution is not of paramount importance in the work described here, because the large bands are broad.

(ii) UNICAM SP200G

This instrument, obtained in November 1970, comprises

the SP200G spectrometer together with the SP250 scale expansion accessory and the SP19 flat bed strip chart recorder. It was possible to utilise the negative recorder input to provide marker 'pips' on the recorder trace at either 50 cm^{-1} (4000 to 1300 cm^{-1}) or 100 cm^{-1} (2000 to 650 cm^{-1}) intervals. The trigger pulses were supplied by a microswitch operated by a disc on the cam stack, which provided a switching mode at periodic intervals. These were differentiated using the simple circuit shown in Figure 8-2, and provided a series of marker pulses of about 1 mV, which were applied to the recorder input.

The spectrometer employed a Nernst source and Golay detector and had variable energy facilities. The monochromator employed a diffraction grating (3000 and 6000 lines/inch) and this eliminated the necessity for thermostating. A ray diagram of the optical system is shown in Figure 8-3, the main features of which are as follows.

The photometer, a double beam type, makes use of the optical null method for measurement. Light from the Nernst source was split into separate beams by mirrors M1, M1* and focused through the sample area by mirrors M3, M3*. The reference beam was brought to a focus at the reference beam attenuator and the sample beam converged at the cell mounting. The beams were chopped by a rotating sectored mirror at 15 Hz and facilities provided for synchronous signal rectification. An attenuator comb was placed in the reference beam and connected to the pen and driven by

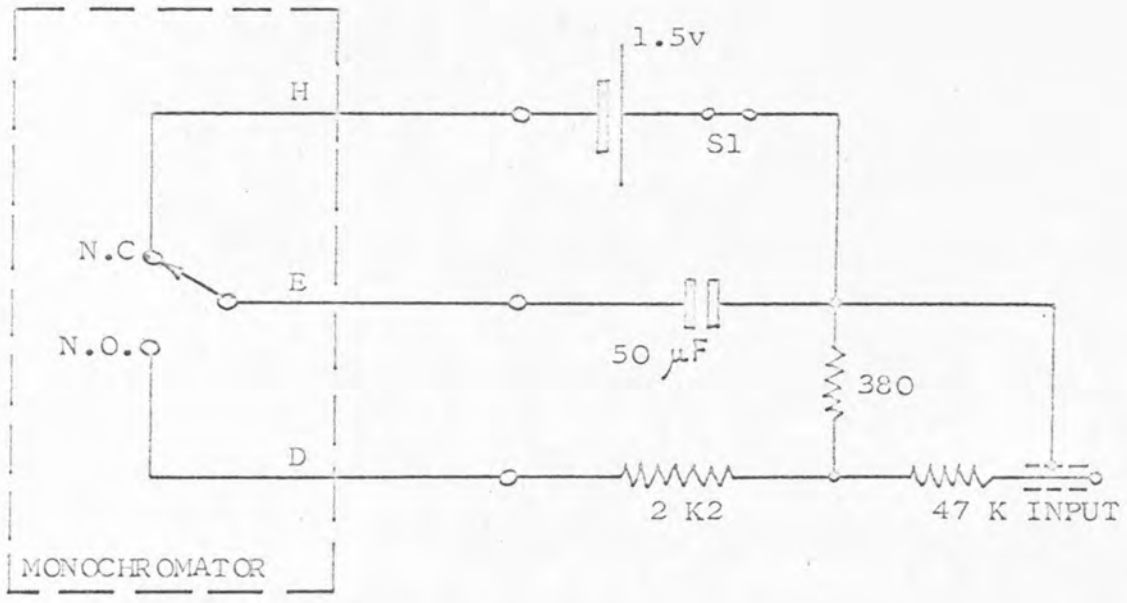

FIGURE 8-2 Marker Circuit

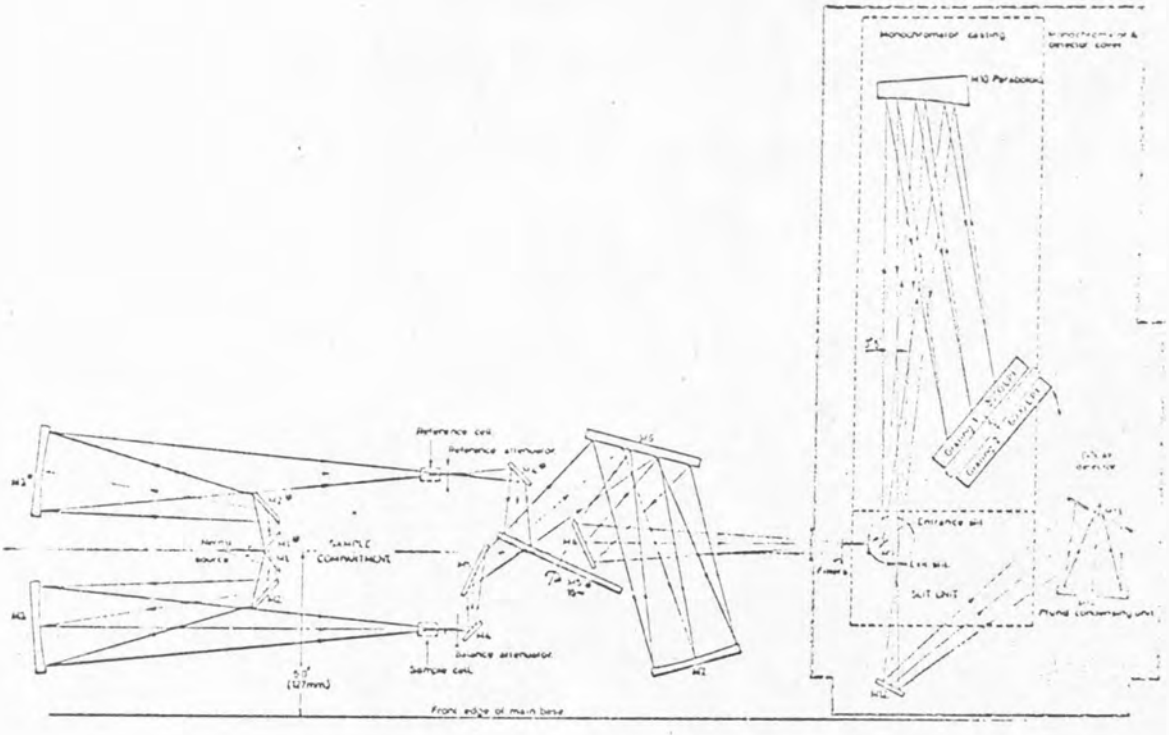

FIGURE 8-3 SP200G Optics

a servo motor. The attenuator was arranged to give a linear transmission scale. The monochromator was of the Littrow type. Light entering the monochromator, after passing through a filter, was reflected by mirror M9 onto M10, an off axis paraboloid mirror. This then produced a parallel beam which fell onto and was dispersed by the selected grating. The beam returned along a similar path to the exit slit and into the Pfund condenser and thence to the Golay detector.

The resolution was better than 2 cm^{-1} and the calibration which was checked with methane and polystyrene, was accurate to $\pm$ 2 cm^{-1}, using the SP19 recorder.

(iii) BECKMAN DK-2A

Near infra-red spectra were recorded in all cases using this instrument, which was essentially a UV-visible instrument fitted with a lead sulphide photocell extending its range into the near infra-red ($\sim$ 1600 nm). The source was a tungsten lamp.

(iv) SAMPLE HANDLING AND THERMOSTATING

Variable path length cells supplied by BECKMAN-R.I.I.C. and fitted with calcium fluoride windows (CaF_2) were used for single beam infra red measurements. For double beam infra red measurement a variable path length cell was used in conjunction with a demountable cell (Type FH-01) supplied by BECKMAN-R.I.I.C., or two such demountable cells, fitted with appropriate teflon spacers, were used.

Thermostating to about $\pm$ 2 K was achieved using a large tank of water maintained a little above (or below in the case of temperature less than ambient) the desired temperature, using a contact thermometer and relay device. Water was circulated around a water jacket type WJ-2supplied by BECKMAN-R.I.I.C. which supported the FH-01 cells. Temperatures were measured using a calibrated copper-constantan thermocouple inserted into a recess in one of the cell windows. The thermostating system was not very satisfactory for two reasons. Firstly, low temperatures were difficult to obtain because the coolant was heated by the pump. Secondly, the small pipe diameter in the water jacket WJ-2 allowed only a low flow rate of thermostating fluid. A greater flow rate around the jacket could only be achieved following extensive redesign of the BECKMAN-R.I.I.C. jacket.

In the near infra-red region 1 cm silica cells similar to those employed in U.V. spectrophotometry were used. These were thermostated at the desired temperature by fluid circulated through the cell mounting block from a Townson and Mercer thermostat bath. Temperatures were measured by means of a copper-constantan thermocouple dipping into the liquid. The error in temperatures recorded was of the order of $\pm$ 0.5K.

8-3 LASER-RAMAN INSTRUMENTATION

A Raman spectrometer must have the following:-

(a) A source of coherent monochromatic light of high intensity (high intensity since often raman spectra are weak) is conveniently provided by a gas laser, of the He-Ne or A^+ types, nowadays.

(b) The sample mounting area should provide facilities for placing solid, liquid and gaseous samples within the laser beam close to the monochromator entrance slit.

(c) A high quality monochromator such as a double grating type is essential since the Raman scattering is of low intensity compared with the exciting line. The essential requirements of the monochromator in addition to calibration accuracy are,

(i) low stray light passage,

(ii) optical precision, and

(iii) maximum resolution.

(d) The detector is usually a very sensitive photomultiplier tube. An improved signal to noise ratio is obtained by cooling the photomultiplier.

(e) A stable H.T. supply for the photomultiplier and a D.C. amplifier are required, together with a strip chart recorder and monochromator scanning facilities.

(i) THE CODERG PH_o AND PH_1 RAMAN SPECTROMETERS

The optical system and transfer plate optics of the CODERG PH_o and PH_2 laser Raman spectrometers are illustrated in Figure 8-4. The monochromator (focal length 600 mm)

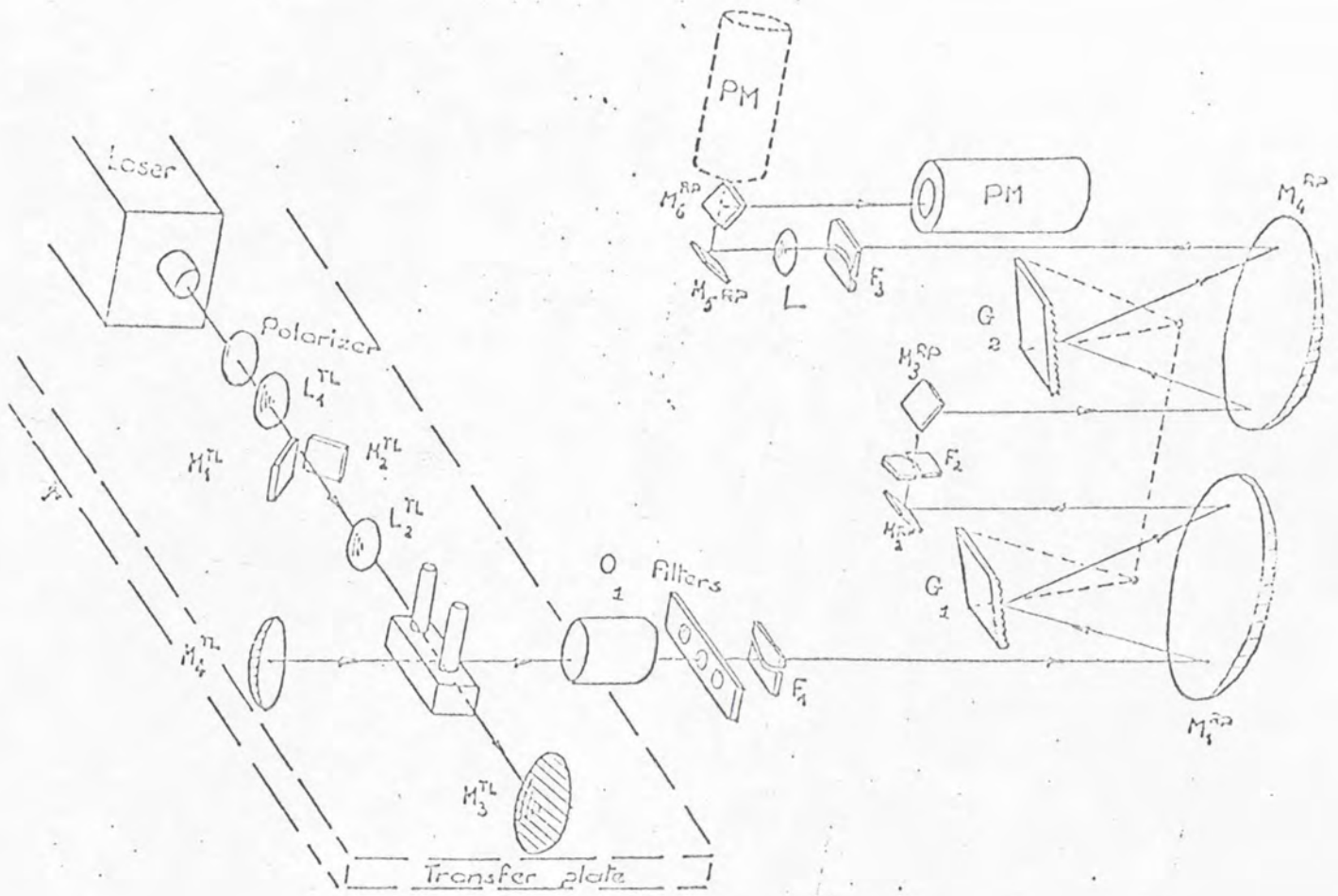

FIGURE 8-4 CODERG Optics

was rigidly constructed of aluminium alloy. Light scattered by the sample entered the spectrometer via the objective lens (O_1), passed through an appropriate filter and was incident upon the entrance slit F_1. To ensure high reliability, F_1 and F_3 were 30 mm commutable fixed slits, whose curvature lay on the 'Fastie circle'. These slits were mounted horizontally to eliminate bubble effects in liquid samples. The slits were calibrated directly in resolution at 488.0 nm. After passing slit F_1 the light fell upon mirror M1 which reflected this onto grating G_1 (1200 g/mm). The beam of light underwent diffraction by the grating and then two further reflections at mirrors M1 and M2. At this stage an intermediate slit F_2 was interposed which was adjusted using an external micrometer control. The light next entered the second half of the double grating monochromator and underwent further diffraction. The light left the monochromator via the exit slit F_3 and struck a plane mirror M5 after focussing by lens L. In the PH_1 (the earlier model) the detector (PM) was mounted horizontally, a sixth mirror M6 being used to reflect the light into it. The PH_0 has the detector vertically mounted to facilitate cooling of the phototube by liquid nitrogen. The gratings were mounted in ball races and grating transport was arranged to be linear in wavenumber by means of a cosecant bar. The drive was provided by a step drive motor. The double grating monochromator, having coupled gratings and an intermediate, slit had identical resolution to a double

pass monochromator but a much reduced stray light level. Thus it was better suited to Raman work.

The detector was a specially selected high performance photomultiplier supplied with a stabilised variable high tension source. The phototube was a high quality, high gain, DC amplifier ($\sim 10^6$). Suitable voltage for recording was obtained using a low gain integrated circuit DC amplifier which did not introduce much noise. A further reduction in noise level for very weak signals may be achieved using a cooled phototube or photon counting techniques.

The amplifier input incorporated a series of selectable Resistance-Capacitance filters which, together with automatic electronic coupling to the slits, ensured optimum recording conditions. Control light indicated on the PH_1 when this condition was fulfilled.

The amplifier output was recorded on a strip chart recorder and a marker device (similar to that previously described for the SP200G) provided calibration points at 50 cm^{-1} intervals. The major features of the electronics are summarised in Figure 8-5.

The transfer plate is shown in plan in Figure 8-6. The plate was supported by a kinematic mounting such that the sample area was opposite the projection objective (O_1 Figure 8-4). Essentially it was an optical bench providing support for collimating and focussing lenses and mirrors and sample holders. The collimated coherent plane polarised laser beam (with the electric vector vertical with respect to the entrance slit of the monochromator)

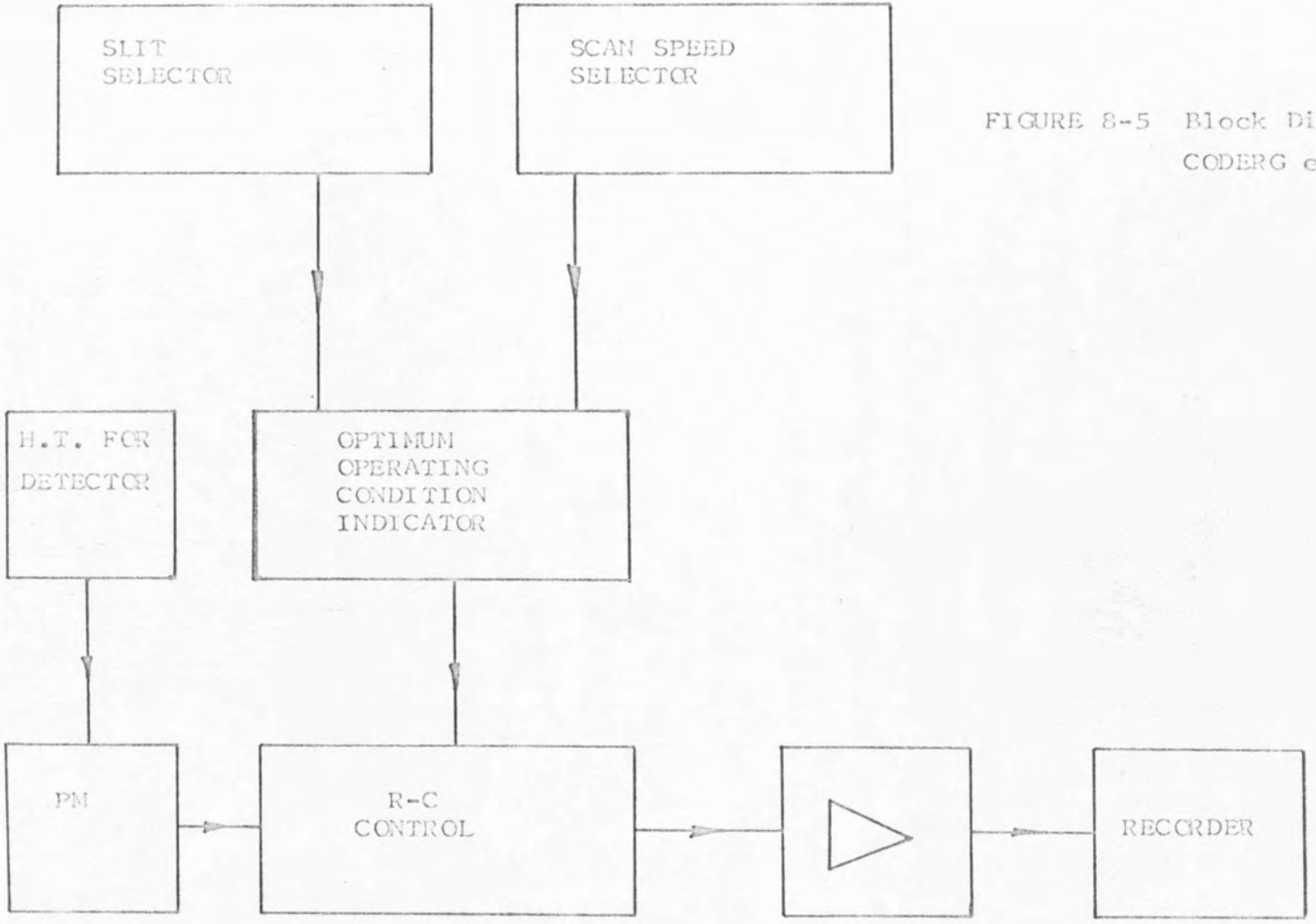

FIGURE 8-5 Block Diagram of
CODERG electronic system

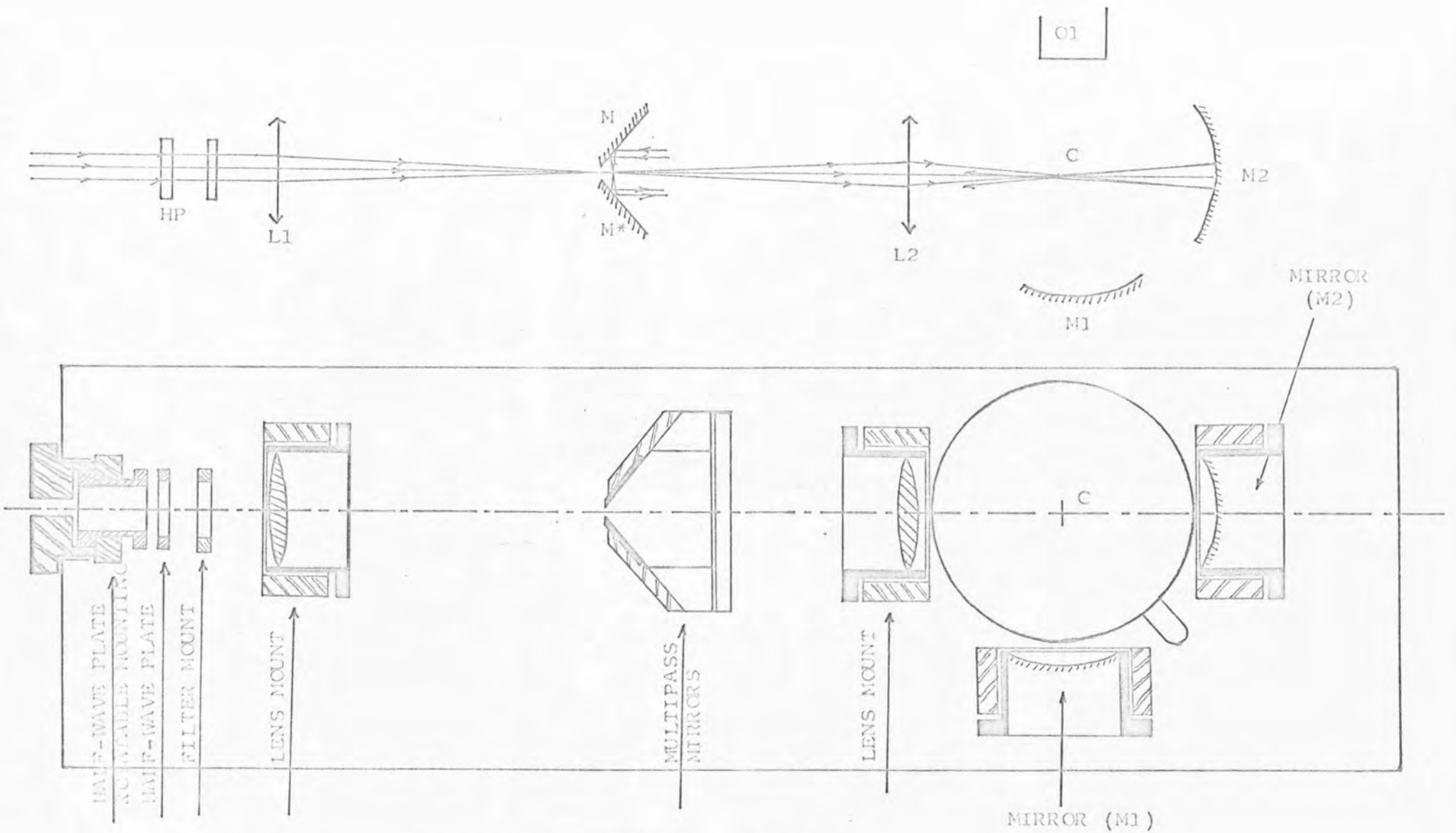

FIGURE 8-6 CODERG Transfer Plate

passed through a half wave plate (HP). When this was rotated by 45° the electric vector of the incoming beam was rotated by 90°. The beam was then focussed by a convex lens (all lenses involved were 'thick lenses') at the junction of the multipass mirror system M,M*. The beam then diverged until it struck lens L2 and was brought to a focus at C (the centre of the sample holding area) and from there diverged to reach mirror M2. A ray leaving M2 was arranged (by adjustment of M2) to take a slightly different path (i.e. the foci of M2 and L2 were not coincident at C). Thus, when the ray struck the multipass mirror system, it impinged on one of the plane mirrors M,M* and was reflected between these and back to L2. Thus the ray may execute several passes through the region of C and the optical system. A cell placed at C would thus have several beams of light passing through it. The mirror M_1 served to reflect the scattered Raman light into the projection lens O_1. The multipass system had the advantage that more scattered light was collected by the monochromator, thus increasing the overall sensitivity of the spectrometer.

(ii) ALIGNMENT OF SPECTROPHOTOMETER AND RECORDING OF THE RAMAN SPECTRUM OF A LIQUID SAMPLE

Brief details will be given for the alignment procedure of the multipass optics and the operation of the instrument for the case of a liquid sample (say H_2O). Further information (in French) is available from the CODERG Operation Manual.

(a) Aligning the multipass optics

The laser was lined up so that the beam lies along the centre line of the transfer plate using the device provided by CODERG for this purpose. It is assumed that the instrument has been set up for the exciting line used (say 488.0 nm), that is the wavenumber counter has been set for zero at the exciting line wavenumber.

The multipass system was most conveniently aligned by positioning the optical components as indicated in Figure 8-6. With a cell containing distilled water in the cell holder (described later) and with mirror M1 removed, the three screws at the back of the M2 mirror mount were adjusted whilst viewing the cell from above (with the electric vector vertical) until about 6 to 9 narrow beams of light were visible crossing the cell. With the electric vector horizontal (HP rotated through 45^{o} from vertical vector position) the beams should all be in one plane when the cell is viewed from the direction of mirror M1. Further adjustments in the locations of the mirrors and lenses may be necessary and the method of trial and error had to be used to obtain a maximum number of passes.

(b) Recording a Spectrum

When this condition had been achieved mirror M1 was replaced. The long lever on the projection objective was placed in a midway position. (This lever caused rotation of a collecting tube mounted off axis) A moderate laser power (for water say 600 mW) and a slit width of about 2 or 4 cm^{-1} were selected. About 900 to 1000 v

was applied to the photomultiplier (dependent on PM). The gain (R) control was set to maximum and an appropriate combination of time constant (C) and scan speed selected until the indicator lamps were simultaneously illuminated. (For the PH_o these latter values were found from tables supplied).

The monochromator was set to the wavenumber value at which the desired band was to be observed. The recorder pen should have deflected. If it did not, the laser power, slit width, or photomultiplier voltage was increased. If the pen did deflect the gain, slit width, laser power or recorder attenuation were reduced until the deflection covered a good portion of the chart. The position of maximum deflection was located by scanning over this region and stopping the scan at that position. The three screws on the mounting of M1 were adjusted to maximise this deflection. Having reached this position, the lever and knurled brass ring on the lens O1 were rotated (image focusing;focuses image onto slit) separately until maximum deflection was again achieved (during these processes it may have been necessary to reduce the gain or laser power since the function of this process was to focus the maximum Raman scattered light into the monochromator). The intermediate slit (F2) was closed up until the minimum setting was located, which did not cause a reduction in band intensity. At this stage recording of a preliminary spectrum could be carried out.

The laser used for our studies was the COHERENT RADIATION ARGON ION LASER MODEL 52A with a maximum output

of 1300 mw at 488 nm.

(iii) CELL HOLDER DESIGN AND THERMOSTATING SYSTEM

CODERG do not supply a thermostated liquid cell holder for their PH_o or PH_1 spectrometers, and thus the design of a suitable device was undertaken. Certain criteria for the thermostated cell holder may be set out as indicated below.

Firstly, the cell mounting system must be such that light may pass on all four sides; secondly, the dimensions were quite critical,and finally thermostating must be such that convection currents are not set up in the liquid since these give rise to light scattering. The cell is shown in diagramatic form in Figures 8-7a and 8-7b. The main features are described below.

The central component of the cell holder was a copper tank (T) sealed and fitted with inlet and outlet pipes as illustrated. This was supported by a copper ring (R), insulated from the aluminium mounting block (MB) by a Tufnel washer. The mounting block had standard dimensions for the PH_o and PH_1 transfer plates. The tank, which had a domed roof for minimising the trapping of air thus reducing efficiency, was surmounted by the cell holder (H). This is shown in detail in Figure 8-7a and consisted of a copper block braised to the top of the tank, fitted with four sides (two tensioned by springs) and cut as indicated. This will be more clearly visible from the plan - Figure 8-7b.

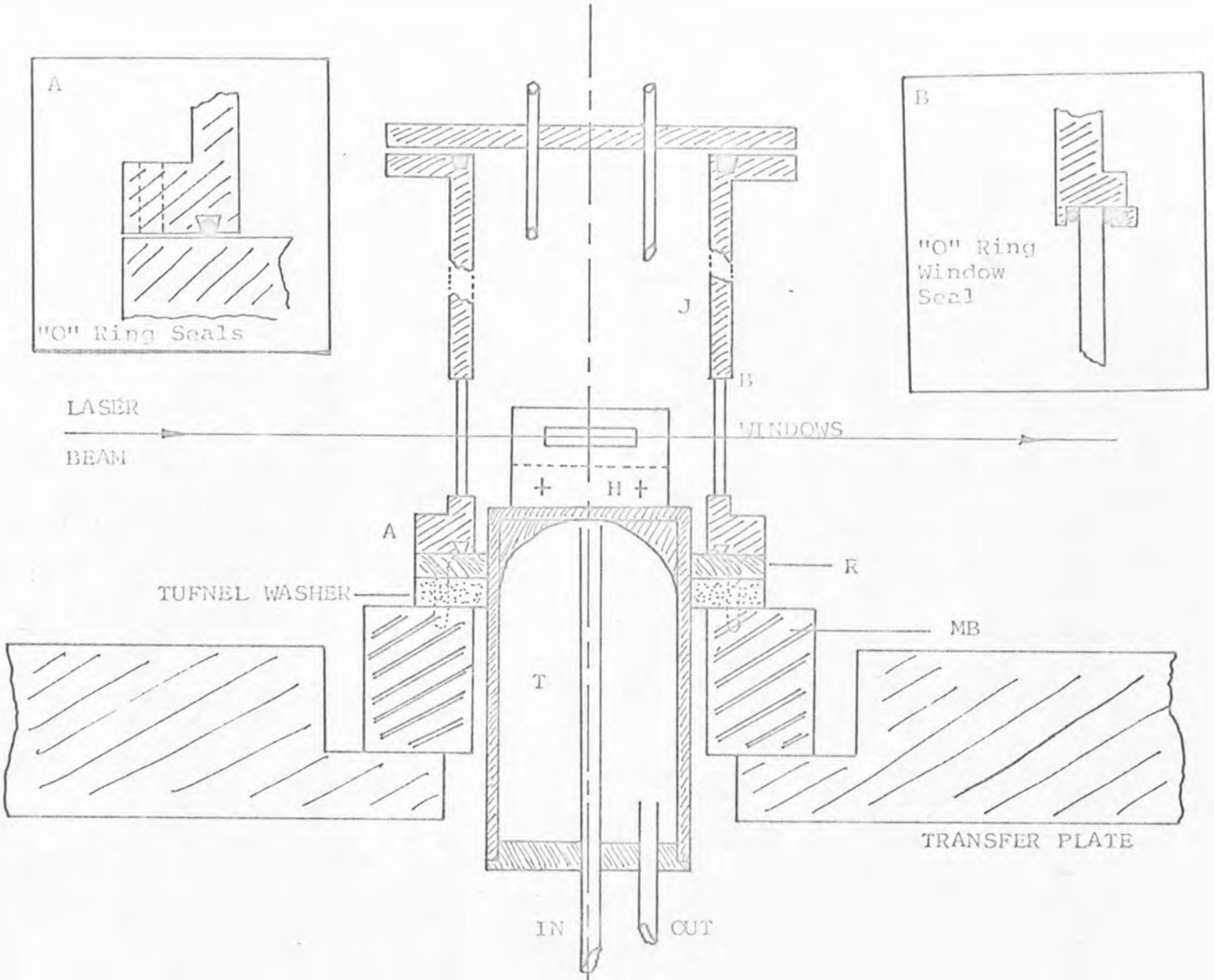

FIGURE 8-7a Thermostated Cell Design - Section.
(FULL SCALE - APPROX.)

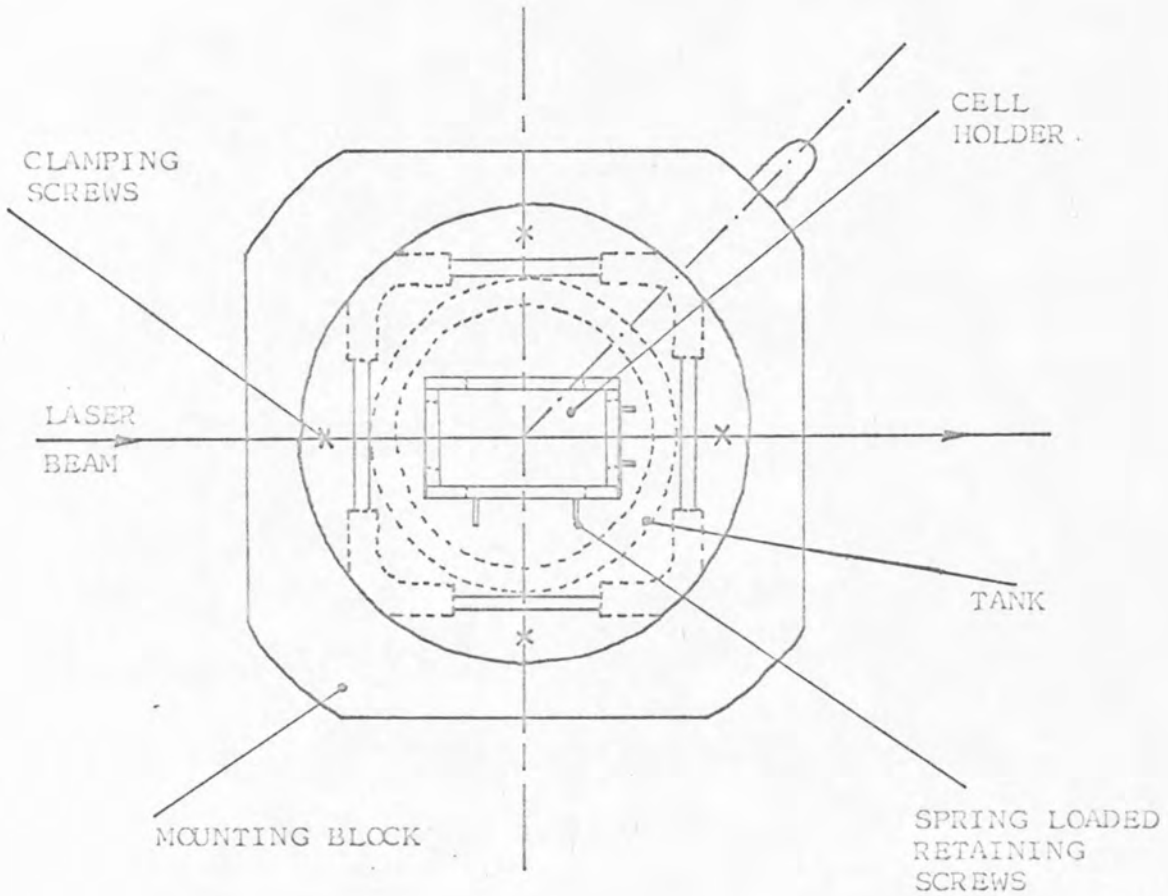

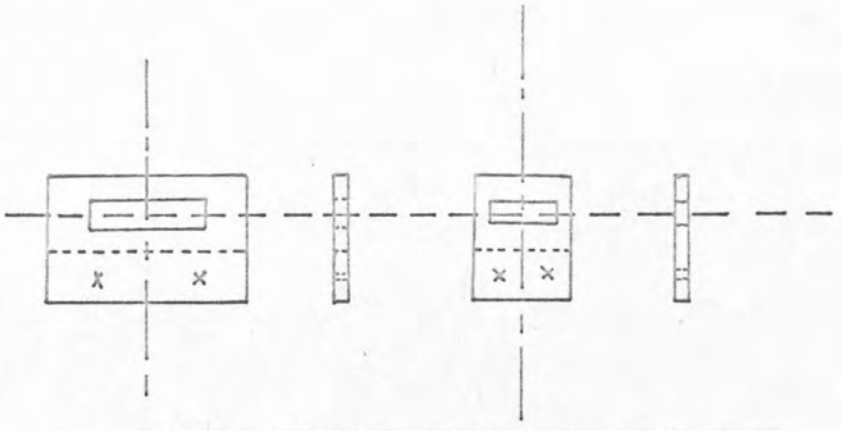

DETAIL OF CELL HOLDER CONSTRUCTION

FIGURE 8-7b Thermostated Cell Design - Plan.
(FULL SCALE- Approx.)

The whole upper part or jacket (J) of the holder was surrounded by a cylinderical jacket fitted with four optically flat windows at right angles with respect to each other. This jacket was sealed to the base by an "o"-ring and a cover fitted with two tubes was also screwed to the top of the jacket incorporating an "o"-ring seal. Thus the whole upper jacket could be evacuated, or filled with some dry gas for greater efficiency. Facility was also provided for the insertion of a thermocouple into one limb of the Raman cell.

Thermostating fluid from a contact thermometer controlled tank was conveniently fed by a Stuart-Turner pump to the small cell holder tank (T) from below the transfer plate. Figure 8-7b also shows certain details not shown on Figure 8-7a which clarify the cell holder construction. Over the range 283 K to 373 K liquid temperatures were stable to $\pm$ 0.5 K after 40 minutes. Due to the relatively large volume of the tank ($\sim$ 50 cm^3) compared to the small volume of fluid to be thermostated ($\sim$ 2 cm^3), thermostating was quite rapid. The 'cell' behaved quite well at low temperature when cooled nitrogen was used as a coolant in place of water.

(iv) ADAPTATION OF CODERG PH_1 FOR DIGITAL OUTPUT AND ASSOCIATED BAND DECONVOLUTION PROGRAMS.

(a) Digital Output Electronics

If the spectrum can be recorded digitally, that is, if the recorder pen position can be recorded at constant wavenumber intervals, the resulting information will be

available for mathematical band shape analysis. CODERG do not supply a simple system to do this, and for digital output the photon counting accessory is required. This is very expensive. However, digitisation of the spectra may be obtained with reasonable accuracy by a simpler method which we have used.

The CODERG instruments employ step drive motors in their scanning systems. Pulses are supplied by an oscillator and binary dividers and these pulses may readily be used to trigger a data logging device which would record the potential across the recorder, and hence the position of the pen on the recorder chart.

The SOLARTRON DATA LOGGER, together with an ADDO digital output punch, was used and triggering was achieved by closing two contacts provided for this purpose, using a relay. The pulses required for driving the step drive scanning motor were found to be available at pins 7 and 9 of plug CA12F (reference to instrument wiring diagrams). The pulse rate obtained was 8 per cm^{-1} and at a scanning speed of 60 cm^{-1}/min this would mean that one voltage reading would be taken every $\frac{1}{8}$th of a second. Since the data logger cannot sample faster than 3 readings per second, this means that we require an electronic device to divide down the pulse repetition frequency. This was constructed and the relevant circuit diagrams are shown in Figure 8-8. Figure 8-8a shows a block diagram of the device. The signal from the motor is fed to a buffer amplifier. This has a gain of

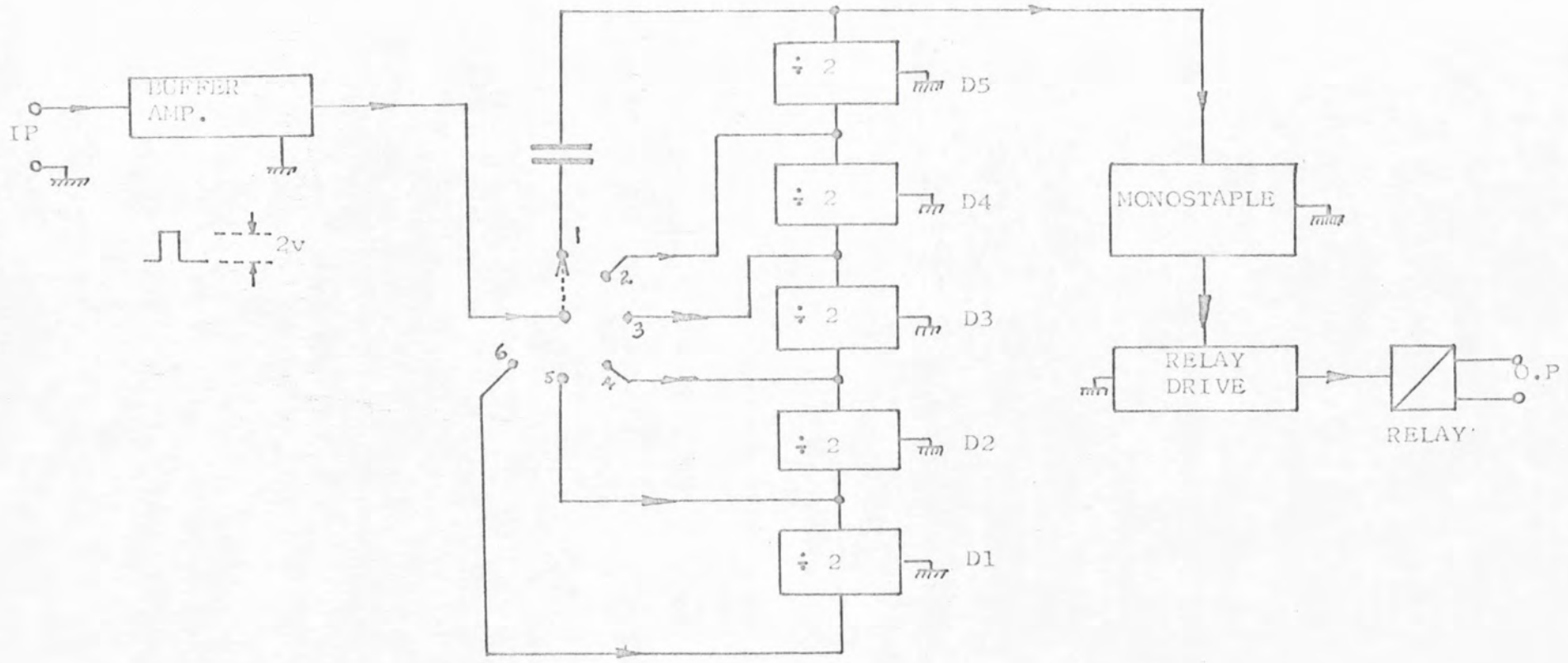

FIGURE 8-8a Block Diagram of Binary Divider Unit.

about 1 and an input impedence of ~14 MΩ, and so protects the instrument from damage due to the drawing of excessive currents. The output of the buffer amplifier is fed via a selector switch S1 to a bank of five binary divider units, such that 0 to 5 of these units can be incorporated into the circuit. The final output after the dividers is fed to a monostable and thence to a relay drive circuit and relay. The relay contacts are connected to the data logger.

Figures 8-8b and 8-8c show, respectively, the buffer amplifier, and final divider (D5) circuits, and the monostable and relay drive circuits. Some further test data is included in Appendix 8-1 together with correlation tables relating selector position (S1), scanning speed, and points output per cm^{-1}.

With the spectrometer set up to record a spectrum, for which a digital record is required, the selector switch S1 was set to a suitable value (see Appendix 8-1 to provide the desired number of wavenumbers per point. The recorder attenuation was noted together with the voltage corresponding to 0% and 100% per deflection. The spectrometer was then switched to SCAN and the wavenumber, indicated by the counter at which the first triggering of the data logger takes place, was recorded. Points (voltage readings) were then punched out at the selected wavenumber intervals, until the spectrometer was switched to STOP SCAN. The digitally output data of voltage on recorder versus chosen wavenumber interval was converted

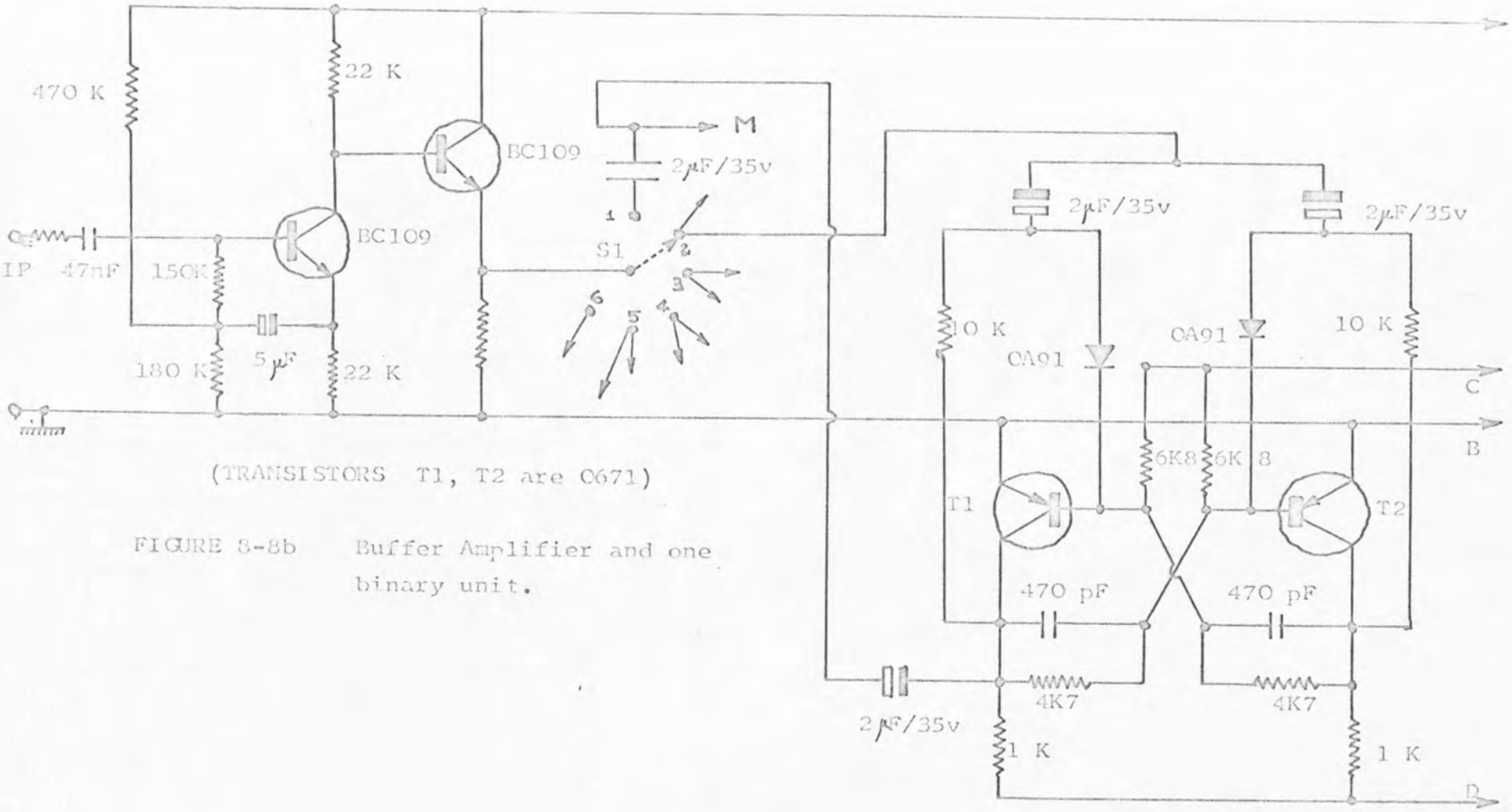

(TRANSISTORS T1, T2 are O671)

FIGURE 8-8b Buffer Amplifier and one binary unit.

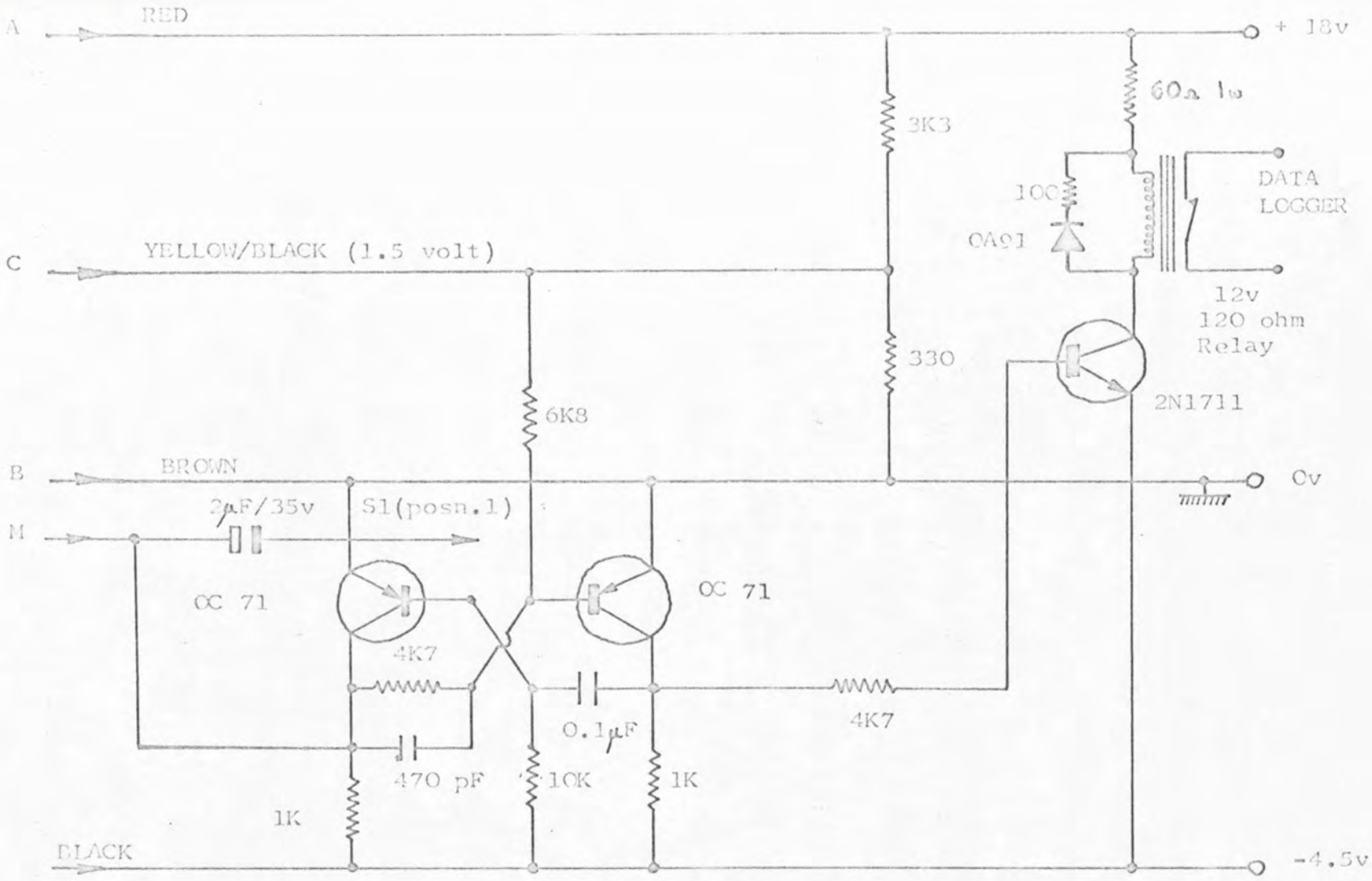

FIGURE 8-8c Final Monostable and Relay Drive

to a table of wavenumber versus percentage pen deflection using the program described in Appendix 8-2

(b) Computer Deconvolution of Band Envelopes

Often infra-red and Raman bands are composite features incorporating two or more bands, possibly on a curved 'background'. The process of obtaining these components is called Deconvolution and a least squares program similar to that described by Stone[177] was written to perform such deconvolution into Gaussian or Lorentzian Components. The method employed is described below and a summary of the order of data input is given, together with a listing of the ALGOL program, in Appendix 8-2
If the band shape represented by ϕ is some function, say Gauss or Lorentz, of the parameters ν°, the frequency of maximum intensity and $\Delta\nu$ the half width of the band,

then $\phi_i = \phi\,(\nu_i^{\circ}, \Delta\nu_i)$ . . . . . (8-1)

for any band i.

If the contour is a convolution of n bands, then

$$I_c(\nu) = \alpha + \beta\nu + \gamma\nu^2 + \sum_{i=1}^{n} a_i\,\phi(\nu_i^{\circ}, \Delta\nu_i) \qquad \text{. . . . . (8-2)}$$

where $I_c(\nu)$ is the contour intensity calculated at wavenumber ν. If we have m data points on the observed experimental curve, then the sum of the squares of the deviations F is given by

$$F = \sum^{m} \left(I_e(\nu) - I_c(\nu)\right)^2 \qquad \text{. . . . . (8-3)}$$

$I_e(\nu)$ is the experimentally observed intensity at and $I_c(\nu)$ the calculated intensity.

Band parameters for the components of the envelope are required which satisfy the relation

$$\frac{\partial F}{\partial p_i} = 0 \quad (\forall i \text{ to } 3n+3) \qquad \ldots\ldots (8\text{-}4)$$

The specific parameters are now represented by a series of $3n + 3$ parameters p_i (called general parameters). Suppose we have a function

$$F = f(p_1, p_2, p_3 \text{ ---} p_k \text{ ---} p_{3n+3}) \qquad \ldots\ldots (8\text{-}5)$$

Expansion, using a Taylor Series, gives

$$\partial F = \frac{\partial F}{\partial p_1}\delta p_1 + \frac{\partial F}{\partial p_2}\delta p_2 + \frac{\partial F}{\partial p_3}\delta p_3 + \text{---} + \frac{\partial F}{\partial p_{3n+3}}\delta p_{3n+3} \qquad \ldots\ldots (8\text{-}6)$$

$$\text{so} \quad \partial F = \sum_{k=1}^{3n+3} \frac{\partial F}{\partial p_k}\delta p_k \qquad \ldots\ldots (8\text{-}7)$$

If it is supposed that we chose an initial parameter p_i°, then $\frac{\partial F}{\partial p_i}^{\circ}$ can be calculated as follows:

$$\frac{\partial F}{\partial p_i}^{\circ} = \sum_{k=1}^{3n+3} \frac{\partial^2 F}{\partial p_k^{\circ}\partial p_i^{\circ}}(p_k - p_k^{\circ}) \qquad \ldots\ldots (8\text{-}8)$$

$$\frac{\partial F}{\partial p_i} = 0 \simeq \sum_{k=1}^{3n+3} \frac{\partial^2 F}{\partial p_k^{\circ}\partial p_i^{\circ}}(p_k^{\circ} - p_k) + \frac{\partial F}{\partial p_i}^{\circ} \qquad \ldots\ldots (8\text{-}9)$$

Thus, the problem has been linearised.

Let g be a matrix having elements $\frac{\partial F}{\partial p_i}^{\circ}$ $\forall i$ and H be a matrix having elements $\frac{\partial^2 F}{\partial p_k^{\circ}\partial p_i^{\circ}}$ $\forall i, k \rightarrow 3n + 3$. Equation (8-9) may be written in matrix form.

$$0 \approx g + H(p - p^{\circ}) \qquad \ldots\ldots (8\text{-}10)$$

p and p° are vectors containing the elements p_k and p_k° $\forall k$. Thus equation (8-10) becomes

$$p \approx p^{\circ} - H^{-1}g \qquad \ldots\ldots (8\text{-}11)$$

Since H^{-1} is difficult to obtain, we approximate H by $\mathcal{H}\tau$ where $\mathcal{H}$ is a matrix for which all the off idagonal elements $k \neq i$ are zero and τ is a variable to be discussed later.

This leads to the result that for any parameter with initial value p_i° a "better" value of p_i can be obtained from the relationship

$$p_i = p_i^{\circ} - \tau \left[\frac{\partial F}{\partial p_i^{\circ}} \Big/ \frac{\partial^2 F}{\partial p_i^{\circ 2}} \right] \qquad \ldots\ldots (8\text{-}12)$$

τ is a "damping factor" or step length modifier and is set initially to $\tau = 1.0$ and thereafter varied by $0.5\,\tau$ until a value of F which is smaller than the value of F calculated using the parameters p_i° (i.e. F°) is obtained. The "new" parameters p_i take the place of the parameters p_i° and the process of 'improving' the value of p_i is repeated to obtain a minimum value of F. Various other controls have been included in the program and these are fully described in Appendix 8-2. It is clear that for the program sets of equations giving the values of $\frac{\partial F}{\partial p_i}$ and $\frac{\partial^2 F}{\partial p_i^2}$ are required. The derivation of these is now indicated.

From equation (8-3) we obtain by successive differentiation $\frac{\partial F}{\partial p_i}$ and $\frac{\partial^2 F}{\partial p_i^2}$, the quantities required for equation (8-12).

$$\frac{\partial F}{\partial p_i} = -2 \sum_{k=1}^{m} (I_e - I_c) \frac{\partial I_c}{\partial p_i} \qquad \ldots\ldots (8\text{-}13)$$

$$\frac{\partial^2 F}{\partial p_i^2} = -2\sum_{k=1}^{M}\left\{(I_e - I_c)\frac{\partial^2 I_c}{\partial p_i^2} - \left(\frac{\partial I_c}{\partial p_i}\right)^2\right\} \quad \ldots\ldots \text{(8-14)}$$

These derivative equations are also listed in Appendix 8-3

From equations (8-13) and (8-14) it readily becomes clear that we require expressions for the derivatives

$$\frac{\partial \phi_i}{\partial \nu_i^{\circ}} \; ; \; \frac{\partial \phi_i}{\partial \Delta\nu_i} \; ; \; \frac{\partial^2 \phi_i}{\partial \nu_i^{\circ 2}} \; ; \; \frac{\partial^2 \phi_i}{\partial \Delta\nu_i^2}$$

Taking the case of Gaussian band shapes ϕ_i may be written

$$\phi_i = \exp\left(-((\nu - \nu_i{}^{\circ})/\Delta\nu_i)^2\right); \quad \ldots\ldots \text{(8-15)}$$

for Lorentzian band shape ϕ_i =

$$\frac{1}{1 + \left((\nu - \nu_i{}^{\circ})/\Delta\nu_i\right)^2} \quad \ldots\ldots \text{(8-16)}$$

For the Gaussian case these derivatives are

$$\frac{\partial \phi_i}{\partial \nu_i^{\circ}} = \frac{2(\nu - \nu_i^{\circ})}{\Delta\nu_i^2} \cdot \exp(-u) \quad \ldots\ldots \text{(8-17)}$$

$$\frac{\partial \phi_i}{\partial \Delta\nu_i} = \frac{2(\nu - \nu_i^{\circ})}{\Delta\nu_i^3} \cdot \exp(-u) \quad \ldots\ldots \text{(8-18)}$$

$$\frac{\partial^2 \phi_i}{\partial \nu_i^{\circ 2}} = \left\{\frac{4x}{\Delta\nu_i^4} - \frac{2}{\Delta\nu_i^2}\right\} \cdot \exp\left(-\frac{x}{\Delta\nu_i^2}\right) \quad \ldots\ldots \text{(8-19)}$$

$$\frac{\partial^2 \phi_i}{\partial \Delta\nu_i^2} = -\frac{2u}{\Delta\nu_i^2}\{3 - 2u\} \cdot \exp(-u) \quad \ldots\ldots \text{(8-20)}$$

x and u in the above expressions represent the quantities

$$x = (\nu - \nu_i{}^{\circ})^2$$

$$u = \left((\nu - \nu_i{}^{\circ})/\Delta\nu_i\right)^2$$

A similar set of equations can be derived for the case of Lorentzian band shapes.

Thus the program operates by taking initially estimated values of the set of 3n + 3 parameters (where n is the

number of bands comprising the contour subjected to analysis) and successively refines these. The criterion used to establish that a satisfactory 'fit' of the experimental contour to that calculated being that the sum of the squares of the deviations be minimised.

Some examples of the application of the program are discussed in the following chapter. A flow chart of the ALGOL program, called SPECT 1, is given in Figure 8-9.

8-4 PREPARATION OF SOLUTIONS AND MATERIALS

(i) Materials Used

Water, used in the preparation of solutions, was produced by distillation of deionised water from alkaline potassium permanganate under nitrogen. All solvents used were purchased from B.D.H. or Fisons and were analytical grade. These solvents were dried over molecular sieve and used directly. Absence of water in CH_2Cl_2 and methanol was checked by recording the infra-red spectra of the solvents and in no case did the percentage of water exceed 0.05. All salts used were dried in a vacuum oven for several days prior to use at the appropriate temperature. Deuterium oxide was purchased from Koch-Light Ltd. and was supplied at 99.7 atom per cent D_2O, bottled under nitrogen. This was used directly.

In the case of electrolytes standard concentrated solutions of these in water were prepared. A standard solution of D_2O in water was prepared. The concentration

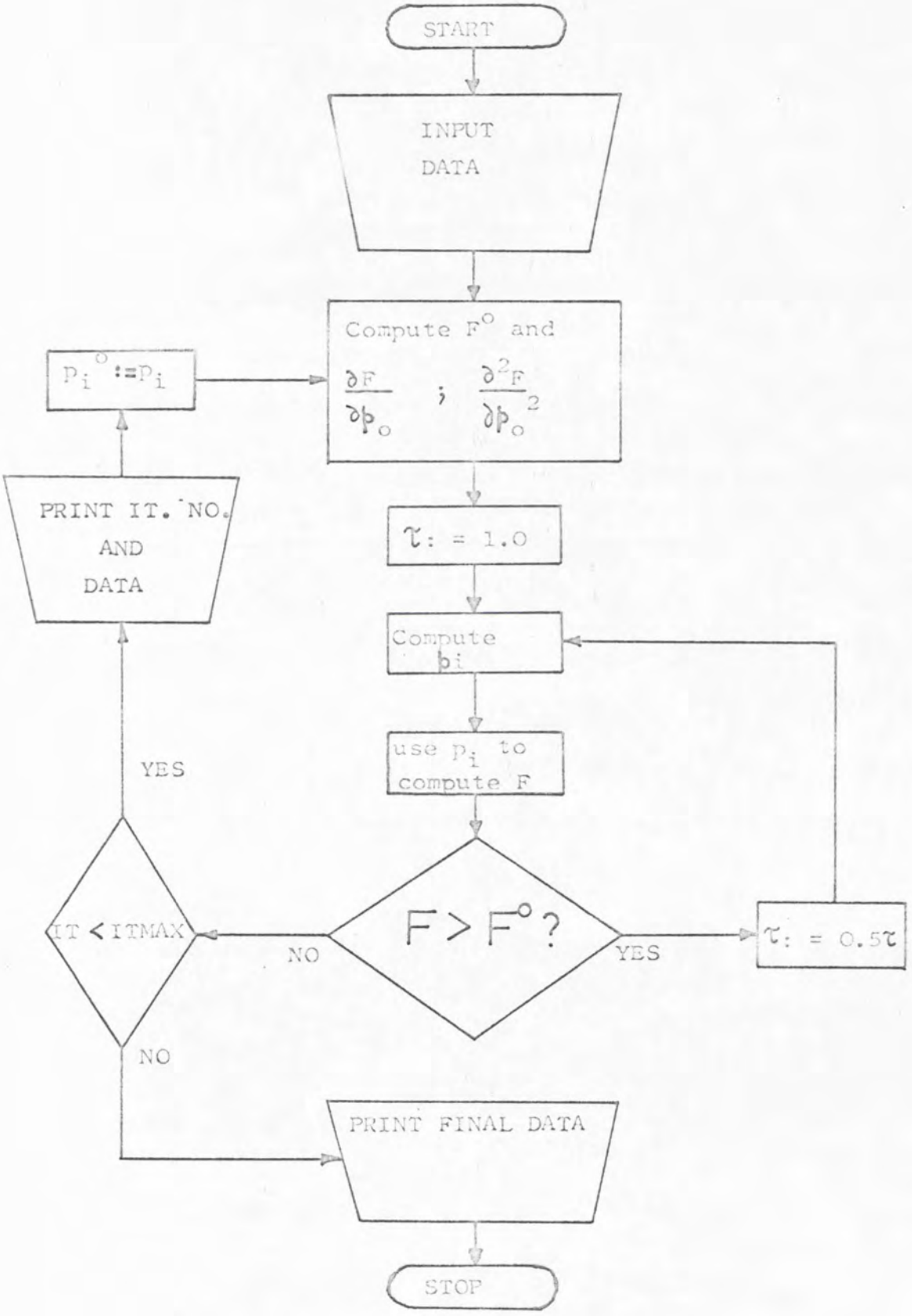

FIGURE 8-9 FLOW DIAGRAM OF DECONVOLUTION PROGRAM

of this solution was so chosen that after dilution of an aliquot of this to the final volume of the working solutions, the concentrations were 2% for infra-red studies and 2 mol dm^{-3} or 6 mol dm^{-3} for Raman studies. Solutions for infra-red spectroscopy were prepared in sets of two 10 cm^3 graduated flasks by mixing suitable aliquots of electrolyte solutions with a fixed quantity of standard D_2O (to prepare the sample solution). The same quantity of electrolyte was added to the reference solution, the D_2O being omitted, and the solutions diluted to the mark. For spectroscopy of organic solutes, the concentrated electrolyte solution was replaced by an appropriate quantity of the pure organic solute.

Solutions for Raman spectroscopy were prepared in a similar fashion to those of the sample solutions for infra-red spectroscopy. These solutions were then filtered between three and five times through 0.22μ millipore filters before transference to the Raman cell. The purpose of this filtration was to remove suspended dust particles which increase the Rayleigh scattering (background scattering) and produce a noisy Raman spectrum.

Sodium and Ammonium Fluoroborates, supplied by B.D.H., were recrystallised twice from water to remove all insoluble material.

Tetrapentylammoniumperchlorate was prepared by reacting equimolar quantities of tetrapentylammonium iodide and silver perchlorate in acetone solution. The silver

iodide was filtered off, the solution evaporated to yield the crude perchlorate, and this latter further recrystallised from an acetone-ether mixture.

CHAPTER NINE

SPECTROSCOPIC RESULTS AND DISCUSSION

9-1 WATER, DEUTERIUM OXIDE AND HOD SOLUTIONS

(i) Results

Raman spectra (10 - 4000 cm^{-1}) of water at 298 K were recorded (Figure 9-1) using the Coderg PH_1 spectrometer as described in Chapter 8. Spectra for the low frequency region are shown in Figure 9-2 together with estimated 'background' and difference spectra. The region having the most intense bands shown in Figure 9-1 (3000 to 4000 cm^{-1}) is shown in greater detail in Figure 9-3. The band was noticeably more intense than that around 1640 cm^{-1} where a second feature was just visible. These bands have been assigned to[36] the O-H stretch (4000 - 3000 cm^{-1}), the water HOH bend (1640 cm^{-1}) and the librational modes of the water molecule (0 - 700 cm^{-1}).

The temperature dependence of the scattering in the region 4000 to 3000 cm^{-1} was recorded between 273 and 323 K and a two component gaussian deconvolution carried out as previously described in Chapter 8. The resulting band parameters are displayed as a function of temperature in Figure 9-4. Raman spectra (2300 - 2800 cm^{-1}) of 6.0 mol dm^{-3} D_2O in H_2O were recorded (Figure 9-5) as a function of temperature. Figure 9-6 summarises the temperature dependence of ν_{max} at the band maximum between 278 and 363 K. The calculated temperature dependence of ν_{max} is 0.6 cm^{-1} K^{-1}.

Raman spectra (2000 to 2800 cm^{-1}) were measured at

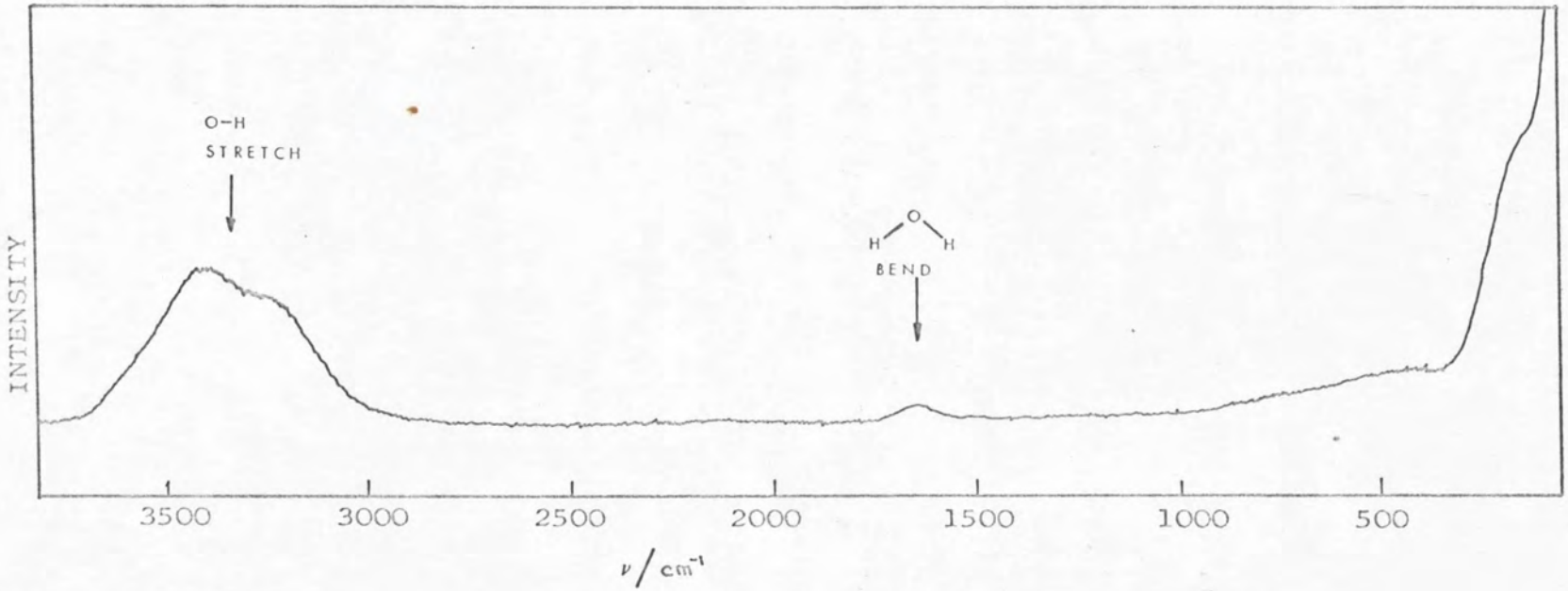

FIGURE 9-1 Raman spectrum of water at 298 K.
Resolution 1 cm^{-1}. Scanning speed 60 cm^{-1}/min.

a - spectrum of water
b - selected 'background'
c - difference spectrum

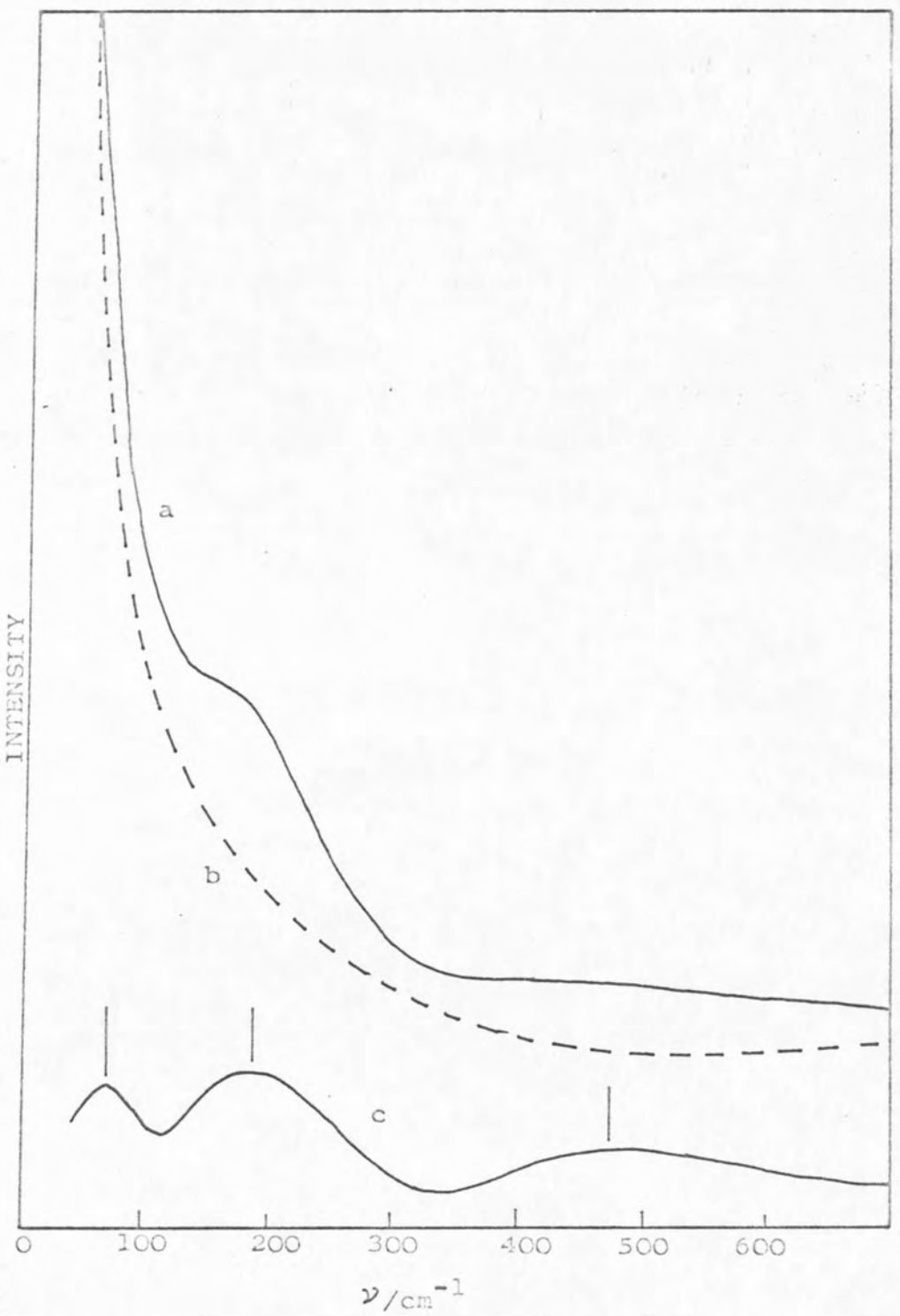

FIGURE 9-2 Raman Spectrum of Water in the Range 0 to 700 cm^{-1}.

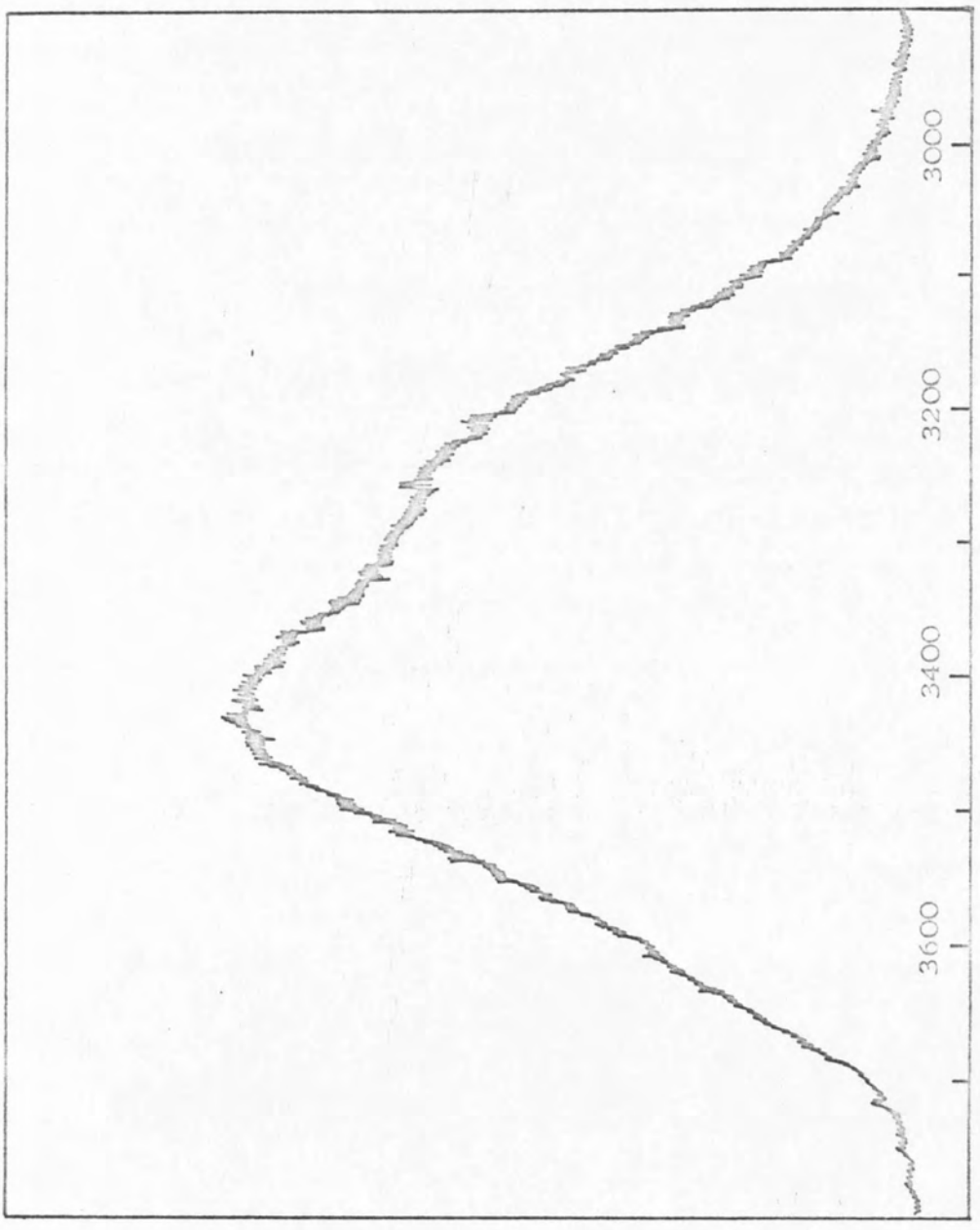

FIGURE 9-3 Raman Spectrum of Water over the range 3000 to 4000 cm^{-1}.

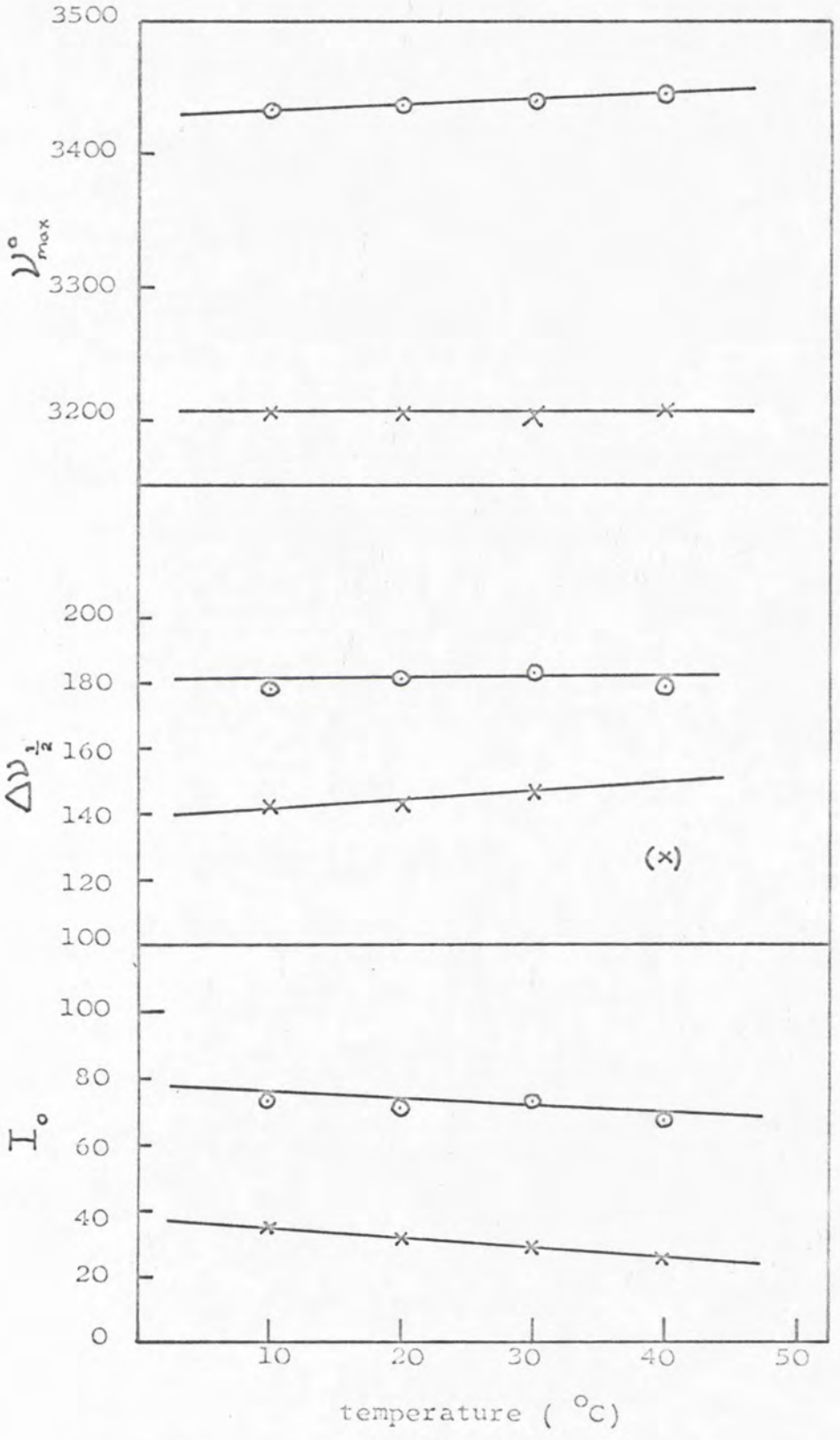

FIGURE 9-4 Results of Gaussian Deconvolution of Raman Spectrum of Pure Water in the range 4000 to 3000 cm^{-1}.

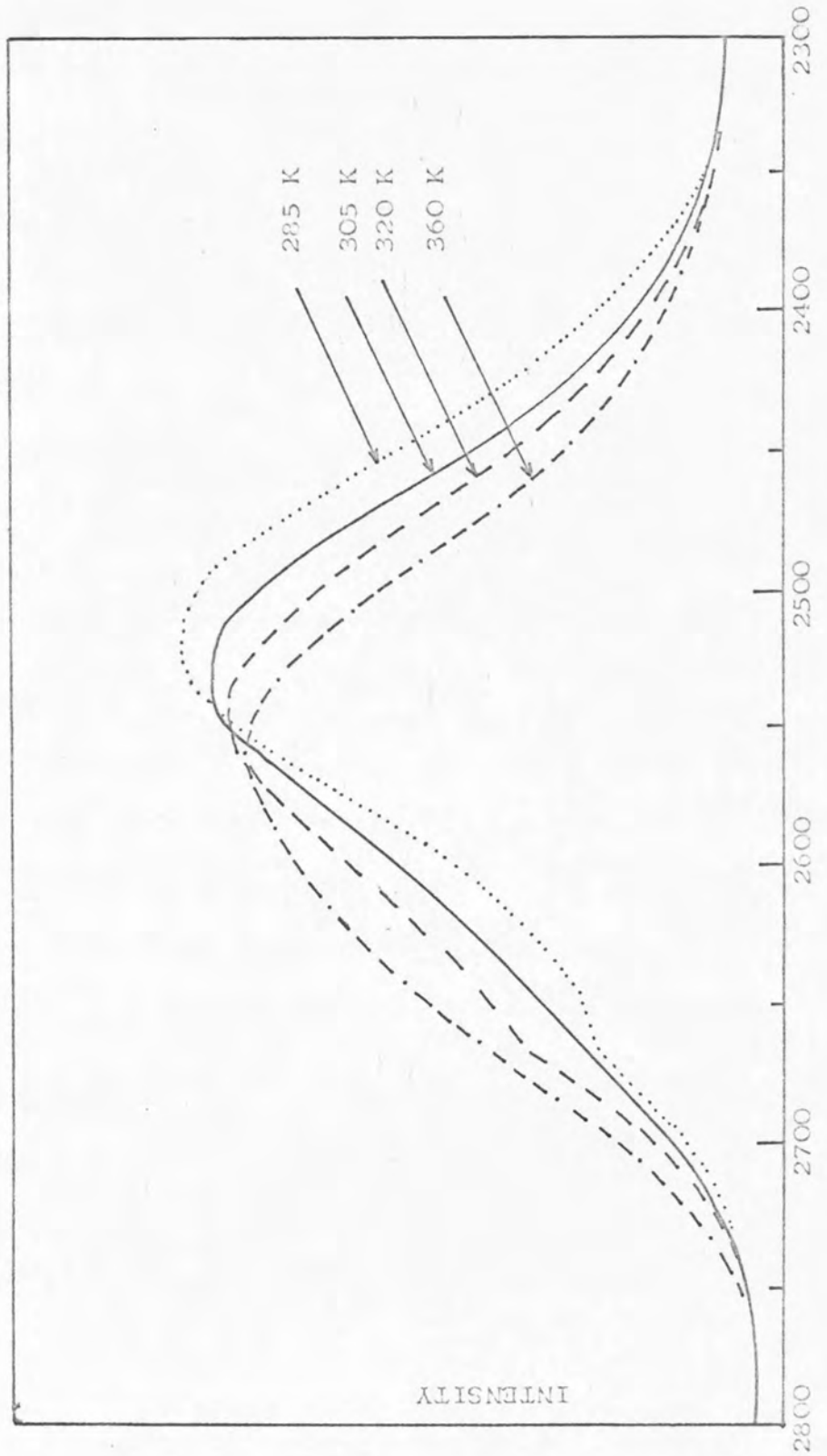

FIGURE 9-5 Raman Spectra of 6.0 mol dm^{-3} D_2O in H_2O at four temperatures.

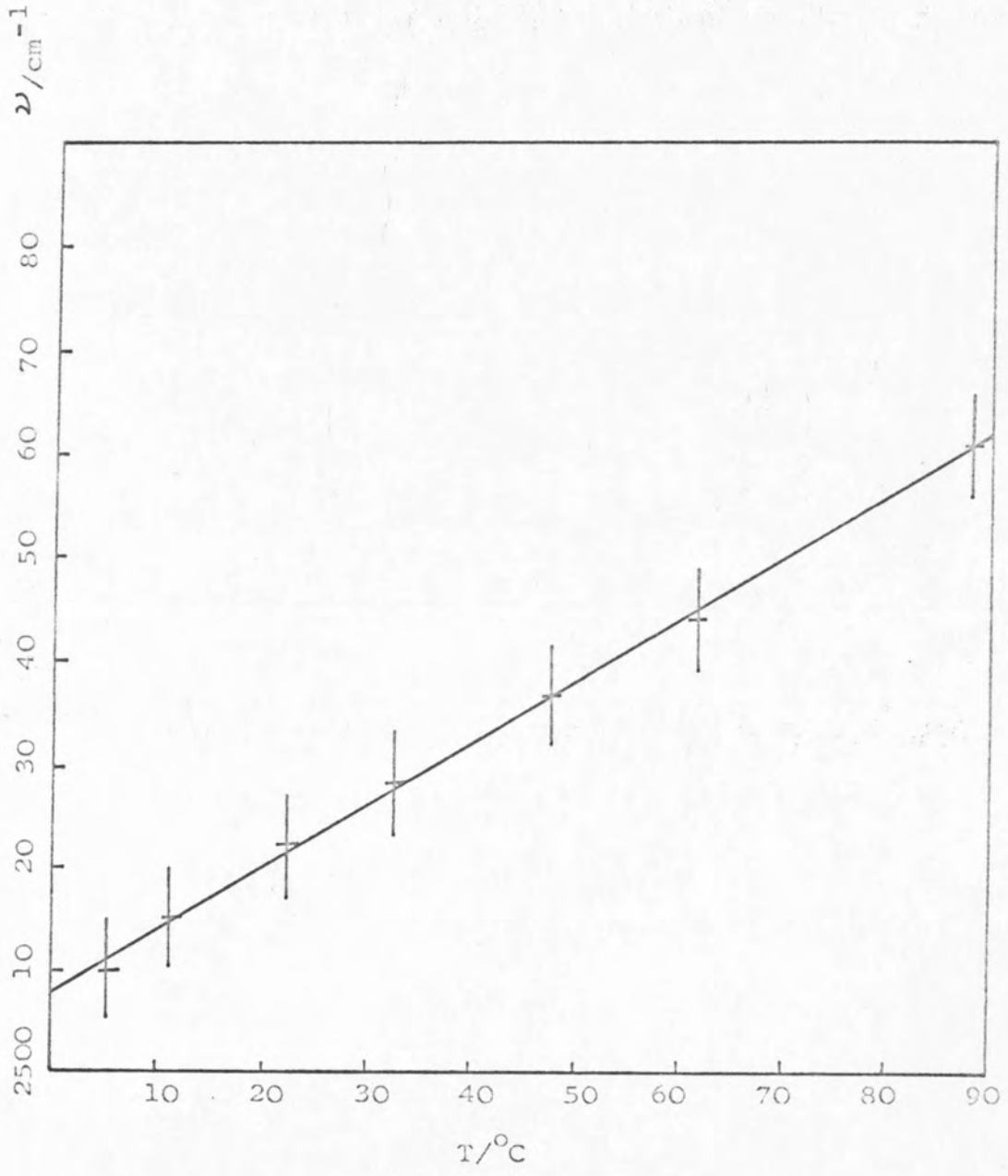

FIGURE 9-6 Dependence of the frequency of the major component maximum upon temperature of the Raman spectra of 6.0 mol dm^{-3} D_2O in H_2O.

several fixed temperatures and each spectrum analysed (see Chapter 8) in terms of two gaussian components. The dependence of band parameters on temperature is summarised in Figure 9-7. Figure 9-8 shows the infra-red spectrum recorded over the range 2000 to 2800 cm^{-1} of a 1.0 mol dm^{-3} solution of HOD in H_2O at 298 K.

(ii) Discussion

The results are in good agreement with those reported by Walrafen[224] for pure water. The prominent features of the Raman spectrum shown in Figure 9-1 are the stretch and bend regions. In addition other bands are present at much lower frequencies. A typical background was obtained from the Raman spectra of carbon tetrachloride (curve (b) in Figure 9-2) which was in turn subtracted from curve (a) (Figure 9-2) to yield a new curve (c), showing bands at about 70, 170 and 480 cm^{-1} similar to those reported by Walrafen.[236,237,242,243] Bands in this low frequency region are observed in other liquids and are tentatively assigned to translatory molecular modes. Neutron inelastic scattering data[36] adds some support to the assignment and position of the hindered translations in water at 70 and 170 cm^{-1}.

Turning to the coupled water stretching region (Figure 9-3) analysis in terms of two gaussian components, leads to the trends summarised in Figure 9-4. It is of interest that the temperature dependence of the bands in this region is not marked. There is some evidence for a band at 3620 cm^{-1} assigned[36] variously as the æsymmetric

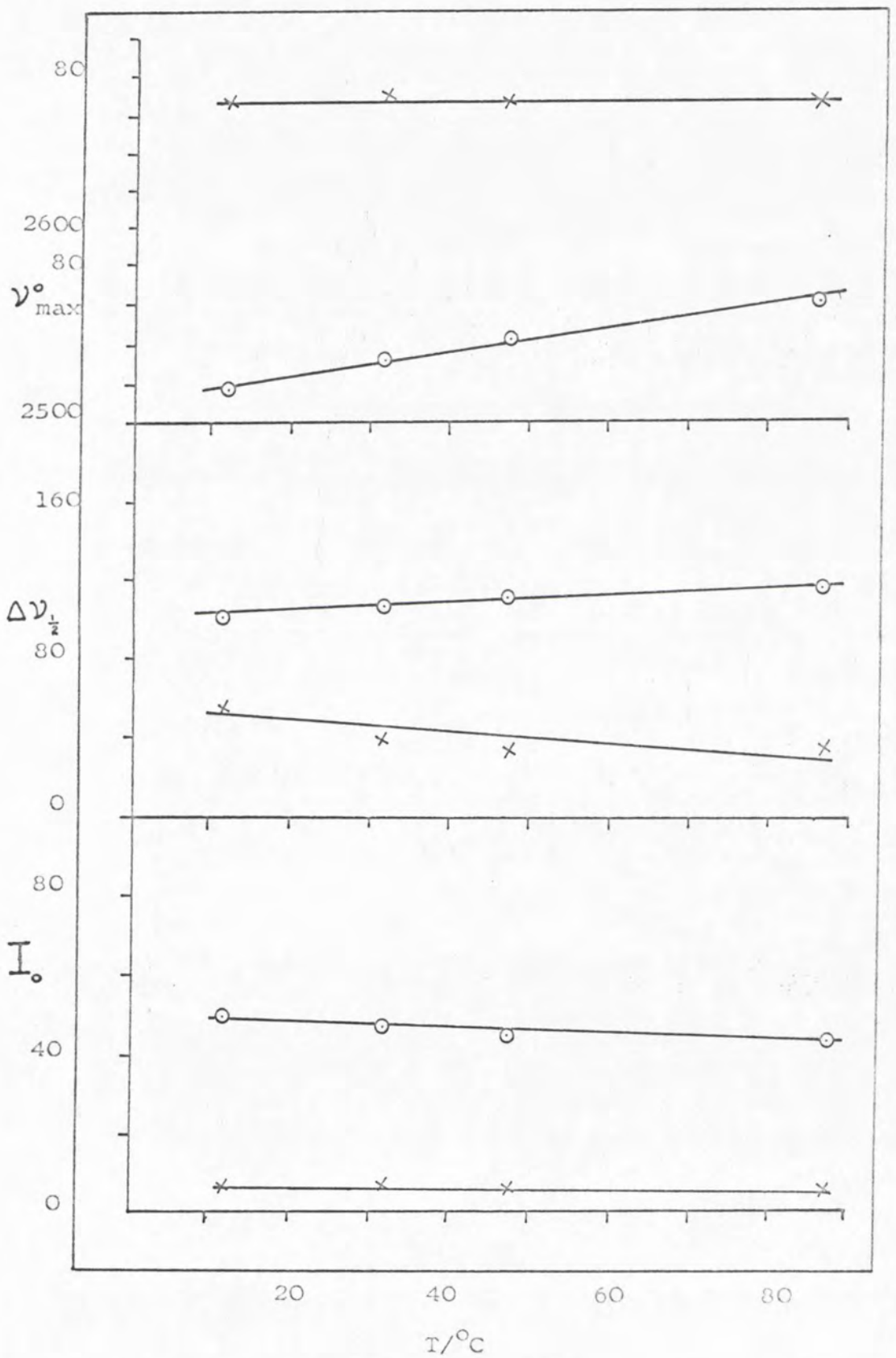

FIGURE 9-7 Gaussian Deconvolution of Raman Spectra of 6.0 mol dm-3 D_2O in H_2O as a function of temperature.

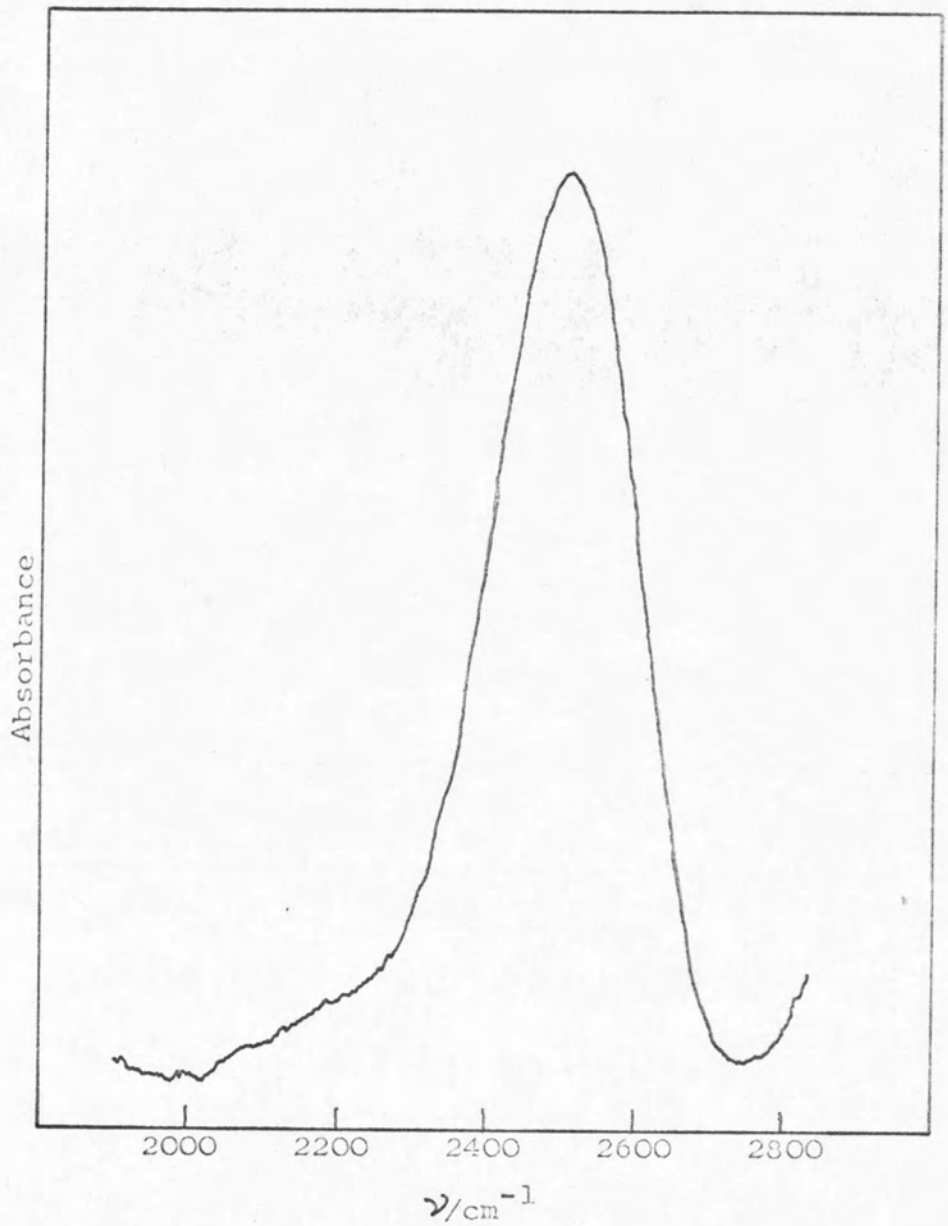

FIGURE 9-8 Infra-red Spectrum of 2 per cent D_2O in H_2O at 298 K.

stretch (ν_3), and as due to free (unbounded) OH groups. Attempts to deconvolute the envelope into three gaussian components have failed to assign a meaningful intensity to a component in this region. Presumably the scattering arising from such a band is within experimental error. This analysis indicates the pitfalls of analogue curve analysis techniques[286] such as those employed by Walrafen. There seems little doubt that such a feature does appear in the stretching region of the Raman spectrum close to 3620 cm^{-1}, but its position and band shape are critically dependent upon the band shape of the major component at 3450 cm^{-1}. It is clear that a band at 3620 cm^{-1} must be less than a few percent of the total contour intensity.

The uncoupled O-D stretching vibration is shown at 285, 305, 320 and 360 K in Figure 9-5. Three features of these spectra are noteworthy;

(i) an isosbestic point (or region) at 2570 cm^{-1},

(ii) a marked temperature dependence of the band contour, (cf Figures 9-5 and 9-6), and

(iii) a high frequency shoulder at about 2660 cm^{-1}.

These observations confirm the work of Walrafen.[241] Two further features were apparent. The overall band intensity was relatively constant. The low frequency component, obtained from double gaussian deconvolution of the observed contours at various temperatures, moved to higher frequencies with increase in temperature. The maximum ν_{max} of the high frequency component was independent of temperature. The half-bandwidth of the high frequency component decreased

whilst that of the low frequency component increased with increasing temperature. With increase in temperature the component at 2660 cm^{-1} sharpens and decreases in intensity whilst the component at lower frequency shows a small decrease in intensity and moves to higher frequency. Overall the contour intensity increases in the 2660 cm^{-1} region and falls in the 2500 cm^{-1} region with increase in temperature. These results are in broad agreement with the measurements of Walrafen,[241] who assigns the 2645 - 2660 cm^{-1} component to free (unbonded) OD, and the 2525 component to hydrogen bonded OD. If these two species, bonded and non-bonded OD groups, characterise a mixture model for water, Walrafen[241] has calculated from his data that ΔH° for the breaking of a hydrogen bond is 11 $\pm$ 2 kJ mol^{-1}. The value of ΔH°, as calculated from the spectra and analysis given here, is 8 $\pm$ 2.5 kJ mol^{-1} of hydrogen bonds.

The infra-red spectra of solutions of HOD in H_2O (Figure 9-8) do not show any visible indication of a high frequency component. Walrafen[224] reconciled this observation with the Raman data by assigning a lower oscillator strength to 'free' OD in the infra-red than in the Raman spectra. At least one group of workers, using differential analysis techniques, claim to have observed an asymmetry in the infra-red spectra of dilute D_2O solutions in water.[245]

These assignments by Walrafen are, however, the subject of considerable controversy.[36] In the work

described here, it was felt that some of these difficulties could be resolved following an examination of the effects on the bands of various inorganic and organic solutes which were thought to modify the structure of water.[222]

9-2 INORGANIC SOLUTES

(i) Results

The effects of a wide range of electrolytes upon the Raman spectra of dilute solutions of D_2O in H_2O were investigated (Appendix 9-1). Figure 9-9 shows the effect of added sodium iodide upon the O-D stretching oscillator, and dramatic changes in bandshape and band intensity took place with increase in salt concentration. Addition of potassium fluoride at 295 and 279 K produced an overall decrease in band intensity and some change of bandshape (Figures 9-10 and 9-11). A third type of behaviour was found when magnesium nitrate was added, (9-12). The band was broadened, particularly in the 2650 cm^{-1} region and the feature around 2650 cm^{-1} in HOD was apparently lost. Figures 9-13, 9-14 and 9-15 summarise the dependence upon salt concentration of the OD stretching band maximum for a typical selection of electrolytes. For the systems given in Figure 9-13, the band shift initially increased linearly with added salt concentration but at higher concentrations began to level off. Salts with a common anion but different cations showed (see Figure 9-14) remarkably small shifts compared with

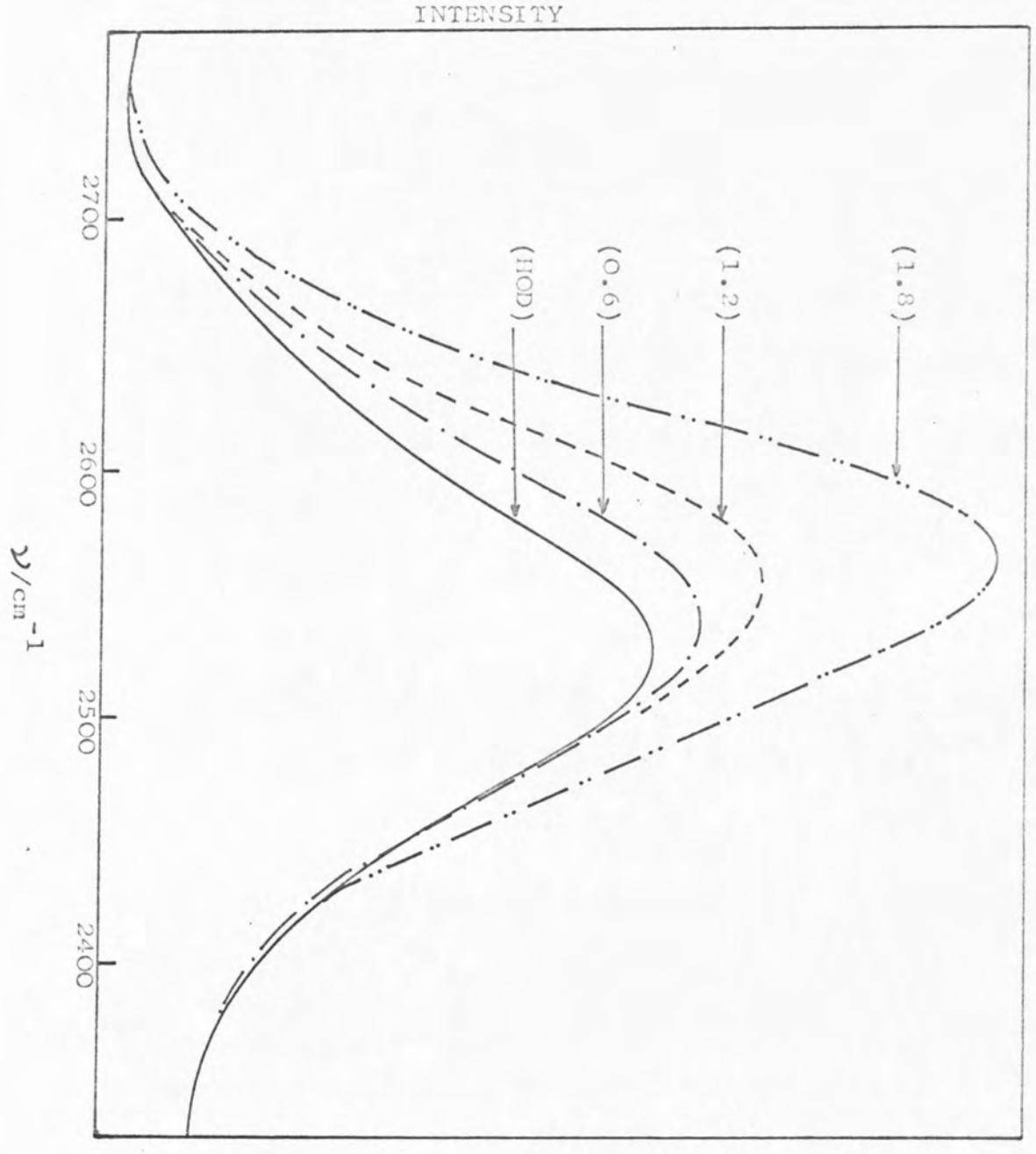

FIGURE 9-9 Raman Spectra of solutions of D_2O in H_2O containing various concentrations (in parenthesis) of Sodium Iodide at 298 K.

FIGURE 9-10 Raman Spectra of solutions of D_2O in H_2O containing Potassium Fluoride (concentrations mol dm^{-3} indicated in parenthesis), at 295 K.

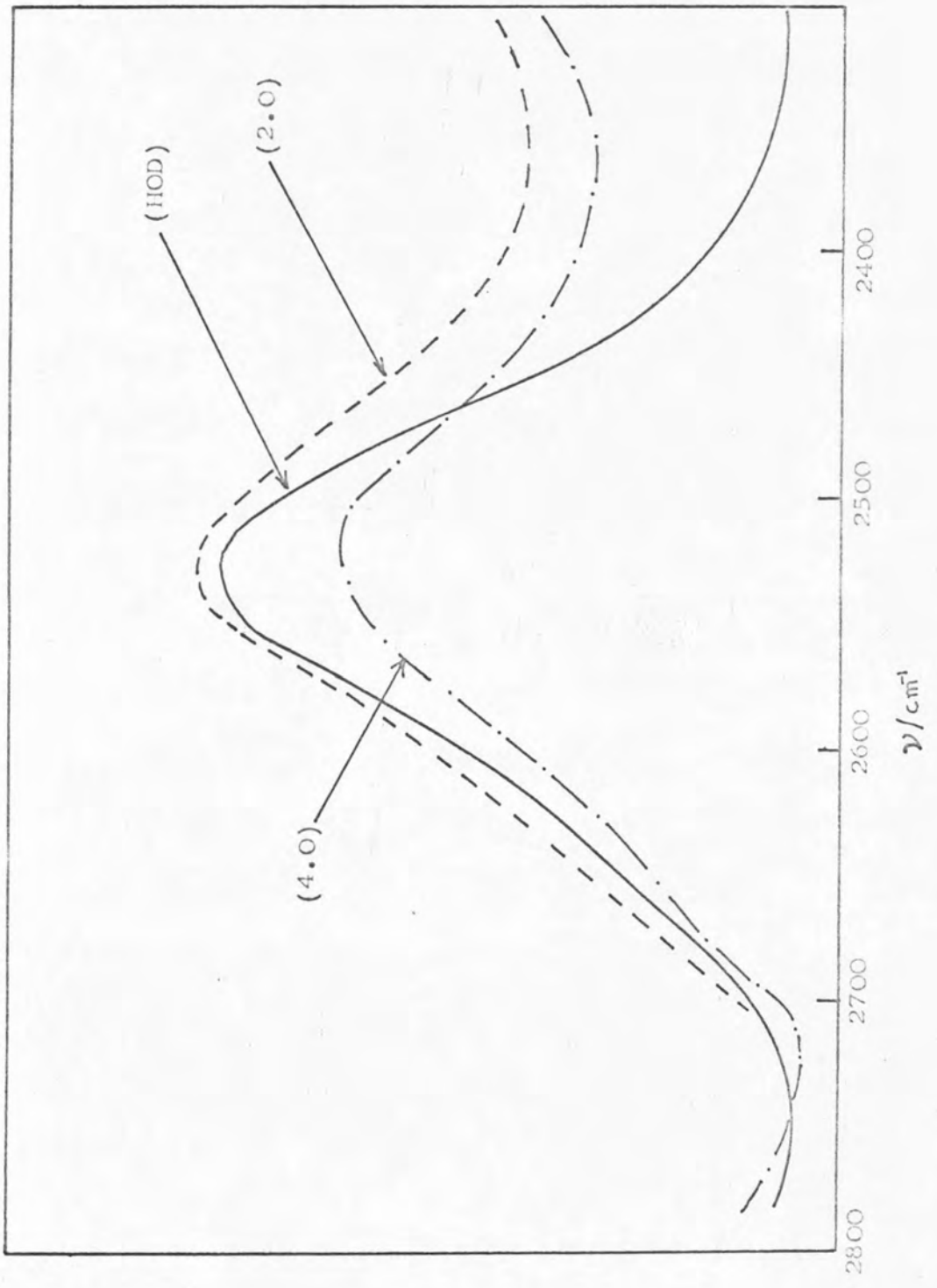

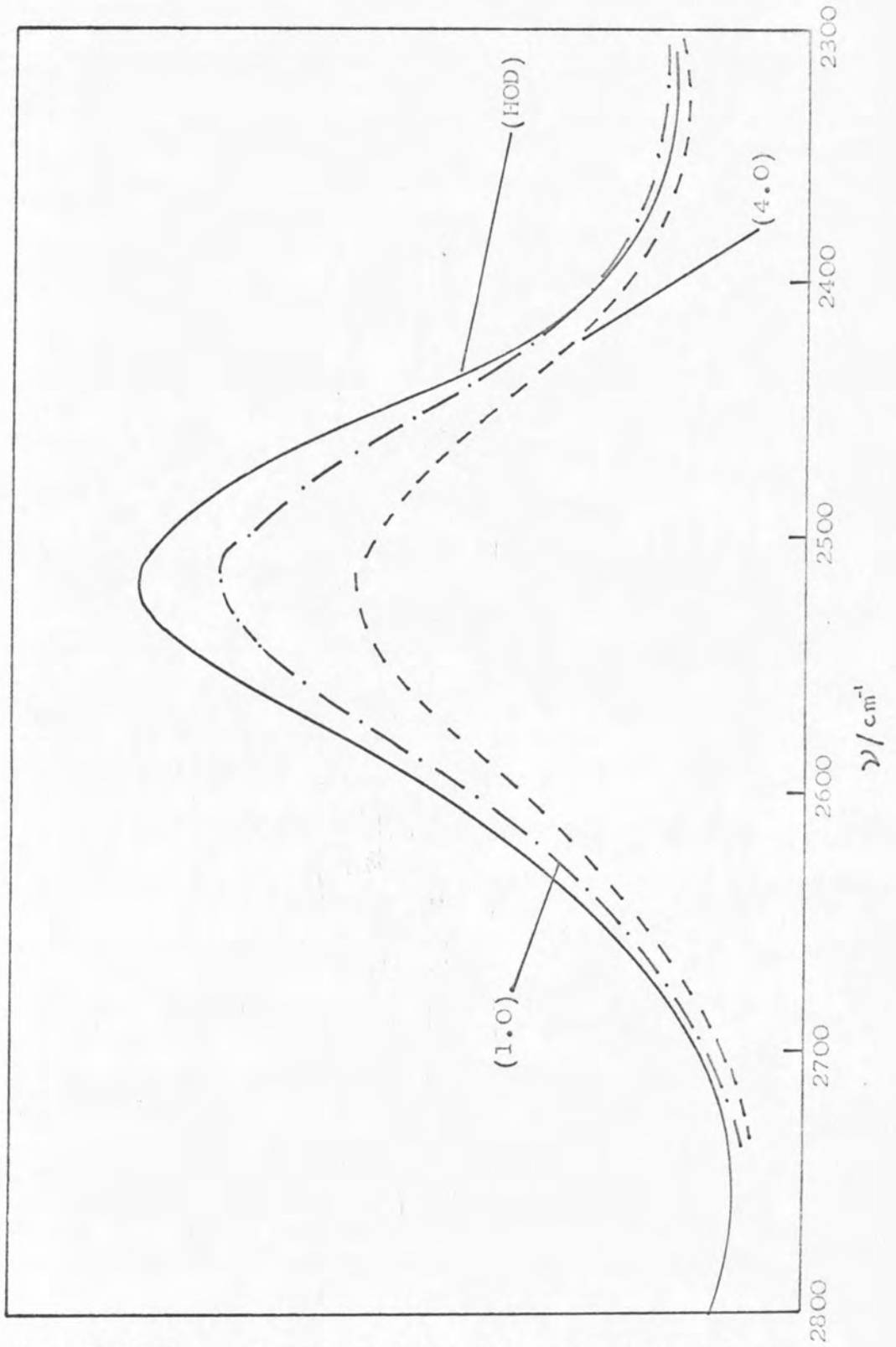

FIGURE 9-11 Raman Spectra of D_2O/H_2O solutions containing 1.0 and 4.0 mol dm^{-3} of Potassium Fluoride at 279 K.

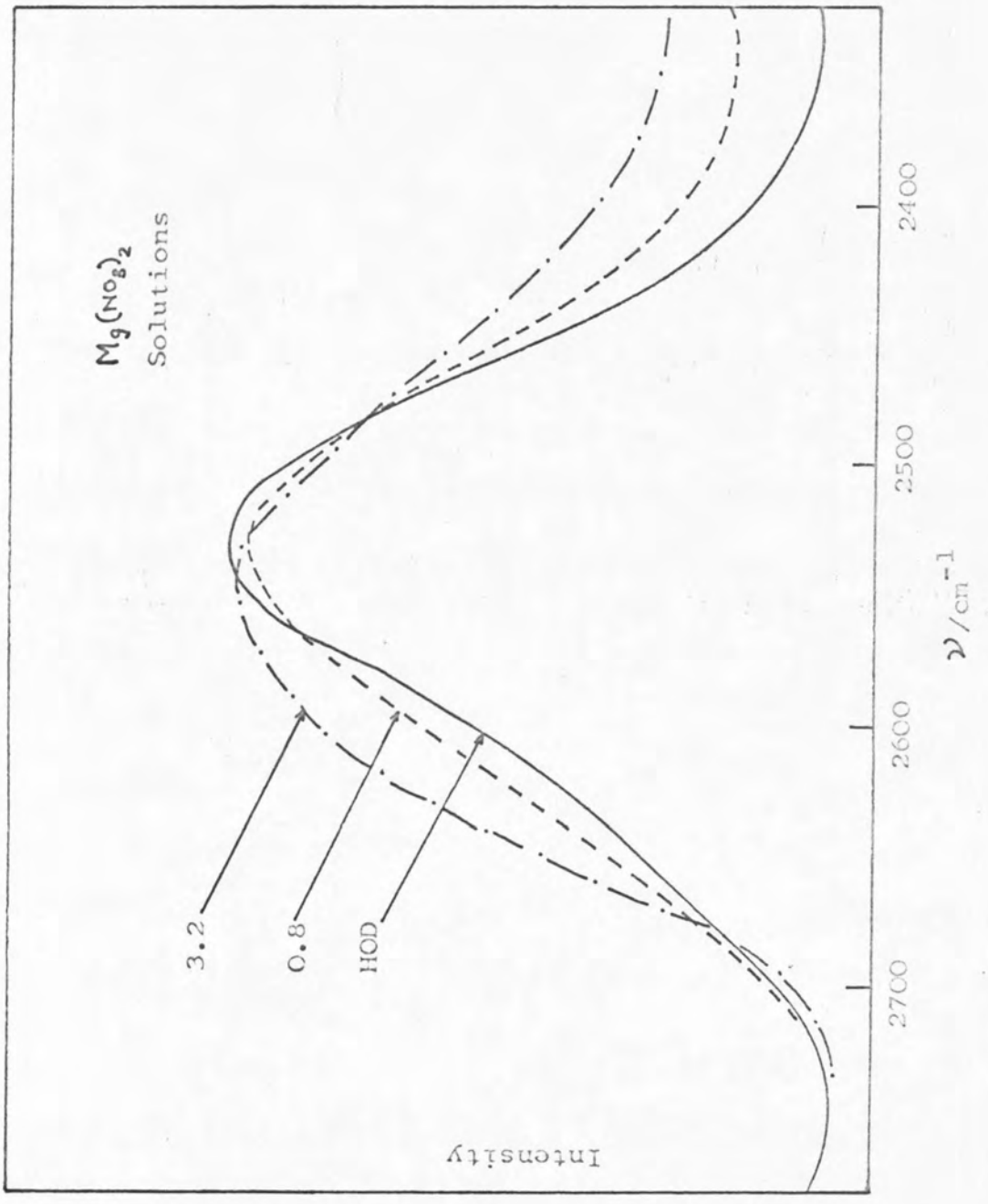

FIGURE 9-12 Raman Spectra of Magnesium nitrate solutions in D_2O/H_2O at concentration of 3.2 and 0.8 mol dm^{-3} and 298 K.

FIGURE 9-13 Dependence of major frequency maximum on concentration (mol dm^{-3}) of added salt in D_2O/H_2O solutions (Raman Spectra).

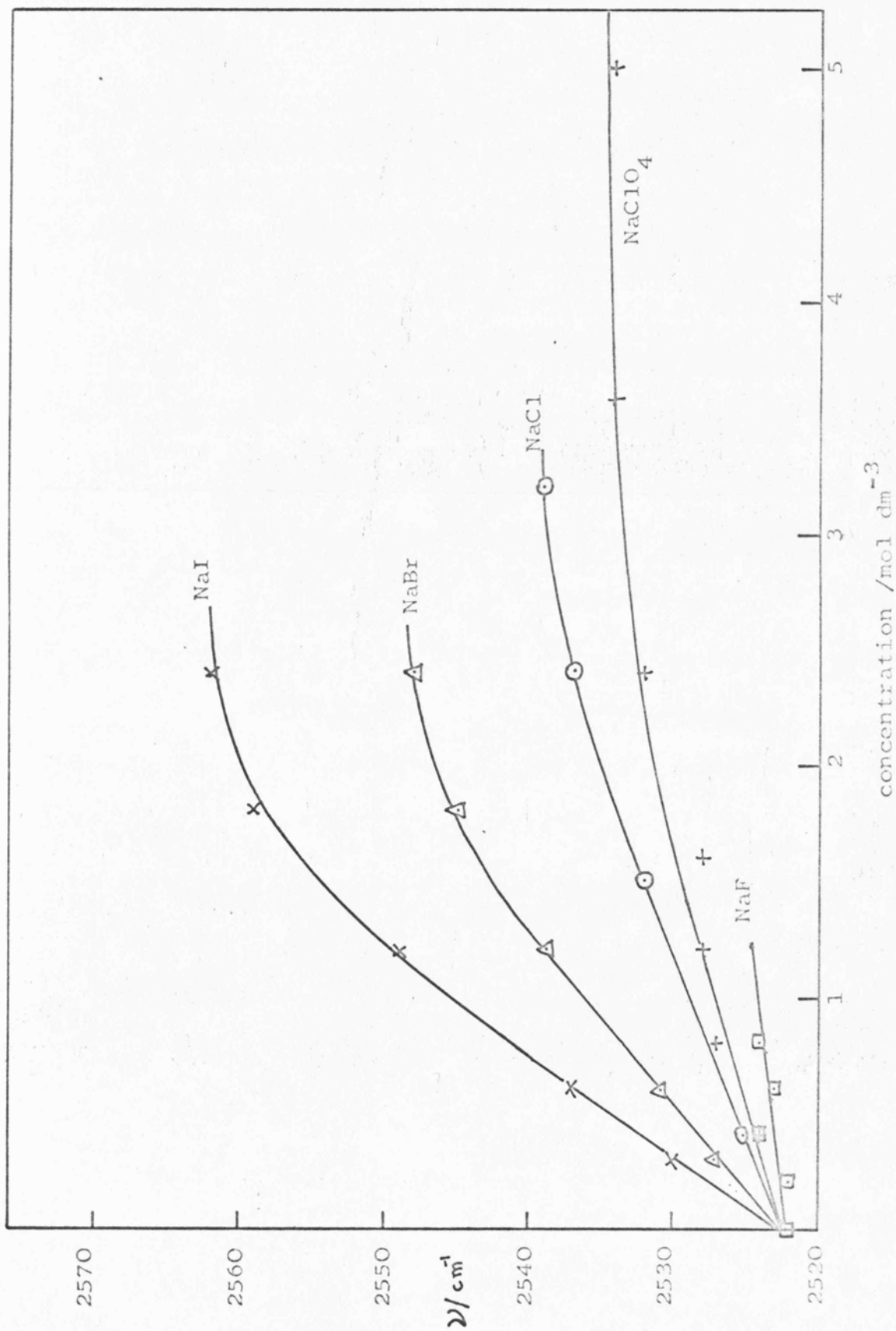

FIGURE 9-14 Dependence of frequency of major component maximum of solutions of salt in D_2O/H_2O mixtures (Raman Spectra).

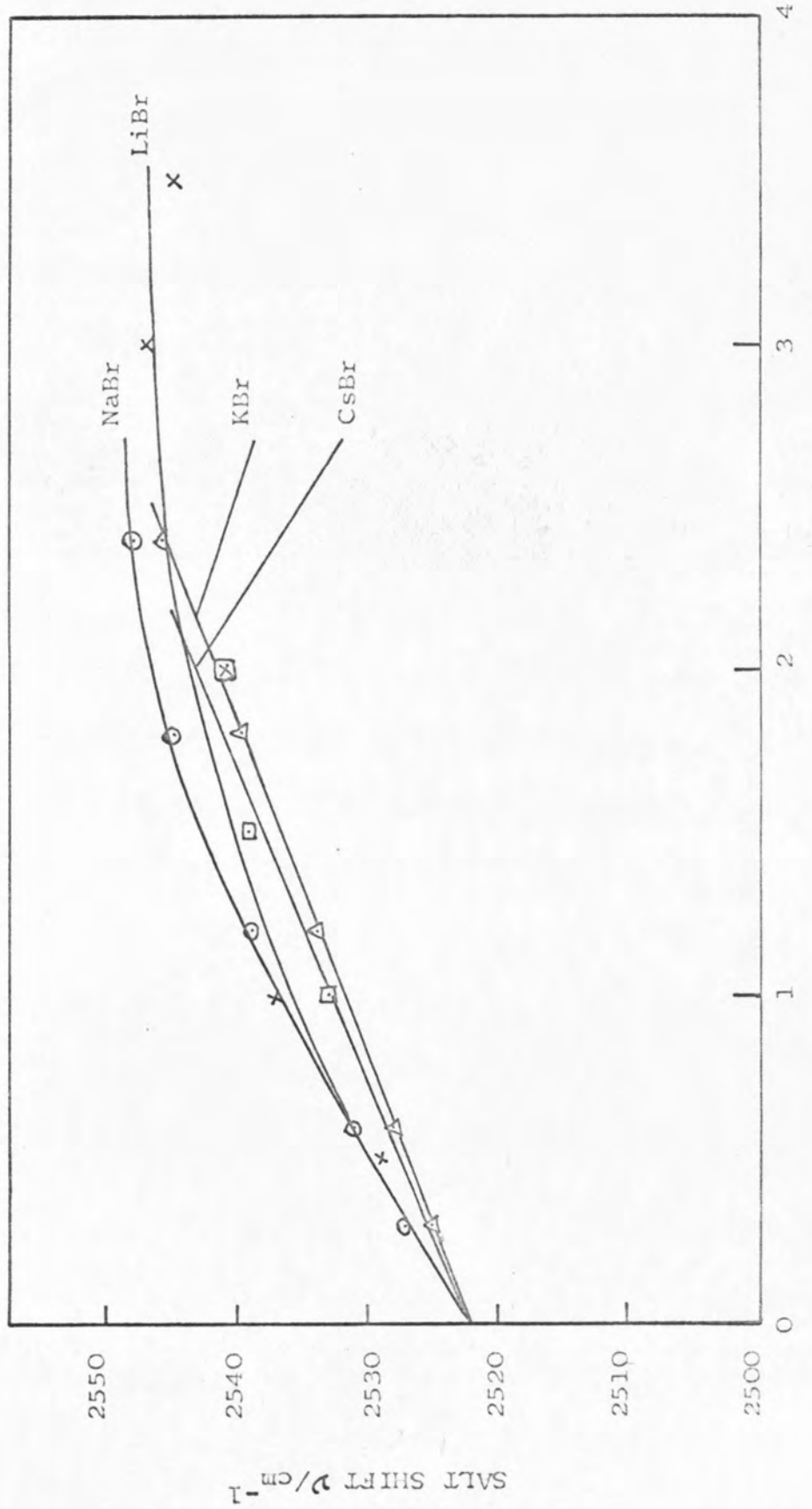

FIGURE 9-15 Dependence of major component frequency maximum on salt concentration in D_2O/H_2O (Raman Spectra).

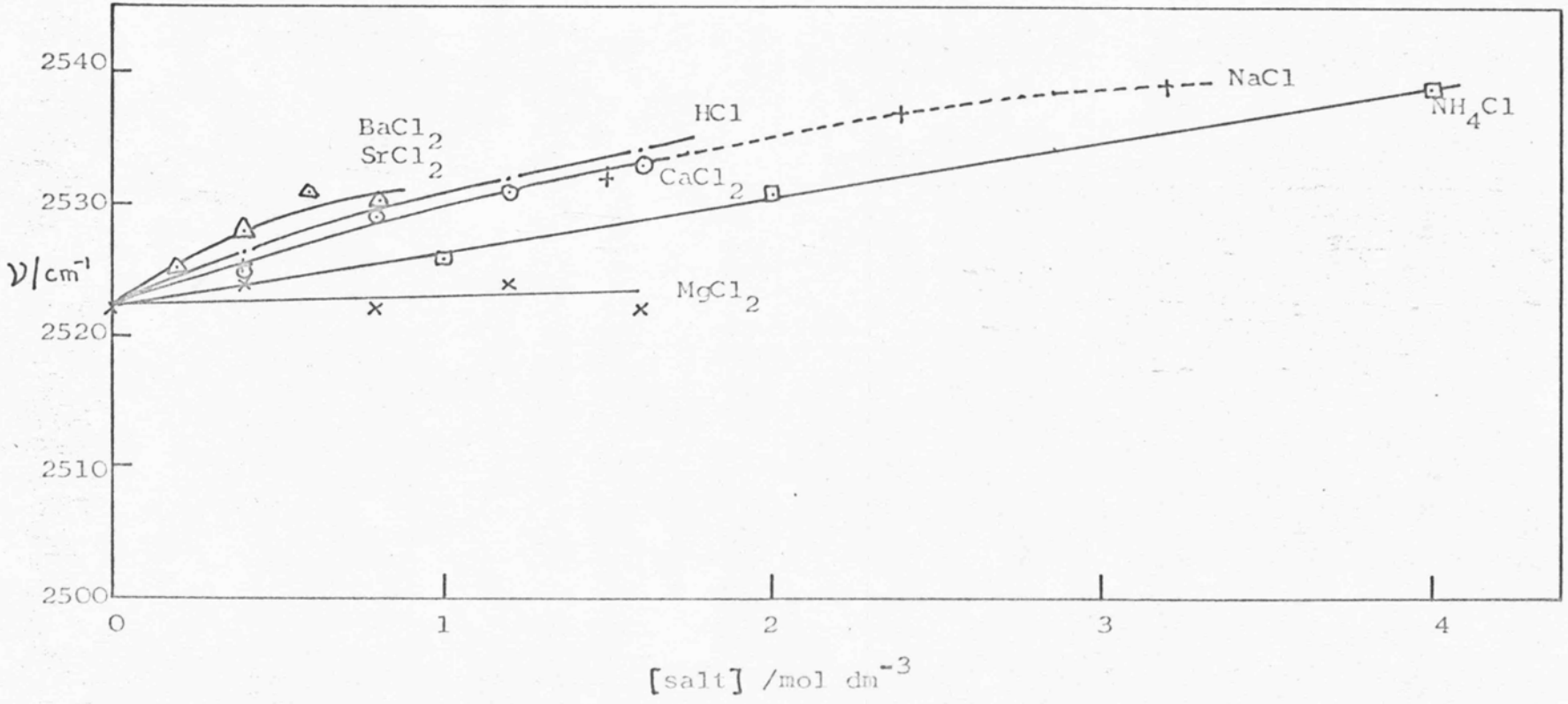

different anions having a common cation (Figure 9-13). The molar single ion shifts relative to that for Na^+ ($\delta_+ = 5\ cm^{-1}\ mol^{-1}$) are plotted against charge to radius ratio in Figure 9-16. These 'single ion' quantities were derived using the same technique as applied to n.m.r. data.[287] The shapes of the curves for both anions and cations show a striking qualitative resemblance to similar curves resulting from n.m.r. measurements.[287]

Raman spectra (Figure 9-17) over the region 2000 to 2800 cm^{-1} for solutions containing various concentrations of sodium perchlorate showed an important new feature in the 2630 cm^{-1} region. On lowering the temperature (see Figure 9-18) to 279 K, only a small change in the position and intensity of this new feature was observed. Similar behaviour was noticed for lithium perchlorate solutions (Figure 9-19). Magnesium perchlorate also showed similar trends (Figures 9-20 and 9-21 at 298 and 275 K). The effects of various concentrations of lithium, sodium, magnesium and zinc perchlorates on the Raman spectra of 2 mol dm^{-3} D_2O in H_2O at 298 K over the range 2300 to 2800 cm^{-1} are summarised in Figure 9-22.

A new absorption band was also observed in the infra-red spectra when perchlorates were added to dilute D_2O in H_2O. The effects of metal perchlorates upon the Raman and infra-red spectra of pure water in the OH stretch region (3700 to 3100 cm^{-1}) are summarised for saturated solutions in Figure 9-23 and Figure 9-24 respectively. The approximate positions of the infra-red contour maxima

FIGURE 9-16 Correlation between change to radius ratio and salt shifts.

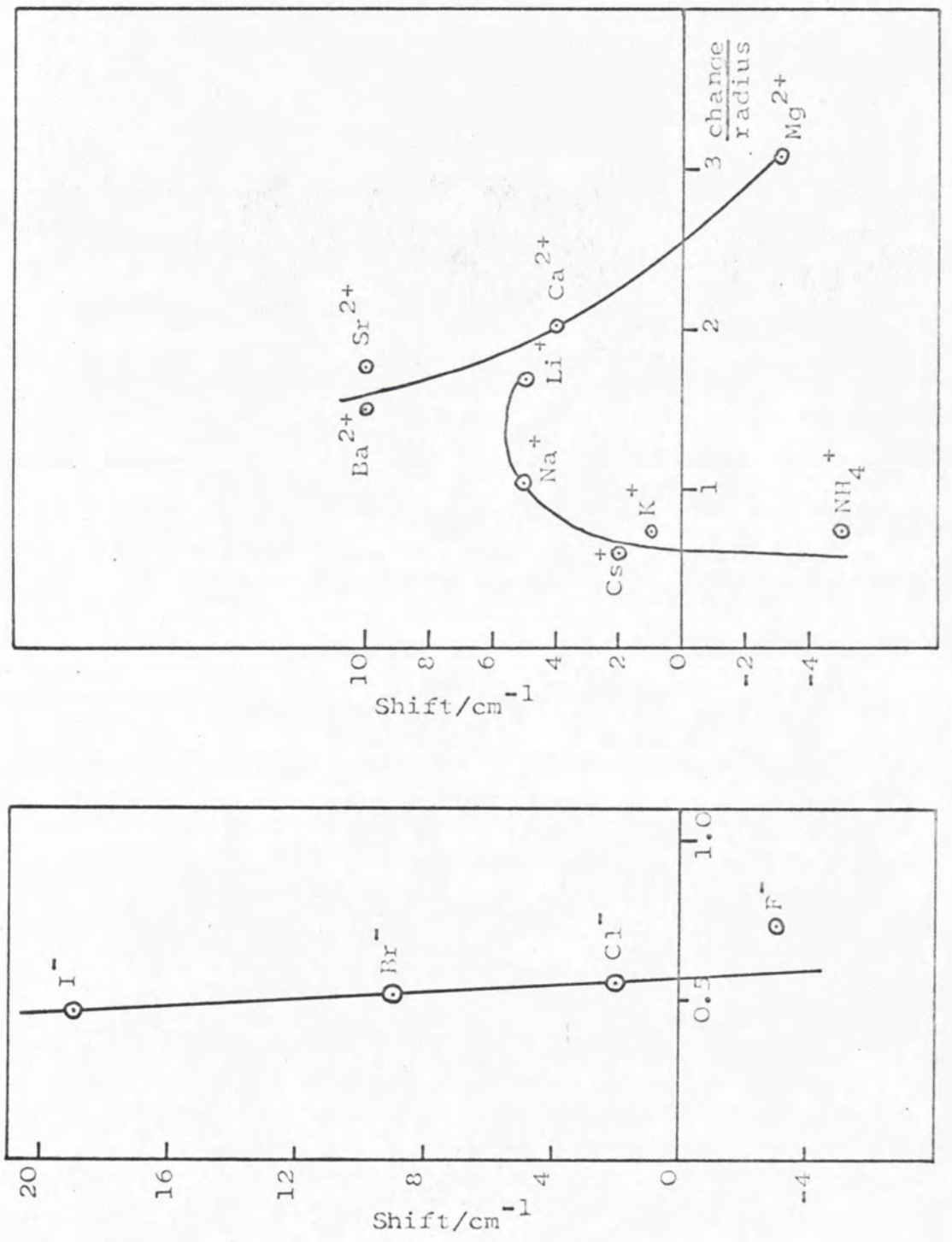

FIGURE 9-17 Raman spectra of D_2O/H_2O solutions containing various concentrations (mol dm^{-3}) of Sodium Perchlorate.

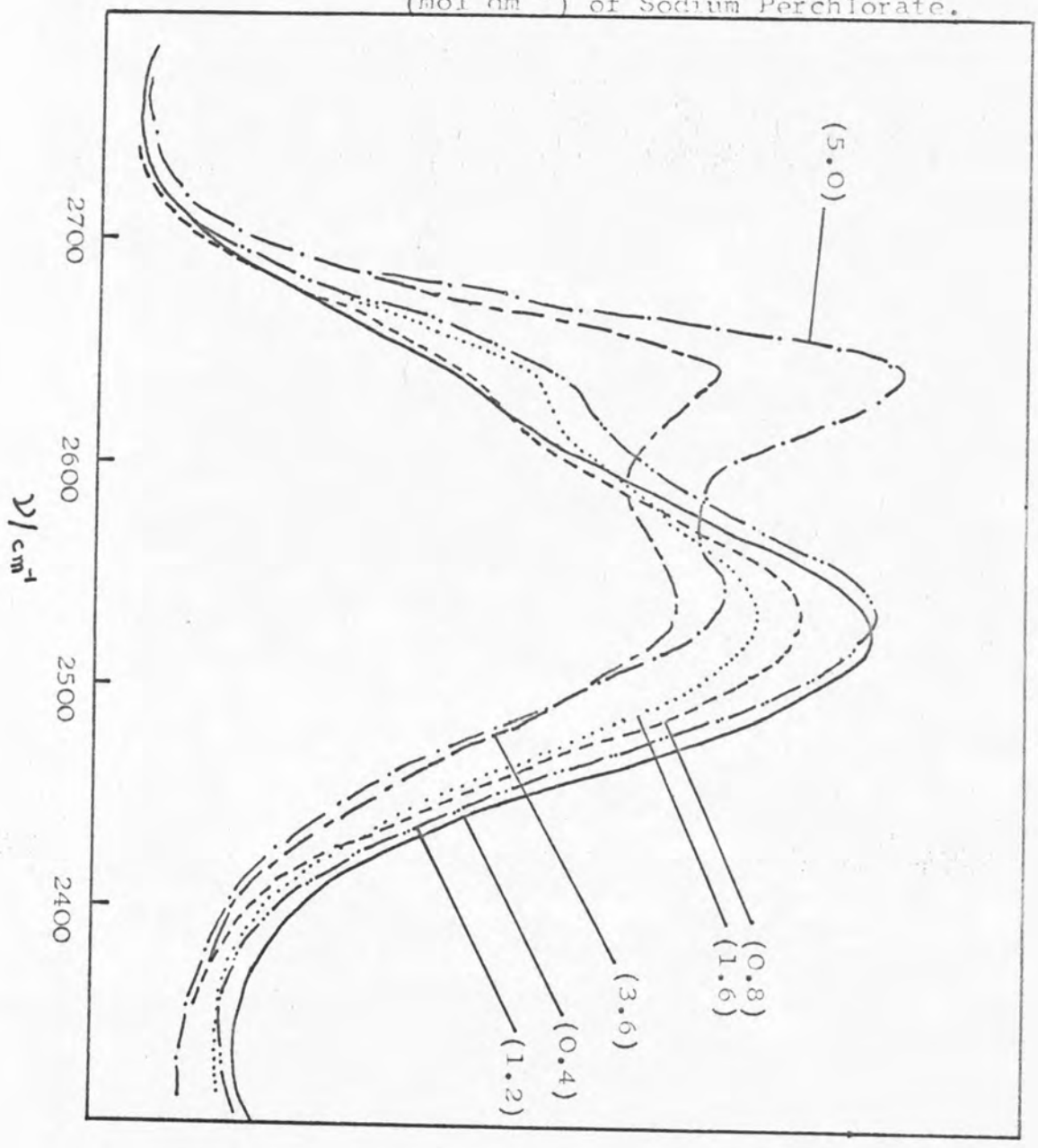

FIGURE 9-18 Raman spectra of solutions of Sodium Perchlorate (5.0 mol dm^{-3}) in D_2O/H_2O solutions at two temperatures 295 K and 279 K.

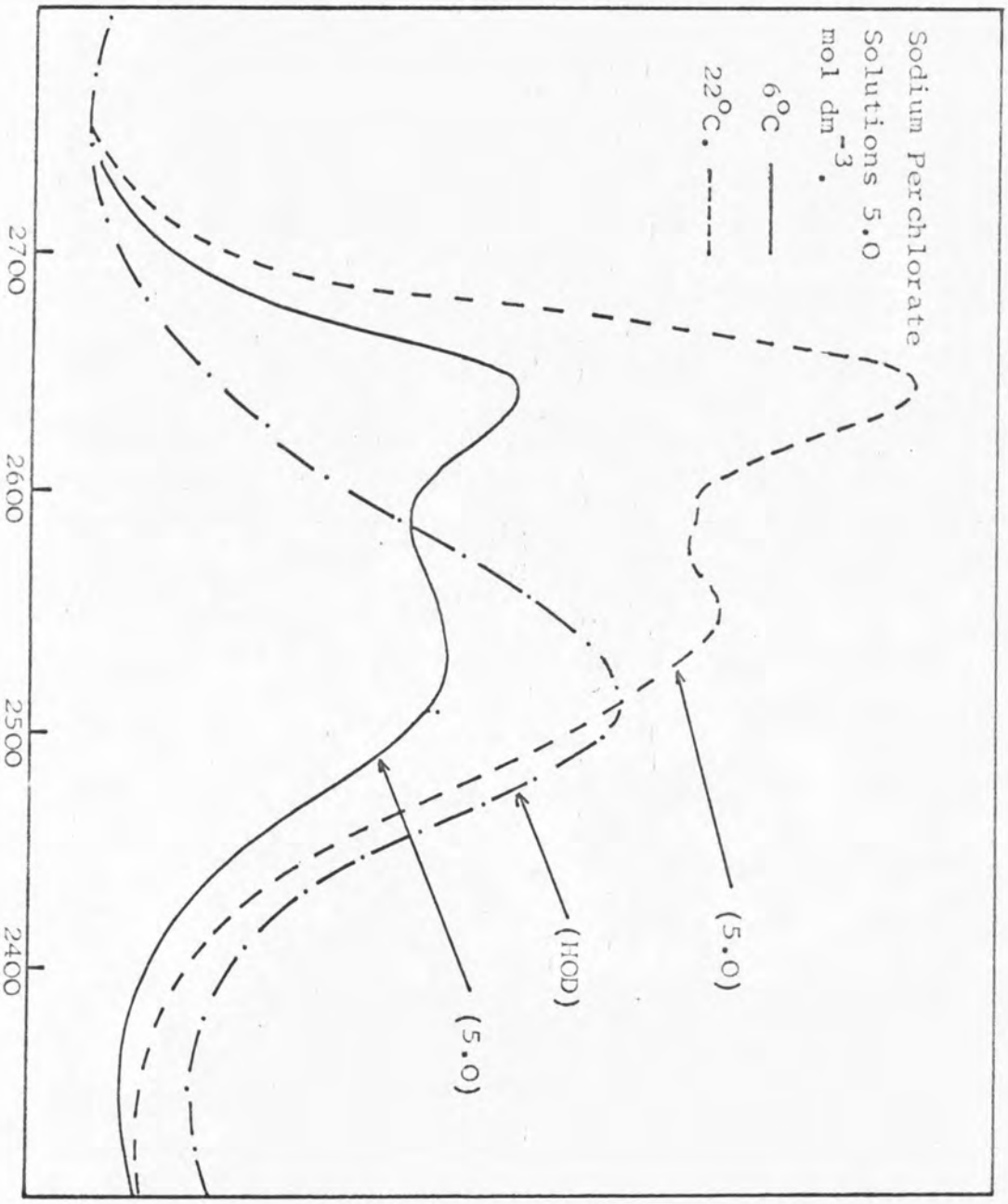

FIGURE 9-19 Raman Spectra of solutions of Lithium Perchlorate at several concentrations (mol dm^{-3}) in D_2O/H_2O at 298 K.

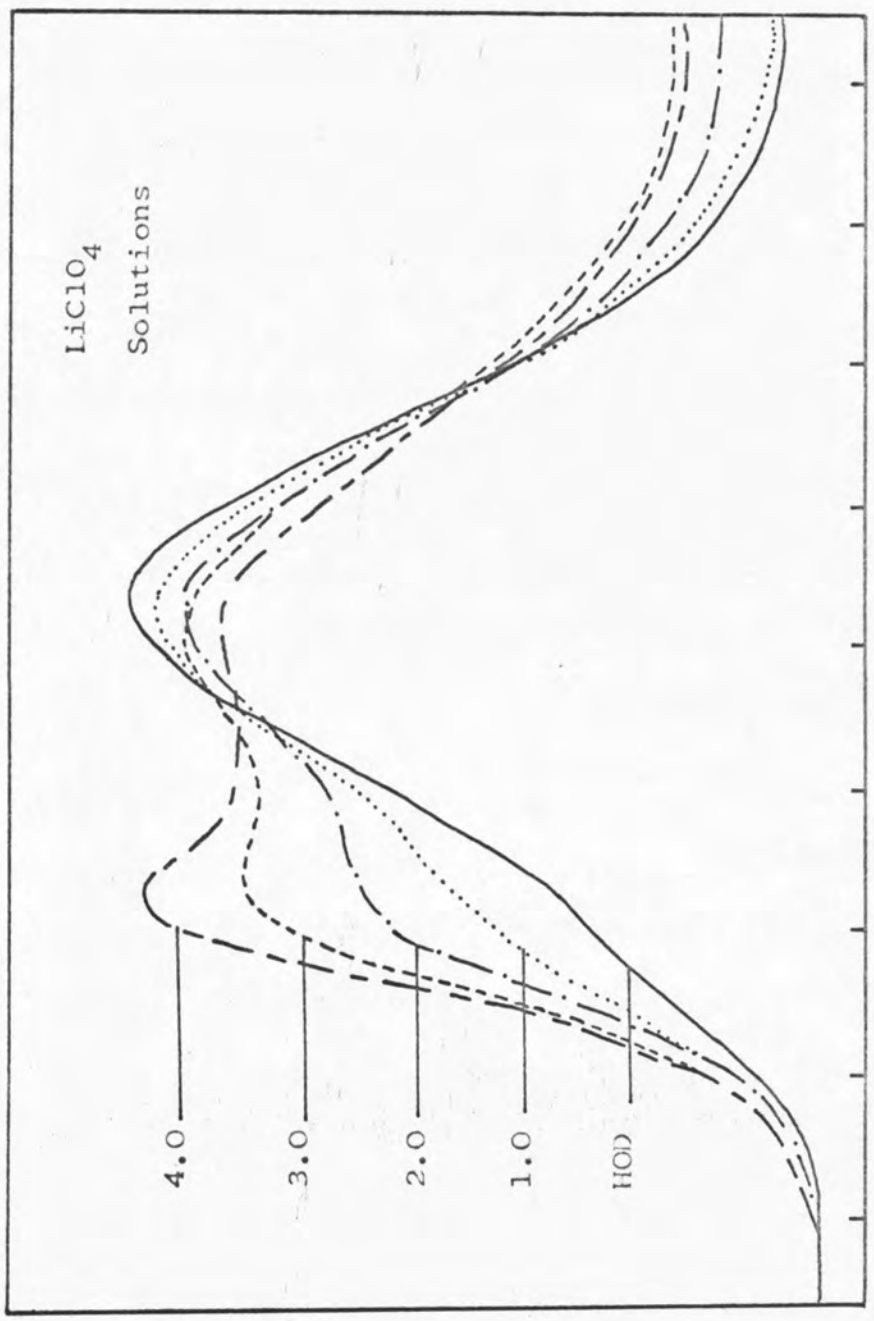

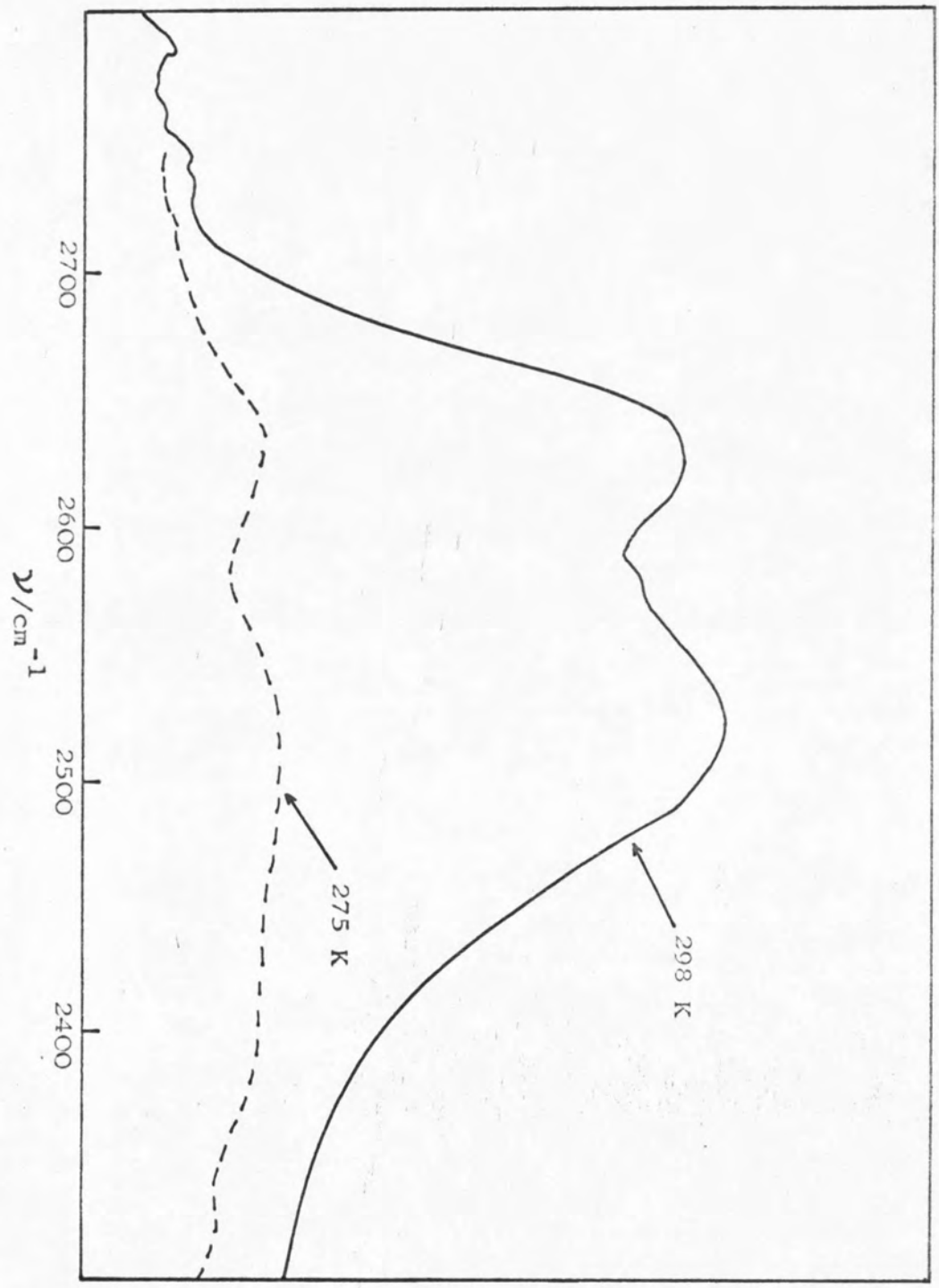

FIGURE 9-20 Raman Spectra of 2.0 mol dm^{-3} solutions of Magnesium Perchlorate in D_2O/H_2O at 298 K and 275 K.

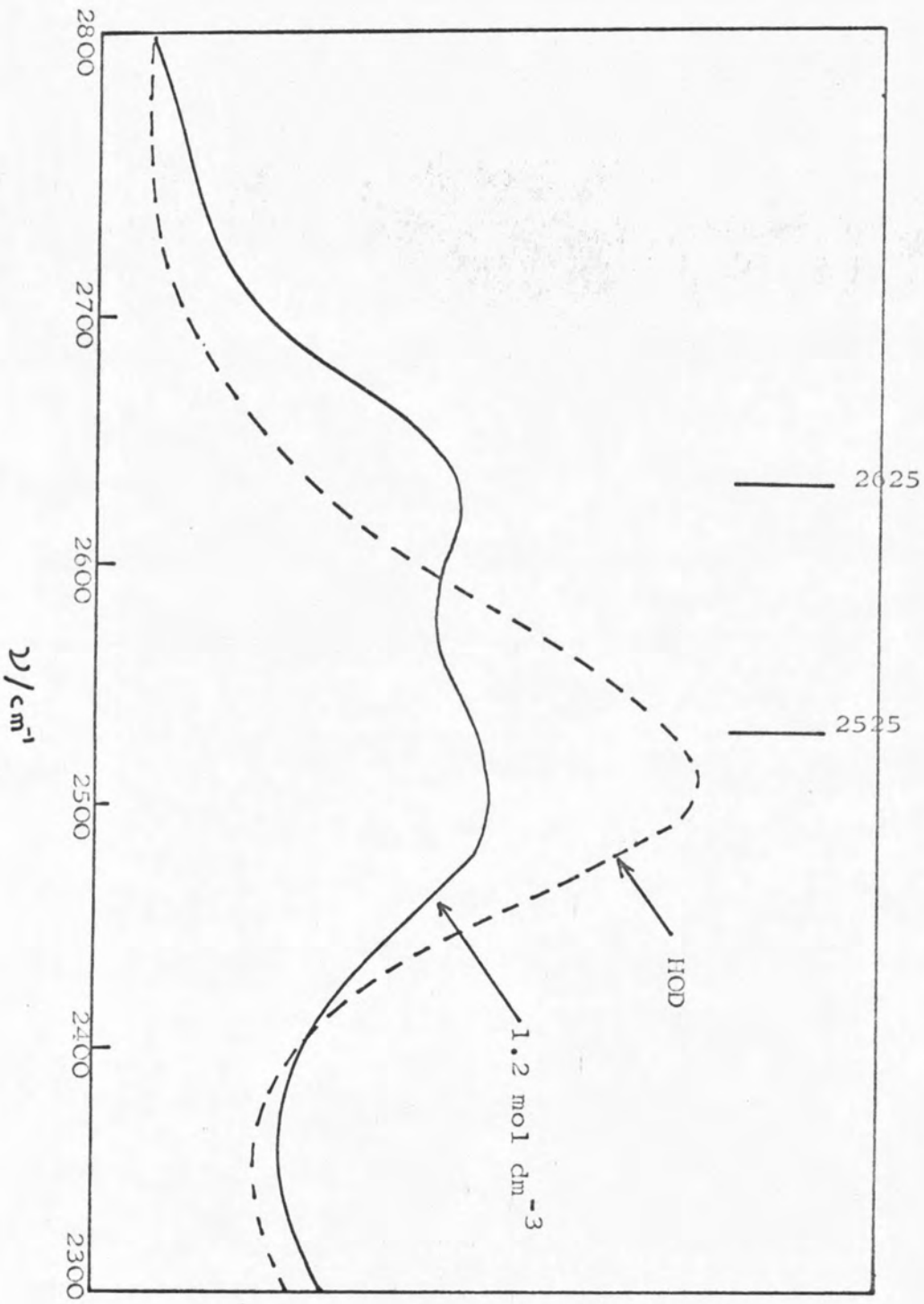

FIGURE 9-21 Raman Spectra of D_2O/H_2O and D_2O/H_2O containing 1.2 mol dm^{-3} of Magnesium Perchlorate at 279 K.

FIGURE 9-22 Raman Spectra of several metal perchlorates in 2 mol dm^{-3} D_2O/H_2O at 298 K

(a) D_2O in water; (b) 1.6 mol dm^{-3} $Mg(ClO_4)_2$;

(c) 1.6 mol dm^{-3} $Zn(ClO_4)_2$; (d) 2.0 mol dm^{-3} $LiClO_4$;

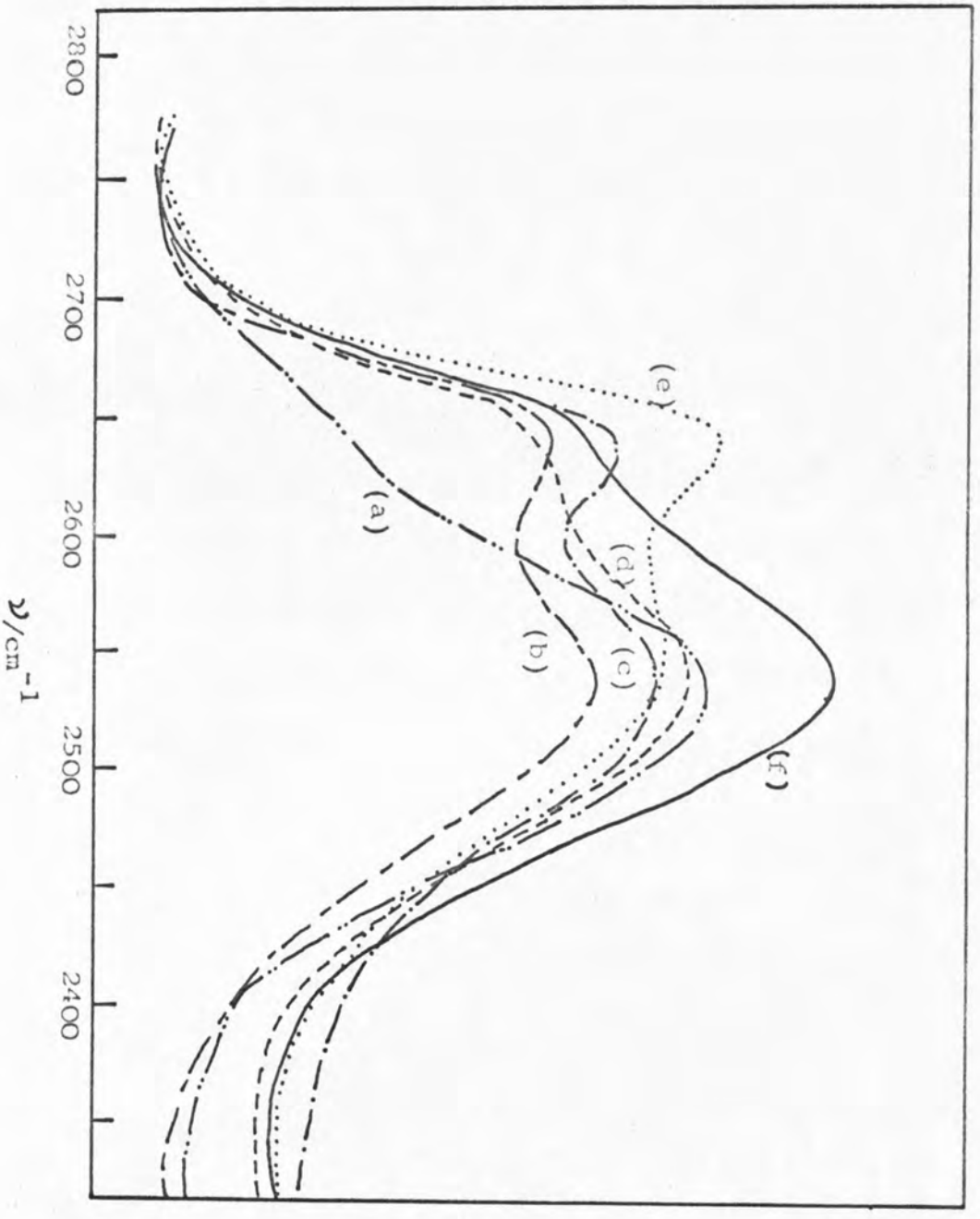

(e) 4.0 mol dm^{-3} $LiClO_4$; (f) 1.6 mol dm^{-3} $NaClO_4$.

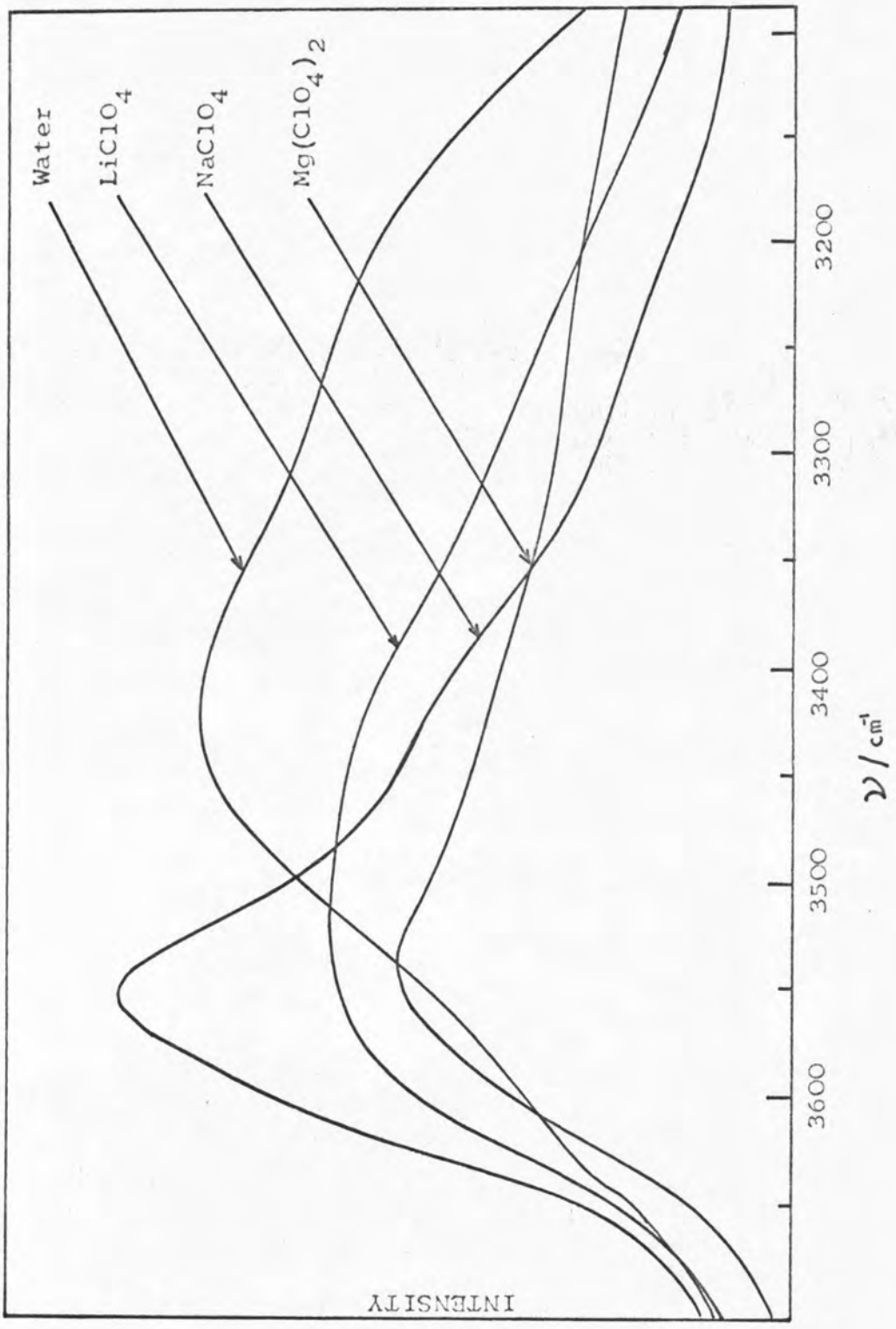

FIGURE 9-23 Raman Spectra of Saturated Solutions of metal perchlorates in water at 298 K.

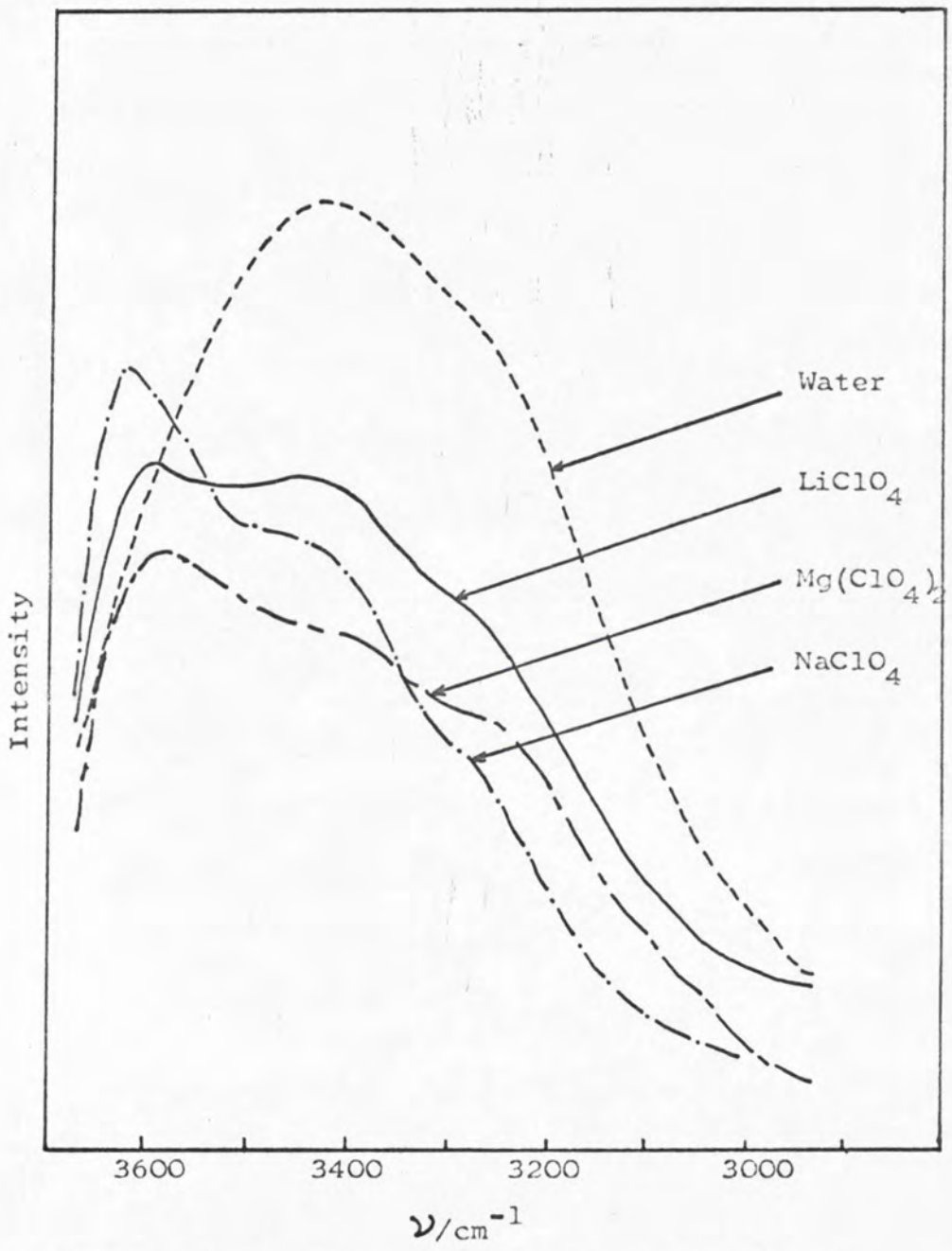

FIGURE 9-24 Infra-red Spectra of Saturated Solutions of metal perchlorates in water at 298 K.

are summarised in Figure 9-25.

An intensive search was made for other electrolytes which would also cause contour changes similar to those produced by perchlorates. Two electrolytes, sodium fluoroborate and sodium chlorate, were considered since they were known to show anomalous behaviour in the n.m.r. spectra[288] of aqueous solutions. The Raman spectra of aqueous (HOD) solutions of sodium fluoroborate and sodium perchlorate are shown in Figure 9-26. Two features are of paramount importance;

(i) the high frequency contour maxima are not in the same position but separated by 16 $\pm$ 2 cm^{-1}, and

(ii) the positions of the broad low frequency maxima have been shifted, both to the same extent, from the position in 6.0 mol dm^{-3} D_2O in H_2O.

The Raman spectra of sodium chlorate solutions did not (Fig 9-27) display any new features in the band contour, but the frequency position of the band maximum was considerably shifted from that of bulk OD. Figure 9-28 illustrates the effect of added lithium perchlorate on the absorption band assigned to water H–O–H bend. A narrowing (or sharpening) of the band was noticed at about 1640 cm^{-1} accompanied by a small low frequency shift. A small shift has also been noticed in the near infra-red spectra of 6.0 mol dm^{-3} HOD in D_2O,[254] (Figure 9-29).

The effects of perchlorate (Na^+, Li^+, Mg^{2+} and Zn^{2+}) were investigated in pure methanol. In this system no

FIGURE 9-25 Location of IR bands in metal perchlorate solutions in water.

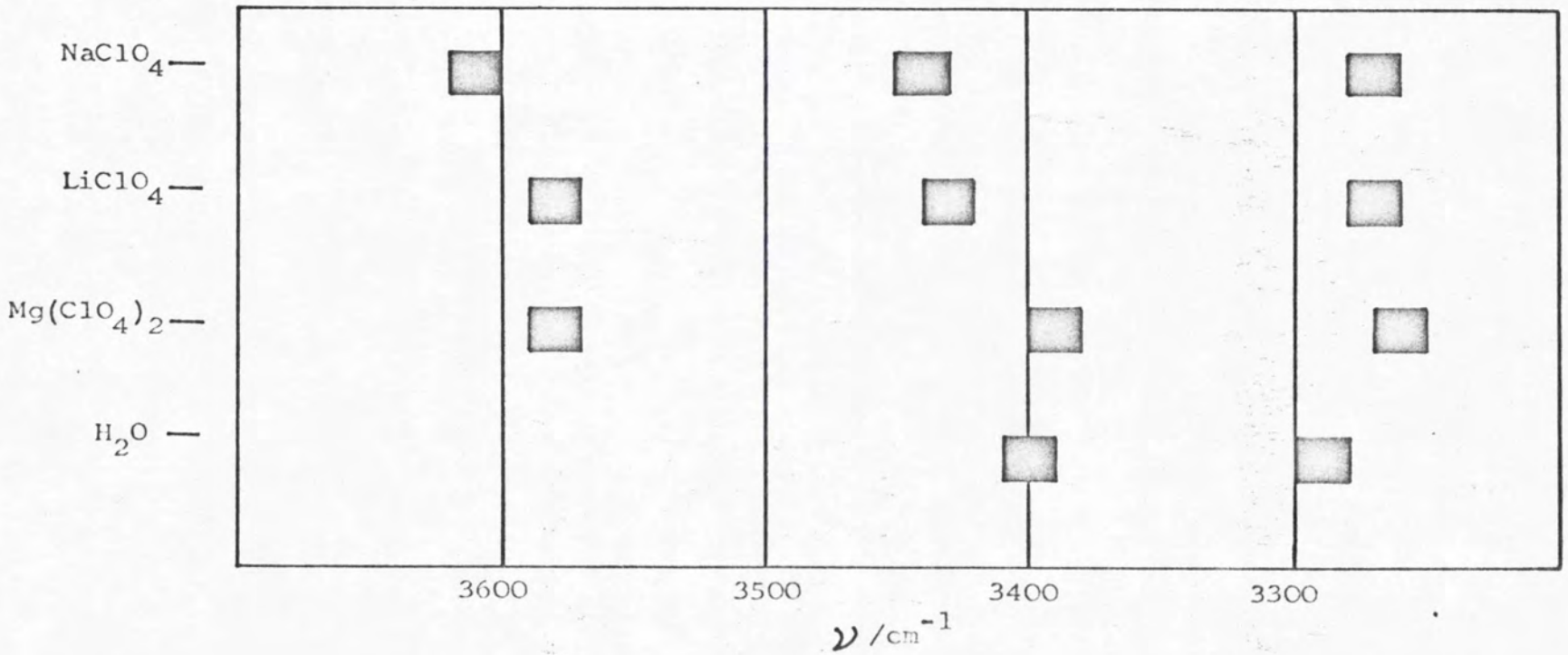

FIGURE 9-26 Raman spectra of 6.0 mol dm^{-3} D_2O in H_2O containing:

(a) 4.5 mol dm^{-3} $NaBF_4$; (b) 5.0 mol dm^{-3} $NaClO_4$;
(c) 3.7 mol dm^{-3} $NaClO_4$; (d) 6.0 mol dm^{-3} D_2O in H_2O;
(e) Background scattering, 4.5 mol dm^{-3} $NaBF_4$ at 298 K.

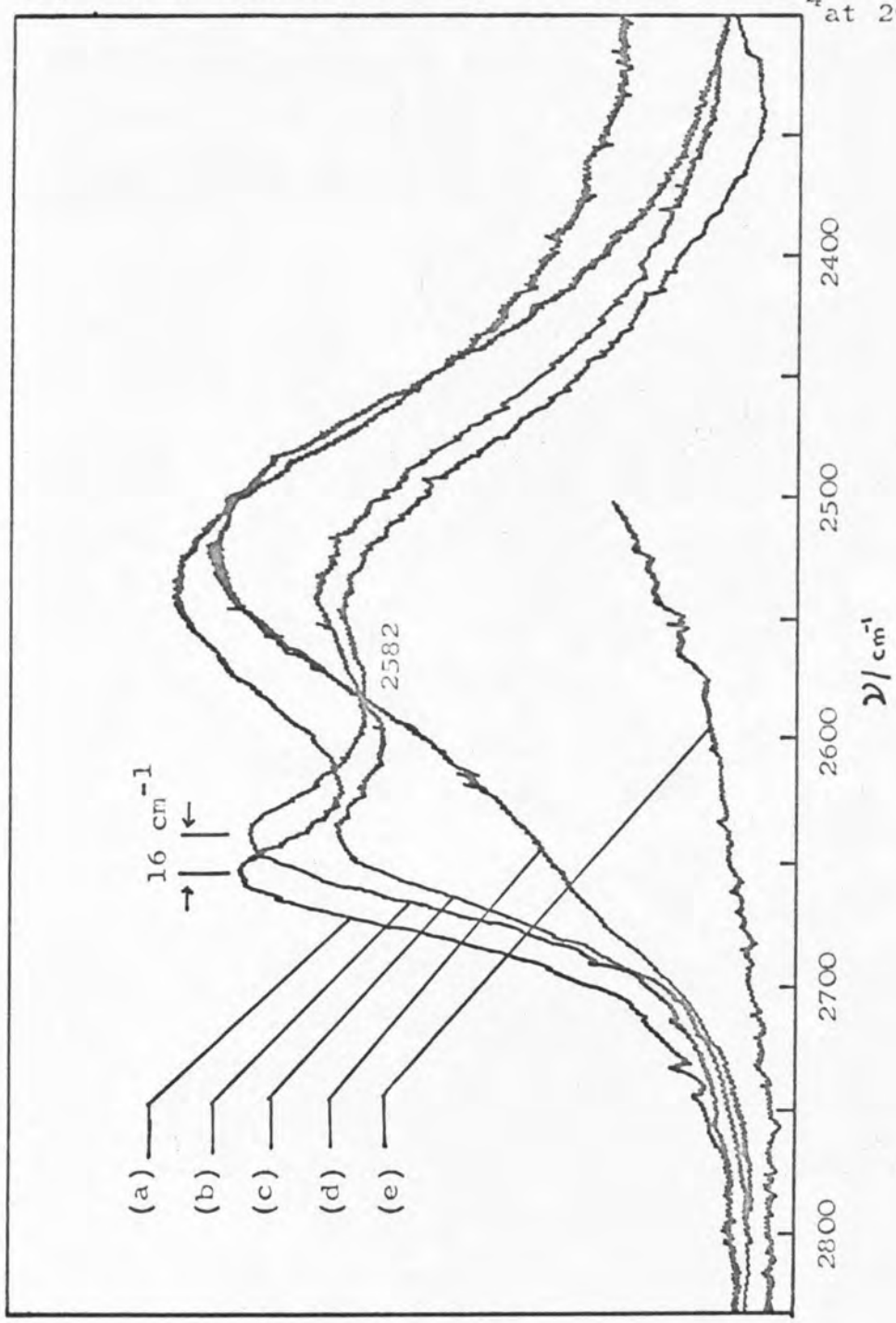

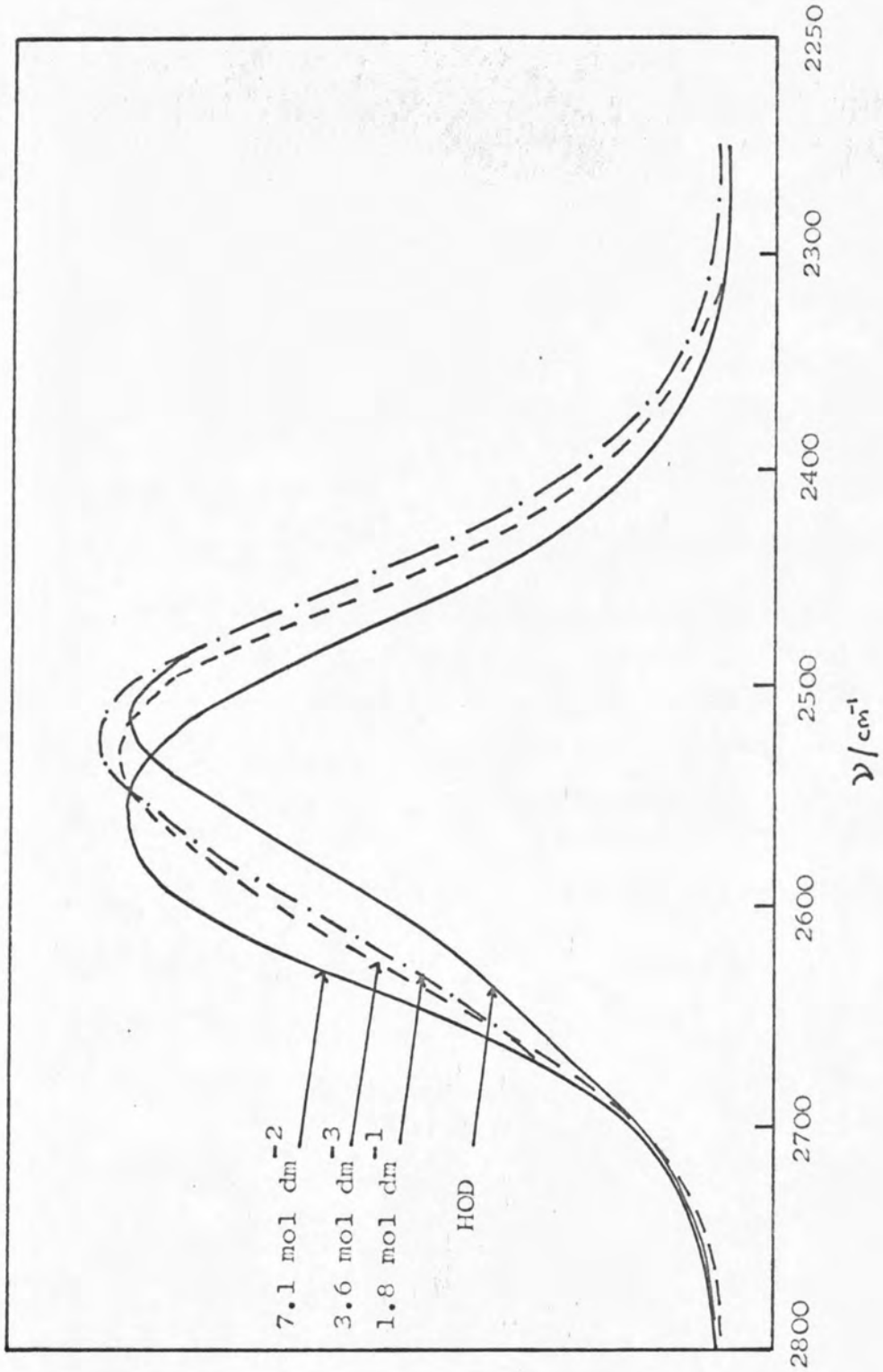

FIGURE 9-27 Raman Spectra of solutions of sodium chlorate at various concentrations in 6.0 mol dm^{-3} D_2O/H_2O at 298 K.

FIGURE 9-28 Raman Spectrum of Bending region of liquid water containing (a) 6.0 mol dm^{-3}, $LiClO_4$ and (b) pure water at 298 K.

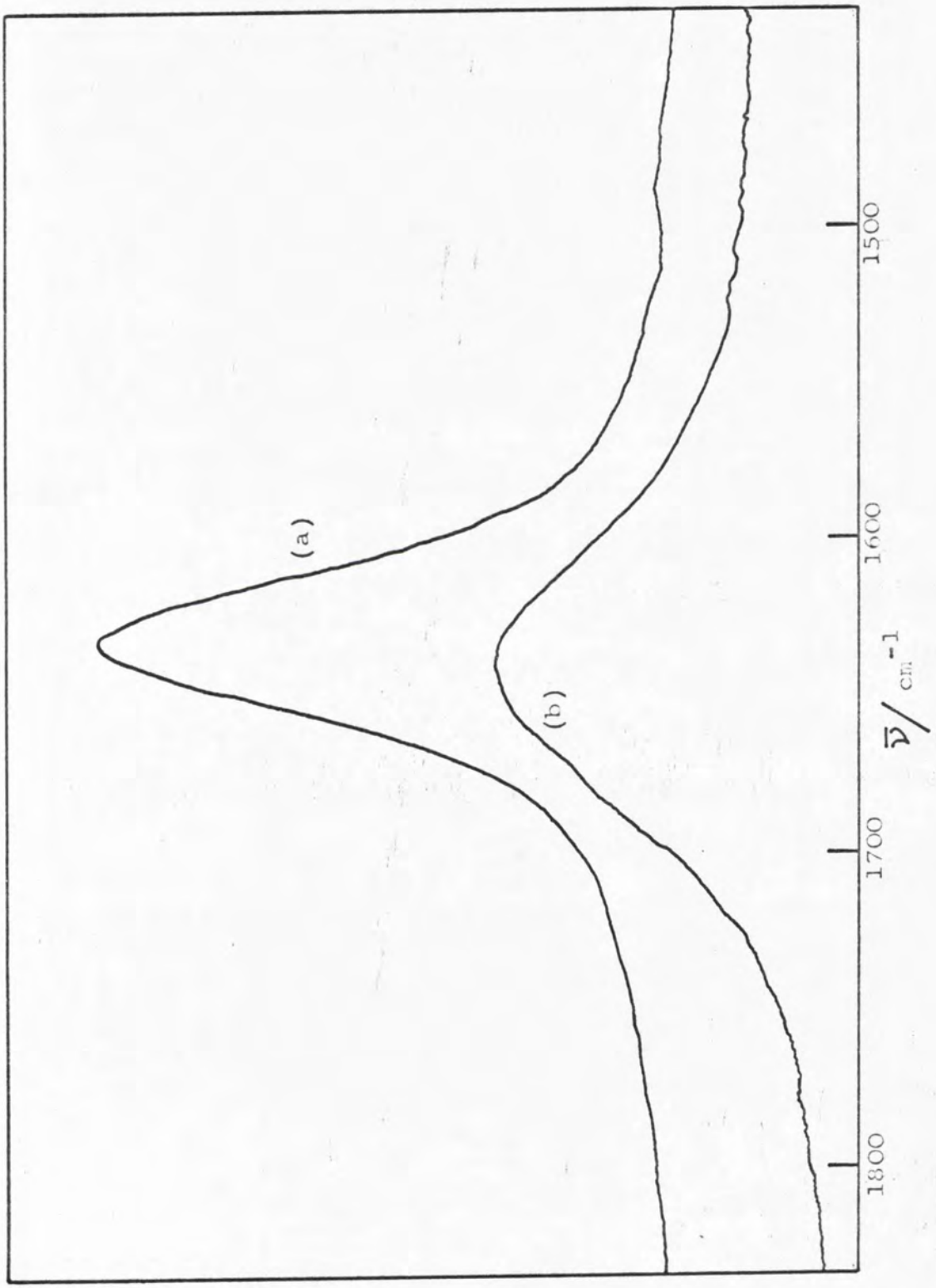

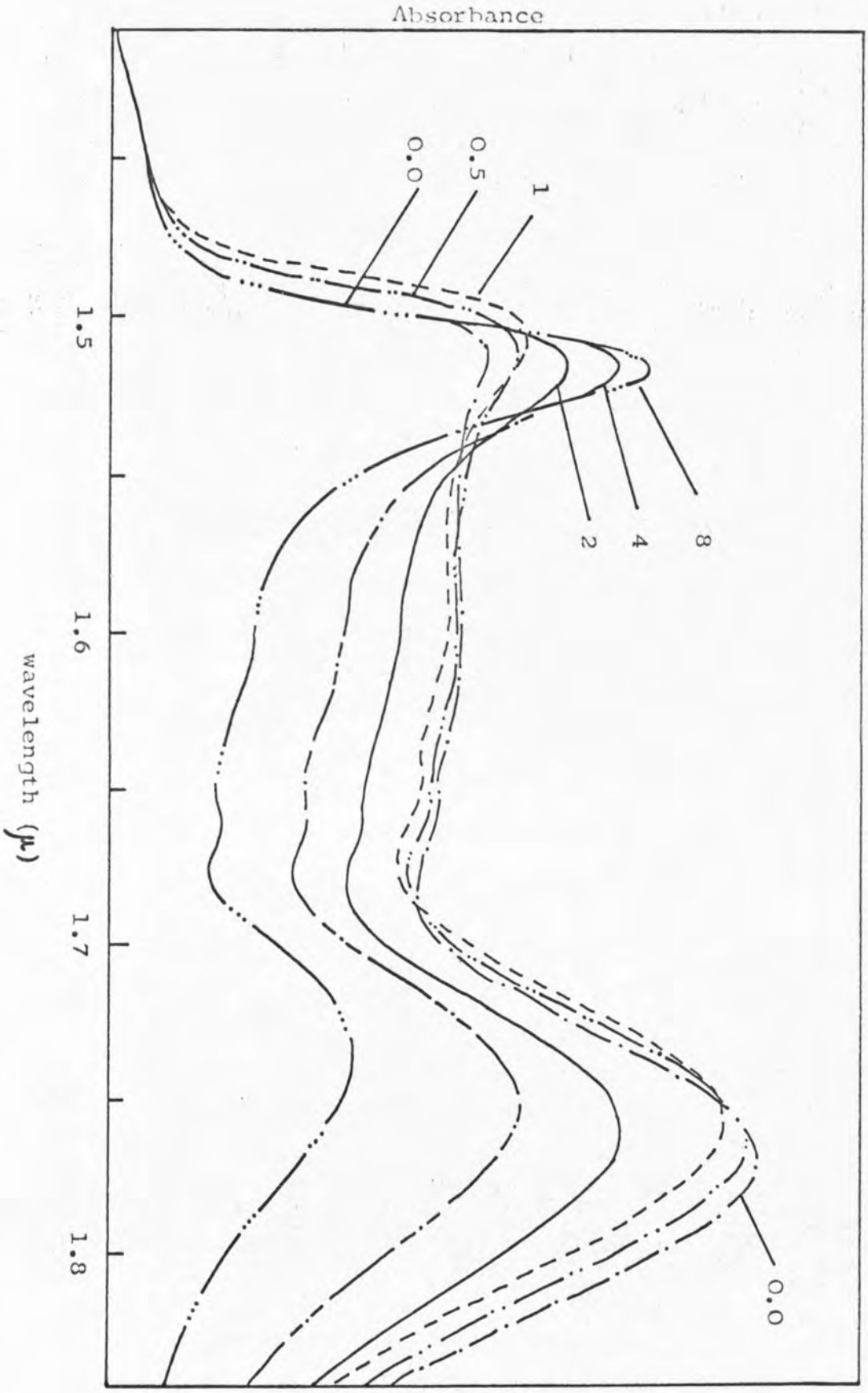

FIGURE 9-29 Near Infra-red spectra of 6.0 mol dm^{-3} H_2O in D_2O containing sodium perchlorate (concentration, mol dm^{-3} $NaClO_4$, indicated).

coupling occurs between the OH stretching modes. The results are summarised in Figure 9-30. Figure 9-31 shows the Raman spectrum of methanol and methanol containing 6.0 mol dm^{-3} lithium perchlorate. The wavenumber of the major components are summarised in Figure 9-32. The infra-red spectra of dilute solutions of methanol in dichloromethane show two features, one at 3640 and one at 3460 cm^{-1} assigned to 'free' (unbonded) OH oscillators and bonded OH oscillators respectively.[289] The spectra of methanol in methylene dichloride containing added alkylammonium perchlorate are shown in Figure 9-33 and 9-34.

(ii) Discussion

Salts

The infra-red spectra of inorganic salts in water reproduce closely the trends observed by Hartmann.[265] The Raman spectra are in accord with those observed by Wall and Hornig.[272,273] Since no vibrational bands of water of hydration are resolved, it may be that hydration of ions for long time intervals in solution does not take place. Alternatively well defined bands which could be assigned to water of hydration are hidden under the broad band envelope. The data does not lead to a clear cut choice between these alternatives. The fact that two very similar salts (e.g. NaI and KF) give contradictory spectroscopic effects makes it probable that simple structural interpretations are not valid.

Wall and Hornig[272,273] favour the absence of distinct

FIGURE 9-30 Infra-red spectra of solutions of metal perchlorates in pure methanol at 298 K:
(a) 3.5 mol dm^{-3} $Zn(ClO_4)_2$; (b) 2.5 mol dm^{-3} $NaClO_4$;
(c) 4.0 mol dm^{-3} $Mg(ClO_4)_2$; (d) 6.0 mol dm^{-3} $LiClO_4$;

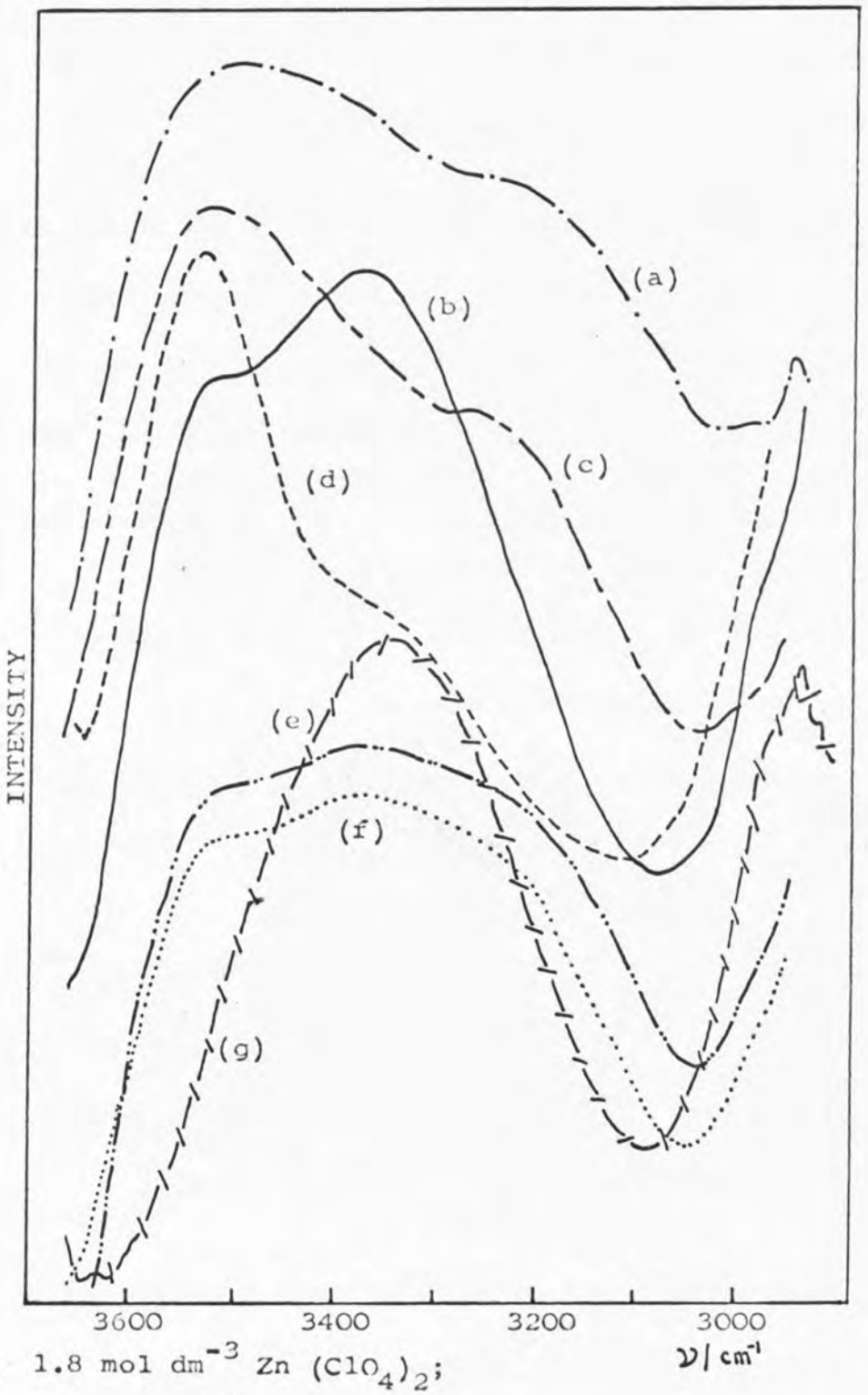

(e) 1.8 mol dm^{-3} $Zn(ClO_4)_2$;
(f) 2.0 mol dm^{-3} $Mg(ClO_4)_2$; (g) pure methanol.

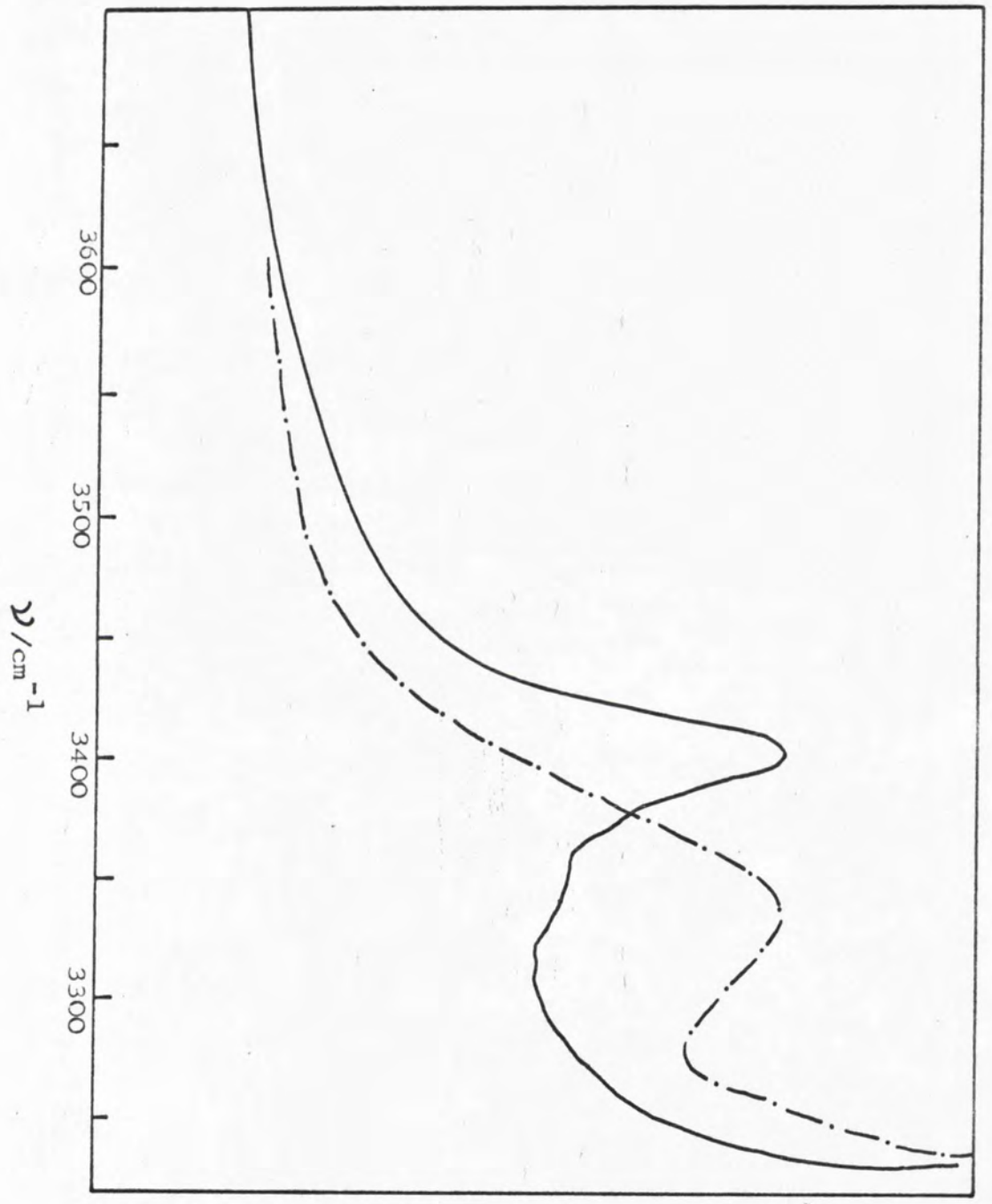

FIGURE 9-31 Raman Spectra of 6.0 mol dm^{-3} Lithium Perchlorate in methanol (____) and pure methanol (-.-.-) at 298 K.

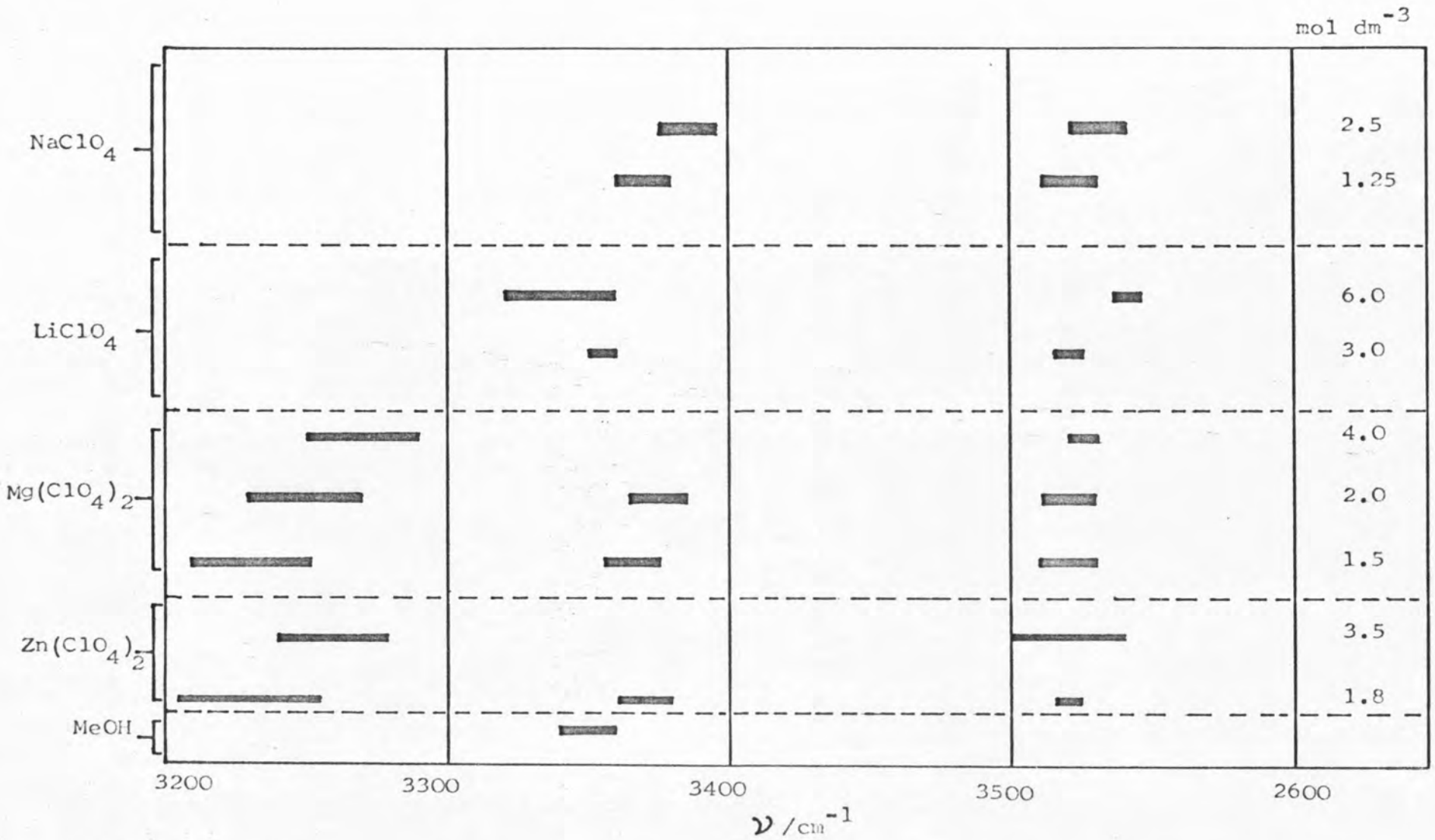

FIGURE 9-32 Correlation of major component bands observed in the infra-red spectra of metal perchlorates in methanol at 298 K.

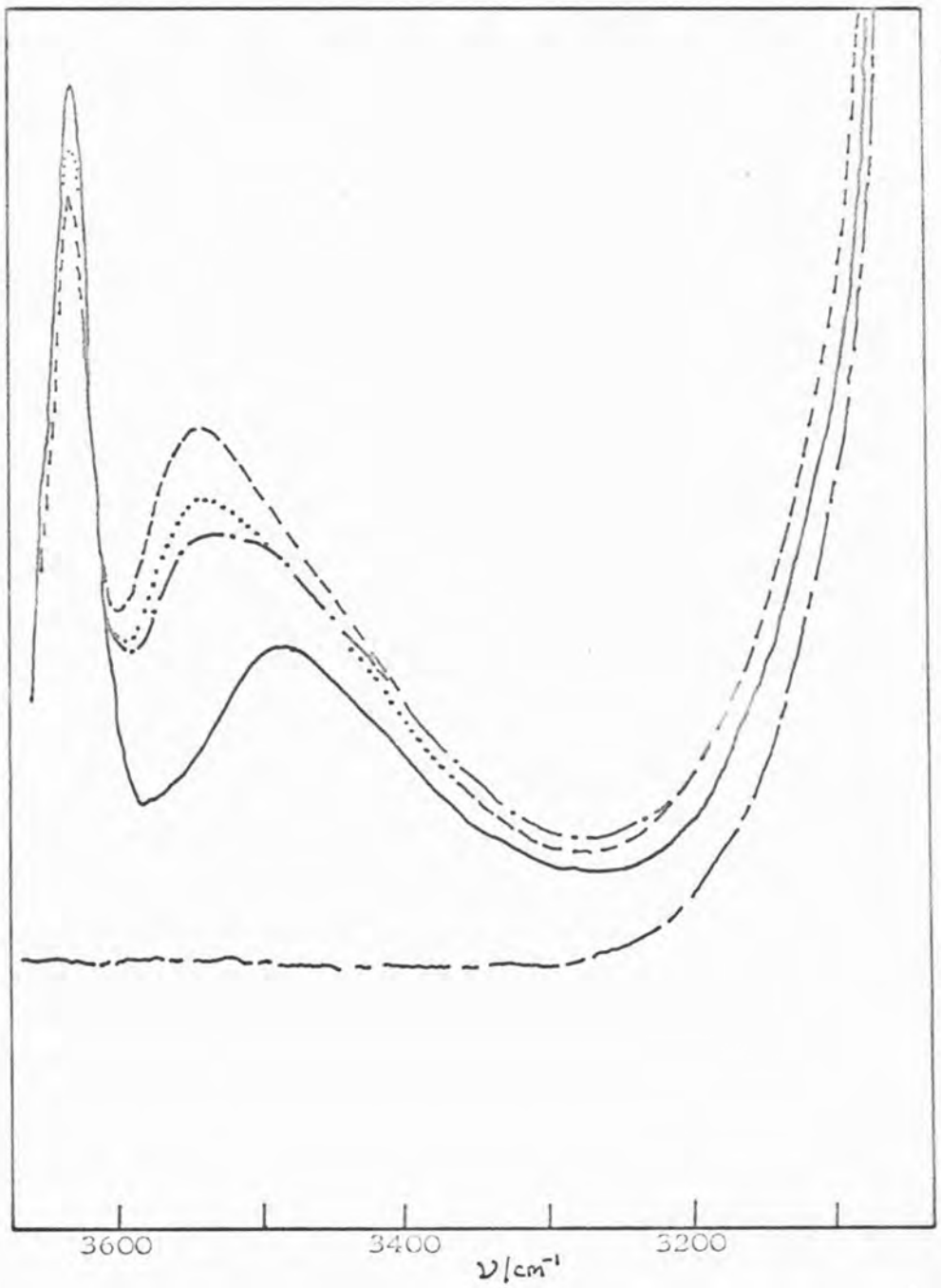

FIGURE 9-33 Infra-red spectra of tetraethylammonium perchlorate colutions in dilute methanol (2%) in methylene dichloride.

——— MeOH;
—·—· 0.11 mol dm^{-3};
..... 0.15 mol dm^{-3};
– – – – 0.22 mol dm^{-3};
——– – Solvent

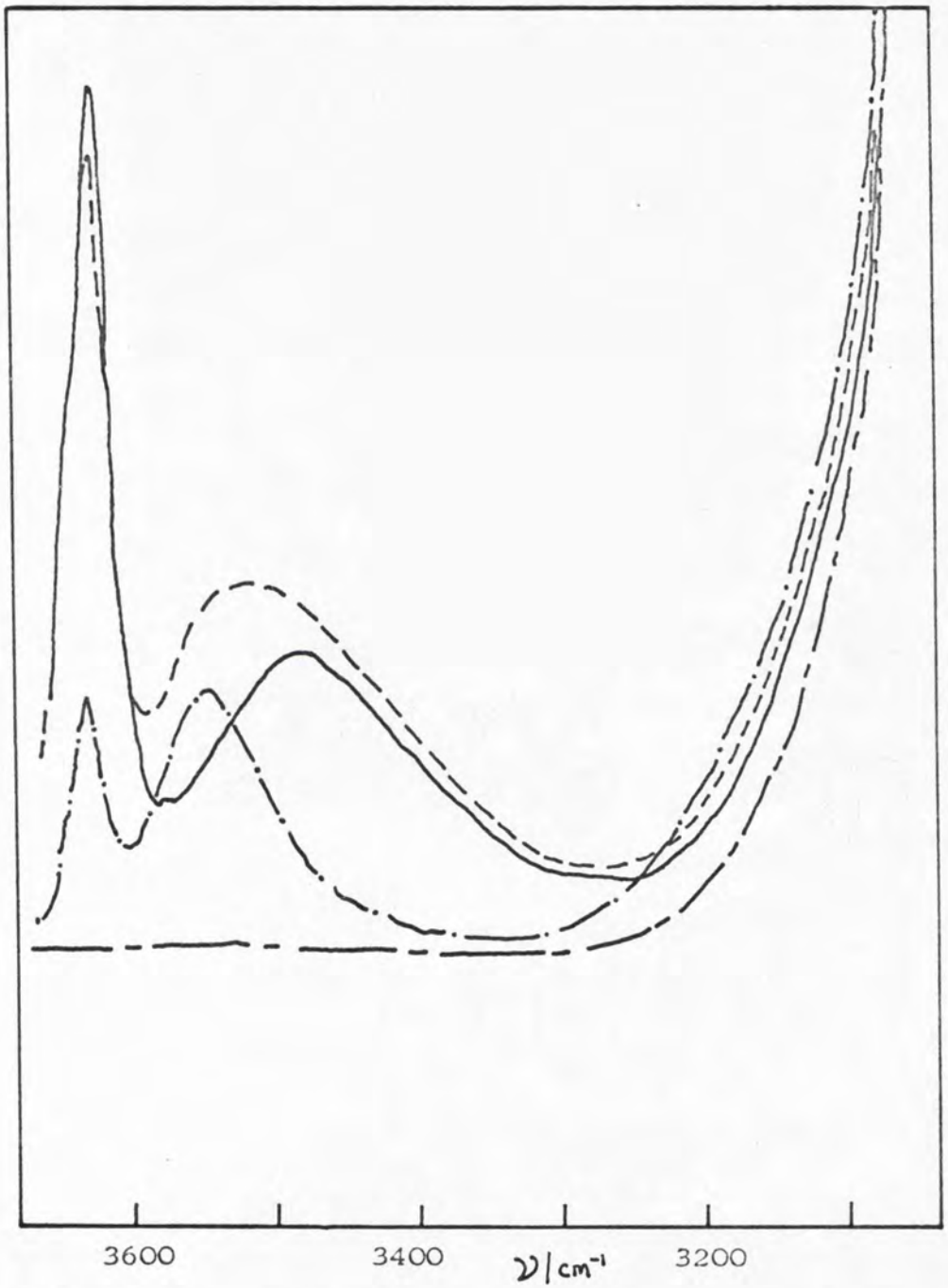

FIGURE 9-34 Infra-red spectra of tetra-n-pentyl perchlorate in dilute methanol (2%) in dichloromethane.

——— MeOH;

—·—·— 0.567 mol dm^{-3};

- - - - - - 0.113 mol dm^{-3};

——·—· Solvent.

water hydrates, whilst Hartmann[265] suggests that hydration does in fact occur, particularly in the case of sodium perchlorate.

Walrafen[224] has suggested that the high frequency shoulder on the OD stretching band is due to the presence of 'free' OD (unbonded) oscillators in the liquid. He concludes from the temperature dependence and isosbestic behaviour of the Raman spectra that a simple two state model suffices to account in general for this temperature dependence. In a study of the effects of sodium perchlorate on the OD stretching mode of water, Walrafen[276] suggests that hydration of the ions in solution, even up to high concentrations is not the dominant effect. Rather, the addition of salt induces the formation of 'free' OD, and this produces an increase in intensity near 2640 cm^{-1}.

Perchlorates, Chlorates and Fluoroborates

Two theories have been outlined above and in Chapter 7 in regard to the effects of salts upon the OD stretching region of the Raman spectrum of dilute solutions of D_2O in H_2O. Briefly, one[276] suggests that addition of sodium perchlorate induces the formation of non-hydrogen bonded OD oscillators, leading to increased intensity around 2640 cm^{-1}. The second suggests that bands characteristic of solvated species are observed.[265]

All metal perchlorates increased the intensity in the 2640 cm^{-1} region (Figure 9-22). Further, the increase

was always located at the same frequency ($\pm$ 5 cm^{-1}). This indicated that the new feature was a property of the perchlorate and not of the cation. The Raman and infra-red spectra of perchlorates in water, shown in Figures 9-23 and 9-24 respectively, also confirmed that the intensity change was due to added perchlorate. The same increase in intensity was produced by exactly half as much magnesium perchlorate as lithium or sodium perchlorate.

Thus the theories outlined above (and in Chapter 7) can be re-stated as follows. Given that the 'new' feature is due to the effect of perchlorate,is the 'new' feature an increase in the intensity of the 2640 cm^{-1} band due to perchlorate inducing the formation of non bonded OD groups, or is the feature a band due to OD groups attached to (i.e. hydrating) the perchlorate ion?

One aim of this work was therefore to find other experimental data which would help to distinguish between these theories. A second aim, based on the expectation that the perchlorate-hydrate theory was correct, was to deduce the influence of cations on these spectra.

In principle, separate bands will be formed for solvent molecules bonded to cations and anions, and five main types of O-D (H) oscillator can be distinguished, I, IIa, IIb, IIIa, IIIb. (The oscillator under consideration is marked *).

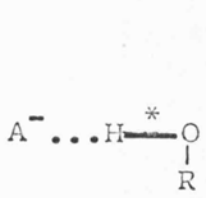

I

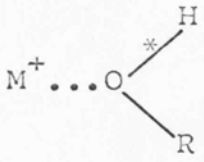

IIa

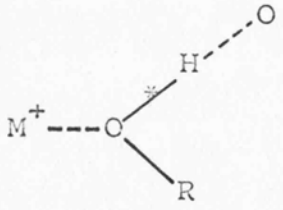

IIb

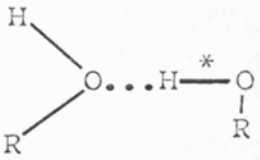

IIIa

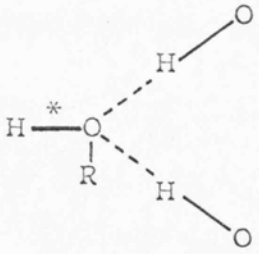

IIIb

Clearly it is necessary to make comparisons between such entities as

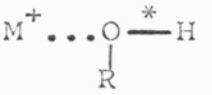 and 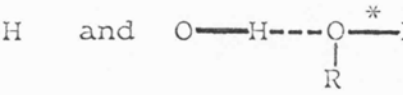 and not with the monomeric solvent molecules. (For water R = H). It is to be expected that the O-D (H) oscillator will be considerably affected when its D (or H) is involved in different sorts of hydrogen bonding as in I, IIb, and IIIa, but will be much less affected when its oxygen acts as a hydrogen bond acceptor as in IIIb, or becomes co-ordinated to cations as in IIa. These simple models would indicate that the effects of cations may well be second order in the sense that they may strengthen or weaken the extent to which the O-H (D) hydrogen (or deuterium) participates in hydrogen bonding of the type shown in IIb.

In all pure solvents there is a wide range of types of molecules in varying environments, all of which will give rise to different absorption bands. The recorded spectrum will be a broad envelope comprising these bands arising from combinations of I, II and III types of environment.

For most salts this is the case and separate species are not observed or resolved. For perchlorates and fluoroborates there is, however, clear evidence (Figures 9-17 and 9-24) for the existence of separate species. As indicated above this could be caused by the formation of 'free' (non hydrogen bonded) O-D (H) groups.[36,224,276]

However, the results shown in Figures 9-30 to 9-32 indicate that methanol behaves quite analogously to water. Consideration of Figure 9-26 reveals a small but definite difference (16 cm^{-1}) between the position of the new band in perchlorate solution and that formed on addition of the fluoroborate.

There is strong evidence that the new band formed when tetraethyl or tetrapentylammonium perchlorates were added to dilute solutions of methanol in dichloromethane (Figures 9-33 and 9-34), is associated with ClO_4^----HOMe units. In a previous study[289,290] it was shown that when tetra-n-butylammonium iodide is added to carbon tetrachloride containing a small amount of methanol, the anion becomes solvated by the methanol.[291] There is a good correlation between the infra-red spectra of the O-H groups

and the ultraviolet absorption spectra of iodide. It may be assumed that the same situation arises in this present system. Consequently the new band formed for both salts around 3540 cm^{-1} (at high concentration of alkylammonium salt) has been assigned to the O-H in the unit ClO_4^----H—*OMe.

If perchlorate is able to induce the formation of 'free' OD (H) groups, then the intensity of the 'free' OH in methanol band at 3640 cm^{-1} should increase in intensity as the concentration of perchlorate is increased. This does not happen. The 'new' band formed is shifted from that of monomeric methanol. The shift is less than the average value for liquid methanol, indicating that the perchlorate ion is a somewhat weaker acceptor than the oxygen atom of methanol. The same conclusion has been reached in nuclear magnetic resonance studies.[292]

Therefore, for perchlorates in methanol there is no evidence for the induced formation of free OH and the new feature is caused by methanol associated with perchlorate ions.

Since the results for water resemble those for methanol, it seems likely that the same situation applies, the proximity of the 'new' band to the weak shoulder detected in pure water being fortuitous. The Raman spectra (see Figure 9-23) for perchlorates in aqueous solution show a band, which is probably due to solvated perchlorate, at 3550 cm^{-1} and not 3600 cm^{-1}, the slight shoulder assigned by Walrafen[224,276] to 'free' O—H.

The position of the 'perchlorate-solvate' band in these spectra is at higher energy than the contour maximum of pure water (3450 cm^{-1}) and this indicates that the perchlorate-water interaction is somewhat weaker than the water-water interaction. The fact that the fluoroborate-solvate band is 16 cm^{-1} toward the high energy side of the perchlorate-solvate band, indicates that the fluoroborate-water interaction is weaker than the perchlorate-water interaction, the order being

$$BF_4^-\text{---}D\text{—}O \;<\; ClO_4^-\text{---}D\text{—}O \;<\; O\text{---}D\text{—}O.$$

The separation between the mean bulk OD frequency $\nu(\ O\overset{*}{\text{—}}D\text{---}O)$ and $\nu(O\overset{*}{\text{—}}D\text{---}ClO_4^-)$ the perchlorate-solvate maximum frequency for perchlorate dissolved in dilute solutions of D_2O in H_2O is equal, as now expected, to the separation between the band observed in pure water and the perchlorate-solvate band (see Figures 9-23 and 9-26).

The analogue computer analysis reported by Walrafen[241] predicts that the high frequency shoulder is centered on 2645 cm^{-1}. This requires that the D—O bond is stronger when fluoroborate is added than in the solvent. The gaussian computer analysis described in Chapter 8 gives the high frequency component position as 2660 cm^{-1} which is at higher frequencies than the fluoroborate and perchlorate-solvate bands and is consistent with the experimental observations.

The effect of cations upon the band not associated with the perchlorate-solvate band was relatively small.

The trends predicted in Figure 9-22 are in the same sense as that predicted by nuclear magnetic resonance measurements,[287,288,292] and reflect the effect upon hydrogen bonding of cations bonded to solvent molecules. Sodium ions have a smaller effect than the O---D - O bonding and magnesium ions increase the acidity of the O-D group and hence the strength of the hydrogen bond.

A somewhat analogous situation is provided by the solid hydrates studied by Brink and Falk.[279] Cations shift, slightly, the band for water associated with perchlorate, the order being $Na^+ < Ba^+ \approx$ water $< Li^+$.

It may be concluded that the replacement of a water molecule hydrogen bonded to the oxygen of an O-H (D) oscillator by a cation has only a minor effect upon that oscillator. However, a similar replacement of a water molecule, bound to a hydrogen, by an anion has a much greater effect. When the anion is perchlorate or fluoroborate a 'new' band due to the solvated species is observed, and the location of the bulk water maximum is dependent upon the cation.

In the case of salts such as sodium iodide or potassium chlorate (Figures 9-9 and 9-27) it seems likely that the band attributed to solvated anion is concealed within the broad contours since it is neither of sufficient intensity (oscillator strength) nor sufficiently separated from the bulk solvent band to be resolved. If this is the case it must be concluded that the limiting position of the plot of shift (cm^{-1}) against concentration reflects the position of the new solvated species band. Thus from

Figure 9-13 the order predicted of X^----D——O interaction would be

$$(OD---I^-) < (OD---BF_4^-) \approx (OD---Br^-) < (OD---Cl^-) \approx (OD---ClO_4^-) < (OD---F^-) \approx (OD---O).$$

A band due to the species ($OD---I^-$), ($OD---Br^-$) and ($OD---Cl^-$) may not be resolved because the exchange process in these systems is much faster than in the perchlorate and fluoroborate solutions. This is possible since in the perchlorate and fluoroborate ions the negative charge is localised along four directions in space tetrahedrally disposed about the central atom, thus facilitating hydrogen bonding. Wall and Hornig[272,273] suggest that ions in solution are able to affect all the water oscillators equally and shift the whole distribution of frequencies across the range available to liquid water. However in view of the spectroscopic evidence for hydration of perchlorate and fluoroborate it would not be unreasonable to extend this model to other ions. One final piece of evidence for solvation of perchlorate was obtained[293] from a near infra-red study of 6.0 mol dm^{-3} HOD in D_2O in the region studied by Worley and Klotz (Chapter 7). The band assigned to 'free' OH and the 'new' band produced at concentrations of perchlorate greater than 2 mol dm^{-3} are not co-incident (see Figure 9-29).

Solvation Number for Perchlorate and Fluoroborate

An approximate solvation number for perchlorate and

fluoroborate was obtained from the Raman spectra recorded at various concentrations of salt. Brink and Falk[282] reported infra-red studies of perchlorates and fluoroborates in dilute D_2O in H_2O. Using this data it has also been possible to derive solvation numbers for fluoroborate and perchlorate.

Suppose the low frequency band in the OD spectra is denoted B and the high frequency band A. A has been assigned above to (O—D---A^-) and B to (O—D---O). As salt is added (MA) the intensity of B decreases. Suppose the Raman scattering (or IR transmittance) of the unit (O—D---O) is S.

For n moles of water the initial band intensity would be I (initial) and

$$I\ (\text{initial}) = 2Nn\mathcal{S}\ ;\quad (N = \text{Avogadro's Number})$$

If, on addition of m moles of salt MA, x bonds are formed to A^-, then the final intensity will be I (final) and

$$I\ (\text{final}) = 2N(n-m)\mathcal{S} - Nmx\mathcal{S}$$

Thus $$\frac{I\ (\text{final})}{I\ (\text{initial})} = R = 1 - \{m/(2(n-m))\}x$$

R is the ratio of the total band integrated intensities. A graph of (1-R) against $(m/2(n-m))$ should have gradient x and should pass through the origin.

The value of x derived in the case of sodium perchlorate (Appendix 9-2) and fluoroborate is between 4 to 5, closer to 4.

The solvation number of perchlorate and fluoroborate

(i.e. the number of OH (D) bonds which it forms in solution) is probably 4. The rather higher value may be due to a statistical averaging of the number of water molecules associated with any perchlorate ion.

9-3 ORGANIC SOLUTES

(i) Results

The effects of added organic solutes on the O—D stretching band in the Raman spectra of dilute solutions of D_2O in H_2O were studied. Examples of spectra are shown in Figures 9-35 and 9-36. The shifts of the infra-red and Raman band maxima are plotted against mole fraction of organic solute in Figures 9-37, 9-38 and 9-39, for acetone and t butyl alcohol respectively. Further data is tabulated in Appendix 9-3.

(ii) Discussion

Walrafen[276] has studied the effect of dimethyl sulphoxide (DMSO) upon the O—D stretching oscillator. Following Safford[294] Walrafen suggests that hydrogen bonding between OD groups in HDO and DMSO would be expected to occur. Since the spectra from DMSO solutions are similar to those obtained when KCl or KBr are dissolved in the solvent, it was suggested[276] that the observed bands can be assigned to interactions of the type $\rangle S{=}O\cdots D{-}O$, since these latter salts are known to undergo anionic hydration. (See Chapter 7). These spectroscopic observations have

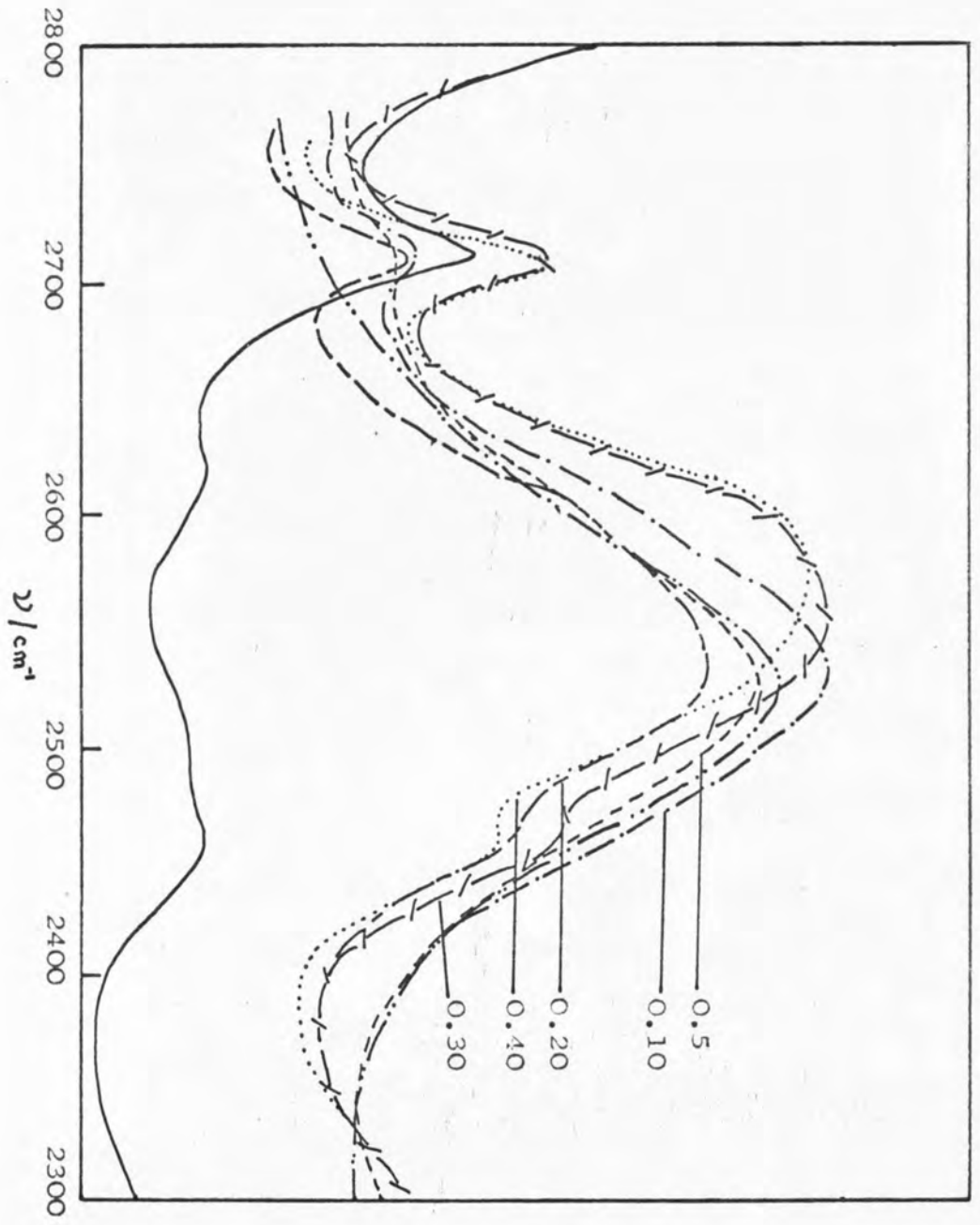

FIGURE 9-35 Raman spectra obtained from solutions of acetone in 6.0 mol dm^{-3} D_2O in H_2O at several concentrations and 298 K.

FIGURE 9-36 Raman Spectra obtained from solutions of t butanol in D_2O/H_2O (6.0 mol dm^{-3}) at 298 K. (mole fraction of t BuOH as indicated).

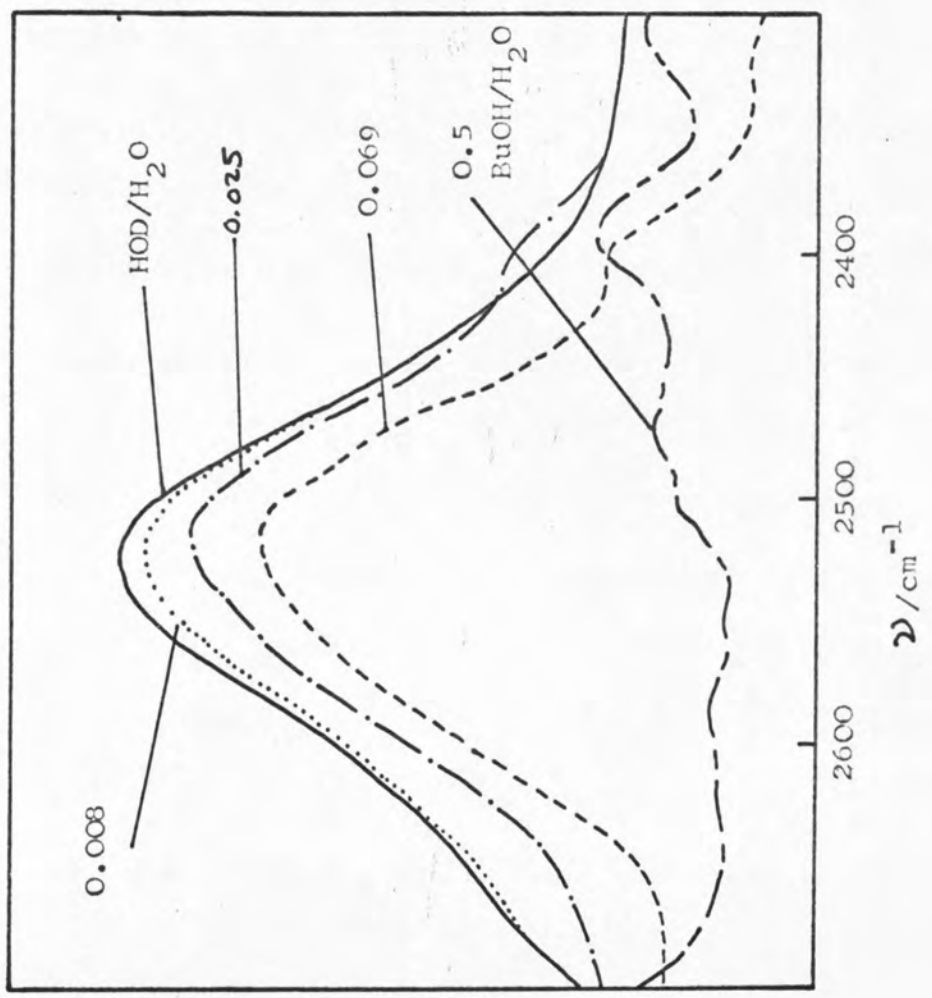

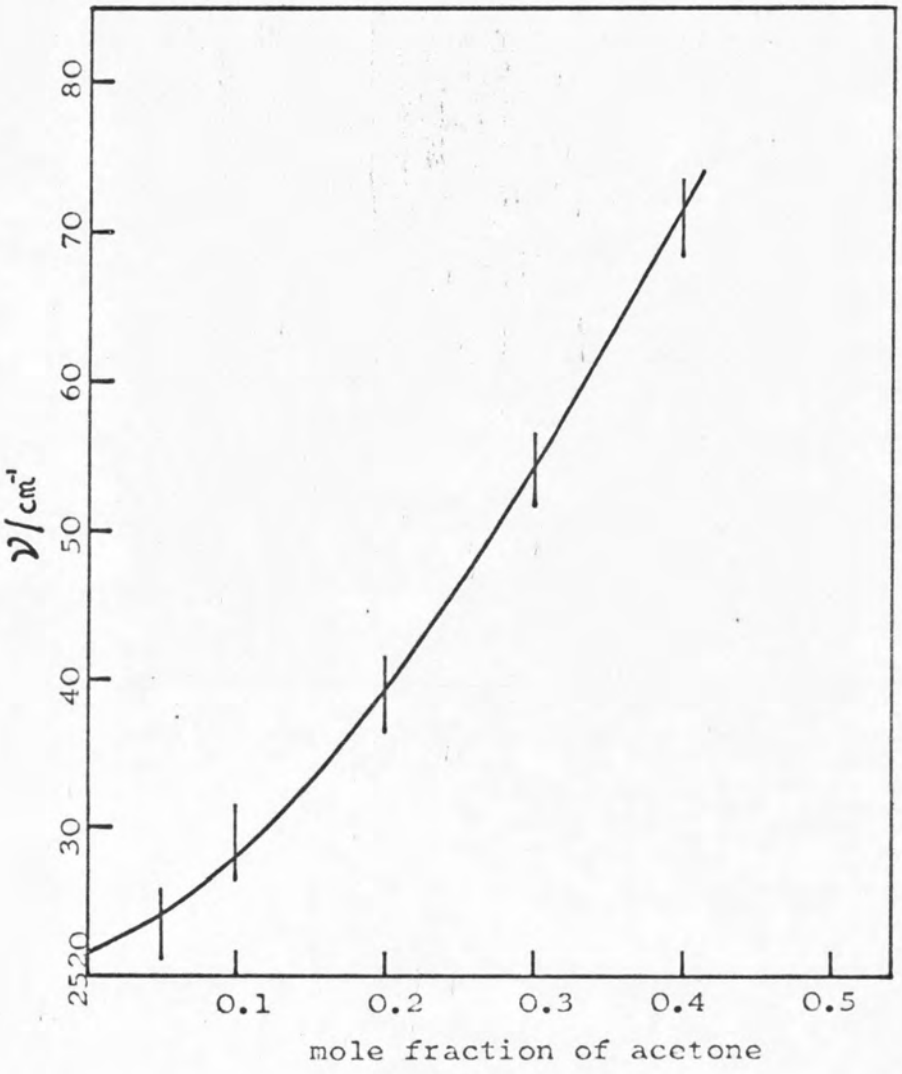

FIGURE 9-37 Dependence of major component frequency maximum on mole fraction added acetone at 298 K. (in D_2O/H_2O - Raman Spectra).

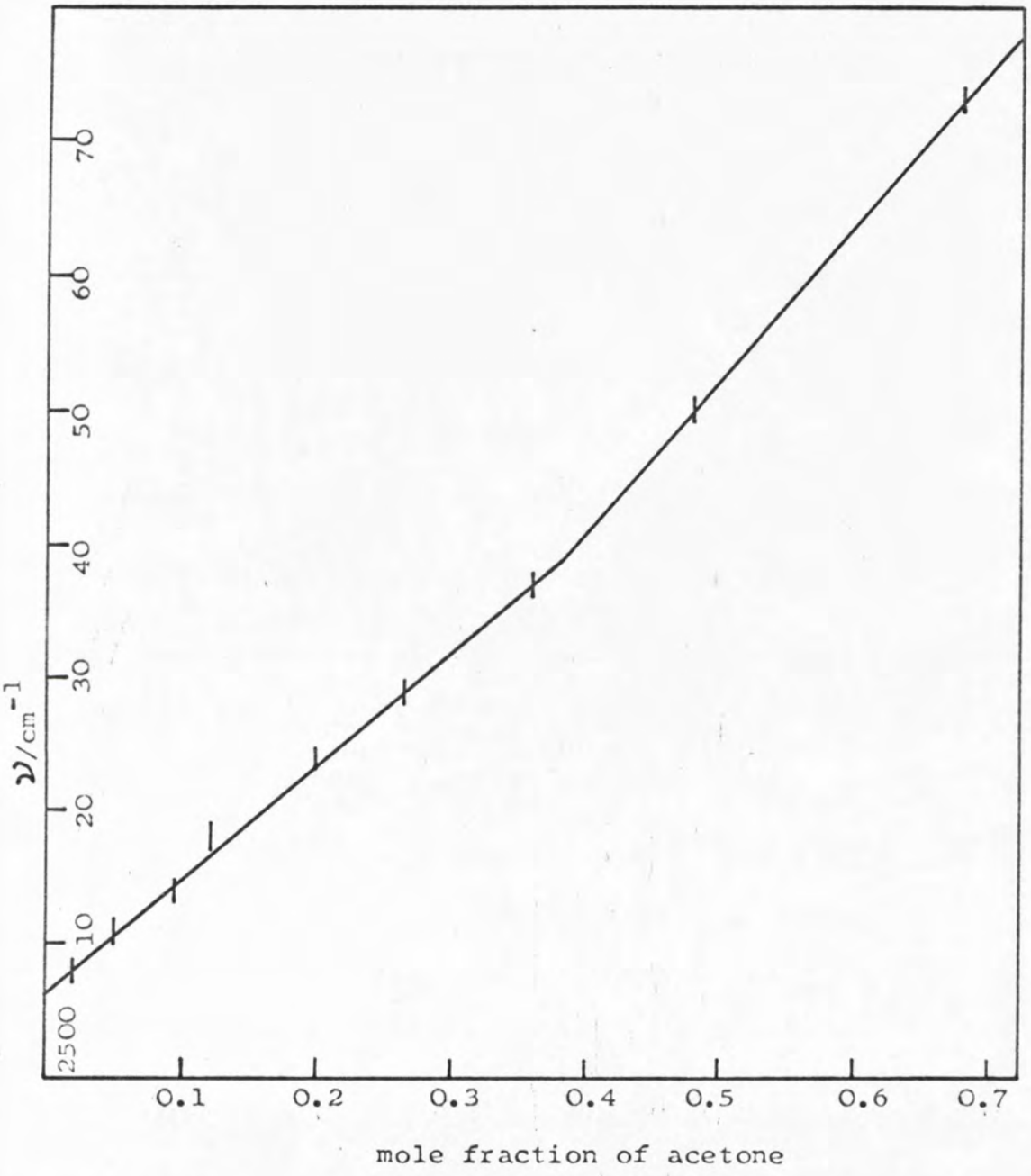

FIGURE 9-38 Dependence of major component frequency maximum upon mole fraction of added acetone for solutions of D_2O/H_2O at 298 K. (Infra-red spectra).

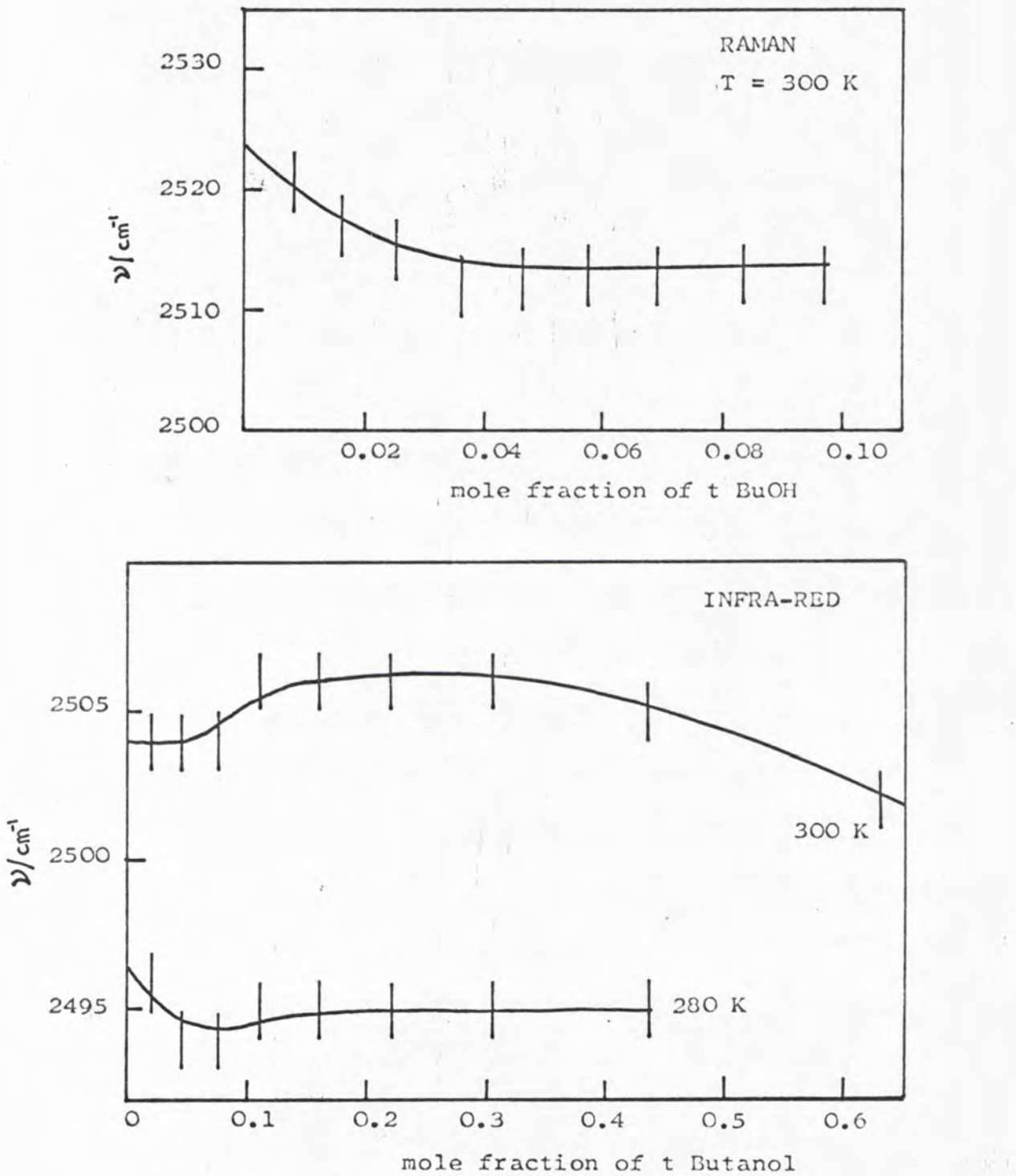

FIGURE 9-39 Correlation of major component frequency maximum with mole fraction of added solute (t butanol).

been confirmed.[295] However, the changes in the spectra are so small as to be unconvincing, unless it can be considered that the O---D——O interaction is almost identical with the >S=O---D——O interaction.

Extensive studies of the alcohol series t butyl-alcohol, n-propyl alcohol, ethyl alcohol, methyl alcohol, revealed that little or no shift in OD band position occurs. However it is probable that ROH is converted, partially at least to ROD, this masking subtle changes which take place when alcohol is added. However replacement of an oxygen of a water atom hydrogen bonded to an OD oscillator (H_2O---D——O) by an alcohol would not be expected to shift the OD oscillator frequency by a large amount. The results for t butylalcohol are represented in Figures 9-36 and 9-39.

The affects of added acetone and dioxan have also been studied in the infra-red and Raman. The Raman spectra of the OD stretching region for acetone are shown in Figure 9-35 from which it is clear that added acetone brings about a significant shift in the frequency of the band maximum, together with a considerable increase in breadth of the maximum.

A similar shift occurred when dioxan was added (Appendix 9-3). It seems that in these cases the situation is much more clear cut than that for DMSO. The high frequency shift for acetone suggests that a new band clearly not visible in the alcohol-water mixtures (shown for t butyl alcohol in Figure 9-36) is being formed. This

new feature was tentatively assigned to ($\rangle$C =O---D—O) interactions. Similarly the large shift of the infra-red OD oscillator towards higher frequencies for dioxan was assigned to specific interaction between OD and dioxan.

Therefore acetone-water and dioxan-water interactions are weaker than the water-water interactions. Further, the DMSO interaction is probably the strongest of the series DMSO, acetone, dioxan,and is about equivalent to the O---D—O interaction. The order being

(O---D—O) $\approx$ (DMSO---D—O) $>$ (DIOXAN---D—O) $>$ (ACETONE---D—O).

It is interesting to note that the infra-red results for acetone in dilute D_2O in H_2O predict a change in slope of the plot of ν_{max} versus composition at about 0.4 mole fraction of acetone. This corresponds to the peak sound absorption concentration at 70 MHz and 298 K. The plot of the ratio R determined from a near infra-red study of acetone in 6.0 mol dm^{-3} HOD in D_2O[296] (Chapter 7) shows an increase up to 0.07 mole fraction of acetone. This corresponds to the composition of the acetone hydrate reported by Frank and Quist.[173]

9-4 DILUTE SOLUTIONS OF WATER IN ORGANIC PHASES

(i) Introduction

The infra-red spectra of small amounts of water diluted

in organic solvents show two bands due to the asymmetric (ν_3) stretching vibration of water and the symmetric (ν_1) vibration. Some years ago Saumagne[297] demonstrated, by infra-red studies, the existence of two water-complex species with organic solvents. In the 1:1 complex (HOH---A) observed in water-organic solute mixtures at low concentrations in carbon tetrachloride the symmetry of the water molecules is lost, whereas for the 2:1 complex (A---HOH---A) it is retained. The latter complex is formed when water is diluted by an organic solvent. In addition a recent matrix isolation study by Tursi and Nixon[298] has yielded values of ν_1 and ν_3 for water molecules in different environments. For the dimer ($HOH---OH_2$) and the trimer ($H_2O---HOH---OH_2$) values of ν_1 and ν_3 (ν_{ass} and ν_{free}) were obtained.

Glew[256] has also recently drawn attention to the linear correlation which exists between the values of ν_1 (ν_{ass}) and ν_3 (ν_{free}) plotted against each other. The relationship given by Glew is

$$(3657 - \nu_1) = 0.8333\ (3756 - \nu_3).$$

(ii) Discussion

Using the data of Bellamy,[299] Glew,[256] Stevenson,[300] Greinacher[301] and Barrow[302] in addition to that of Saumagne, it was possible to construct the more detailed plot shown in Figure 9-40. The data used in the construction of this diagram is recorded in Appendix 9-4.

Data points for ice and many crystal hydrates also

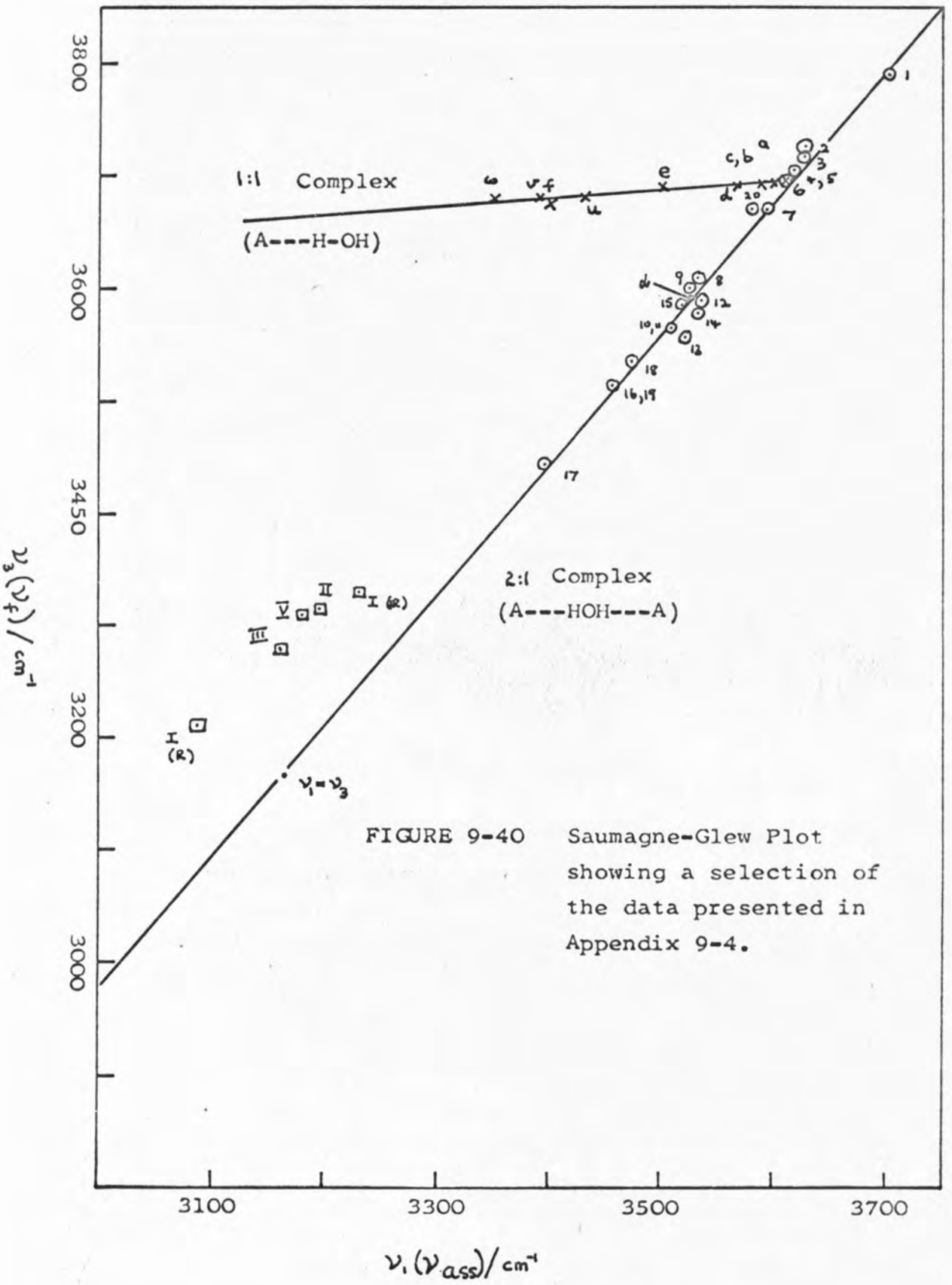

FIGURE 9-40 Saumagne-Glew Plot showing a selection of the data presented in Appendix 9-4.

fit onto the line for the 2:1 complex. Then, as the environment of water becomes more ice-like, so the linear relationship predicted by Glew breaks down. This diagram can be used to predict the environment of any given water molecule whose symmetric and asymmetric stretching frequencies can be measured. Thus the perchlorate hydrates lie on this curve, confirming the presence in these hydrates of a perchlorate-water interaction. The data point for the stimulated Raman scattering spectra for perchlorate in water is on this line, adding further weight to the previous assignments (section 9-2).

The locations of the 1:1 complexes of dioxan, DMSO and acetone with water show that the interaction in the DMSO-water complex is greater than in dioxan and acetone. This confirms the conclusion reached in the previous section.

CHAPTER TEN

CONCLUSION

The investigations reported in the foregoing chapters have been concerned with the elucidation of the structure of aqueous solutions. Particular emphasis was placed on the nature of the solute-water interactions and the ways in which the experimental observations can reveal this. Two basic techniques have been employed, ultrasonic absorption, and vibrational spectroscopy.

The former technique was used to study methyl cyanide + water, and acetone + water mixtures in detail, including investigations at low frequencies (200 to 1500 kHz). This information, together with other data from the literature, was used to test two theoretical models. Of these two models, the first interpreted the ultrasonic absorption in terms of simple chemical equilibria, whilst the second used a concentration fluctuation approach. It was shown that the former model could only account for the observed ultrasonic absorption in cases where a specific and simple chemical equilibrium was known to be present in the mixture; and then only qualitatively. The latter model proved more rewarding and led to the establishment of a direct link between the thermodynamic and ultrasonic absorption properties of several aqueous binary mixtures. This model was also extended to provide a description of ultrasonic absorption (PLOT A) in aqueous electrolyte solutions and aqueous solutions of urea. In all cases studied good agreement was found between the experimental and theoretical treatments of the systems studied. In particular, it was possible to highlight those thermo-

dynamic parameters which control the absorption process (e.g. the enthalpy for methyl cyanide + water; the volume for acetone + water).

Two important regions have been identified in the plot of (α/f^2) against mixture composition (PLOT A). These are the highly aqueous or 'plateau' region, and the peak sound absorption region around the PSAC (Chapter 2).

In the highly aqueous region, water accommodates the solute. At the end of this region (the end of the 'plateau') further addition of the solute establishes simple equilibria in solution which are thought, according to the first model described above, to be responsible for the absorption process.

In the study of the vibrational spectra of aqueous solutions by Raman and infra-red spectrophotometry, the studies have been centered around electrolyte solutions. Two recent studies of solutions of sodium perchlorate in water (using D_2O as a convenient probe) have led to conflicting views in respect of the ability of perchlorate ions to be solvated in solution. One view considers solvation of perchlorate as responsible for the appearance of a new feature in the Raman spectra of these solutions. A second believes that addition of alkali metal perchlorates to water encourages the formation of non-hydrogen bonded OH (OD) groups which are responsible for the new features observed.

It has been possible, partly by consideration of

data taken from the literature reporting a water-perchlorate interaction, and partly by detailed experimental studies, to show that the hydration approach is the correct one. Sodium fluoroborate has been shown to cause similar changes in the spectra to sodium perchlorate and fluoroborate solvation is indicated. A solvation number of four for the perchlorate and fluoroborate ions has been derived. Solutions of perchlorates in anhydrous methanol display similar spectra to aqueous solutions. The study of methanol in dilute solution in dichloromethane containing tetra-alkylammonium perchlorates has led to the characterisation of a methanol-perchlorate solvate, and this can be considered as good evidence for the solvation of perchlorate by water.

In addition, an investigation of the changes in the Raman and infra-red spectra of aqueous solutions containing organic solutes (and D_2O as a convenient probe) was undertaken. The results of this study, and a parallel study of the effect of organic solutes upon the near infra-red spectra of HOD in D_2O, reveal similar regions of behaviour to those characterised in the ultrasonic studies.

The spectroscopic and ultrasonic absorption properties of aqueous solutions seem to divide into two separate regions. In the highly aqueous region of binary liquid mixtures, both techniques (ultrasonics and vibrational spectroscopy) show extrema. Similarly, extrema are also provided by both methods of investigation in the more concentrated mixtures, close to the ultrasonic PSAC. A

similar type of behaviour was noted by Hyne[108] in a study of the effects of pressure and temperature on reaction rates. Hyne assigned these extrema to the 'buttressing' effect of added co-solvent as demonstrated previously by Franks and Ives.[45] He considers that the first extremum (cf the end of the ultrasonic 'plateau' region) represents the situation at which water structure is at a maximum due to co-solvent occupying all the preformed holes in the solvent structure. A prerequisite of further solvent dissolution is the formation of further holes (or cavities). This requires the breakdown of the water structure. Blandamer[303] has taken a somewhat similar approach in so far as considering the initial water rich region and the eventual extremum at high solute concentrations. In this model the initial insensitivity to added solute, as reflected in the near infra-red and the ultrasonic absorption, corresponds to the accommodation of the co-solvent by water, the co-solvent fitting into the water structure in much the same way as in clathrate hydrates. At this stage, e.g. the end of the 'plateau' region, the water structure is at a maximum. Addition of further solute causes the breakdown of this structure since the availability of cavities for accommodation of the solute has reached a minimum. Blandamer[303] suggested that the degree of structuring caused by the addition of an alcohol, say, is reflected in the magnitude of the catastrophic breakdown of water structure at higher solute concentrations (the ultrasonic PSAC). Thus the large

ultrasonic absorption exhibited by t butylalcohol + water mixtures is a consequence of the catastrophic destructuring brought about by the addition of further t butylalcohol.

Consequently, the situation is now one in which 'enclathrated' solute, represented by ($S \bullet_n H_2O$) is essentially 'disolved' in the co-solvent (S). An equilibrium may then be considered to be established as follows:

$$S + nH_2O \rightleftharpoons S \bullet nH_2O$$

One may speculate that the peak sound absorption composition corresponds to the situation where all semblance of water structure has left the mixture.

It is hard to translate observations made on aqueous solutions back to pure water, since addition of a small amount of solute may change the nature of the structure. The above evidence (the initial insensitivity to solute) would at face value suggest, however, that this is not the case. It is clear that the ability of water to accommodate a solute is limited, but over a small initial region the addition of solute seems, from the ultrasonic observations, to have little structural effect. Perhaps, however, evidence from the near infra-red region is more revealing. This implies an immediate structural change, interpreted as a structure making or structure breaking effect, in the solvent. This situation is not yet fully resolved, but if the near infra-red results are to be believed, then arguments concerning water structure based

upon information obtained from studies of aqueous solutions should be avoided.

It was noted earlier (Chapter 9) that the extrema in the highly aqueous liquid mixtures can be correlated with the compositions of the clathrate hydrates, e.g. the alcohols and acetone. This is of considerable importance and adds credence to the above theories of Hyne[108] and Blandamer.[303] This does not imply that definite clathrate hydrate structures exist in the dynamic medium of water, but rather that 'hydrate-like' species are present having a life time of the order of 10^{-10} second, that is slightly longer than the ultrasonic absorption on vibrational spectroscopic time scales.

APPENDICES

APPENDIX TO CHAPTER 4

TABLE 4 - 1 Sound Velocity Measurements:

Methyl Cyanide + Water

Mole Fraction MeCN (x_2)	Sound Velocity/(ms^{-1}) 273.2 K	298.2 K	308.2 K
0.000	1495	1490	1520
0.025	1468	1510	1527
0.050	1517	1520	1538
0.075	1531	1530	1537
0.100	1516	1518	1527
0.125	1510	1515	1512
0.150	1505	1505	1499
0.200	1495	1481	1480
0.300	1463	1425	1430
0.400	1436	1386	1387
0.500	1426	1364	1334
0.600	1414	1338	1305
0.700	1402	1318	1293
0.800	1393	1308	1270
0.900	1388	1304	1248
1.000	1385	1300	1245

TABLE 4 - 2 Ultrasonic Absorption Measurements

(200 to 1500 kHz)

(a) Calibration* data at 298 K; large transducers

k/s^{-1} - calibration constants

Frequency kHz	Run 1	Run 2	Run 3	Run 4
200	39	43	37	36
250	46	40	50	57
300	57	47	51	54
350	63	44	56	60
400	62	50	67	69
450	54	50	51	55
500	52	48	49	-
550	47	45	46	46
600	50	49	59	46
650	59	59	58	54
700	60	63	60	53
750	69	70	75	70
800	72	67	76	79
850	76	74	98	93
900	89	120	112	120
1000	100	-	-	137
1100	154	-	-	-
1200	-	-	-	160
1300	-	-	-	166
1400	-	-	-	170
1500	167	-	-	170

*Pure degassed, deionised water was used for calibration.

TABLE 4 - 2 Ultrasonic Absorption Measurements

(200 to 1500 kHz)

(b) Calibration data at 298 K; small transducers

Frequency kHz	k/s^{-1}	τ/s
250	46	22
300	48	21
350	51	19
400	50	20
450	48	21
500	48	21
550	53	19
600	59	17
650	72	14
700	68	15
750	74	14
800	81	12
850	100	10
900	110	9
1000	121	8
1100	154	6.5
1200	175	5.7
1300	190	5.3
1400	-	-
1500	250	4

TABLE 4 - 2 Ultrasonic Absorption Measurements

(200 to 1500 kHz)

(c) For methyl cyanide + water mixtures

Frequency kHz	$(\alpha/f^2) \times 10^{17}$/nepers s^2 cm^{-1}	
	0.1 mole fraction MeCN + H_2O at 298 K	
200	667	870
250	298	550
300	85	208
350	117	316
400	67	96
450	130	140
500	86	84
550	80	80
600	78	78
650	60	59
700	71	71
750	106	108
800	89	101
850	76	69
900	71	77
950	-	-
1000	72	61
1100	120	73
1200	-	100
1300	-	88
1400	-	-
1500	198	-

TABLE 4 - 2 Ultrasonic Absorption Measurements

(200 to 1500 kHz)

(d) For methyl cyanide + water mixtures

Frequency kHz	$(\alpha/f^2) \times 10^{17}$/nepers s^2 cm^{-1}
	0.3 mole fraction MeCN + H_2O at 298 K
200	1235
250	1322
300	635
350	907
400	934
450	789
500	845
550	821
600	894
650	917
700	1659
750	1653
800	1093
850	1088
900	1413
1000	1020

	711
	990
	808
	957
	690
	819
	737
	821
	993
	1069
	1254
	1305
	1141
	1264
	1111
	963

TABLE 4 - 2 Ultrasonic Absorption Measurements

(200 to 1500 kHz)

(e) For methyl cyanide + water mixtures

Frequency kHz	$(\alpha/f^2)\ 10^{17}$/nepers s^2 cm^{-1}		
	mole fraction methyl cyanide at 298 K		
	0.4	0.5	
200	1239	-	272
250	799	625	469
300	901	418	602
350	627	398	464
400	957	399	492
450	740	521	368
500	642	535	497
550	804	478	621
600	1054	413	550
650	883	463	453
700	1123	473	485
750	967	654	488
800	918	507	454
850	746	734	508
900	562	514	519
1000	759	967	454
1100	890	-	605
1200	-	400	601
1300	-	-	760
1400	-	-	-
1500	657	388	-

TABLE 4 - 3 Ultrasonic Absorption Measurements (1 to 230 MHz) for Acetone + Water Mixtures

(a) Composition Dependence of the Ultrasonic Absorption

Mole fraction acetone x_2	$10^{17}(\alpha/f^2)$/nepers s^2 cm^{-1} 263 K	273 K	283 K	298 K
0.00	-	55	35	20
0.02	-	55	34	20
0.04	-	53	35	20
0.06	-	57	36	22
0.08	-	61	42	26
0.10	124	77	51	32
0.12	-	91	61	41
0.14	-	104	69	49
0.16	-	119	83	57
0.18	-	131	95	67
0.20	198	144	102	74
0.30	225	179	137	104
0.40	201	179	143	108
0.50	167	145	122	93
0.60	137	99	95	65
0.70	102	64	71	46
0.80	68	47	46	34
0.90	39	46	32	27
1.00	-	44	30	28

TABLE 4 - 3 (b) Ultrasonic Relaxation Data (1 to 230 MHz) for Acetone + Water Mixtures; at 273 K

Frequency MHz	$10^{17}(\alpha/f^2)$/nepers s^2 cm^{-1}			
	0.1 mf.	0.3 mf.	0.4 mf.	0.5 mf.
3	113	212	308	183
5	86	210	282	205
7	82	242	240	205
9	90	238	243	201
11	94	248	210	195
13	93	239	225	192
15	97	234	234	193
17	94	224	225	193
19	94	238	227	182
21	94	219	218	175
23	100	219	224	181
25	94	201	-	-
27	94	-	-	-
29	-	-	-	-
30	85	184	196	170
70	78	170	177	155
110	67	154	152	130
170	64	136	123	107
230	66	118	112	104

TABLE 4 - 3 (c) Ultrasonic Relaxation Data (1 to 230 MHz) for Acetone + Water Mixtures; at 283 K

Frequency MHz	$10^{17}(\alpha/f^2)$/nepers s^2 cm^{-1}		
	0.1 mf.	0.3 mf.	0.4 mf.
3	114	210	257
5	-	-	180
7	54	178	214
9	57	172	198
11	57	172	178
13	59	170	182
15	61	186	170
17	62	193	190
19	63	182	176
21	56	164	167
23	59	165	179
25	66	172	178
27	-	-	-
29	-	-	-
30	50	140	151
70	46	136	141
110	47	117	122
170	46	88	119
230	40	69	80

TABLE 4 - 3 (d) Ultrasonic Absorption Data (1 to 230 MHz) for Acetone + Water Mixtures; at 298 K

Frequency MHz	$10^{17}(\alpha/f^2)$/nepers s^2 cm^{-1}		
	0.1 mf.	0.3 mf.	0.4 mf.
3	30	200	156
5	30	149	150
7	35	130	141
9	42	142	130
11	34	131	140
13	31	130	130
15	31	120	128
17	37	141	133
19	40	130	135
21	38	137	132
23	38	124	136
25	38	-	138
27	-	-	-
29	-	-	-
30	40	112	108
70	35	103	87
110	32	95	85
170	31	78	81
230	30	68	83

TABLE 4 - 3 (e) Measured Corrections for Diffraction Losses at 298 K and 3, 5, 7, 9 MHz

Frequency MHz	$10^{17}(\alpha/f^2)$/nepers s^2 cm^{-1}
3	55 ± 5
5	30 ± 5
7	20 ± 5
9	5 ± 5

TABLE 4 - 4 Measured Ultrasonic Absorption (200 to 1500 kHz) for Acetone + Water Mixtures at 298 K

Frequency kHz	$10^{17}(\alpha/f^2)$/nepers s^2 cm^{-1}			
	0.1 mf.		0.3 mf.	
250	50	20	295	565
300	138	138	219	243
350	34	25	210	175
400	55	52	190	234
450	30	28	162	167
500	58	52	219	204
550	61	63	190	-
600	45	49	161	162
650	54	46	194	-
700	36	40	214	203
750	43	49	151	-
800	52	62	-	221
850	-	59	165	-
900	-	37	255	-
1000	-	13	246	246
1100	-	-	-	-
1200	-	-	259	-
1300	-	67	-	-
1400	-	-	-	-
1500	-	-	174	-

TABLE 4 - 5 Ultrasonic Absorption Data for Acetonylacetone + Water at 70 MHz

Mole fraction acetonylacetone x_2	$10^{17}(\alpha/f^2)$/nepers s^2 cm^{-1}		
	273 K	283 K	298 K
0.00	-	35	21
0.05	84	54	29
0.10	161	101	58
0.15	207	138	86
0.20	213	157	98
0.30	192	147	98
0.40	165	128	79
0.50	129	99	65
0.60	103	87	53
0.70	91	64	46
0.80	78	58	42
0.90	75	53	40
1.00	-	53	-

APPENDIX TO CHAPTER 5

5 - 1 Ultrasonic Relaxational Analysis Program

Summary of Input Data

```
M1          N

1           N

X(1)        D(1)        L(1)        U(1)
 :           :           :           :
X(I)        D(I)        L(I)        U(I)
 :           :           :           :
X(N)        D(N)        L(N)        U(N)

7           1

/title and description of calculation\

M1

NU(1)       US(1)       WT(1)
 :           :           :
NU(M)       US(M)       WT(M)
 :           :           :
NU(M1)      US(M1)      WT(M1)

7   2

N1   N2        N3

7   3

7   4
```

Where the above symbols represent:

M1 = total number of frequencies for which the ultrasonic absorption was measured.

N = total number of relaxation parameters X(I).

X(I) = relaxation parameter I (original graphical estimate). Note that X(1) is equal to B and the order of the subsequent parametersis $A_{(i)}$, $fc_{(i)}$ ---.

D(I) = step length modifier, usually X(I)/5.

L(I) = lower limit of variation permitted for X(I).

U(I) = upper limit of variation permitted for X(I).

NU(M) = Mth measurement frequency at which the ultrasonic absorption US(M) was determined.

WT(M) = a weighting parameter, when WT(M) is set equal to US(M) each data point is given equal weighting in compounding the sum of the squares F.

N1 = output after N1 curve fits.

N2 = output after N2 minhunts.

N3 = total number of iterations required.

The numbers in the above description of the input data are control numbers used to specify the input data format. The output consists of the values of the parameters after each interation together with F, the sum of the squares of the deviations.

The program input data summarised above refers to the program listed on tape entitled ULTRAS which has dynamic arrays defined for the data points and the parameters. The listing which follows has fixed dimension arrays.

The program listing, which follows, was written in ALGOL for an Elliott 4130 computer.

```
 &JOB; CHE  131  DW; ULTRASON 1969;


 &ALGOL;
LIBRARY
ALGOL



 &LIST;


 &TIME;10;;
 RELAXATIONAL ANALYSIS PROGRAM 1969;
 "BEGIN"
 "INTEGER" M1,S,N,M,N1,N2,N3;
 "BEGIN"
 "PRINT" ''L2`DAVID WADDINGTON`,SAMELINE,''S80`1969`,''L2``,
 ''S30`ULTRASONIC RELAXATIONAL ANALYSIS PROGRAM  ONE`,''L2``;
 "END" OF TITLE PRINT STATEMENT;
 "BEGIN"
 "REAL" "ARRAY" X,D,L,U[1:200],Y,US,NU,WT[1:100];
 "INTEGER" "ARRAY" I1[1:2000];
 "INTEGER" IC;
 "INTEGER" "ARRAY" P[1:3];
 "SWITCH"  SS:=L1,L2,L3,L4,L5;

 "PROCEDURE" SET;
 "BEGIN"
 "INTEGER" M;
 IC:=1;
 INSTRING(I1,IC);
 "READ" M1;
 "FOR" M:=1 "STEP" 1 "UNTIL" M1 "DO"
 "BEGIN"
 "READ" NU[M],US[M],WT[M];
 Y[M]:=(US[M]/WT[M]);
 "END";
 "END" OF PROCEDURE SET;

 "PROCEDURE" PREPARE;
 "BEGIN"
 "END" OF PROCEDURE PREPARE;

 "REAL" "PROCEDURE" G(M,X);
 "VALUE" M,X;
 "ARRAY" X;
 "INTEGER" M;
 "BEGIN"
 "INTEGER" K,I,J,V;
 "REAL" DAVE,FUN;
 "REAL" GG;
 DAVE:=0;
```

```
V:= ((N-1) "DIV" 2);
"BEGIN"
"FOR"  I:=1  "STEP"  1  "UNTIL"  V "DO"
"BEGIN"
J:=2*I;
K:=J+1;
FUN:=((NU[M]/X[K])*(NU[M]/X[K]) + 1);
DAVE:=DAVE + (X[J]/FUN);
"END";
"END";
GG:=DAVE + X[1];
G:=(GG/WT[M]);
"END" OF PROCEDURE FUNCTION    ENTER CURVE FIT;

"PROCEDURE" RAPM(N,X,D,L,U,S); "INTEGER" N,S;
"ARRAY" X,D,L,U;
"BEGIN" "SWITCH" SS:=S1,S2,S3,S4,S5,S6,S7,S9;
"INTEGER" I;
"PROCEDURE" PRH; "BEGIN"
"PRINT" ''L4'INPUT DATA'L2''S3'I'S7'XI'S10'DI'S15'LI'S15'UI'L1'';
"END" PRH;
"PROCEDURE" PRD(I); "VALUE" I;  "INTEGER" I;
"BEGIN" "PRINT" DIGITS(3),I,PREFIX('    '),SCALED(4),
X[I],D[I],L[I],U[I];
"END" PRD;
"PROCEDURE" RAS(X,L);  "VALUE" X; "ARRAY" X; "LABEL" L;
"BEGIN" PRH; "FOR" I:=1 "STEP" 1 "UNTIL" N "DO"
"BEGIN" "READ" X[I]; PRD(I) "END";
"PRINT" ''L2'';
"GO TO" L;
"END" RAS;
S9:"READ" I;
"IF" I "LE" 6 "THEN"
"PRINT" ''L10'AW.19.12.1966.CCM PROCEDURE AND CONTROLS';
"GO TO" SS[I];
S1 : "READ" N; PRH; "FOR" I:=1 "STEP" 1 "UNTIL" N "DO"
"BEGIN" "READ" X[I],D[I],L[I],U[I]; PRD(I) "END" I;
"PRINT" ''L2''; "GO TO" S9;
S2: RAS(X,S9);
S3: RAS(D,S9);
S4: RAS(L,S9);
S5: RAS(U,S9);
S6: PRH; "FOR" I:=1 "STEP" 1 "UNTIL" N "DO" "BEGIN" "READ" X[I],D[I];
PRD(I) "END";
"PRINT" ''L2''; "GO TO" S9;
S7: "READ" S;
"END" RAPM;
"PROCEDURE" PRI1(J1,J2,F,K1,K2); "VALUE" J1,J2,F,K1,K2;
"INTEGER" J1,J2,K1,K2; "REAL" F;
"BEGIN" "PRINT" ''L2'IT',SAMELINE, DIGITS(4),(J1+J2),
''L1'',J1,' CUFS ', DIGITS(6), K1, ' FUN EVALS',
''L1'', DIGITS(4), J2, ' MINS ', DIGITS(6), K2,' FUN EVALS',
''L1'', 'F:= ', SCALED(9), F;
"END" PRI1;
"PROCEDURE" PRI2(N,X,D); "VALUE" N,X,D; "INTEGER" N; "ARRAY" X,D;
"BEGIN" "INTEGER" I;
"PRINT" ''L2''S2'I'S10'XI'S11'DI'L1'';
"FOR" I:=1 "STEP" 1 "UNTIL" N "DO"
"BEGIN" "PRINT" DIGITS(3), I, PREFIX('    '), SCALED(9), X[I],
SCALED(4), D[I]; "END";
```

```
"END" PRI2;
"PROCEDURE" RAPS(S,N);  "VALUE" S; "INTEGER" S; "INTEGER" "ARRAY" N;
"BEGIN" "INTEGER" I;
"FOR" I:=1 "STEP" 1 "UNTIL" S "DO" "READ" N[I];
"END" RAPS;
"PROCEDURE" TEST(J1,J2,F,K1,K2,X,D,L); "VALUE" J1,J2,F,K1,K2,X,D;
"INTEGER" J1,J2,K1,K2; "REAL" F; "ARRAY" X,D; "LABEL" L;
"BEGIN"
"INTEGER" I,Q; "SWITCH" S:=S1,S2,S3,S4; "OWN" "INTEGER" M1,M2;
I:=J1+J2; "IF" I=0 "THEN" "BEGIN" M1:=M2:=0; "GO TO" S1 "END";
"IF" I "GE" N3 "THEN" "BEGIN" I:=1; "GO TO" S1 "END";
I:=3;
"IF" J1 "LE" M1 "THEN" "GO TO" S2;
M1:=J1; Q:=J1-N1*(J1"DIV"N1);
"IF" Q=0 "THEN" I:=2;
S2: "IF" J2 "LE" M2 "THEN" "GO TO" S4;M2:= J2; Q:=J2-N2*(J2"DIV"N2);
"IF" Q=0 "THEN" I:=2;
S4: "IF" I=3 "THEN" "GO TO" S3;
S1: PRI1(J1,J2,F,K1,K2);
"IF" I=0 "THEN" "GO TO" S3; PRI2(N,X,D);
"IF" I=1 "THEN" "GO TO" L;
S3:
"END" OF TEST;
"PROCEDURE" CCM(M1,Y,X,D,L,U,N);  "VALUE" M1,Y,X,D,L,U,N;
"ARRAY" Y,X,D,L,U;   "INTEGER" M1,N;
"BEGIN"
"REAL" F,F1;  "INTEGER" I,J1,J2,K1,K2,V1; "ARRAY" X1[1:N];
"SWITCH" SS:=S1,S2,S3,S4,S5,S6;
"REAL" "PROCEDURE" FUN(X); "VALUE" X; "ARRAY" X;
"BEGIN"
"INTEGER" M; "REAL" A,Z;
Z:=0;
"FOR" M:=1 "STEP" 1 "UNTIL" M1 "DO"
"BEGIN" A:=Y[M]-G(M,X);  Z:=Z+A*A;
"END";
FUN:=Z;
K2:=K2+1;
"END" FUN;
"PROCEDURE" LIM(X);  "ARRAY" X;
"BEGIN"
"REAL" Z,Y; "INTEGER" I; "SWITCH" S:=L1,L2;
"FOR" I:=1 "STEP" 1 "UNTIL" N "DO"
"BEGIN" Z:=L[I]; Y:=X[I]; "IF" Y>Z "THEN" "GO TO" L1;
X[I]:=Z; "GO TO" L2;
L1: Z:=U[I]; X[I]:= "IF" Y<Z "THEN" Y "ELSE" Z;
L2: "END";
"END" OF LIM;
"PROCEDURE" MINHUNT(Y,X,D,L,U,N); "VALUE" L,U,N;
"REAL" Y; "ARRAY" X,D,L,U;  "INTEGER" N;
"BEGIN"
"REAL" "ARRAY" P,Q,R,W[1:N]; "REAL" A,B,C,Z;
"INTEGER" I; "SWITCH" S:=L1,L2,L3,L4,L5,L6;
"REAL" "PROCEDURE" LIMITS(P); "VALUE" P; "REAL" P;
"BEGIN" "REAL" Z; "SWITCH" S:=L1,L2;
Z:=L[I]; "IF" P > Z "THEN" "GO TO" L1;
LIMITS:=Z; "GO TO" L2;
L1: Z:=U[I]; LIMITS:= "IF" P < Z "THEN" P "ELSE" Z;
L2: "END" OF LIMITS;
"PROCEDURE" SUB(A,B,M); "VALUE" M; "ARRAY" A,B; "INTEGER" M;
"BEGIN" "FOR" I:=1 "STEP" 1 "UNTIL" N "DO"
```

```
"BEGIN" "REAL" T; "SWITCH" S:=L1,L2,L3,L4,L5;
"GO TO" S[M];
L1: A[I]:=B[I];  "GO TO" L5;
L2: T:=B[I]+W[I]; "GO TO" L4;
L3: T:=B[I]+C*W[I];
L4: A[I]:=LIMITS(T);
L5: "END";
"END" OF SUB;
Z:=Y; SUB(P,X,1); SUB(W,D,1);
"FOR" I:=1 "STEP" 1 "UNTIL" N "DO"
"BEGIN" "REAL" A,B,C;  "SWITCH" S:=L1,L2,L3;
B:=P[I]; C:=W[I]; P[I]:=LIMITS(B+C);
A:=FUN(P);
"IF" A<Z "THEN" "GO TO" L1;
P[I]:=LIMITS(B-C); A:=FUN(P);
"IF" A<Z "THEN" "GO TO" L2;
P[I]:=B; W[I]:=0.5*C; "GO TO" L3;
L2: W[I]:=-C;
L1: Z:=A;
L3: "END" I;
SUB(Q,P,2);
A:=FUN(Q); "IF" A "GE" Z "THEN" "GO TO" L1;
SUB(R,Q,2);
B:=FUN(R); C:=B-2*A+Z;
"IF" C "LE" 0 "THEN" "GO TO" L2;
C:=(Z-B)/(2*C);
SUB(P,Q,3);
Z:=FUN(P);
"IF" Z "GE" A "THEN" "GO TO" L2;
"IF" Z "GE" B "THEN" "GO TO" L2;
"GO TO" L1;
L2: "IF" B<A "THEN" "GO TO" L3;
SUB(P,Q,1);
Z:=A; "GO TO" L1;
L3: C:=2; SUB(Q,R,1);
L4: SUB(P,R,3);
Z:=FUN(P); "IF" Z "GE" B "THEN" "GO TO" L5;
B:=Z; SUB(Q,P,1); C:=2*C; "GO TO" L4;
L5: SUB(X,Q,1); Y:=B; "GO TO" L6;
L1: SUB(X,P,1); Y:=Z;
L6: SUB(D,W,1);
"END" OF MINHUNT;
"PROCEDURE" CUF(Y,X1,D,N,M1,E,S); "VALUE" Y,D,E,N,M1;
"ARRAY" Y,X1,D; "INTEGER" N,M1; "LABEL" S; "REAL" E;
"BEGIN"
"REAL" "ARRAY" F,X[1:N], Z[1:(N*N+N)];
"INTEGER" I,J,K,L,M,I1,I2,I3; "REAL" T,A,W;
"FOR" I:=1 "STEP" 1 "UNTIL" N "DO" X[I]:=X1[I]; K:=N*N+N;
"FOR" I:=1 "STEP" 1 "UNTIL" K "DO" Z[I]:=0;
"FOR" M:=1 "STEP" 1 "UNTIL" M1 "DO"
"BEGIN" A:=G(M,X); T:=Y[M]-A;
"FOR" I:=1 "STEP" 1 "UNTIL" N "DO"
"BEGIN" W:=X[I]; X[I]:=W+D[I];
F[I]:=G(M,X)-A; X[I]:=W "END" I;
"FOR" I:=1 "STEP" 1 "UNTIL" N "DO"
"BEGIN" A:=F[I]; W:=T*A; Z[I]:=Z[I]+W;
K:=N*I;
"FOR" J:=I "STEP" 1 "UNTIL" N "DO"
"BEGIN" L:=K+J; Z[L]:=Z[L]+A*F[J];
"END" J;
```

```
"END" I;
"END" M;
"FOR" I:=1 "STEP" 1 "UNTIL" N"DO"
"BEGIN" K:=N*I;
"FOR" J:=I "STEP" 1 "UNTIL" N"DO"
"BEGIN" L:=N*J; Z[L+I]:=Z[K+J];
"END" J;
"END" I;.
I2:=N-1;
"FOR" K:=1 "STEP" 1 "UNTIL" I2 "DO"
"BEGIN" I:=K*N; I1:=K+1; W:=Z[I+K];
"IF" ABS(W) < E "THEN" "GO TO" S;
W:=1/W;
"FOR" J:=I1 "STEP" 1 "UNTIL" N "DO"
"BEGIN" L:=I+J; Z[L]:=W*Z[L]; "END" J;
Z[K]:=W*Z[K]; Z[I+K]:=1;
"FOR" L:=I1 "STEP" 1 "UNTIL" N "DO"
"BEGIN" M:=L*N; W:=Z[M+K];
"FOR" J:=K "STEP" 1 "UNTIL" N "DO"
"BEGIN" I3:=M+J; Z[I3]:=Z[I3]-Z[I+J]*W;
"END" J;
Z[L]:=Z[L]-Z[K]*W;
"END" L;
"END" K;
I:=N*N;
W:=Z[I+N]; "IF" ABS(W) < E "THEN" "GO TO" S;
Z[N]:=Z[N]/W;
Z[I+N]:=1;
"FOR" K:=I2 "STEP" -1 "UNTIL" 1 "DO"
"BEGIN" I:=K*N; I1:=K+1; W:=0;
"FOR" J:=I1 "STEP" 1 "UNTIL" N "DO" W:=W+Z[I+J]*Z[J];
Z[K]:=Z[K]-W;
"END" K;
"FOR" I:=1 "STEP" 1 "UNTIL" N "DO" X1[I]:=X[I]+D[I]*Z[I];
"END" CUF;
J1:=J2:=K1:=K2:=V1:=0;
F:=FUN(X);
S5: TEST(J1,J2,F,K1,K2,X,D,S6);
S1: K1:=K1+N+1;  J1:=J1+1;
"FOR" I:=1 "STEP" 1 "UNTIL" N "DO" X1[I]:=X[I];
CUF(Y,X1,D,N,M1,10₁₀-76,S2);
LIM(X1); F1:=FUN(X1);
"IF" F1 "GE" F "THEN" "GO TO" S3;
"IF" F1 < 0.5*F "THEN" "GO TO" S4;
"FOR" I:=1 "STEP" 1 "UNTIL" N "DO" D[I]:=0.125*D[I];
S4:F:=F1; "FOR" I:=1 "STEP" 1 "UNTIL" N "DO" X[I]:=X1[I];
"GO TO" S5;
S2: V1:=1;
S3: MINHUNT(F,X,D,L,U,N); J2:=J2+1;
TEST(J1,J2,F,K1,K2,X,D,S6);
"IF" V1=1 "THEN" "GO TO" S3;
"GO TO" S1;
S6:;



"BEGIN"
"INTEGER" M;
"REAL" CFUNC;
"BEGIN"
```

```
  "PRINT" ''F'',
  'DAVID WADDINGTON',SAMELINE,''S68'ULTRASONIC RELAXATIONAL ANALYSIS',
  ''L2'';
  IC:=1;
  OUTSTRING(I1,IC);
  "PRINT" ''L5'THE RELAXATION PARAMETERS',''L2'',
  ''S8'XI',SAMELINE,''S10'RELAXATION PARAMETERS',''L'';
  "END";
  "BEGIN"
  "FOR" M:=1 "STEP" 1 "UNTIL" N "DO"
  "PRINT" ''L'',''S11'',M,SAMELINE,SCALED(9),''S12'',X[M];
  "END";
  "BEGIN"
  "REAL" RMS,SDEV;
  RMS:=SQRT(F/M1);
  SDEV:=SQRT(F/(M1 - 1));
  "PRINT" ''L2'',
  'R.M.S.  DEVIATION = ',SAMELINE,FREEPOINT(9),RMS,''L2'',
  'STANDARD DEVIATION  =',SAMELINE,FREEPOINT(9),SDEV,''L2'',
  'SUM OF SQUARES OF DEVIATIONS  = ',SAMELINE,FREEPOINT(9),F;
  "END";
  "BEGIN"
  "PRINT" ''L5'THE COMPUTED VALUES OF THE FUNCTION',''L2'',SAMELINE,
  ''S8'M',''S12'FREQUENCY MHZ',''S10'ABSORPTION CALCD ',
  ''S10'ABSORPTION EXPTL',''L'';
  "END";
  "BEGIN"
  "FOR" M:=1 "STEP" 1 "UNTIL" M1 "DO"
  "BEGIN"
  CFUNC:=US[M]*G(M,X);
  "PRINT" SAMELINE,M,FREEPOINT(9),''S12'',NU[M],
  ''S14'',CFUNC,''S16'',US[M],''L'';
  "END";
  "END";
  "END" OF COMPUTED VALUES OF THE FUNCTION;
  "END" OF CCM;
  L5: RAPM(N,X,D,L,U,S);
  "GO TO" SS[S];
  L1: SET; "GO TO" L5;
  L2: RAPS(3,P);
  N1:=P[1];N2:=P[2];N3:=P[3];"GO TO" L5;
  L3: PREPARE;
  CCM(M1,Y,X,D,L,U,N);
  "GO TO" L5;
  L4:
  "END";
  "END" OF PROGRAM;
    1060     MC
    2810   CODE
    3870  TOTAL


 &RUN;
RELAXA
DR0


 DAVID WADDINGTON
```

5 - 2 Summary of Input Data to Program for evaluation of the parameter Q.

Summary of Input Data

/title of calculation, name of system to be studied \

M1 = total number of compositions at which Q is to be evaluated.

N = number of parameters used in fitting excess functions.

TEMP = temperature in kelvin.

PHI = estimated coefficient of volume expansion.

V1 = molar volume of pure component 1 (usually water).

V2 = molar volume of pure component 2 (usually organic).

K = Boltzman constant.

R = Gas constant.

MA = molecular weight of component 1.

MB = molecular weight of component 2.

GG(O)	HH(O)	VV(O)
GG(I)	HH(I)	VV(I)
GG(N-1)	HH(N-1)	VV(N-1)

X2(1)	C(1)	RHO(1)	CP(1)
X2(M1)	C(M1)	RHO(M1)	CP(M1)

GG, HH and VV are the parameters in the equation (see section 5-53) used for fitting the excess functions of mixing. X2, C, RHO and CP are the mole fraction, sound velocity, density and molar heat capacity of the solution of composition X2 for which the parameter Q is to be computed.

The program which follows then outputs the values of Q, along with other parameters such as g",h",v" used in the foregoing discussions. The program was written in ALGOL for an Elliott 4130 computer.

```
? JOB;CHF 196 DW; QCALC;


 & ALGOL;
LIBRARY
ALGOL



 & LIST;



 & TIME;2;2;

 QCALC  REVISED VERSION;
 "BEGIN"
 "INTEGER" "ARRAY" II[1:2000];
 "INTEGER" IC;
 "INTEGER" M,M1,N,I;
 "REAL" TEMP,PHI,V1,V2,K,R,MA,MB;
 "COMMENT" INSERT PROCEDURES AFTER THIS CARD;

 "REAL" "PROCEDURE" SUM(A,K,N);
 "INTEGER" N,K;
 "REAL" "ARRAY" A;
 "BEGIN" "INTEGER" I;
 "REAL" S;    S:=0;
 "FOR" I:=1 "STEP" 1 "UNTIL" N "DO"
 S:=S+A[I-K];
 SUM:=S;
 "END" REAL PROCEDURE SUM;

 "REAL" "PROCEDURE" D1XE(A,N,X1);
 "INTEGER"     N;
 "REAL" X1;
 "REAL" "ARRAY" A;
 "BEGIN"    "INTEGER" I;
 "REAL" X2,Z;
 "REAL" "ARRAY" V1,V2[0:N-1];
 X2:=1-X1;
 Z:=X1-X2;
 "FOR" I:=0 "STEP" 1 "UNTIL" N-1 "DO"
 "BEGIN"
 V1[I]:=A[I]*Z↑I;
 V2[I]:=I*A[I]*Z↑(I-1);
 "END";
 D1XE:=Z*SUM(V1,1,N) - 2*X1*X2*SUM(V2,1,N);
 "END" OF REAL PROCEDURE D1XE;

 "REAL" "PROCEDURE" D2XE(A,N,X1);
 "INTEGER" N;
 "REAL" X1;
 "REAL" "ARRAY" A;
```

```
"BEGIN"
"INTEGER" I;
"REAL" X2,Z;
"REAL" "ARRAY" P,P1,P2[0:N-1];
"FOR" I:=0 "STEP" 1 "UNTIL" N-1 "DO"
"BEGIN"
X2:=1-X1;          Z:=X1-X2;
P[I]:=(I+1)*A[I]*Z↑I;
P1[I]:=I*A[I]*Z↑I;
P2[I]:=I*(I-1)*A[I]*Z↑(I-2);
"END" I;
D2XE:=4*X1*X2*SUM(P2,1,N) - 2*(SUM(P,1,N)+SUM(P1,1,N));
"END" OF REAL PROCEDURE D2XE;

"REAL" "PROCEDURE" VEC(A,N,X1);
"INTEGER" N;
"REAL" X1;
"REAL" "ARRAY" A;
"BEGIN" "INTEGER" I;
"REAL" X2,Z;
"REAL" "ARRAY" D[0:N-1];
X2:=1-X1;      Z:=X1-X2;
"FOR" I:=0 "STEP" 1 "UNTIL" N-1 "DO"
D[I]:=A[I]*Z↑I;

VEC:=X1*X2*SUM(D,1,N);
"END" OF REAL PROCEDURE VEC;

IC:=1; INSTRING(II,IC);
"READ" M1,N,TEMP,PHI,V1,V2,K,R,MA,MB;
"BEGIN"
"REAL" "ARRAY"  GG,HH,VV[0:N-1],G1,G,H,V,VM,VE,X1,X2,GF,HF,VF,
RHO,C,CP,P,T,W,Q[1:M1];
"PRINT" ''F'DAVID  WADDINGTON',SAMELINE,
''S70'CALCULATION OF Q VALUES';
"PRINT" ''L6'',''S2'';
IC:=1; OUTSTRING(II,IC);
"FOR" I:=0 "STEP" 1 "UNTIL" N-1 "DO"
"READ"  GG[I],HH[I],VV[I];
"FOR" M:=1 "STEP" 1 "UNTIL" M1 "DO"
"READ" X2[M],C[M],RHO[M],CP[M];

"BEGIN"
"FOR" M:=1 "STEP" 1 "UNTIL" M1 "DO" "BEGIN"
GF[M]:=D1XE(GG,N,X2[M]);
HF[M]:=D1XE(HH,N,X2[M]);
VF[M]:=D1XE(VV,N,X2[M]);
G[M]:=D2XE(GG,N,X2[M]);
H[M]:=D2XE(HH,N,X2[M]);
V[M]:=D2XE(VV,N,X2[M]);

VE[M]:=VEC(VV,N,X2[M]);
VM[M]:=(VE[M] + ((1-X2[M])*V1)+(X2[M]*V2));
P[M]:=(1.00₁₀+07/(RHO[M]*C[M]*C[M]));
"END";     "END";
"BEGIN"
"FOR" M:=2 "STEP" 1 "UNTIL" M1-1 "DO"
"BEGIN"
G1[M]:=G[M] + ((R*TEMP)/(X2[M]*(1-X2[M])));
CP[M]:=CP[M]*4.1840;
```

```
T[M]:=((V[M]/VM[M]) -((PHI*H[M])/CP[M]));
W[M]:=(T[M]↑2);
Q[M]:=((8*(3.1416↑5)*(VM[M]↑2)*K*TEMP*W[M])/
(C[M]*P[M]*C1[M]*C1[M]));
"END";      "END";
"BEGIN"
"PRINT"
''L6'TEMPERATURE = ',SAMELINE,FREEPOINT(6),TEMP,'DEG. C.';
"PRINT"
''L4'COEFFICIENT OF VOLUME EXPANSION = ',SAMELINE,
SCALED(4),PHI;
"PRINT"
''L6'MOLAR VOLUME OF ONE = ',SAMELINE,FREEPOINT(4),V1,
''S20'MOLAR VOLUME OF TWO = ',V2;
"PRINT" ''L6'',SAMELINE,FREEPOINT(4),
'MOLECULAR WEIGHT OF ONE = ',MA,
''S20'MOLECULAR WEIGHT OF TWO = ',MB;
"PRINT" ''F'';
"PRINT" ''L5'MOLE FRACTION',SAMELINE,''S10'EXCESS VOLUME';
"FOR" M:=1 "STEP" 1 "UNTIL" M1 "DO"
"PRINT" ''L'',FREEPOINT(9),X2[M],SAMELINE,SCALED(9),''S10'',VE[M];
"PRINT" ''F'MOLE FRACTION',SAMELINE,''S14'D1GE',''S21'D1HE',''S21'D1VE';
"FOR" M:=1 "STEP" 1 "UNTIL" M1 "DO"
"PRINT" ''L'',FREEPOINT(9),X2[M],SAMELINE,SCALED(9),PREFIX(''S10''),
GF[M],HF[M],VF[M];
"PRINT" ''F'MOLE FRACTION',SAMELINE,''S14'D2GE',''S21'D2HE',''S21'D2VE';
"FOR" M:=1 "STEP" 1 "UNTIL" M1 "DO"
"PRINT" ''L'',FREEPOINT(9),X2[M],SAMELINE,SCALED(9),PREFIX(''S10''),
G[M],H[M],V[M];
"PRINT" ''F'MOLE FRACTION',SAMELINE,''S15'VOLUME (MOLAR).',
''S9'COMPRESSIBILITY   BETA - 0';
"FOR" M:=2 "STEP" 1 "UNTIL" M1-1 "DO"
"PRINT" ''L'',FREEPOINT(9),X2[M],SAMELINE,''S15'',VM[M],SCALED(9),
''S15'',P[M];
"PRINT" ''F'MOLE FRACTION',SAMELINE,
''S12'VALUE OF Q - FACTOR          CMS↑2.SEC.';
"FOR" M:=2 "STEP" 1 "UNTIL" M1-1 "DO"
"PRINT" ''L'',''S20'',FREEPOINT(9),X2[M],SAMELINE,''S20'',
SCALED(9),Q[M];
"END";
"END";
"END" OF Q CALCULATION;
   530   MC
  1476  CODE
  2006 TOTAL


 &RUN;
QCALCR
DR0
```

5 - 3 Summary of Input Data to Romanov-Solovyev Curve Fitting Program RSCF.

Summary of Input Data

This program employs the same basic minimisation procedure as ULTRAS, details of which were given in 5-1.

```
1          N          (N.B. in this case N = 4)

X(1)       D(1)       L(1)       U(1)
 :          :          :          :
X(I)       D(I)       L(I)       U(I)
 :          :          :          :
X(N)       D(N)       L(N)       U(N)

7          1          M1

NU(1)      US(1)      Y(1)
 :          :          :
NU(M1)     US(M1)     Y(M1)

7          2
N1         N2   N3
7          3
7          4
```

The symbols have similar significance to those used in 5-1. N=4 since there are only four parameters:

X(1) = B

X(2) = Q

X(3) = DC

X(4) = LM

where B is the high frequency residual absorption, Q is the constant defined in chapter 5, DC is the diffusion coefficient and LM is the interaction length.
M1 is again the total number of observations of the ultrasonic absorption.
Y is a weighting parameter and in all cases was set equal to US so that each data point was given equal weighting in the evaluation of the sum of the squares.

The output lists the parameters evaluated together with a table of the computed and experimental ultrasonic absorption at each measurement frequency.

The program listing is not included since it is essentially identical to ULTRAS. The PROCEDURE G(M,X) calculated values of α/f^2 using the equation of Romanov and Solovyev (Chapter 5).

APPENDIX TO CHAPTER 6

6 - 1 Input data to QCALC program for the system t butyl alcohol + water at 298 K.

Input:

/t butyl alcohol + water at 298 K\

16
6
273.16 (T)
$1.00_{10}-3$ (α_e)
18.016 (V1)
95.020 (V2)
$1.38_{10}-23$ (k)
8.3144 (R)
18.016 (MA)
74.120 (MB)

G^E parameters	H^E parameters	V^E parameters
4078.91	92.83740	-3.0385908
1236.83	-3466.0859	-13.857002
1090.14	2433.2887	28.562546
416.26	1104.4473	66.210554
-311.17	-9608.1430	-223.13861
-122.70	-9289.8323	137.77913

Mole fraction t BuOH	Sound Velocity/cm s^{-1}	Density/ grm cm^{-3}	Heat Capacity $J\ mol^{-1}\ K^{-1}$
0.0000	$1500 \times 10^{+5}$	0.99707	160
0.0035	$1505 \times 10^{+5}$	0.99466	160
0.0103	$1555 \times 10^{+5}$	0.98936	160
0.0179	$1575 \times 10^{+5}$	0.98609	160
0.0265	$1590 \times 10^{+5}$	0.98190	160
0.0394	$1595 \times 10^{+5}$	0.97592	160
0.0572	$1585 \times 10^{+5}$	0.96669	160
0.0749	$1545 \times 10^{+5}$	0.95608	160
0.0951	$1500 \times 10^{+5}$	0.94482	160
0.1384	$1435 \times 10^{+5}$	0.92264	160
0.1979	$1385 \times 10^{+5}$	0.89739	160
0.2746	$1335 \times 10^{+5}$	0.87341	160
0.3653	$1280 \times 10^{+5}$	0.85103	160
0.4955	$1230 \times 10^{+5}$	0.82775	160
0.6850	$1175 \times 10^{+5}$	0.80419	160
1.0000	$1100 \times 10^{+5}$	0.78052	160

Output Data from Q-CALC Program: t-butyl alcohol + water

Mole fraction t BuOH	Q-FACTOR $cm^2 s$
0.0035	$4.248_{10}-28$
0.0103	$3.304_{10}-27$
0.0179	$8.859_{10}-27$
0.0265	$1.698_{10}-26$
0.0394	$2.776_{10}-26$
0.0572	$4.553_{10}-26$
0.0749	$5.898_{10}-26$
0.0951	$7.070_{10}-26$
0.1384	$8.673_{10}-26$
0.1979	$9.008_{10}-26$
0.2746	$5.887_{10}-26$
0.3653	$2.394_{10}-27$
0.4955	$3.987_{10}-26$
0.6860	$1.849_{10}-23$

Output from Q-Calc. Program t-butyl alcohol + water

Mole fraction t BuOH	$\left(\frac{v''}{V}\right)$	$\left(\frac{\alpha_p h''}{Cp}\right)$	$10^{-4} \times g''$ /J mol^{-1}
0.0000	-	-	-
0.0035	+ 1.300	- 0.77	-
0.0103	+ 1.200	- 0.70	24.00
0.0179	+ 1.090	- 0.60	14.00
0.0265	+ 1.030	- 0.53	9.25
0.0394	+ 0.910	- 0.34	6.10
0.0572	+ 0.775	- 0.26	4.10
0.0749	+ 0.640	- 0.18	3.15
0.0951	+ 0.520	- 0.13	2.45
0.1384	+ 0.320	- 0.10	1.50
0.1979	+ 0.140	- 0.10	1.00
0.2746	+ 0.100	- 0.10	0.65
0.3653	- 0.04	- 0.06	0.50
0.4955	- 0.015	+ 0.035	0.45
0.6860	+ 0.16	- 0.04	0.10
1.0000	-	-	-

6 - 2 Input Data to QCALC program for the system Acetone + Water at 293.15 K

Input:

/ACETONE + WATER - 293.15 K \

21	7
293.15	(T)
$1.0_{10}-3$	(α_2')
18.016	(V1)
73.462	(V2)
$1.38_{10}-23$	(k)
8.31	(R)
18.016	(MA)
58.08	(MB)

G^E parameters	H^E parameters	V^E parameters
3570.1725	-987.602866	-5.7184746
-8.6821132	4756.250282	2.0099595
-174.56722	-3865.215433	-0.70794019
-48.351698	2196.551507	1.2511168
0.19959572	9936.261942	-0.63571719
-0.26878290	1665.571572	-1.2503269
-0.25256430	-13732.466647	1.5025413

Mole fraction acetone x_2	Sound Velocity /cm s^{-1}	Density /gcm^{-3}	Heat Capacity / J mol^{-1} K^{-1}
0.000	1.4857_{10}+05	0.99826	100
0.0078	1.500_{10}+05	.99532	100
0.0151	1.520_{10}+05	.99180	100
0.024	1.540_{10}+05	.98858	100
0.034	1.550_{10}+05	.98469	100
0.040	1.560_{10}+05	.98241	100
0.070	1.580_{10}+05	.97262	100
0.083	1.590_{10}+05	.96837	100
0.119	1.585_{10}+05	.95667	100
0.179	1.550_{10}+05	.93716	100
0.236	1.510_{10}+05	.92056	100
0.313	1.450_{10}+05	.89969	100
0.411	1.390_{10}+05	.87647	100
0.527	1.335_{10}+05	.85332	100
0.739	1.260_{10}+05	.82015	100
0.857	1.220_{10}+05	.80544	100
0.881	1.215_{10}+05	.80259	100
0.907	1.210_{10}+05	.79974	100
0.941	1.200_{10}+05	.79631	100
0.969	1.195_{10}+05	.79349	100
1.000	1.1898_{10}+05	.79061	100

Output:

Mole fraction x_2	$\left[\frac{v''}{V}\right]$	$\left[\frac{\alpha_e h''}{Cp}\right]$	10^{-4} g'' J mol^{-1}	10^{25} Q (calcd,thermo) cm^{2}s
0.0078	-0.098	0.663	30.86	0.003
0.0151	0.137	0.588	15.76	0.004
0.0240	0.380	0.507	9.78	0.0001
0.0340	0.603	0.426	6.79	0.004
0.0400	0.714	0.384	5.72	0.020
0.0700	1.063	0.221	3.11	0.512
0.0830	1.134	0.172	2.56	1.044
0.1190	1.168	0.086	1.67	3.546
0.1790	0.962	0.038	0.98	9.117
0.2360	0.705	0.034	0.66	12.696
0.3130	0.445	0.030	0.42	14.751
0.4110	0.285	0.004	0.27	20.528
0.5270	0.213	-0.015	0.23	23.722
0.7390	0.107	-0.014	0.56	1.627
0.8570	0.065	-0.076	1.36	0.443
0.8810	0.053	-0.078	1.72	0.251
0.9070	0.035	-0.065	2.31	0.083
0.9410	-0.006	-0.006	3.85	v.small
0.9690	-0.060	0.096	7.60	v.small

Estimated value of $\alpha_e = 1.0 \times 10^{-3}$ K^{-1}

Estimated heat capacity Cp = 100 J/mol/K.

6 - 3 Input and Output data for QCALC program for the system methyl cyanide + water at 298 K

Input:

/Methyl cyanide + water at 298.16 K\

21

5

298.16 (T)

$1.0_{10}-3$ (α_e)

18.016 (V1)

52.495 (V2)

$1.38_{10}-23$ (k)

8.31 (R)

18.016 (MA)

41.05 (MB)

$G^E(I)$	$H^E(I)$	$V^E(I)$
5490.985	3740.5812	-1.9819
-705.2755	-1536.9844	-1.1816
375.5685	4853.3435	-1.0231
-393.1694	-2467.2992	-1.3744
710.9772	-6160.6210	-0.006529

Mole fraction acetone x_2	Sound Velocity /cm s^{-1}	Density /g cm^{-3}	Heat Capacity / J mol^{-1} K^{-1}
0.00	1.490_{10}+05	0.9982	100
0.01	1.500_{10}+05	0.9930	100
0.02	1.508_{10}+05	0.9898	100
0.03	1.513_{10}+05	0.9888	100
0.04	1.517_{10}+05	0.9858	100
0.05	1.520_{10}+05	0.9799	100
0.06	1.5222_{10}+05	0.9769	100
0.07	1.524_{10}+05	0.9748	100
0.08	1.524_{10}+05	0.9733	100
0.09	1.524_{10}+05	0.9669	100
0.10	1.522_{10}+05	0.9567	100
0.15	1.505_{10}+05	0.9402	100
0.20	1.481_{10}+05	0.9240	100
0.30	1.425_{10}+05	0.8956	100
0.40	1.385_{10}+05	0.8641	100
0.50	1.365_{10}+05	0.8406	100
0.60	1.338_{10}+05	0.8175	100
0.70	1.320_{10}+05	0.8170	100
0.80	1.308_{10}+05	0.8055	100
0.90	1.304_{10}+05	0.7943	100
1.00	1.300_{10}+05	0.7829	100

Output:

Mole fraction MeCN	Q-factor /$cm^2 s$	$10^{25}Q$ /$cm^2 s$
0.01	$4.02377612_{10}-28$	0.1
0.02	$1.683121_{10}-27$	0.1
0.03	$3.90969997_{10}-27$	0.1
0.04	$7.03226853_{10}-27$	0.1
0.05	$1.08225296_{10}-26$	0.11
0.06	$1.49129887_{10}-26$	0.15
0.07	$1.86206329_{10}-26$	0.19
0.08	$2.09921347_{10}-26$	0.21
0.09	$2.08804368_{10}-26$	0.21
0.10	$1.75208951_{10}-26$	0.18
0.15	$3.68686859_{10}-26$	0.37
0.20	$8.56829031_{10}-25$	8.57
0.30	$9.69609869_{10}-24$	97.00
0.40	$1.68233367_{10}-23$	168.23
0.50	$3.38890833_{10}-24$	33.89
0.60	$1.87655279_{10}-24$	18.76
0.70	$5.37244804_{10}-25$	5.37
0.80	$3.98109928_{10}-25$	3.98
0.90	$1.70632532_{10}-25$	1.71

Mole fraction x_2	$\left[\frac{v''}{V}\right]$	$\left[\frac{\alpha_e h''}{Cp}\right]$	$10^{-4} g''$ /J mol^{-1}
0.01	-0.595118051	0.0114455351	21.4998
0.02	-0.528648751	-0.000216204	9.3021
0.03	-0.467337735	-0.0143398	5.3526
0.04	-0.410837526	-0.0251628	3.4573
0.05	-0.358826975	-0.03470418	2.3779
0.06	-0.311008617	-0.04303541	1.7019
0.07	-0.267106354	-0.05022634	1.2527
0.08	-0.226863415	-0.0563451	0.9421
0.09	-0.190040555	-0.061458116	0.7214
0.10	-0.156414460	-0.06563012	0.5614
0.15	-0.0293688318	-0.07452195	0.2045
0.20	+0.0441860463	-0.06862310	0.1117
0.30	+0.0919804299	-0.0361265	0.0413
0.40	+0.0770302684	-0.00488494	-0.0217
0.50	+0.0551668188	+0.00531913	-0.0320
0.60	+0.0627489930	-0.00833432	0.0657
0.70	+0.124352431	-0.03170302	0.2918
0.80	0.256932105	-0.0336824	0.6761
0.90	0.47700926	+0.0337945	1.6663

6 - 4 Results of Application of RSCF program to ultrasonic relaxation data for the system Methyl Cyanide + Water at 273 K.

Mole fraction Methyl Cyanide x_2		$10^{17}B$ /nepers s^2cm^{-1}	$10^{25}Q$ /cm^2s	10^5D	ℓ_m/nm	R.M.S. deviation
0.1		89.993	0.099	5.187	2.095	<0.1
0.2		66.146	1.068	4.480	3.221	<0.1
0.3		131.627	11.663	3.351	6.053	<0.1
0.4		138.254	14.828	2.744	6.007	<0.1
0.5	*	104.716	16.108	5.705	6.172	0.1
0.6	*	83.379	14.729	7.709	7.542	0.1
0.7		58.418	2.392	9.928	5.789	<0.1

* These results were not well fitted by the Romanov-Solovyev equation, and in all cases this seemed to be connected with the large absorption at 1.5 MHz.

6 - 5 Reanalysis of Relaxation Data for Methyl Cyanide + Water Mixtures at 273 K.

2 Relaxations; using weighted version of program, (cf results using unweighted version in reference 148)

Composition	$10^{17}A_1$	$10^{-6}fc_1$	$10^{17}A_2$	$fc_2 \times 10^{-6}$
0.1	90.19	5.88	75.36	145.42
0.2	882.55	1.53	449.66	60
0.3	4966.18	4.99	713.54	54.13
0.4	13863.2	3.11	957.22	50
0.5	5628.2	3.46	880.17	51.16
0.6	1441.6	6.08	823.8	33.60
0.7	269.52	2.82	229.68	49.80

Calculated values of the maximum absorption per wavelength .

Composition x_2	$10^6 \mu_{1_{max}}$	$10^6 \mu_{2_{max}}$
0.1	0.4	8.3
0.2	1.0	20.2
0.3	18.1	28.25
0.4	31.0	34.4
0.5	14.0	32.1
0.6	6.2	19.6
0.7	0.5	8.0
0.8	-	-
0.9	-	-

x_2	$10'' A_1fc_1$	$10''A_2fc_2$
0.1	530.3	10960
0.2	1350	26980
0.3	24780	38620
0.4	43110	47860
0.5	19470	45030
0.6	8765	27680
0.7	760	11440

6 - 6 Application of the Romanov-Solovyev treatment to electrolyte solutions, tetraethylammonium bromide and tetra-n-butylammonium bromide.

The modified program used in this analysis is not included, it being essentially similar to that in Appendix 5-2. A program was written to fit the excess function data to equation 6-30. This program has not been included but is a substantially modified version of a curve analysis routine described by Armitage et al. (see reference 182).

(a) tetra-n-butylammonium bromide:

Input data:

22	(number of data points)
7	(number of parameters)
298.15	(temperature /K)
18.016	(molecular weight of solvent)
322.0	(molecular weight of solute)
303.0	(molar volume of solute)

Salt Molality m_2	Sound Velocity 10^{-5}C/cm s^{-1}	Density /g cm^{-3}	Volume Expansion coeffts/K $\underline{\alpha_e}$	Heat Capacity $J\ mol^{-1}\ K^{-1}$ $\underline{C_p}$
0.1	1.500	0.99925	0.012	90
0.2	1.500	1.0015	0.012	90
0.3	1.503	1.0037	0.012	90
0.4	1.507	1.0060	0.012	90
0.5	1.509	1.0082	0.012	90
0.6	1.511	1.0103	0.012	90
0.7	1.514	1.0124	0.012	90
0.8	1.520	1.0143	0.012	90
0.9	1.520	1.0162	0.012	90
1.0	1.520	1.0180	0.012	90
1.2	1.520	1.0212	0.012	90
1.4	1.520	1.0242	0.012	90
1.6	1.520	1.0268	0.012	90
1.8	1.520	1.02921	0.012	90
2.0	1.520	1.0314	0.012	90
2.5	1.520	1.0357	0.012	90
3.0	1.520	1.0365	0.012	90
3.5	1.520	1.0410	0.012	90
4.0	1.520	1.0429	0.012	90
7.0	1.520	1.0491	0.012	90
10.0	1.520	1.0511	0.012	90
17.0	1.520	1.0535	0.012	90

	G^E(salt)	H^E(salt)	V^E(salt)
Ao	-3941.43376	-6218.86188	0.110627118
A_1	647.461219	18522.49375	-0.289733722
A_2	-55.6005190	-3186.26385	0.054047308
A_3	5.61068049	303.8269	0.005105600
A_4	-0.299074708	-14.638825	0.000251303
A_5	-0.007981062	0.271944	-0.000005036
A_6	-0.000084499	0.0004956	0.00000000

C_2 / Mol dm^{-3}	$\{v''/V\}$	$\{\alpha_{eh}''/C_p\}$	$10^{-4}g''$ / J mol^{-1}	$10^{24}Q$(calcd) / cm^2 s
0.0968	-31.85	38.2	58.2	0.8
0.1882	- 8.59	43.3	27.5	2.2
0.2746	- 3.07	44.2	17.7	4.8
0.3565	- 0.90	43.6	12.9	8.9
0.4342	0.14	42.5	10.1	14.4
0.5080	0.70	41.0	8.2	21.2
0.5783	1.02	39.4	6.9	29.4
0.6452	1.21	37.7	6.0	38.8
0.7091	1.31	35.9	5.2	48.9
0.7700	1.37	34.2	4.7	59.7
0.8800	1.40	30.7	3.8	31.7
0.9883	1.38	27.3	3.2	102.4
1.084	1.31	24.0	2.7	119.4
1.173	1.24	20.9	2.4	130.8
1.255	1.17	18.0	2.1	135.1

(b) tetra-ethylammonium bromide

Input Data:

22 7 298.15 18.016 210.2 173.7

Concentration /mol kg^{-1}	Sound Velocity 10^{-5} C/cm s^{-1}	Density /g cm^{-3}	Expansion coefft/K^{-1}	Heat Capacity / J mol^{-1} K^{-1}
0.1	1.495	1.000625	0.006	100
0.2	1.495	1.004178	0.006	100
0.3	1.520	1.007642	0.006	100
0.4	1.520	1.01105	0.006	100
0.5	1.520	1.0014362	0.006	100
0.6	1.530	1.017606	0.006	100
0.7	1.540	1.020788	0.006	100
0.8	1.550	1.023910	0.006	100
0.9	1.550	1.046175	0.006	100
1.0	1.550	1.029986	0.006	100
1.2	1.550	1.035856	0.006	100
1.4	1.550	1.041423	0.006	100
1.6	1.550	1.046793	0.006	100
1.8	1.550	1.051982	0.006	100
2.0	1.550	1.057006	0.006	100
2.5	1.550	1.068645	0.006	100
3.0	1.550	1.079423	0.006	100
3.5	1.550	1.089248	0.006	100
4.0	1.550	1.098167	0.006	100
5.0	1.550	1.113722	0.006	100
7.0	1.550	1.139249	0.006	100
10.0	1.550	1.165203	0.006	100

	G^E(salt)	H^E(salt)	V^E(salt)
A_o	-3676.61753	-525.4470	-0.12336378
A_1	380.233505	-2650.53898	0.328469054
A_2	188.870632	915.211	-0.27873279
A_3	-54.9094202	-155.4850	0.113039802
A_4	8.34524939	15.20161	-0.023791127
A_5	0.6094211773	-0.78190	0.002354393
A_6	0.016822983	0.01653	-0.000089298

Output Data from QCALC.

c_2	$\{v''/V\}$	$\{\alpha_{eh}''/Cp\}$	$10^{-4}g''$ / J mol^{-1}	$10^{25}\Omega$(thermo) (cm^2 s)
0.0980	20.5	-5.06	58.5	0.99
0.1927	-3.4	-4.38	27.7	0.01
0.2844	-7.6	-3.90	17.9	0.25
0.3731	-8.2	-3.48	13.2	0.79
0.4589	-7.7	-3.11	10.5	1.29
0.5422	-6.9	-2.77	8.8	1.58
0.6229	-6.0	-2.46	7.5	1.65
0.7012	-5.1	-2.17	6.7	1.52
0.7772	-4.2	-1.90	6.0	1.25
0.8511	-3.4	-1.65	5.5	0.94
0.9926	-2.1	-1.21	4.8	0.34
1.1260	-1.2	-0.82	4.3	0.07
1.2530	-0.5	-0.49	3.9	v. small

6 - 7 Modified Version of QCALC program and Input Data for the system Urea + Water at 298 K.

The modified version of the QCALC program was described in Chapter 6-5.

Input Data:

12	(number of data points)
4	(number of parameters)
298.15	(temperature)
18.016	(molecular weight of solvent)
60.06	(molecular weight of solute)
44.2	(molar volume of solute)

Concentration of Urea /mol kg^{-1}	Sound Velocity /cm s^{-1}	Density /g cm^{-3}	Expansion Coefficient /K^{-1}	Heat Capacity /J mol^{-1} K^{-1}
1.0	1.522_{10}+05	1.013	0.0015	75.73
2.0	1.544_{10}+05	1.026	0.0015	76.27
3.0	1.564_{10}+05	1.038	0.0015	76.57
4.0	1.582_{10}+05	1.050	0.0015	77.15
5.0	1.599_{10}+05	1.061	0.0015	77.53
6.0	1.613_{10}+05	1.070	0.0015	78.37
7.0	1.626_{10}+05	1.078	0.0015	78.78
8.0	1.638_{10}+05	1.086	0.0015	79.37
9.0	1.649_{10}+05	1.094	0.0015	80.17
10.0	1.660_{10}+05	1.101	0.0015	80.83
11.0	1.670_{10}+05	1.108	0.0015	81.33
12.0	1.679_{10}+05	1.114	0.0015	82.26

I	GA(I)	HA(I)	VA(I)
0	0.042783	359.3	0.212
1	0.15	28.51	0.15
2	0.0004198	1.912	0.00
3	0.00	0.06151	0.00

Output Data from QCALC

Mole fraction of Urea	Concentration /mol kg^{-1}	$\left[\frac{V''}{V}\right]$	$\left[\frac{d_{eh}''}{Cp}\right]$
.0177	1.000	8.53686_{10}-01	1.49402_{10}+00
.0348	2.000	5.20644_{10}-01	3.88668_{10}+00
.0513	3.000	2.78107_{10}-01	6.40442_{10}+00
.0672	4.000	9.69787_{10}-02	9.01313_{10}+00
.0826	5.000	-4.14618_{10}-02	1.17604_{10}+01
.0976	6.000	-1.49551_{10}-01	1.45479_{10}+01
.1120	7.000	-2.35616_{10}-01	1.75285_{10}+01
.1260	8.000	-3.05408_{10}-01	2.05959_{10}+01
.1395	9.000	-3.62985_{10}-01	2.37267_{10}+01
.1527	10.00	-4.11259_{10}-01	2.70202_{10}+01
.1654	11.00	-4.52362_{10}-01	3.05066_{10}+01
.1778	12.00	-4.87876_{10}-01	3.39685_{10}+01

Mole fraction of Urea	Concentration /mol kg^{-1}	Concentration /mol dm^{-3}	Ω(thermo) /cm^{2}s
.0177	1.000	.9556	3.28213_{10}-31
.0348	2.000	1.832	1.42410_{10}-28
.0513	3.000	2.639	2.34589_{10}-27
.0672	4.000	3.386	1.54428_{10}-26
.0826	5.000	4.080	6.49749_{10}-26
.0976	6.000	4.719	2.05097_{10}-25
.1120	7.000	5.313	5.44788_{10}-25
.1260	8.000	5.868	1.26377_{10}-24
.1395	9.000	6.391	2.64315_{10}-24
.1527	10.00	6.879	5.13663_{10}-24
.1654	11.00	7.339	9.42562_{10}-24
.1778	12.00	7.769	1.62672_{10}-23

APPENDIX TO CHAPTER 8

8 - 1 Binary Divider Interface Unit for Coderg PH_1 Raman Spectrometer

Input Impedance = ~ 14 MΩ

Selector Switch Position S1	Function	Sampling Interval* cm^{-1}
1	direct	0.25
2	÷ 2	0.5
3	÷ 4	1
4	÷ 8	2
5	÷ 16	4
6	÷ 32	8

*To some extent the action of the binary dividers is dependent upon the pulse frequency from the step drive motor. Nominally four pulses are utilised per cm^{-1} and for medium scanning speeds (60 cm^{-1}/min) the above table is applicable. At very high or low scanning speeds some divergence from the above table was noticed.

8 - 2 Summary of Input Data and Controls for Gaussian and Lorentzian Spectral Band Deconvolution Program

(a) Digital Voltmeter Output Conversion Program

This program converts voltage readings output by the Solartron Data Logger into the corresponding percentage reading on the recorder scale, and outputs a tape comprising suitable input data for SPECT 1.

Input data required:

N - number of data points.

VFSD - full scale deflection voltage on recorder.

V100 - voltage corresponding to 100% reading on recorder scale. (N.B. - a negative value and negative sign must be included).

NUSTART - wavenumber corresponding to first sample point recorded by D.V.M.

INC - sampling interval in wavenumbers.

Then follows digital voltmeter (D.V.M.) readings on 8 hole paper tape.

(b) The program SPECT 1

This program executes Gaussian and Lorentzian spectral band contour deconvolution as described in Chapter 8. (The program is filed on magnetic tape).

Input data required:

KURVE - for Gaussian analysis set KURVE = 1

- for Lorentzian analysis set KURVE = 0

M - number of data points to be input.

N - number of bands comprising envelope.

WRITE - if WRITE is greater than, or equal to, one then a table of input and computed contour intensity values is output. Setting WRITE to any other value suppresses this output.

TAUMIN - limiting minimum value of step length modifier.

ITMAX - maximum permitted number of interactions.

TIMAX - maximum permitted run time in minutes.

ALPHA	BETA	GAMMA
I (1)	NUMAX(1)	DELTANU(1)
⋮	⋮	⋮
I(N)	NUMAX(N)	DELTANU(N)

NU(1)	INT(1)	Spectral envelope data generated by above D.V.M. program on paper tape (8 bit).
⋮	⋮	
NU(M)	INT(M)	

Alpha, Beta and Gamma are the constants in a quadratic equation used to fit the background. I is the band component intensity at NUMAX, the frequency of the intensity maximum. DELTANU is the half-band width.

```
  1
  2   DIGITAL VOLTMETER CONVERSION PROGRAM;
  3   "BEGIN" "INTEGER" N,I,J;
  4   "REAL" V100,VFSD,INC,NUSTART;
  5   "REAL" "ARRAY" PD,NU[1:2000];
  6   "READ" N,VFSD,V100,NUSTART,INC;
  7   "FOR" I:=1 "STEP" 1 "UNTIL" N "DO" "BEGIN"
  8   "READ" READER(1),PD[I];
  9   PD[I]:=PD[I]/10000;
 10   PD[I]:=((V100-PD[I])*100)/VFSD;
 11   PD[I]:=100.0-PD[I];
 12   "END";
 13   NU[1]:=NUSTART;
 14   "FOR" I:=2 "STEP" 1 "UNTIL" N "DO"
 15   NU[I]:=NU[I-1]+INC;
 16   "FOR" I:=1 "STEP" 1 "UNTIL" N "DO"
 17   "PRINT" PUNCH(1),FREEPOINT(6),''L``,SAMELINE,NU[I],''S2``,PD[I];
 18
 19   "PRINT" ''L6`***DATA OUTPUT TO PAPER TAPE***`;
 20   "PRINT" ''F''L10`***CALCULATED TRANSMISSION***`;
 21   "FOR" I:=0 "STEP" 11 "UNTIL" N+11 "DO" "BEGIN"
 22   "PRINT" ''L``;
 23   "FOR" J:=1 "STEP" 1 "UNTIL" 10 "DO"
 24   "PRINT" ''S5``,PD[I+J];
 25   "END";
 26   "END";
  256    M:
  248  CODE
  504 TOTAL
```

```
& JOB;CHE 131 DW;SPECT 1;


& ALGOL;
LIBRARY
ALGOL


& LIST;


& TIME;15:15;
    1   SPECT 1
    2   DECONVOLUTION OF INFRA RED AND RAMAN SPECTRA
    3   D WADDINGTON 1969 UNIVERSITY OF LEICESTER;
    4
    5   "BEGIN" "INTEGER" KURVE;
    6
    7   "COMMENT"            *SUMMARY OF INPUT DATA*
    8   KURVE-FOR GAUSSIAN ANALYSIS SET KURVE=1
    9         -FOR LORENTZIAN ANALYSIS SET KURVE=0
   10   M-NUMBER OF DATA POINTS TO BE INPUT
   11   N-NUMBER OF BANDS COMPRISING ENVELOPE
   12   WRITE-IF WRITE IS GREATER THAN OR EQUAL TO ONE THEN
   13         A TABLE OF INPUT AND COMPUTED VALUES OF INTENSITY IS
   14         OUTPUT, TOGETHER WITH THE RESPECTIVE DEVIATIONS
   15         IF WRITE TAKES ANY OTHER VALUE THEN NO OUTPUT
   16         IS OBTAINED
   17   TAUMIN-LIMITING MINIMUM VALUE OF STEP LENGTH MODIFIER
   18   ITMAX-MAXIMUM PERMITTED NUMBER OF ITERATIONS
   19   TIMAX-MAXIMUM PERMITTED RUN TIME IN MINUTES
   20   *DATA FOR BAND ENVELOPE READ FROM PAPER TAPE
   21   *FOLLOWED BY INDIVIDUAL ESTIMATED BAND PARAMETERS ON CARDS
   22   INTENSITY, NUMAX, HALF-WIDTH, FOR EACH BAND;
   23
   24
   25   "READ" KURVE;
   26   "IF" KURVE=1 "THEN"
   27
   28
   29   "BEGIN" "INTEGER" I,J,K,M,N,NIT,COUNT,WRITE,ITMAX;
   30   "INTEGER" MINS, SECS, TSECS;
   31   "INTEGER" TIMAX;
   32   "REAL" F,FO,TAU,TAUMIN;
   33   "COMMENT"    *GAUSSIAN ANALYSIS;
   34   "COMMENT" INSERT PROCEDURES AFTER THIS CARD;
   35
   36
   37
   38   "PROCEDURE" TIME(MINS, SECS, TSECS);
   39   "INTEGER" MINS, SECS, TSECS;
   40   "BEGIN" "INTEGER" T1, T2;
   41   "CODE"
   42
```

```
 43   %LD:LST1
 44   %LDR:LS0
 45   %SUBR:LS2
 46   %JIL$177;
 47
 48   MINS:=T1;
 49   SECS:=T2;
 50   TSECS:=60*T1+T2;
 51   "END" PROCEDURE TIME;
 52
 53
 54   "REAL" "PROCEDURE" INCALC(NU,P,IC,N,M);
 55   "INTEGER" M,N;
 56   "REAL" "ARRAY" NU,P,IC;
 57   "BEGIN" "INTEGER" I,J;
 58   "FOR" I:=1 "STEP" 1 "UNTIL" M "DO" "BEGIN"
 59   "REAL" S;    S:=0;
 60   "FOR" J:=0 "STEP" 1 "UNTIL" N-1 "DO"
 61   S:=S+P[4+3*J]*EXP(-((NU[I]-P[5+3*J])↑2)/(P[6+3*J]↑2));
 62   S:=S+P[1]+P[2]*NU[I]+P[3]*(NU[I]↑2);
 63   IC[I]:=S;
 64   "END";
 65   "END" OF INCALC;
 66
 67
 68   "REAL" "PROCEDURE" FCALC(II,IC,M);
 69   "INTEGER" M;
 70   "REAL" "ARRAY" II,IC;
 71   "BEGIN" "INTEGER" I;
 72   "REAL" S;    S:=0;
 73   "FOR" I:=1 "STEP" 1 "UNTIL" M "DO"
 7      :=S+((II[I]-IC[I])↑2);
      FCALC:=S;
 76   "END" OF FCALC;
 77
 78
 79   "REAL" "PROCEDURE" DGIA(NU,Y,Z);
 80   "REAL" NU,Y,Z;
 81   "BEGIN"
 82   DGIA:=(2*(NU-Y)/(Z*Z))*EXP(-(((NU-Y)/Z)↑2));
 83   "END" OF DGIA;
 84
 85
 86   "REAL" "PROCEDURE" DGIB(NU,Y,Z);
 87   "REAL" NU,Y,Z;
 88   "BEGIN"
 89   DGIB:=(2*((NU-Y)↑2)/(Z↑3))*EXP(-(((NU-Y)/Z)↑2));
 90   "END" OF DGIB;
 91
 92
 93
 94   "REAL" "PROCEDURE" D2GIA(NU,Y,Z);
 95   "REAL" NU,Y,Z;
 96   "BEGIN" "REAL" XX;     XX:=((NU-Y)↑2);
 97   D2GIA:=((4*XX/(Z↑4))-(2/(Z↑2)))*EXP(-(XX/(Z↑2)));
 98   "END" OF D2GIA;
 99
100
101   "REAL" "PROCEDURE" D2GIB(NU,Y,Z);
102   "REAL" NU,Y,Z;
```

```
103   "BEGIN" "REAL" U;
104   U:=(((NU-Y)/Z)↑2);
105   D2GIB:=-(((2*U)/(Z↑2))*(3.0-2.0*U)*EXP(-U));
106   "END" OF D2GIB;
107
108   "REAL" "PROCEDURE" SUMPROD(R,Q,J,K,M);
109   "VALUE" J,K;
110   "INTEGER" J,K,M;
111   "REAL" "ARRAY" R,Q;
112   "BEGIN" "INTEGER" I; "REAL" S; S:=0;
113   "FOR" I:=1 "STEP" 1 "UNTIL" M "DO"
114   S:=S+((R[I]↑J)*(Q[I]↑K));
115   SUMPROD:=2*S;
116   "END" OF SUMPROD;
117
118
119   "REAL" "PROCEDURE" FIRSTD(II,IC,NU,A,P,M,N);
120   "INTEGER" M,N;
121   "REAL" "ARRAY" II,IC,NU,A,P;
122   "BEGIN" "INTEGER" I,J;
123   "REAL" "ARRAY" Q,R[1:M];
124
125   "FOR" I:=1 "STEP" 1 "UNTIL" M "DO"
126   R[I]:=II[I]-IC[I];
127   "FOR" I:=1 "STEP" 1 "UNTIL" M "DO"
128   Q[I]:=-1.00;
129   A[1]:=SUMPROD(R,Q,1,1,M);
130   "FOR" I:=1 "STEP" 1 "UNTIL" M "DO"
131   Q[I]:=-NU[I];
132   A[2]:=SUMPROD(R,Q,1,1,M);
133   "FOR" I:=1 "STEP" 1 "UNTIL" M "DO"
134   Q[I]:=-(NU[I]↑2);
135   A[3]:=SUMPROD(R,Q,1,1,M);
136
137   "FOR" J:=0 "STEP" 1 "UNTIL" N-1 "DO"
138   "BEGIN"
139   "FOR" I:=1 "STEP" 1 "UNTIL" M "DO"
140   Q[I]:=EXP(-(((NU[I]-P[5+3*J])/(P[6+3*J]))↑2));
141   A[4+3*J]:=SUMPROD(R,Q,1,1,M);
142   A[4+3*J]:=-A[4+3*J];
143
144   "FOR" I:=1 "STEP" 1 "UNTIL" M "DO"
145   Q[I]:=P[4+3*J]*DGIA(NU[I],P[5+3*J],P[6+3*J]);
146   A[5+3*J]:=SUMPROD(R,Q,1,1,M);
147   A[5+3*J]:=-A[5+3*J];
148
149   "FOR" I:=1 "STEP" 1 "UNTIL" M "DO"
150   Q[I]:=P[4+3*J]*DGIB(NU[I],P[5+3*J],P[6+3*J]);
151   A[6+3*J]:=SUMPROD(R,Q,1,1,M);
152   A[6+3*J]:=-A[6+3*J];
153
154   "END" "END" OF FIRSTD;
155
156
157   "REAL" "PROCEDURE" SECONDD(NU,II,IC,P,B,M,N);
158   "INTEGER" M,N;
159   "REAL" "ARRAY" II,IC,NU,P,B;
160   "BEGIN" "INTEGER" I,J;
161   "REAL" "ARRAY" R,Q[1:M];
162
```

```
163   B[1]:=2*M;
164   B[2]:=SUMPROD(NU,NU,1,1,M);
165   B[3]:=SUMPROD(NU,NU,2,2,M);
166
167   "FOR" J:=0 "STEP" 1 "UNTIL" N-1 "DO" "BEGIN"
168
169   "FOR" I:=1 "STEP" 1 "UNTIL" M "DO" "BEGIN"
170   R[I]:=EXP(-(((NU[I]-P[5+3*J])/(P[6+3*J]))↑2));
171   Q[I]:=R[I];
172   "END";
173   B[4+3*J]:=SUMPROD(R,Q,1,1,M);
174
175   "FOR" I:=1 "STEP" 1 "UNTIL" M "DO" "BEGIN"
176   R[I]:=P[4+3*J]*DGIA(NU[I],P[5+3*J],P[6+3*J]);
177   Q[I]:=R[I];
178   "END";
179   B[5+3*J]:=SUMPROD(R,Q,1,1,M);
180   "FOR" I:=1 "STEP" 1 "UNTIL" M "DO" "BEGIN"
181   R[I]:=(II[I]-IC[I]);
182   Q[I]:=D2GIA(NU[I],P[5+3*J],P[6+3*J]);
183   "END";
184   B[5+3*J]:=B[5+3*J]-SUMPROD(R,Q,1,1,M);
185
186
187   "FOR" I:=1 "STEP" 1 "UNTIL" M "DO" "BEGIN"
188   R[I]:=P[4+3*J]*DGIB(NU[I],P[5+3*J],P[6+3*J]);
189   Q[I]:=R[I];
190   "END";
191   B[6+3*J]:=SUMPROD(R,Q,1,1,M);
192   "FOR" I:=1 "STEP" 1 "UNTIL" M "DO" "BEGIN"
193   R[I]:=(II[I]-IC[I]);
194   Q[I]:=D2GIB(NU[I],P[5+3*J],P[6+3*J]);
195   "END";
196   B[6+3*J]:=B[6+3*J]-SUMPROD(R,Q,1,1,M);
197
198   "END" "END" OF SECONDD;
199
200
201   "REAL" "PROCEDURE" PRINTOUT(F,FO,TAU,NU,II,IC,P,K,M,NIT,COUNT,N,WRITE);
202   "INTEGER" N,NIT,K,M,COUNT,WRITE;
203   "REAL" F,FO,TAU;
204   "REAL" "ARRAY" NU,II,IC,P;
205   "BEGIN" "INTEGER" I,J;
206   "REAL" RMS,SIGMA;
207   "REAL" "ARRAY" DEV[1:M];
208
209   "FOR" I:=1 "STEP" 1 "UNTIL" M "DO"
210   DEV[I]:=II[I]-IC[I];
211
212   RMS:=SQRT(SUMPROD(DEV,DEV,1,1,M)/M);
213   SIGMA:=SQRT(SUMPROD(DEV,DEV,1,1,M)/(M-N));
214
215   "PRINT" ''F''S55'ITERATION NUMBER  ',SAMELINE,DIGITS(4),COUNT,''L5'';
216   "PRINT" ''S10'R.M.S. DEVIATION = ',SAMELINE,FREEPOINT(9),RMS,''L'',
217   ''S10'STANDARD DEVIATION SIGMA = ',SAMELINE, FREEPOINT(9),SIGMA,''L'',
218   ''S10'VALUE OF FO = ',SAMELINE,FREEPOINT(9),FO,''L'',
219   ''S10'VALUE OF  F = ',SAMELINE,FREEPOINT(9),F,''L'',
220   ''S10'FINAL VALUE OF STEP LENGTH MODIFIER (TAU) = ',SAMELINE,
221   FREEPOINT(9),TAU,''L'',
222   ''S10'NIT = ',SAMELINE,DIGITS(3),NIT,''L6'';
```

```
223   "PRINT" ''L`PARAMETERS EVALUATED ******************************`,''L2``;
224
225
226   "PRINT" ''L`ALPHA  = `,SAMELINE, FREEPOINT(9),P[1],
227   ''S15`BETA  = `,P[2],
228   ''S15`GAMMA  = `,P[3],''L2``;
229
230   "FOR" J:=0 "STEP" 1 "UNTIL" N-1 "DO"
231   "PRINT" ''L``,PREFIX(''S15``),FREEPOINT(9),
232   P[4+3*J],P[5+3*J],P[6+3*J];
233
234   "IF" WRITE "GE" 1 "THEN" "BEGIN"
235   "PRINT" ''F`COMPUTED SPECTRAL DATA *************************`,''L``;
236
237   "FOR" I:=1 "STEP" 1 "UNTIL" M "DO"
238   "PRINT" ''L``,SAMELINE,FREEPOINT(9),PREFIX(''S10``),
239   NU[I],II[I],IC[I],DEV[I];
240   "END";
241   "PRINT" ''L2`ITERATION COMPLETED ******************************`,''L2``;
242   "END" OF PRINTOUT;
243
244
245
246   "READ" M,N,WRITE,TAUMIN,ITMAX;
247   "READ" TIMAX;
248   TIMAX:=60*TIMAX;
249   K:=3*N + 3;    COUNT:=0;
250   "BEGIN" "REAL" "ARRAY" NU,II,IC,A,B[1:M],P,PO[1:K];
251
252   "COMMENT" INPUT  DATA NOW READ;
253
254   READER(1);
255   "FOR" I:=1 "STEP" 1 "UNTIL" M "DO"
256   "READ" NU[I], II[I];
257   READER(6);
258   "FOR" J:=1 "STEP" 1 "UNTIL" K "DO"
259   "READ" PO[J];
260
261
262
263   "COMMENT" INPUT DATA NOW PRINTED OUT;
264   "PRINT" ''F''S20`* INFRA RED AND RAMAN SPECTRAL BAND FITTING PROGRAM *`
265   ''L4`D. WADDINGTON.  ***  1970.`,
266   ''L`UNIVERSITY OF LEICESTER.`,''L5``,
267   ''L8`INPUT VALUES OF PARAMETERS ***********************`,''L2``;
268
269   "PRINT" ''L`ALPHA = `,SAMELINE,FREEPOINT(9),PO[1],
270   ''S15`BETA = `,PO[2],
271   ''S15`GAMMA = `,PO[3],''L2``;
272
273   "FOR" J:=0 "STEP" 1 "UNTIL" N-1 "DO"
274   "PRINT" ''L``,PREFIX(''S15``),FREEPOINT(8),SAMELINE,
275   PO[4+3*J],PO[5+3*J],PO[6+3*J];
276
277   "GOTO" START;
278
279   "COMMENT" PRINTOUT OBTAINED AT THIS STAGE;
280
281   RESTART: PRINTOUT(F,FO,TAU,NU,II,IC,P,K,M,NIT,COUNT,N,WRITE);
282   TIME(MINS, SECS, TSECS);
```

```
"PRINT" ''L2` TIME: `,DIGITS(3),SAMELINE,
MINS,' MINS. `,SECS, ' SECS. `,''L6``;
"IF" TSECS "GE" TIMAX "THEN"
"GOTO" LLL;
"FOR" J:=1 "STEP" 1 "UNTIL" K "DO"
PO[J]:=P[J];
COUNT:=COUNT+1;
"IF" ITMAX-COUNT=2 "THEN"
WRITE:=1;
"IF" COUNT "GE" ITMAX "THEN"
"GOTO" LL;

"COMMENT" CALCULATION OF FIRST AND SECOND DERIVATIVES OF
          LEAST SQUARES FUNCTION;

START:      INCALC(NU,PO,IC,N,M);
FO:=FCALC(II,IC,M);
FIRSTD(II,IC,NU,A,PO,M,N);
SECONDD(NU,II,IC,PO,B,M,N);
TAU:=1.000;
NIT:=0;

"COMMENT" VALUE OF DAMPING FACTOR TAU IS INITIALLY SET
                  EQUAL TO ONE;

L:      "FOR" J:=1 "STEP" 1 "UNTIL" K "DO"
            P[J]:=PO[J]-TAU*(A[J]/B[J]);

"COMMENT" NEW VALUES OF INITIAL PARAMETERS EVALUATED;

INCALC(NU,P,IC,N,M);
F:=FCALC(II,IC,M);
NIT:=NIT+1;

"COMMENT" PROGRAM NOW ENTERS TEST SUBROUTINE;



"IF" TAU "LE" TAUMIN "THEN" "BEGIN"
"PRINT" ''L10`CALCULATION TERMINATED (TAU LESS THAN TAUMIN)`;
"GOTO" RESTART;
"END" OF TEST;


"IF" F "GE" FO "THEN"
"BEGIN"
TAU:=0.500*TAU;
"GOTO" L;
"END" OF TEST TWO;


"COMMENT" IF F IS LESS THAN FO THEN INTERCHANGE P AND PO
                AND RESTART MINIMISATION;

"GOTO" RESTART;
LL: "PRINT" ''L10`CALCULATION TERMINATED  ***  ITMAX REACHED  ***`;
LLL: "PRINT" ''L10`CALCULATION TERMINATED *** MAX. TIME REACHED *`;

"END" "END"
```

```
343
344
345   "ELSE"
346
347
348   "BEGIN" "INTEGER" I,J,K,M,N,NIT,COUNT,WRITE,ITMAX;
349   "INTEGER" MINS, SECS, TSECS;
350   "INTEGER" TIMAX;
351   "REAL" F,FO,TAU,TAUMIN;
352
353   "COMMENT"     *LORENTZIAN ANALYSIS;
354   "COMMENT" INSERT PROCEDURES AFTER THIS CARD;
355
356
357
358   "PROCEDURE" TIME(MINS, SECS, TSECS);
359   "INTEGER" MINS, SECS, TSECS;
360   "BEGIN" "INTEGER" T1, T2;
361   "CODE"
362
363   %LD:L$T1
364   %LDR:L$0
365   %SUBR:L$2
366   %JIL$177;
367
368   MINS:=T1;
369   SECS:=T2;
370   TSECS:=60*T1+T2;
371   "END" PROCEDURE TIME;
372
373
374   "REAL" "PROCEDURE" INCALC(NU,P,IC,N,M);
375   "INTEGER" M,N;
376   "REAL" "ARRAY" NU,P,IC;
377   "BEGIN" "INTEGER" I,J;
378   "FOR" I:=1 "STEP" 1 "UNTIL" M "DO"
379   "BEGIN" "REAL" S;     S:=0;
380   "FOR" J:=0 "STEP" 1 "UNTIL" N-1 "DO"
381   S:=S+P[4+3*J]/(1+(((NU[I]-P[5+3*J])/P[6+3*J])↑2));
382   S:=S+P[1]+P[2]*NU[I]+P[3]*NU[I]*NU[I];
383   IC[I]:=S;
384   "END";
385   "END" OF INCALC;
386
387
388
389   "REAL" "PROCEDURE" FCALC(II,IC,M);
390   "INTEGER" M;
391   "REAL" "ARRAY" II,IC;
392   "BEGIN" "INTEGER" I;
393   "REAL" S;     S:=0;
394   "FOR" I:=1 "STEP" 1 "UNTIL" M "DO"
395   S:=S+((II[I]-IC[I])↑2);
396   FCALC:=S;
397   "END" OF FCALC;
398
399
400   "REAL" "PROCEDURE" DGIA(NU,Y,Z);
401   "REAL" NU,Y,Z;
402   "BEGIN" "REAL" X,A,D1;
```

```
403   X:=(((NU-Y)/Z)↑2);
404   A:=-1/((1+X)↑2);
405   D1:=-2*(NU-Y)/(Z*Z);
406   DGIA:=A*D1;
407   "END" OF DGIA;
408
409
410   "REAL" "PROCEDURE" DGIB(NU,Y,Z);
411   "REAL" NU,Y,Z;
412   "BEGIN" "REAL" X,A,D2;
413   X:=(((NU-Y)/Z)↑2);
414   A:=-1/((1+X)↑2);
415   D2:=-2*((NU-Y)↑2)/(Z↑3);
416   DGIB:=A*D2;
417   "END" OF DGIB;
418
419   "REAL" "PROCEDURE" SUMPROD(R,Q,J,K,M);
420   "VALUE" J,K;
421   "INTEGER" J,K,M;
422   "REAL" "ARRAY" R,Q;
423   "BEGIN" "INTEGER" I; "REAL" S; S:=0;
424   "FOR" I:=1 "STEP" 1 "UNTIL" M "DO"
425   S:=S+((R[I]↑J)*(Q[I]↑K));
426   SUMPROD:=2*S;
427   "END" OF SUMPROD;
428
429
430   "REAL" "PROCEDURE" FIRSTD(II,IC,NU,A,P,M,N);
431   "INTEGER" M,N;
432   "REAL" "ARRAY" II,IC,NU,A,P;
433   "BEGIN" "INTEGER" I,J;
434   "REAL" "ARRAY" Q,R[1:M];
435
436   "FOR" I:=1 "STEP" 1 "UNTIL" M "DO"
437   R[I]:=II[I]-IC[I];
438   "FOR" I:=1 "STEP" 1 "UNTIL" M "DO"
439   Q[I]:=-1.00;
440   A[1]:=SUMPROD(R,Q,1,1,M);
441   "FOR" I:=1 "STEP" 1 "UNTIL" M "DO"
442   Q[I]:=-NU[I];
443   A[2]:=SUMPROD(R,Q,1,1,M);
444   "FOR" I:=1 "STEP" 1 "UNTIL" M "DO"
445   Q[I]:=-(NU[I]↑2);
446   A[3]:=SUMPROD(R,Q,1,1,M);
447
448   "FOR" J:=0 "STEP" 1 "UNTIL" N-1 "DO"
449   "BEGIN"
450   "FOR" I:=1 "STEP" 1 "UNTIL" M "DO"
451   Q[I]:=1/(1+(((NU[I]-P[5+3*J])/P[6+3*J])↑2));
452   A[4+3*J]:=SUMPROD(R,Q,1,1,M);
453   A[4+3*J]:=-A[4+3*J];
454
455   "FOR" I:=1 "STEP" 1 "UNTIL" M "DO"
456   Q[I]:=P[4+3*J]*DGIA(NU[I],P[5+3*J],P[6+3*J]);
457   A[5+3*J]:=SUMPROD(R,Q,1,1,M);
458   A[5+3*J]:=-A[5+3*J];
459
460   "FOR" I:=1 "STEP" 1 "UNTIL" M "DO"
461   Q[I]:=P[4+3*J]*DGIB(NU[I],P[5+3*J],P[6+3*J]);
462   A[6+3*J]:=SUMPROD(R,Q,1,1,M);
```

```
A[6+3*J]:=-A[6+3*J];

"END" "END" OF FIRSTD;


"REAL" "PROCEDURE" SECONDD(NU,II,IC,P,B,M,N);
"INTEGER" M,N;
"REAL" "ARRAY" II,IC,NU,P,B;
"BEGIN" "INTEGER" I,J;
"REAL" "ARRAY" R,Q[1:M];

B[1]:=2*M;
B[2]:=SUMPROD(NU,NU,1,1,M);
B[3]:=SUMPROD(NU,NU,2,2,M);

"FOR" J:=0 "STEP" 1 "UNTIL" N-1 "DO" "BEGIN"

"FOR" I:=1 "STEP" 1 "UNTIL" M "DO" "BEGIN"
R[I]:=1/(1+(((NU[I]-P[5+3*J])/P[6+3*J])↑2));
Q[I]:=R[I];
"END";
B[4+3*J]:=SUMPROD(R,Q,1,1,M);

"FOR" I:=1 "STEP" 1 "UNTIL" M "DO" "BEGIN"
R[I]:=P[4+3*J]*DGIA(NU[I],P[5+3*J],P[6+3*J]);
Q[I]:=R[I];
"END";
B[5+3*J]:=SUMPROD(R,Q,1,1,M);


"FOR" I:=1 "STEP" 1 "UNTIL" M "DO" "BEGIN"
R[I]:=P[4+3*J]*DGIB(NU[I],P[5+3*J],P[6+3*J]);
Q[I]:=R[I];
"END";
B[6+3*J]:=SUMPROD(R,Q,1,1,M);

"END" "END" OF SECONDD;


"REAL" "PROCEDURE" PRINTOUT(F,FO,TAU,NU,II,IC,P,K,M,NIT,COUNT,N,WRITE);
"INTEGER" N,NIT,K,M,COUNT,WRITE;
"REAL" F,FO,TAU;
"REAL" "ARRAY" NU,II,IC,P;
"BEGIN" "INTEGER" I,J;
"REAL" RMS,SIGMA;
"REAL" "ARRAY" DEV[1:M];

"FOR" I:=1 "STEP" 1 "UNTIL" M "DO"
DEV[I]:=II[I]-IC[I];

RMS:=SQRT(SUMPROD(DEV,DEV,1,1,M)/M);
SIGMA:=SQRT(SUMPROD(DEV,DEV,1,1,M)/(M-N));

"PRINT" ''F''S55`ITERATION NUMBER  `,SAMELINE,DIGITS(4),COUNT,''L5'';
"PRINT" ''S10`R.M.S. DEVIATION = `,SAMELINE,FREEPOINT(9),RMS,''L'',
''S10`STANDARD DEVIATION SIGMA = `,SAMELINE, FREEPOINT(9),SIGMA,''L'',
''S10`VALUE OF FO = `,SAMELINE,FREEPOINT(9),FO,''L'',
''S10`VALUE OF  F = `,SAMELINE,FREEPOINT(9),F,''L'',
''S10`FINAL VALUE OF STEP LENGTH MODIFIER (TAU) = `,SAMELINE,
FREEPOINT(9),TAU,''L'',
```

```
''S10`NIT = `,SAMELINE,DIGITS(3),NIT,''L6``;
"PRINT" ''L`PARAMETERS EVALUATED ****************************`,''L2``;

"PRINT" ''L`ALPHA  = `,SAMELINE, FREEPOINT(9),P[1],
''S15`BETA  = `,P[2],
''S15`GAMMA  = `,P[3],''L2``;

"FOR" J:=0 "STEP" 1 "UNTIL" N-1 "DO"
"PRINT" ''L``,PREFIX(''S15``),FREEPOINT(9),
P[4+3*J],P[5+3*J],P[6+3*J];

"IF" WRITE "GE" 1 "THEN" "BEGIN"
"PRINT" ''F`COMPUTED SPECTRAL DATA **************************`,''L``;

"FOR" I:=1 "STEP" 1 "UNTIL" M "DO"
"PRINT" ''L``,SAMELINE,FREEPOINT(9),PREFIX(''S10``),
NU[I],II[I],IC[I],DEV[I];
"END";
"PRINT" ''L2`ITERATION COMPLETED ****************************`,''L2``;
"END" OF PRINTOUT;



"READ" M,N,WRITE,TAUMIN,ITMAX;
"READ" TIMAX;
TIMAX:=60*TIMAX;
K:=3*N + 3;     COUNT:=0;
"BEGIN" "REAL" "ARRAY" NU,II,IC,A,B[1:M],P,PO[1:K];

"COMMENT" INPUT  DATA NOW READ;

READER(1);
"FOR" I:=1 "STEP" 1 "UNTIL" M "DO"
"READ" NU[I], II[I];
READER(6);
"FOR" J:=1 "STEP" 1 "UNTIL" K "DO"
"READ" PO[J];



"COMMENT" INPUT DATA NOW PRINTED OUT;
"PRINT" ''F``S20`* INFRA RED AND RAMAN SPECTRAL BAND FITTING PROGRAM *`
''L4`D. WADDINGTON.  ***  1970.`,
''L`UNIVERSITY OF LEICESTER.`,''L5``,
''L8`INPUT VALUES OF PARAMETERS ***********************`,''L2``;

"PRINT" ''L`ALPHA = `,SAMELINE,FREEPOINT(9),PO[1],
''S15`BETA = `,PO[2],
''S15`GAMMA = `,PO[3],''L2``;

"FOR" J:=0 "STEP" 1 "UNTIL" N-1 "DO"
"PRINT" ''L``,PREFIX(''S15``),FREEPOINT(8),SAMELINE,
PO[4+3*J],PO[5+3*J],PO[6+3*J];

"GOTO" START;

"COMMENT" PRINTOUT OBTAINED AT THIS STAGE;

RESTART: PRINTOUT(F,FO,TAU,NU,II,IC,P,K,M,NIT,COUNT,N,WRITE);
```

```
583   TIME(MINS, SECS, TSECS);
584   "PRINT" ''L2` TIME: `,DIGITS(3),SAMELINE,
585   MINS,' MINS. `,SECS, ' SECS. `,''L6``;
586   "IF" TSECS "GE" TIMAX "THEN"
587   "GOTO" LLL;
588   "FOR" J:=1 "STEP" 1 "UNTIL" K "DO"
589   PO[J]:=P[J];
590   COUNT:=COUNT+1;
591   "IF" ITMAX-COUNT=2 "THEN"
592   WRITE:=1;
593   "IF" COUNT "GE" ITMAX "THEN"
594   "GOTO" LL;
595
596   "COMMENT" CALCULATION OF FIRST AND SECOND DERIVATIVES OF
597             LEAST SQUARES FUNCTION;
598
599   START:      INCALC(NU,PO,IC,N,M);
600   FO:=FCALC(II,IC,M);
601   FIRSTD(II,IC,NU,A,PO,M,N);
602   SECONDD(NU,II,IC,PO,B,M,N);
603   TAU:=1.000;
604   NIT:=0;
605
606   "COMMENT" VALUE OF DAMPING FACTOR TAU IS INITIALLY SET
607                    EQUAL TO ONE;
608
609   L:       "FOR" J:=1 "STEP" 1 "UNTIL" K "DO"
610                P[J]:=PO[J]-TAU*(A[J]/B[J]);
611
612   "COMMENT" NEW VALUES OF INITIAL PARAMETERS EVALUATED;
613
614   INCALC(NU,P,IC,N,M);
615   F:=FCALC(II,IC,M);
616   NIT:=NIT+1;
617
618   "COMMENT" PROGRAM NOW ENTERS TEST SUBROUTINE;
619
620
621
622   "IF" TAU "LE" TAUMIN "THEN" "BEGIN"
623   "PRINT" ''L10`CALCULATION TERMINATED (TAU LESS THAN TAUMIN)`;
624   "GOTO" RESTART;
625   "END" OF TEST;
626
627
628   "IF" F "GE" FO "THEN"
629   "BEGIN"
630   TAU:=0.500*TAU;
631   "GOTO" L;
632   "END" OF TEST TWO;
633
634
635   "COMMENT" IF F IS LESS THAN FO THEN INTERCHANGE P AND PO
636                    AND RESTART MINIMISATION;
637
638   "GOTO" RESTART;
639   LL: "PRINT" ''L10`CALCULATION TERMINATED  ***  ITMAX REACHED  ***`;
640   LLL: "PRINT" ''L10`CALCULATION TERMINATED *** MAX. TIME REACHED *`;
641
642   "END" "END" OF PROGRAM;
      "END";
```

(c) The program SPECTPLOTTING

This program consists of two procedures SPECPLOT and BANDPLOT. The former plots out the original contour from the spectral data (on 8 bit paper tape) supplied to SPECT 1. The latter plots out the computed component band envelopes on the same scale (but a different grid) as the above.

Input data required:

M - total number of data sample points on input paper tape (8 bit).

N - total number of derived Gaussian parameters; three per band (for J bands N = 3 J).

PLOT - if PLOT = 1 then both procedures are executed.

SCX - number of wavenumbers per inch of scale required.

A(1)
⋮
A(N)

This is followed by the 8 bit paper tape used for input to SPECT 1. (This program lising has not been included).

The above programs were all written in ALGOL for an Elliott 4130 computer.

8 - 3 Additional Equations used in SPECT 1

The variables in these equations were defined in Chapter 8.

Lorentzian bandshapes:

$$\phi_i = \frac{1}{1 + ((\nu - \nu_i^{\circ})/\Delta\nu_i)^2} \qquad \text{(from equation 8-16)}$$

For a Lorentzian bandshape the derivates used $\frac{\partial \phi_i}{\partial \nu_i^{\circ}}$ and $\frac{\partial \phi_i}{\partial \Delta\nu_i}$ are as follows. It was found to be unnecessary to use the second derivatives of these two functions.

$$\frac{\partial \phi_i}{\partial \nu_i^{\circ}} = \frac{2((\nu - \nu_i^{\circ})/\Delta\nu_i)}{\Delta\nu_i(1 + ((\nu - \nu_i^{\circ})/\Delta\nu_i)^2)^2}$$

$$\frac{\partial \phi_i}{\partial \Delta\nu_i} = \frac{2((\nu - \nu_i^{\circ})^2/\Delta\nu_i^3)}{(1 + ((\nu - \nu_i^{\circ})/\Delta\nu_i)^2)^2}$$

APPENDIX TO CHAPTER 9

9 - 1 (a) Dependence of frequency of major component maximum in the Raman spectra of 6.0 mol dm^{-3} HOD in H_2O on concentration of added salt

Salt	Salt Concentration /mol dm^{-3}	Frequency/cm^{-1}
Lithium Bromide	0.0	2522
	0.5	2529
	3.0	2547
	3.5	2545
Sodium Bromide	0.0	2522
	0.3	2527
	0.6	2531
	1.2	2539
	1.8	2545
	2.4	2548
Caesium Bromide	0.0	2522
	0.5	2531
	1.0	2533
	1.5	2539
	2.0	2541
Potassium Bromide	0.0	2522
	0.3	2525
	0.6	2528
	1.2	2534
	1.8	2540
	2.4	2546
Sodium Chloride	0.0	2522
	0.4	2525
	1.5	2532
	2.4	2537
	3.2	2539
Hydrochloric Acid	0.0	2522
	0.4	2528

Salt	Salt Concentration /mol dm^{-3}	Frequency/cm^{-1}
Hydrochloric Acid	0.8	2529
	1.2	2532
	1.6	2534
Ammonium Chloride	0.0	2522
	1.0	2526
	2.0	2531
	4.0	2539
Magnesium Chloride	0.0	2522
	0.4	2524
	0.8	2522
	1.2	2524
	1.6	2522
Calcium Chloride	0.0	2522
	0.4	2525
	0.8	2529
	1.2	2531
	1.6	2533
Strontium Chloride	0.0	2522
	0.2	2525
	0.4	2528
	0.6	2532
	0.8	2530
Barium Chloride	0.0	2522
	0.2	2525
	0.4	2528
	0.6	2531
	0.8	2530
Sodium Iodide	0.0	2522
	0.3	2530
	0.6	2537
	1.2	2549
	1.8	2559
	2.4	2562

Salt	Salt Concentration /mol dm^{-3}	Frequency/cm^{-1}
Sodium Fluoride	0.0	2522
	0.2	2522
	0.4	2524
	0.6	2523
	0.8	2524
Sodium Sulphate	0.0	2522
	0.4	2522
	0.8	2525
	1.2	2526
Sodium Chlorate	0.0	2519
	0.5	2521
	0.9	2523
	1.8	2527
	3.6	2539
	7.1	2563
Sodium Perchlorate	0.0	2522
	0.4	2524
	0.8	2527
	1.2	2528
	1.6	2528
	2.4	2532
	3.6	2534
	5.0	2536

9 - 1 (b) Summary of two component Guassian deconvolution of Raman spectra of water between 287 and 323 K.

Temp. /K	Io /%	ν_{max} /cm^{-1}	$\Delta\nu_{\frac{1}{2}}$ /cm^{-1}	Standard Deviation /cm^{-1}
283	35	3204	142	2.21
	73	3433	178	
293	31	3204	143	4.47
	71	3436	181	
303	29	3204	147	2.47
	73	3439	183	
313	25	3209	127	6.62
	67	3445	179	
323	31	3165	190	2.75
	66	3386	179	

9 - 1 (c) Summary of two component Gaussian deconvolution of Raman spectra of water containing 6.0 mol dm^{-3} D_2O between 285 K and 360 K

Temp. /k	Io /%	ν_{max} /cm^{-1}	$\Delta\nu_{\frac{1}{2}}$ /cm^{-1}	Standard Deviation /cm^{-1}
285	50	2517	101	1.5
	7	2665	55	
305	47	2532	106	1.5
	7	2667	39	
320	44	2543	112	1.5
	6	2664	32	
360	38	2570	122	1.5
	8	2665	12	

9 - 2 Solvation Numbers for Perchlorate and Fluoroborate*

Infra Red Spectra (calculated from data in reference)

		Solvation Number
Sodium Perchlorate	-	4.5 ± 0.5
Sodium Fluoroborate	-	4.7 ± 0.5
Magnesium Perchlorate	-	3.5 ± 0.5

Raman Spectra

Sodium Perchlorate	-	4.4 ± 0.5
Lithium Perchlorate	-	4.7 ± 0.5
Sodium Fluoroborate	-	4.4 ± 0.5

*These solvation numbers were calculated as outlined in Chapter 9. The quantity x, defined as the solvation number of the anion, was obtained from a graph of (1-R) against (m/2(n-m)), an example of which is given for sodium perchlorate on the following page.

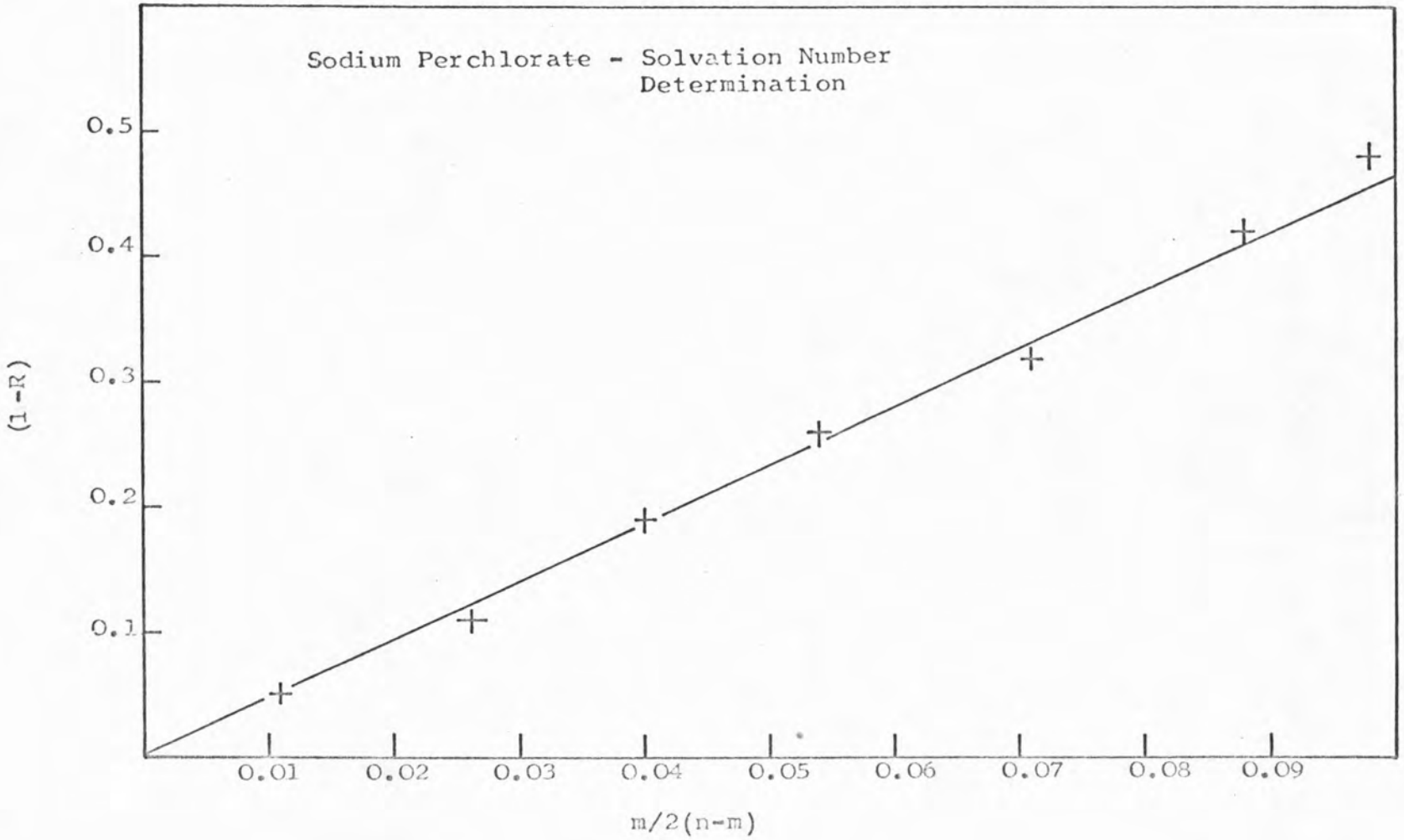
Sodium Perchlorate - Solvation Number Determination
0.5
0.4
0.3
0.2
0.1
(1-R)
0.01
0.02
0.03
0.04
0.05
0.06
0.07
0.08
0.09
m/2(n-m)

9 - 3 (a) Dependence of frequency of the major component maximum, in the Raman spectra of 6.0 mol dm^{-3} solutions of D_2O in H_2O at 298 K on composition of added solute.

	Composition /mol dm^{-3}	Frequency ν/cm^{-1}
Acetamide	0	2521
	1	2521
	2	2520
	3	2521
	4	2517
	5	2517

Composition /mol dm^{-3}	Frequency ν/cm^{-1}		
	Methanol	Ethanol	D.M.S.O.
0	2520	2519	2517
2	2517	2520	2517
4	2517	2520	2517
6	2517	2521	2519
8	2523	2526	2521
10	2527	2531	-

(b) Dependence of frequency of the band maximum, in the infra-red spectra of 2% solutions of D_2O in H_2O at 298 K, upon mole fraction added solute.

	Composition mole fraction	Frequency ν/cm^{-1}
Dimethyl Sulphoxide (DMSO)	0.00	2520
	0.09	2520
	0.38	2538
	0.49	2538
	0.70	2538

	Composition mole fraction	Frequency ν/cm^{-1}
Dioxan	0.00	2520
	0.10	2534
	0.28	2548
	0.54	2571
	0.73	2606

9 - 4 Data used in the compilation of the Saumagne-Glew plot presented in Chapter 9.

The data used in compiling Figure 9-40 is listed in the tables below, and was obtained from references given in Chapter 9.

Data for 2:1 Complexes and Hydrates

System (water in)	$\nu_3(\nu_f)$ /cm^{-1}	$\nu_1(\nu_{as})$ /cm^{-1}
1 gas	3756	3657
2 nitrogen matrix	3725	3627
3 perfluorobenzene	3719	3626
4 carbon tetrachloride	3705	3614
5 perchloroethylene	3705	3613
6 1,1,1-trichloroethane	3698	3610
7 1,2-dichloroethane	3670	3592
8 ethylene oxide (EO)	3608	3528
9 propylene oxide (PO)	3602	3525
10 1,4 dioxane (DI)	3565	3509
11 tetrahydrofuran (THF)	3565	3500
12 $NaClO_4 . H_2O$	3592	3536
13 $LiClO_4 . 3H_2O$	3560	3519
14 $Ba(ClO_4)_2 . 3H_2O$	3579	3529
15 $Ba(ClO_3)_2 . H_2O$	3584	3518
16 $Ba(BrO_3)_2 . H_2O$	3516	3456
17 $Ba(IO_3)_2 . H_2O$	3443	3393
18 $Ca(BrO_3)_2$	3534	3471
19 $Sr(BrO_3)_2$	3518	3455

System (water in)		$\nu_3(\nu_f)$ /cm^{-1}	$\nu_1(\nu_{as})$ /cm^{-1}
20	nitromethane	3670	3580
21	nitrobenzene	3675	3590
22	dimethylphthalate	3650	3565
23	acetonitrile	3640	3545
24	ethyl acetate	3640	3550
25	methylal	3650	3570
26	acetone	3610	3530
27	dioxane	3585	3525
28	ethylether	3600	3525
29	N.N. dimethylformamide	3550	3490

Data for 1:1 complexes: water + organic phase diluted in an 'inert' solvent (CCl_4)

System (water in)		$\nu_3(\nu_f)$ /cm^{-1}	$\nu_1(\nu_{as})$ /cm^{-1}
a	CH_3CN/CCl_4	3697	3555
b	H_2O/N_2 solid matrix	3697	3548
c	cyclohexanone/CCl_4	3695	3550
d	dioxan/CCl_4	3690	3515
e	d.m.s.o./CCl_4	3690	3450
f	pyridine/CCl_4	3675	3400
g	nitromethane	3700	3610
h	nitrobenzene	3700	3585
i	trioxan	3695	3580
j	dimethylphthalate	3695	3575
k	3,4-dimethoxybenzaldehyde	3690	3560
l	acetonitrile	3690	3555
m	butyrolactone	3690	3550
n	ethylacetate	3690	3545
o	methylal	3690	3525
p	acetone	3690	3525
q	dioxane	3690	3520
r	t butyl peroxide	3690	3500

System (water in)	$\nu_3(\nu_f)$ /cm^{-1}	$\nu_1(\nu_{as})$ /cm^{-1}
s ethylether	3687	3490
t N,N dimethylformamide	3688	3490
u pyridazine	3682	3430
v pyridine	3682	3390
w 4-picoline N-oxide	3680	3350

Data for ices and perchlorate

Ice	ν_3 /cm^{-1}	ν_1 /cm^{-1}
I (H-disordered)	3210	3085
II	3314	3194
III	3281	3160
V	3312	3181
I	3330	3230*

* infra-red data, the above are taken from Raman spectral data reported by Eisenberg and Kauzman.[36]

The point marked α corresponds to the values of $\nu_{a.ss}$ and ν_{free} obtained from the stimulated Raman spectra of 5.0 mol dm^{-3} sodium perchlorate solutions (3580,3520 cm^{-1}).

REFERENCES

References

1. Much of the material presented in this chapter was published with Dr. M.J. Blandamer in Adv. in Mol. Relaxation Proc., 1970, 2, 1.
2. D. Sette, Nuovo Cimento, 1955, 1, N5, 800.
3. D. Sette, Natl. Bur. Std., (U.S.), Misc. Publ., 1965, 273, 183.
4. R.O. Davies and J. Lamb, Quart. Rev., 1957, 11, 134.
5. J. Lamb, in W.P. Mason (ed.), 'Physical Acoustics', Vol. 2A, Academic Press, London, 1965, p.203.
6. M.C.R. Symons and M.J. Blandamer, in A.K. Covington and P. Jones (editors), 'Hydrogen Bonded Solvent Systems', Taylor and Francis, London, 1968.
7. D.E. Clarke, Ph.D. Thesis, University of Leicester, 1967.
8. E.F. Caldin, 'Fast Reactions in Solution', Wiley, New York.
9. E. Wynne-Jones, Roy. Inst. Chem. Reviews, 1969, 2(1), 59.
10. G.L. Gooberman, 'Ultrasonics', The English University Press, London, 1968.
11. K. Herzfeld and T.A. Litovitz, 'Absorption and Dispersion of Ultrasonic Waves', Academic Press, London, 1959.
12. T.A. Litovitz and C.M. Davies, in W.P. Mason (ed), 'Physical Acoustics', Vol. 2A, Academic Press, London, 1965, p.281.

13. A.B. Bhatia, 'Ultrasonic Absorption', Oxford University Press, Oxford, 1967.

14. J. Blitz, 'Fundamentals of Ultrasonics', Butterworths, London, 1967.

15. M. Eigen and L. De Mayer, in S.L. Friess, E.S. Lewis and A. Weissberger (editors), Techniques of Organic Chemistry, Vol. 8, Part 2, Interscience N.Y., 1963, p.895.

16. W.T. Richards, Rev. Mod. Phys., 11 (1939) 36.

17. T.A. Litovitz, J. Acoust. Soc. Amer., 1959, 31, 681.

18. M.J. Blandamer, D.E. Clarke, N.J. Hidden and M.C.R. Symons, Trans. Faraday Soc., 1968, 64, 2691.

19. M.J. Blandamer, D.E. Clarke, N.J. Hidden and M.C.R. Symons, Chem. Commun., 1966, 342.

20. A.G. Chynoweth and W.G. Schreider, J. Chem. Phys., 1951, 19, 1566.

21. M.J. Blandamer, N.J. Hidden, M.C.R. Symons and N.C. Treloar, Trans. Faraday Soc., 1969, 65, 2663.

22. C.J. Burton, J. Acoust. Soc. Amer., 1948, 20, 186.

23. M.J. Blandamer, N.J. Hidden, M.C.R. Symons and N.C. Treloar, Trans. Faraday Soc., 1968, 64, 3242.

24. J.H. Andreae, P.D. Edmonds and J.F. McKellar, Acustica, 1965, 15, 74.

25. L.R.O. Storey, Proc. Phys. Soc., 1952, B65, 943.

26. M.J. Blandamer, N.J. Hidden, M.C.R. Symons and N.C. Treloar, Trans. Faraday Soc., 1969, 65, 1805.

27. J. Thamsen, Acustica, 1965, 26, 185.

28. M.J. Blandamer, N.J. Hidden and M.C.R. Symons, Trans. Faraday Soc., 1970, 66, 316.

29. R.N. Barfield and W.G. Schneider, J. Chem. Phys., 1959, 31, 488.

30. F.H. Willis, J. Acoust. Soc. Amer., 1947, 19, 242.

31. G.W. Willard, J. Acoust. Soc. Amer., 1941, 12, 1941.

32. C.G. Hammes and W. Knoche, J. Chem. Phys., 1966, 45, 4041.

33. M.J. Blandamer, N.J. Hidden, K.W. Morcom, R.W. Smith, N.C. Treloar and M.J. Wootten, Trans. Faraday Soc., in press.

34. M.J. Blandamer, M.J. Foster and D. Waddington, Trans. Faraday Soc., 1970, 66(6), 1369.

35. D.A. Armitage, M.J. Blandamer, M.J. Foster, N.J. Hidden, K.W. Morcom, M.C.R. Symons and M.J. Wootten, Trans. Faraday Soc., 1968, 64, 1193.

36. D. Eisenberg and W. Kauzmann, 'The Structure and Properties of Water', Oxford University Press, Oxford, 1969.

37. D.J.G. Ives and J.H. Lemon, R.I.C. Revs., 1968, 1, 62.

38. H.J.C. Berendsen, 'Theoretical and Experimental Biophysics', Vol. 1, Arnold, London, 1967.

39. C.M. Davis Jr. and J. Janzynski, Adv. Mol. Relaxation Proc., 1967, 1, 155.

40. L. Hall, Phys. Rev., 1948, 73, 775.

41. H. Frank, Federation Proc., 1965, 24, 2.

42. J.D. Bernal and R.H. Fowler, J. Chem. Phys., 1933, 1, 515.

43. H.S. Frank and W.Y. Wen, Discussion Faraday Soc., 1957, No. 24, 133.

44. G.A. Jeffrey and R.K. McMullan, Progr. Inorg. Chem., 1967, 8, 43.

45. F. Franks and D.J.G. Ives, Quart Rev., 1966, 20, 1.

46. F. Franks, Ann. N.Y. Acad. Sci., 1965, 125, 277.

47. W. Kauzmann, Adv. Protein Chem., 1959, 14, 1.

48. G. Nemethy and H.A. Scheraga, J. Phys. Chem., 1962, 66, 1773.

49. G. Nemethy, Angew. Chem. Intern. Ed. Engl., 1967, 6, 195.

50. G. Nemethy and W. Kauzmann, J. Phys. Chem., 1968, 72, 1842.

51. J.S. Rowlinson, 'Liquids and Liquid Mixtures', 2nd Ed., Butterworths, London, 1969.

52. F. Franks, in A.K. Covington and P. Jones (ed.) 'Hydrogen Bonded Solvent Systems', Taylor and Francis, London, 1968.

53. I. Prigogine and R. Defay, 'Chemical Thermodynamics', (transl. by D.H. Everett), Longmans-Green, London, 1954.

54. J.L. Copp and D.H. Everett, Diss. Faraday Soc., 1953, 14, 174.

55. J.L. Copp, Trans. Faraday Soc., 1955, 51, 1056.

56. J.L. Copp and D.H. Everett, Trans. Faraday Soc., 1957, 53, 9.

57. J.F. McKellar and J.H. Andreae, Nature, 1962,195,778.

58. J.H. Andreae, Nature, 1962, 195, 865.

59. V.A. Sdovyev, C.J. Montrose, M.H. Watkins and T.A. Litovitz, J. Chem. Phys., 1968, 48, 2155.

60. G.G. Hammes and P.R. Schimmel, J. Amer. Chem. Soc., 1967, 89, 442.

61. K. Arakawa and N. Takenaka, Bull. Chem. Soc., Japan, 1967, 40, 2739.

62. D.V. Beauregard and R.E. Barrett, J. Chem. Phys., 1968, 49, 5241.

63. K.G. Breitschwerdt, H. Kistenmacker and K. Tamm, Phys. Letters, 1967, 244, 550.

64. H.S. Frank and F. Franks, J. Chem. Phys., 1968, 48, 4746.

65. D.B. Wetlaufer, S.K. Malik, L. Stoller and R.L. Coffin, J. Amer. Chem. Soc., 1964, 86, 508.

66. G. Scatchard, W.T. Harrier and S.E. Wood, J. Amer. Chem. Soc., 1938, 75, 5139.

67. R.H. Stokes, Australian J. Chem., 1967, 20, 2087.

68. G.C. Kresheck and H.A. Scheraga, J. Phys. Soc., 1965, 69, 1704.

69. N.C. Treloar, Ph.D. Thesis, University of Leicester,1970.

70. S. Petrucci, J. Phys. Chem., 1967, 71, 1174.

71. S.S. Nun, R.J. Beyer and M.W. Dill, J. Chem. Phys., 1962, 36, 2737.

72. J.H. Andreae, E.L. Heasell and J. Lamb, Proc. Phys. Soc., 1956, B69, 626.

73. J.L. Hunter and H.D. Dardy, J. Chem. Phys., 1966, 44, 3637.

74. J.L. Hunter and H.D. Dardy, J. Chem. Phys., 1965, 42, 2961.

75. For further discussion see, for example, T.L. Hill, 'Statistical Mechanics', McGraw-Hill, London, 1956, Ch. 4.

76. R. Ullmann, J. Chem. Phys., 1968, 49, 831.

77. See also: R. Zwanig, Ann. Rev. Phys. Chem., 1965, 16, 67.

78. J.J. Burke, G.G. Hammes and T.B. Lewis, J. Chem. Phys., 1965, 42, 3520.

79. Unpublished data obtained in these laboratories.

80. E.M. Arnett and D.R. McKelvey, Record. Chem. Progr., 1965, 26, 185.

81. E.M. Arnett, 'Physico-Chemical Processes in Mixed Aqueous Solvents', Heinemann, London, 1967, p.105.

82. J. Lee and J.B. Hyne, Canad. J. Chem., 1968, 46, 2333.

83. J.B. Hyne, H.S. Golinkin and W.G. Laidlaw, J. Amer. Chem. Soc., 1966, 88, 2104.

84. M.J. Blandamer, D.E. Clarke, T.A. Claxton, M.F. Fox, N.J. Hidden, J. Oakes, M.C.R. Symons, G.S.P. Verma, and M.J. Wootten, Chem. Commun., 1967, 273.

85. F. Franks and M.J. Quickenden, Chem. Commun., 1968, 388.

86. F. Franks and H.T. Smith, Trans. Faraday Soc., 1968, 64, 2962.

87. F. Franks and H.H. Johnson, Trans. Faraday Soc., 1962, 58, 656.

88. K. Nakanishi, N. Kato and M. Maruyama, J. Phys. Chem., 1967, 71, 814.

89. M.J. Blandamer and M.F. Fox, Chem. Rev., 1970, 70, 59.

90. M.J. Blandamer, M.F. Fox, M.C.R. Symons, K.J. Wood and M.J. Wootten, Trans. Faraday Soc., 1968, 64, 3210.

91. A.D. Potts and D.W. Davidson, J. Phys. Chem., 1965, 69, 996.

92. M.J. Blandamer, D.E. Clarke, N.J. Hidden and M.C.R. Symons, Trans. Faraday Soc., 1967, 63, 66.

93. D.N. Glew, Nature, 1964, 201, 922.

94. D.N. Glew, Trans. Faraday Soc., 1965, 61, 30.

95. S.U. Pickering, Trans. Chem. Soc., 1893, 63(1), 141.

96. G.A. Jeffrey, T.H. Jorden and R.K. McMullan, Science, 1967, 155, 698.

97. G.A. Jeffrey, T.H. Jorden and R.K. McMullan, J. Chem. Phys., 1967, 47, 1218.

98. T.H. Jordan and T.C.W. Mak, J. Chem. Phys., 1967, 47, 1222.

99. G.L. Bertrand, J.W. Larson and L.G. Hepler, J. Phys. Chem., 1968, 72, 4194.

100. J. Stuehr and E. Yeager, in W.P. Mason (ed.), 'Physical Acoustics', Vol. 2A, Academic Press, London, 1965, p.351.

101. G. Atkinson and S.K. Kor, J. Phys. Chem., 1965, 69, 128.

102. L.G. Jackopin and E. Yeager, J. Phys. Chem., 1966, 70, 313.

103. G. Atkinson and S.K. Kor, J. Phys. Chem., 1965, 69, 128; 1966, 70, 314; 1967, 71, 673.

104. G.H. Czerlinski, 'Chemical Relaxation', Arnold, London, 1966.

105. W.G. Schneider, Colloq. Intern. Centre Natl. Rech. Sci. (Paris), 1959, 77, 259.

106. G.N. Malcolm and J.S. Rowlinson (with A. Davis), Trans. Faraday Soc., 1957, 53, 921.

107. C.J. Clemett, J. Chem. Soc. A, 1969, 455, 458.

108. J.B. Hyne, in A.K. Covington and P. Jones (ed.), 'Hydrogen Bonded Solvent Systems', Taylor and Francis, London, 1968.

109. M.J. Blandamer, N.J. Hidden, M.C.R. Symons and N.C. Treloar, Chem. Commun., 1968, 1325.

110. K.W. Morcom and R.W. Smith, J. Chem. Thermodyn., 1969, 1, 503.

111. M. Fixman, Advan. Chem. Phys., 1964, 4, 175.

112. O. Nomoto, J. Phys. Soc. Japan, 1956, 11, 827.

113. O. Nomoto, J. Phys. Soc. Japan, 1956, 11, 818.

114. O. Nomoto, J. Phys. Soc. Japan, 1957, 12, 300.

115. M.F. Vuks and L.I. Lisnyanski, Ukr. Fiz. Zhur., 1962, 7, 273.

116. V.P. Romanov and V.A. Solovyev, Soviet Phys. Acoust., 1965, 11, 68; Proc. Seminar Properties Water, Leningrad, U.S.S.R., 1965, p.183.

117. V.P. Romanov and V.A. Solovyev, Soviet Phys. Acoust., 1965, 11, 219.

118. J.M. Davenport, J.F. Dill, K. Fritsch and V.A. Solovyev, Akust. Zh. (U.S.S.R.), 1968, 14, 288.

119. J.S. Rowlinson, Natl. Bur. Std. (U.S.), Misc. Publ., 1965, 273, 9.

120. M.E. Fisher, Natl. Bur. Std. (U.S.), Misc. Publ., 1965, 273, 21.

121. P. Heller, Rept. Progr. Phys., 1967, 30(II), 731.

122. M.E. Fisher, Rept. Progr. Phys., 1967, 30(II), 615.

123. L.P. Kadanoff, W. Gotze, D. Hamblen, E.A.S. Lewis, V.V. Palcianskas, M. Rayl, J. Swift, D. Aspnes and J. Kane, Rev. Mod. Phys., 1967, 37, 395.

124. C. Domb, Phys. Today, 1968, 21, 23.

125. W.B. Kay, Accounts Chem. Res., 1968, 1, 344.

126. B. Widom, Science, 1967, 157, 375.

127. M. Cevolani and S. Petralia, Atti. Accad. Nazl. Lincei, Cl. Sc. Fis. Mat. Natur., Rend., 1955, 12, 674.

128. H. Schmidt, G. Jura and J.H. Hilderbrand, J. Phys. Chem., 1959, 63, 297.

129. M.J. Blandamer, D.E. Clarke and M.C.R. Symons, unpublished data.

130. P. White, D. Moule and G.C. Benson, Trans. Faraday Soc., 1958, 54, 1638.

131. H.D. Bale, R.E. Shepler and D.K. Sorgen, 'Phys. and Chemistry of Liquids', 1968, Vol. 1, Gordon and Breach, London, pp. 181-190.

132. R. Lucas, J. Phys. Radium, 1937, 8, 41.

133. M. Fixman, J. Chem. Phys., 1960, 33, 1363.

134. See for example R. Lucas in ref. 132.

135. M. Fixman, J. Chem. Phys., 1960, 33, 1357.

136. M. Fixman, J. Chem. Phys., 1962, 36, 310.

137. M. Fixman, J. Chem. Phys., 1962, 36, 1957.

138. M. Fixman, J. Chem. Phys., 1962, 36, 1961.

139. M. Fixman, J. Chem. Phys., 1962, 36, 1965.

140. J.H. Andreae and P.L. Joyce, Brit. J. Applied Phys., 1962, 13, 462.

141. J.H. Andreae, R. Bass, E.L. Heasell and J. Lamb, Acustica, 1964, 8, 131.

142. K. Tamm, G. Kurtz and R. Kaiser, Acustica, 1965, 4, 380.

143. P.D. Edmonds, V.F. Pearce and J.H. Andreae, Brit. J. Appd. Phys., 1962, 13, 551.

144. J. Karpovitch, J. Acoust. Soc. Amer., 1965, 26, 819.

145. G. Kurtze and K. Tamm, Acustica, 1953, 3, 33.

146. L. Lawley and R. Reed, Acustica, 1955, 5, 316.

147. J. Stuehr, E. Yeager, T. Sachs and F. Havorka, Office of Naval Research Technical Report, Sept. 1962.

148. M.J. Foster, Ph.D. Thesis, University of Leicester, 1968.

149. See ref. 69 and 7 for further details.

150. C.E. Mulders, J. Applied Sci. Research, 1948, B1(3), 149.

151. R.W. Leonard and O.B. Wilson, J. Acoust. Soc. Amer., 1954, 26, 223.

152. C.J. Moen, J. Acoust. Soc. Amer., 1951, 23, 62.

153. D.A. Bies, Tech. Report Number 6, Dept. of Physics, University of California, Research Contract Number N6 - onr - 27507 (1953).

154. M. Cerceo, R. Meister and T.A. Litovitz, J. Acoust. Soc. Amer., 1962, 34, 259.

155. E. Skudrzyk, Ost. Inorg.-Archiv., 1950, 4(5), 418.

156. H. Miller, Z. Phys. Chem. (Lpz), 1960, 215, 238.

157. T. Ohsawa and Y. Wada, Jap. J. App. Phys., 1967, 6(12), 1351.

158. F. Eggers, Acustica, 1967/68, 19, 323.

159. J. Karpovitch, J. Chem. Phys., 1954, 22, 1767.

160. L. Bergman, 'Ultrasonics', 1938, New York, J. Wiley, (6th edition, page 245).

161. J.C. Hubbard and A.L. Loomis, J. Opt. Soc. Amer., 1928, 17, 295.

162. J.C. Hubbard and A.L. Loomis, Nature, 1927, 170,189.

163. J.C. Hubbard and A.L. Loomis, Phys. Rev., 1928, 31(2), 158.

164. J.C. Hubbard and A.L. Loomis, Phil. Mag., 1928, 5(7), 1177.

165. W.P. Mason, 'Electromechanical Transducers and Wave Filters', Van Nostrand, New York, 1948.

166. F.E. Borgnis, Acustica, 1957, 7, 152.

167. E.D. Fletcher and H.D. Parbrook, J. Sound Vib., 1964, 1(2), 179.

168. J.H. Andreae and P.D. Edmonds, J. Scientific Instr., 1961, 38, 508.

169. G.W. Willard, J. Acoust. Soc. Amer., 1941, 12, 438.

170. A.L. Vierk, Z.anorg. Chem., 1950, 261, 283.

171. J. Timmermans, 'The Physico-Chemical Constants of Binary Systems', (Interscience Publishers, Inc., New York, 1960).

172. J. Mobius, J. Prakt. Chem., 1955, 2(4), 95.

173. H.S. Frank and A.S. Quist, J. Phys. Chem., 1961, 65, 560.

174. M. Fixman, in B. Chu(editor), 'Molecular Forces', Interscience, New York, 1967, p.1.

175. J.H. Andreae and J. Lamb, Proc. Phys. Soc., 1956, B69, 814.

176. A.E. Weinman, University of Leicester, unpublished curvefitting routine.

177. H. Stone, J. Opt. Soc. Amer., 1962, 52(9), 998.

178. M.F. Vuks and L.I. Lisnyanskii, Ukr. Fiz. Zhur., 1962, 7(7), 778-781.

179. L.I. Lisnyanskii, Dissertation (Lenningrad Univ.), L.G.U., 1962.

180. M.A. Isakovich, Zhur. Eksp. i Teoret. Fiz., 1948, 18(10), 907.

181. J.A. Barker, Austral. J. Chem., 1953, 6, 207.

182. Modified from an original program by D.A. Armitage.

183. L.S. Ornstein and F. Zernike, Physik. Z., 1918, 19, 134; 1926, 27, 761.

184. P. Debye, J. Chem. Phys., 1959, 31, 680.

185. J. Kentamaa, E. Tommila and M. Martii, Ann. Acad. Scient. Fenn., 1969, AII, 93, 3.

186. D. Nicholsen, J. Chem. Eng. Data, 1960, 5, 309.

187. D. Hansen and M. van Winkle, J. Chem. Eng. Data, 1960, 5, 30.

188. A. Kister and D. Waldman, J. Phys. Chem., 1958, 62, 245.

189. A.E. Taylor, J. Phys. Chem., 1900, 4, 355.

190. J. Griswold and J. Burford, Ind. Eng. Chem., 1949, 41.

191. D. Othmer and F. Morley, Ind. Eng. Chem., 1946, 38, 751.

192. D. Othmer, M. Chugar and S. Levy, Ind. Eng. Chem., 1952, 44, 1872.

193. McElroy and Krug, 1892, 1893, in reference 171.

194. McElroy, 1894, in reference 171.

195. Sapozhnikov, 1896, in reference 171.

196. Barr and Bircumshaw, 1921, in reference 171.

197. Young, 1933, in reference 171.

198. E. Cohen and C.J.G. van der Horst, Z. Physik. Chem., 1938, B40, 231.

199. D.A. Armitage and K.W. Morcom, unpublished work.

200. A.P. Kendig, R.H. Bigelow, P.D. Edmonds and C.J. Pings, J. Chem. Phys., 1964, 40, 1451.

201. A.V. Anantaraman, A.B. Walters, P.D. Edmonds and C.J. Pings, J. Chem. Phys., 1966, 44, 2657.

202. H.W. Thompson, Trans. Faraday Soc., 1941, 37, 344.

203. R.H. Ewell and J.F. Bourland, J. Chem. Phys., 1940, 8, 635.

204. K.A. Valiev and M.I. Emel'yanov, Zhurnal Strukturnoi Khimii, 1964, 5(6), 814.

205. K.A. Valiev and M.I. Emel'yanov, Zhurnal Strukturnoi Khimii, 1964, 5(1), 7.

206. P.A. Johnson and A.L. Baab, Chem. Rev., 1956, 56, 387.

207. M.J. Blandamer, M.J. Foster, N.J. Hidden and M.C.R. Symons, Trans. Faraday Soc., 1968, 64, 3247.

208. M.J. Blandamer, Quart. Rev., 1970, XXIV (2), 169.

209. R.L. Kay, Adv. in Chem., 1968, 73, 1.

210. G. Atkinson, in 'Hydrogen Bonded Solvent Systems', Ed. A.K. Covington, Taylor and Francis, London, 1968.

211. M.J. Blandamer, M.J. Foster, N.J. Hidden and M.C.R. Symons, J. Phys. Chem., 1968, 72, 2268.

212. M.J. Blandamer and D. Waddington, J. Chem. Phys., 1970, 52(12), 6247.

213. R.A. Robinson and R.H. Stokes, 'Electrolyte Solutions', Butterworths, London, 1955 (revised edition).

214. H.L. Friedman and Y.C. Wu, J. Phys. Chem., 1966, 70, 166.

215. S. Lindenbaum and G.E. Boyd, J. Phys. Chem., 1964, 68, 911.

216. S. Lindenbaum, J. Phys. Chem., 1966, 70, 814.

217. W.Y. Wen and S. Saito, J. Phys. Chem., 1964, 68, 2639.

218. F.J. Millero and W. Drost-Hansen, J. Phys. Chem., 1968, 72, 1758.

219. H. Ruterjans, F. Schreiner, U. Saga and Th. Ackermann, J. Phys. Chem., 1969, 73, 986.

220. M.J. Blandamer, in 'Water: A Comprehensive Treatise', (ed. F. Franks), Vol. II, Chapter 9, to be submitted.

221. T. Burdett, University of Leicester, unpublished data.

222. H.G. Hertz, Angew. Chem. Int. Edit., 1970, 9(2), 124.

223. W.A.P. Luck and W. Ditter, J. Phys. Chem., 1970, 74(21), 3687.

224. G.E. Walrafen, in 'Hydrogen Bonded Solvent Systems', A.K. Covington and P. Jones, ed., Taylor and Francis, London, 1968.

225. G. Scatchard, Federation Proc., 1966, 25(3), 954.

226. G. Némethy and H.A. Scheraga, J. Chem. Phys., 1962, 36, 3382, and subsequent papers.

227. J.L. Kavanan, 'Water and Solute-Water Interactions', San Francisco, Holden-Day, 1964.

228. H. Eyring and M.S. Jhon, Chemistry, 1966, 39, 8.

229. R.A. Horne,'Survey of Progress in Chemistry', ed. A.F. Scott, Academic Press, London, 1968, Vol. 4, p. 1.

230. G. Herzberg, 'Molecular Spectra and Molecular Structure', 2nd ed., Van Nostrand, New York, 1950.

231. P.G. Owston, Q. Rev., 1951, 5, 344.

232. C. Haas and D.F. Hornig, J. Chem. Phys., 1960, 32, 1763.

233. M. Magat, Ph. D. Thesis, University of Paris, 1936.

234. T.T. Wall and D.F. Hornig, J. Chem. Phys., 1965, 43, 2079.

235. M. Falk and T.A. Ford, Canad. J. Chem., 1968, 46, 3579.

236. G.E. Walrafen, J. Chem. Phys., 1966, 44(4), 1546.

237. G.E. Walrafen, J. Chem. Phys., 1967, 47(1), 114.

238. D.A. Draegert et al, J. Opt. Soc. Amer., 1966, 56(1), 64.

239. M.D. Cohen and E. Fischer, J. Chem. Soc., 1962, 3044.

240. J.R. Morrey, J. Phys. Chem., 1962, 66, 2169.

241. G.E. Walrafen, J. Chem. Phys., 1968, 48(1), 244.

242. G.E. Walrafen, J. Chem. Phys., 1969, 50(1), 560.

243. G.E. Walrafen, J. Chem. Phys., 1962, 36(4), 1035 and also references 224, 236, 237, 241 and 242.

244. E.U. Franck and K. Roth, Discs. Faraday Soc., 1967, 43, 108.

245. W.A. Senior and R.E. Verrall, J. Phys. Chem., 1969, 73, 4242.

246. J. Schiffer, J. Chem. Phys., 1969, 50, 566.

247. J. Schiffer and D.F. Hornig, J. Chem. Phys., 1968, 49(9), 4150.

248. T.T. Wall, J. Chem. Phys., 1969, 51(1), 113.

249. R.G. Gordon, J. Chem. Phys., 1965, 43, 1307.

250. W. Yellin and W.L. Courchene, Nature, 1968, 219 (5156), 852.

251. K. Buijs and G.R. Choppin, J. Chem. Phys., 1963, 39, 2035.

252. K. Buijs and G.R. Choppin, J. Chem. Phys., 1964, 40, 3120.

253. W. Luck, Ber. Bunsenges. Phys. Chem., 1965, 69, 626.

254. J.D. Worley and I. Klotz, J. Chem. Phys., 1966, 45(8), 2868.

255. D.P. Stevenson, J. Phys. Chem., 1965, 69, 2145.

256. D.N. Glew, in 'Hydrogen Bonded Solvent Systems',

257. M.J. Wootten, Ph.D. Thesis, University of Leicester, 1969.

258. W.A. P. Luck and W. Ditter, J. Mol. Struct., 1967, 1, 339.

259. G. Walrafen, J. Chem. Phys., 1964, 40(11), 3249.

260. P.M. Vollmar, J. Chem. Phys., 1963, 39, 2236.

261. G.E. Walrafen, see reference 243.

262. M. Magat, Ann. Phys. (Paris), 1936, 6, 109.

263. G.E. Walrafen, see reference 236.

264. D.A. Draegert and D. Williams, J. Chem. Phys., 1968, 48(1), 401.

265. K.A. Hartman, J. Phys. Chem., 1966, 70(1), 270.

266. J.C. Hindman, J. Chem. Phys., 1962, 36, 1000.

267. G. Fabbri and S. Roffia, Ann. Chem., 1960, 50, 3.

268. R.D. Waldron, J. Chem. Phys., 1957, 26, 809.

269. R.E. Weston, Spectrochim. Acta, 1962, 18, 1257.

270. C.L. van Panthaleon van Eck et al, Proc. Roy. Soc. (London), 1958, A247, 434.

271. G.A. Krestov, J. Struct. Chem. (U.S.S.R.), 1962, 3, 391.

272. T.T. Wall and D.F. Hornig, J. Chem. Phys., 1967, 47(2), 784.

273. T.T. Wall and D.F. Hornig, J. Chem. Phys., 1966, 45, 3424.

274. G.A. Jeffrey and R.K. McMullan, Progr. In Inorg. Chem., 1967, 8, 43, and references therein.

275. Z. Kecki, P. Dryjanski and E. Kozlowska, Roczniki. Chem., 1968, 42, 1749.

276. G.E. Walrafen, J. Chem. Phys., 1970, 52(8), 4176.

277. M.J. Colles, G.E. Walrafen and K.W. Wecht, Chem. Phys. Letters, 1970, 4(10), 621.

278. H.R. Wyss and M. Falk, Canad. J. Chem., 1970, 48, 607.

279. G. Brink and M. Falk, Canad. J. Chem., 1970, 48, 2096.

280. C.D. West, Z. Kristallogr., 1935, 91, 480.

281. C.D. West, Z. Kristallogr., 1934, 88, 198.

282. G. Brink and M. Falk, Canad. J. Chem., 1970, 48, 3019.

283. G.E. Walrafen, J. Chem. Phys., 1966, 44(10), 3726.

284. J.D. Bernal and R.H. Fowler, J. Chem. Phys., 1933, 1, 515.

285. D.D. Eley and M.G. Evans, Trans. Faraday Soc., 1938, 34, 1093.

286. J. Perram, J. Chem. Phys., 1968, 49, 4245.

287. J. Davies, S. Ormondroyd and M.C.R. Symons, Chem. Comm., 1970, in press.

288. R.N. Butler and M.C.R. Symons, Trans. Faraday Soc., 1969, 65(4), 945; 1969, 65(4), 2559.

289. A. Allerhand and P. Schleyer, J. Amer. Chem. Soc., 1963, 85, 1233.

290. T.E. Gough, Ph.D. Thesis, University of Leicester, 1969.

291. M.J. Blandamer, T.E. Gough and M.C.R. Symons, Trans. Faraday Soc., 1964, 60, 488.

292. R.N. Butler, J. Davies and M.C.R. Symons, Trans. Faraday Soc., 1970, in press.

293. W.V. Nystrom, unpublished results.

294. G.J. Safford, P.C. Schaffer, P.S. Leung, G.F. Doebbler, G.W. Brady and E.F.X. Lyden, J. Chem. Phys., 1969, 50, 2140.

295. W.V. Nystrom and D. Waddington, unpublished results.

296. D. Waddington, unpublished results.

297. P. Saumagne, J. Chem. Phys., 1970, 53, 3768.

298. A.J. Tursi and E.R. Nixon, J. Chem. Phys., 1970, 52, 1521.

299. L.J. Bellamy, private communication.

300. D.P. Stevenson, 'Structural Chemistry and Molecular Biology' (ed. A. Rich and N. Davidson), Freeman, San Francisco, 1968.

301. E. Greinacher, W.Luttke and R. Mecke, Z. Electrochem, 1955, 59, 23.

302. S.C. Mohr, W.D. Wilk and G.M. Barow, J. Amer. Chem. Soc., 1965, 87(14), 3048.

303. M.J. Blandamer and M.F. Fox, to be submitted to 'Water - a Comprehensive Review', (ed. F. Franks) Volume II, Chapter 8, Plenum Press, New York.